

DISSERTATION

VLBI satellite tracking for the realization of frame ties

ausgeführt zum Zwecke der Erlangung des akademischen Grades einer Doktorin der
technischen Wissenschaften unter der Leitung von

Prof. Dr. Dr. h.c. Harald Schuh

E120-4

Department für Geodäsie und Geoinformation

Höhere Geodäsie

eingereicht an der Technischen Universität Wien

Fakultät für Mathematik und Geoinformation

von

Lucia Plank

Wien, August 2013

Thank You - Danke!

Several people have been supporting my research during the past years. This is the place to honor them.

This thesis wouldn't exist without Harald Schuh catching me as a doctorate student. Suggesting to me this exciting new topic of VLBI satellite tracking is evidence of his farsightedness. The work on it and with him was constantly challenging and was built on motivating trust. I expressively thank him for introducing me into the geodetic (VLBI) community and to teach me the principles of internationally recognized research.

Johannes Böhm was my "solution right the next door" without closing hours. I thank him for thinking his way into my problems, his open ears, critical questions, advices & suggestions, his openness and his ability to let me leave his room with a new idea each time I came in.

Big thanks to the VieVS-crowd and all colleagues of the Higher Geodesy group at Vienna University of Technology. I appreciate the meaningless discussions during lunch the same as the scientific ones. You are the reason that I can enjoy my work.

During my doctorate studies I had the chance to spend two weeks at the National Astronomical Observatory in Mizusawa, Japan. I was introduced to the processing of SELENE VLBI data by Sander Goossens, whom I cordially thank, representatively for all the supportive colleagues there.

Chris Jacobs gave me a wonderful time at JPL. His talent, to bring people together and to initiate a fruitful discussion, helped me to put my research goals into concrete terms.

I am glad to acknowledge the steady interest in my work by Vincenza Tornatore. Thank you to all colleagues within the IVS and the whole geodetic community, to whom I had the chance to present parts of my work and gain new ideas through their supportive questions and advice.

Particular (financial) thanks goes to my home institution, the Vienna University of Technology, for my time as University Assistant. It is my pleasure to thank the German Research Foundation for funding my research within the DFG Research Unit FOR 1503: "Space-Time Reference Systems for Monitoring Global Change and for Precise Navigation in Space" - project D-VLBI.

Finally, I thank You - and all readers - for Your interest in my work.

Lucia Plank, August 2013

Kurzfassung

VLBI-Beobachtungen zu Satelliten zur Verknüpfung von Referenzrahmen

Mit der Aussicht auf eine Verbesserung in der Verknüpfung von Referenzrahmen unterschiedlicher Beobachtungsverfahren ist die Idee von VLBI-Beobachtungen zu Satelliten für die heutige Geodäsie von großem Interesse.

Die Radiointerferometrie auf langen Basen (VLBI, *Very Long Baseline Interferometry*) ist ein Standardverfahren in der Geodäsie zur Bestimmung des himmelfesten Referenzrahmens (CRF, *Celestial Reference Frame*), des erdfesten Koordinatenrahmens (TRF, *Terrestrial Reference Frame*) und der Erdorientierungsparameter (EOP, *Earth Orientation Parameter*) zur Verknüpfung dieser beiden. Außerdem kommt die VLBI in der Raumschiffnavigation zum Einsatz, wo in den letzten Jahren gewaltige Entwicklungen zu beobachten waren. Dies wird am Beispiel der japanischen Mondmission SELENE gezeigt, wovon Daten prozessiert wurden. Heutige Realisierungen des TRF kombinieren die Messungen von unterschiedlichen geodätischen Weltraumverfahren und sind auf eine gute Verknüpfung dieser Systeme angewiesen. Für eine weitere Verbesserung, sowie das Ziel einer konsistenten Bestimmung des gesamten Systems aus CRF-EOP-TRF verfolgend, werden alternative Methoden zur Verknüpfung der unterschiedlichen modernen geodätischen Weltraumverfahren gesucht. Eine vielversprechende Methode hierfür sind VLBI-Beobachtungen zu Satelliten. Damit soll die Verknüpfung entweder mittels eines eigens dafür konzipierten Satelliten oder durch direktes Anmessen von Satelliten globaler Satellitennavigationssysteme (GNSS, *Global Navigation Satellite Systems*) erfolgen. Die Untersuchung bereits erfolgreicher Realisierungen im Bereich der Raumschiffnavigation hinsichtlich Methoden für eine nutzbringende Verwendung in der Geodäsie ist Thema dieser Arbeit.

Mit dem Ziel, echte Daten zu verarbeiten wurde die Vienna VLBI Software VieVS um die Möglichkeit erweitert, VLBI-Beobachtungen zu Satelliten zu planen, zu simulieren und zu analysieren. Die Berechnung des beobachteten Laufzeitunterschiedes wird näher erläutert, anschließend wird die Methode der VLBI-Satellitenbeobachtungen mit ihren aktuellen Entwicklungen vorgestellt und auf einige Punkte bezüglich der praktischen Realisierung näher eingegangen. Herzstück der vorgelegten Arbeit ist eine umfassende Simulationsstudie zu geeigneten Beobachtungsstrategien, die eine Ableitung präziser Stationskoordinaten im System des beobachteten Satelliten erlauben. Für Satelliten zwischen 1000 und 20000 Kilometern Flughöhe gelingt dies mit einer Genauigkeit von wenigen Millimetern. Dafür wird der Ansatz von Wochenlösungen

gewählt, d.h. ein Satellit wird von einem regionalen oder globalen Netzwerk für sieben Tage durchgehend beobachtet. Für die untersuchten Satelliten in 2000 bzw. 6000 km Höhe wird ein geeignetes Beobachtungsintervall von einer Minute bestimmt. Unter der Annahme einer relativ turbulenten Atmosphäre, werden in den Simulationen für regionale Netzwerke aus 6-7 Stationen mit Basislinienlängen zwischen 2000 und 3000 km Genauigkeiten von bestimmten Stationskoordinaten zwischen 3 und 14 mm gefunden. Diese sind abhängig von der Bahn bzw. der Höhe des beobachteten Satelliten, sowie von der sich laufend ändernden Geometrie zwischen den Basislinien und dem Satelliten. Im Fall globaler Netze von mindestens 16 bis 32 Stationen werden Genauigkeiten gleicher Größenordnung gefunden wenn ein Satellit auf 6000 km beobachtet wird. Für ein relativ tiefes Ziel auf 2000 km verringert sich die erwartete Genauigkeit für wöchentliche Stationskoordinaten um einen Faktor zwei. Sollen Satelliten des GNSS beobachtet werden, ist die gewählte Beobachtungsstrategie nicht zielführend und es wird die Kombination mit einer klassischen VLBI Session zu Radioquellen bzw. die Beobachtung einer Satellitenkonstellation untersucht.

Eine finale Einschätzung der erzielten Ergebnisse eröffnet eine Vielzahl von unmittelbaren Anwendungen zur Verknüpfung von unterschiedlichen Systemen. Damit werden eine alsbaldige Realisierung von VLBI-Beobachtungen zu Satelliten sowie eine Fortführung intensiver Forschung auf diesem Gebiet gleichermaßen unterstützt.

Abstract

VLBI satellite tracking is a popular topic in geodesy at the moment. Attributed with the potential to solve the pending problem of inter-technique frame ties, the prospect of success provides the impetus of ongoing research in that area.

Very Long Baseline Interferometry (VLBI) is a well-probed space geodetic technique used to determine the Celestial Reference Frame (CRF), the Terrestrial Reference Frame (TRF) and the Earth Orientation Parameters (EOP) in between. Alternatively, VLBI is generally used in spacecraft tracking. Technology in that area has been rapidly advancing in the last years. An overview of present realizations of VLBI spacecraft tracking, including data processing on the example of the Japanese lunar mission SELENE is part of this work. Today's most precise and reliable realizations of the TRF rely on the measurements of several space geodetic techniques and the corresponding inter-technique ties. For future improvement, and also for a rigorous determination of the whole system of CRF-EOP-TRF, alternative methods for connecting the various space geodetic techniques, establishing precise frame ties, are urgently needed. A promising solution is the use of VLBI satellite observations, either in combination with a so-called space tie realized by a dedicated satellite or by directly observing satellites of the Global Navigation Satellite Systems (GNSS) with VLBI. The study of successful realizations of VLBI tracking and identifying proper applications for practical geodetic value summarizes this work.

With the goal to process real data, the Vienna VLBI Software VieVS is extended for the possibilities to schedule, simulate and analyze VLBI satellite observations. Some details on the corresponding delay modeling are provided. The technique of VLBI satellite tracking is introduced, discussing some practical issues as well as the latest developments. This thesis contains a detailed simulation study of VLBI observations to satellites, identifying adequate observing strategies for the precise determination of antenna coordinates on Earth in the satellite's system. For satellites at heights between 1000 and 20000 km, adequate observation strategies are found that allow the determination of the station coordinates at the level of a few millimeters. Therefore, the approach of weekly solutions is chosen, meaning that one satellite is observed by either a regional or a global antenna network during seven consecutive days. For the investigated satellites at 2000 and 6000 km, a feasible observing interval of 1 minute is found. Assuming turbulent tropospheric conditions, in regional networks of 6-7 stations with baseline lengths between 2000 and 3000 km, weekly 3D position rms between 3 and 14 mm can be expected, depending on the orbit, respectively the height, of the observed satellite, as well as on the changing geometry be-

tween the observing baselines and the target satellite. For global networks, a considerable high number of observing telescopes is needed, about 16-32, with expected accuracies at the same level as in regional networks for a higher satellite at 6000 km height and about a factor of two worse for a very low satellite at 2000 km. In the case of VLBI observations to a satellite of the GNSS, alternative observing strategies are needed. In this thesis the combination with a classical VLBI session observing extragalactic radio sources or the observation of a satellite constellation are introduced.

The careful assessment of the presented results reveals valuable application of such observations in the area of frame ties, strongly supporting immediate realization and ongoing research on the topic of VLBI satellite observations.

Contents

1	Introduction	1
1.1	Research task	2
1.2	Route to the goal	3
2	Time and coordinate systems	5
2.1	The framework of Newton and Einstein	6
2.1.1	Relativity in Astronomical Reference Systems	6
2.2	Time Scales	7
2.2.1	Time Scales based on the SI-Second	8
2.2.2	Coordinated Universal Time UTC	9
2.3	Conventional Celestial Reference System and Frame	10
2.3.1	Ephemerides	12
2.3.2	Quasars	13
2.4	International Terrestrial Reference System and Frame	13
2.4.1	Inter-technique ties	14
2.4.2	Transformation between TRS and CRS	16
3	Very Long Baseline Interferometry	17
3.1	Geodetic VLBI	17
3.1.1	Basics	18
3.1.2	Delay model	19
3.1.3	Atmospheric delay models	24
3.1.4	The role of clocks	26
3.1.5	Prospects	26
3.2	VLBI for space applications	27
3.2.1	Technical evolution	28
3.2.2	Overview of VLBI tracking systems	30
3.2.3	Delay model for sources at finite distance	33
3.2.4	Future potential	36

4	Differential VLBI	39
4.1	Measurement principle	39
4.1.1	Scan gaps	40
4.1.2	Separation angles	41
4.1.3	Common media	42
4.1.4	Same beam interferometry	44
4.2	D-VLBI by the example of SELENE	45
4.2.1	SELENE differential VLBI tracking	45
4.2.2	Processing SELENE D-VLBI data in VieVS	47
4.2.3	Investigation of residual effects & level of cancellation	52
5	VLBI satellite tracking	57
5.1	Motivation and previous work	58
5.2	GRASP	59
5.3	Technical aspects	60
5.3.1	Shared visibility	61
5.3.2	Antenna slew speed	62
5.4	VieVS ₂ tie	65
5.4.1	Vienna VLBI software VieVS	65
5.4.2	Satellite tracking in VieVS	65
5.4.3	Satellite delay modeling	68
5.4.4	Simulations	69
6	Simulation studies and results	73
6.1	Composition of the study	73
6.1.1	Satellite orbits	73
6.1.2	Station networks	75
6.1.3	Scheduling	77
6.1.4	Processing options	77
6.1.5	Station position repeatability	78
6.2	Regional networks	78
6.2.1	Weekly solution	83
6.2.2	Cutoff elevation angle	83
6.2.3	Observation interval	85
6.2.4	Influence of simulation parameters	87
6.2.5	Influence of processing options	88
6.2.6	Satellite passes	94
6.2.7	Orbit error	96
6.2.8	Investigated time span	98
6.3	Global networks	98

6.3.1	32 stations	98
6.3.2	16 stations	100
6.3.3	Cluster network	101
6.4	Observations to GNSS-satellites	104
6.4.1	Combined observations of a satellite and radio sources	106
6.4.2	Observing a satellite constellation	108
6.5	Summary of the results	111
7	Conclusions and Outlook	113
A	List of stations	117
B	Figures	119
	Abbreviations	123
	List of Figures	127
	List of Tables	129
	Bibliography	131

Chapter 1

Introduction

The realization of reference frames, as the platform of all kind of measurements on and around the Earth, is one of geodesy's main responsibilities. Today's most precise reference frames are either applicable through positions and velocities at a certain time epoch, which is indicated as kinematic approach, or they are modeled dynamically and represented by ephemerides of celestial bodies or space probes, respectively satellites. On global scales, one distinguishes between celestial, space-fixed, frames and terrestrial systems that are co-rotating with the Earth. The connection between these two systems is the current orientation of the Earth in space, which is monitored by space-geodetic techniques measuring the Earth Orientation Parameters (EOP).

The Very Long Baseline Interferometry (VLBI) technique, measuring signals emitted by extragalactic radio sources, is used to precisely determine the directions to these sources, realizing the International Celestial Reference Frame (ICRF). By monitoring the relative positions of the radio telescopes, VLBI is also capable to determine a reference frame on Earth. However, for highest accuracies and also for control reasons, the International Terrestrial Reference Frame (ITRF) is a combined product of four space geodetic techniques, optimally utilizing the specific strengths of VLBI, the Global Navigation Satellite Systems (GNSS), Satellite Laser Ranging (SLR) and Doppler Orbitography and Radiopositioning Integrated by Satellite (DORIS).

Today's prime challenge in the area of reference systems is a rigorous combination of the various contributing techniques, or the establishment of precise frame ties between the frames realized by the single techniques. VLBI holds a special position, as it is the only technique capable of consistently determining a full set of CRF-EOP-TRF. Therefore, the International Association of Geodesy (IAG) installed Sub-Commission 1.4, investigating the Interaction of Celestial and Terrestrial Reference Frames. One of the proposed possibilities within this group to support this goal is the option of VLBI observations to satellites.

VLBI to other targets than extragalactic radio sources is routinely applied in deep spacecraft tracking. There, in order to enable sufficient accuracy, usually the differential VLBI (D-VLBI) method is applied, where a target is observed alternately to an angularly close radio source. Through the differential approach common error sources on the similar signal ray paths cancel, enabling the precise determination of the target's position relative to the well known reference

source. By applying this technique between deep space probes, that are determined in the dynamical system of the planetary ephemerides, and radio sources of the kinematically determined ICRF, such observations establish the link between these two systems.

At the moment, several ideas are investigated how VLBI observations to satellites can be used to tie the systems of the various space geodetic techniques to one another and thus improve the accuracy and particularly the consistency of the TRF and the entire system of TRF, EOP, and CRF. If it was a proposed mission for a dedicated space tie satellite or successful test observations to GNSS-satellites, VLBI satellite tracking is a hot topic in geodesy today. However, the actual state of the art is only at the beginning of a full establishment of this promising technique. Consequently, research and development in that area are highly desired in the community.

1.1 Research task

The research task of the present thesis is to study the technique of VLBI satellite tracking and its applicability to support the derivation of frame ties. Therefore, the role of this new technique needs to be positioned carefully within the world of VLBI. Against the backdrop of the development of reference frames and completing the efforts done in that area so far and to support future progress. With regard to the latter, one has to face the fact that despite the existence of several prosperous recent studies, mission concepts and field tests, a standardized way of operation has not been identified yet. There is a significant divergence in the technical realization, e.g. with regard to the used signal, the observation strategy, e.g. if observations are done in differenced D-VLBI or single-target mode, and in the orbits of the proposed targets, from satellites at heights of a few hundreds of kilometers up to space probes orbiting the Moon. In brief, there are a lot of open questions to be solved.

With VLBI space applications rather unknown in the geodetic community, a review of available techniques certainly will be an important part of this work. The question to be discussed is, whether existent knowledge can be used for the purposes of geodetic frame ties. This can not happen straightforwardly, as there are different realizations currently in use and because for targets in deep space the geometry between the baseline and the target(s) as well as accuracy demands are different than for probes in near Earth space.

The investigations of this thesis shall be substantially independent of any predefined measurement characteristics that possibly impose restrictions on the way of observation or the use of certain telescopes. Disregarding further applications, the focus is set on the establishment of inter-technique ties, with the aim to connect the space geodetic techniques contributing to the TRF. By the use of VLBI satellite tracking, a rather new technology, the task is to find observing methods that enable research and development of the technique itself and at the same time provide useful results right from the beginning. Within this framework, this thesis intends to identify adequate simple observing strategies towards the goal of frame ties, together with estimates on the expected accuracies. Provided that the findings are promising, they then need to be placed

in the context of geodetic future and possible immediate applications shall be defined.

Ideally, without a loss of scientific objectivity, by the provision of convincing simulations the presented research shall also help to support future work in the covered areas, as e.g. a pending realization of VLBI satellite tracking with good scientific outcome or the approval of a dedicated satellite mission.

1.2 Route to the goal

Following this introduction, the journey through this dissertation starts in chapter 2 with some theoretical background on the definition and realization of reference frames. The provision of highly precise coordinate systems goes hand in hand with the definition of a suitable time frame. Dealing with astronomical distances, but also important at global scales, time and distance have to be treated in accordance with Einstein's theory of relativity, whose basic principles are explained here. Throughout this chapter, the reader is introduced to the definition of frame ties and confronted with the actual problem of establishing precise inter-technique ties during the derivation of the ITRF.

Chapter 3 is devoted to the Very Long Baseline Interferometry (VLBI) technique. Assuming a certain familiarity with the classical geodetic VLBI method, only the basic principles, with emphasis on the geometrical delay model and the treatment of the troposphere, are given here. Some more information is provided on VLBI applications in space, examining the history of and recent developments in VLBI spacecraft tracking. Also the necessary changes in the corresponding delay model compared to the geodetic approach are discussed.

The commonly used approach of differential (D-)VLBI measurements is treated in chapter 4. Here, the clever concept of error cancellation is elaborated in theory first, before experiences of processing VLBI tracking data to the lunar space probes of the SELENE mission are shared. In concrete terms, the factor of cancellation is determined for this actual mission, imparting to the reader a good overall knowledge about the advantage of applying D-VLBI.

From the well-probed VLBI spacecraft tracking with the mostly applied D-VLBI technique, the transition is made to the rather innovative VLBI observations to Earth-orbiting satellites in chapter 5. The available literature in that area, together with the findings of the previous chapters provide the foundations for the following studies. In addition, the exciting mission concept of the Geodetic Reference Antenna in Space (GRASP) is introduced briefly and some technical issues of such observations are considered. With regard to the VLBI prerequisite of shared visibility for at least two separated antennas, the relation between the satellite heights and the consequent maximum baseline lengths is illustrated. In the course of the presented research, a software capable of simulating, processing and analyzing VLBI delays to satellites was created. The most important features and its basic manner of operation is also presented in this chapter.

Chapter 6 comprises the heart of the presented work. Reaching the agreement to concentrate on the determination of precise positions of the observing antennas with respect to the tracked

satellites, a comprehensive simulation study is performed. Using satellites of different heights, from about 1000 kilometers to the GNSS constellation at roughly 20000 km, adequate observing strategies are identified and expected accuracies are determined. Hereby, several decisive factors, as e.g. the observation interval, the simulation parameters, the processing options and the geometrical conditions, as determined through the satellite orbit and the antenna network, are thoroughly investigated. Chapter 6 ends with a summary of the results obtained in this simulation study.

Finally, the overall conclusions are drawn in chapter 7. Trying to quantify the findings and acquisition of this thesis in broader context, some small shortcomings of the presented investigations are identified, and ideas for future research are addressed.

Chapter 2

Time and coordinate systems

The basis for all three-dimensional, time dependent positioning on Earth and in space is a well defined coordinate system. The broad range of demands on such a system, in terms of precision, stability, and accessibility as well as the aim for a clear mathematical and physical theory behind, makes this a challenging topic. In space geodesy, the focus is on global coordinate systems, which can be either co-rotating with the Earth or fixed to distinct directions in space, e.g. stars. In the first case one speaks of a terrestrial system, the latter one is called a celestial system. A reference system is realized through a reference frame. While a reference system consists of definitions, its matching frame enables the user access to the system via the coordinates of distinct markers (e.g. antennas). For one reference system, there usually exist several realizations.

Time enters the system in two ways. First, as absolute time for the epoch of the observation and secondly in an indirect way, when distances are measured via the travel time of a signal in between. Nowadays space-geodetic techniques have reached a level of accuracy where a purely Newtonian description is not sufficient any more; hence, relativity aspects must be considered as well.

This chapter starts with an introduction of the basic Newtonian and relativistic foundation (section 2.1), in which all systems need to be embedded. In section 2.2 information is given on the definition of time and how it is measured in geodesy. In terms of coordinate systems, it is distinguished between celestial systems (sec. 2.3) and terrestrial systems (sec. 2.4), emphasizing the respective theoretical definitions and the practical transformations between the various frames. The important issue of inter-technique frame ties is discussed in section 2.4.1.

The Global Geodetic Observing System (GGOS; Plag & Pearlman, 2009) was established by the IAG to advance the geodetic theory, integrate today's products and support their transfer to applications supporting the society in its needs when living on our changing planet Earth. As the basis of all kinds of geo-referencing, accurate reference frames were identified as one of the main GGOS products, with the ambitious targets for the TRF of 1 mm positional accuracy and 0.1 mm/yr stability.

2.1 The framework of Newton and Einstein

For the description of dynamical processes, coordinate systems are preferred where all common physical and mechanical laws hold. Such systems, called inertial frames, are defined as systems with full validity of Newton's first law, so that a particle is at rest or is moving with constant velocity (Hobson *et al.*, 2006). In Newton's classical mechanics, a space-time event can be specified uniquely, when defining three spatial coordinates and one time coordinate. Time is absolute and events defined in different reference systems can be easily related and compared to each other. In special relativity, Einstein postulates that time runs differently in different inertial systems, in such a way that the speed of light c has the same measured value in all of them (Kaplan, 2005). Now, when two systems are moving relative to each other, space coordinates are related by the appropriate Lorentz transformation. The effects of length contraction and time dilatation can be identified in many common geodetic formulas via the prominent term of $\sqrt{1 - v^2/c^2}$. According to general relativity, time is influenced not only by velocity but also by gravitational fields. In general relativity, there are no preferred reference systems, what opens up the problem of defining useful and adequate systems for one's purposes. Following Einstein's equivalence principle, for the immediate vicinity of a point-like observer so-called locally inertial reference systems can be introduced, where physical laws have the same form as in inertial reference systems in special relativity (Kaplan, 2005). Nevertheless, as soon as two or more reference systems are in use, time events and measured quantities must be connected with a certain system and, if necessary, adequately transformed.

2.1.1 Relativity in Astronomical Reference Systems

Although the theory of relativity has been known since the beginning of the 20th century, the observational effects of special and general relativity are small and for a long time deviations from Newtonian physics were not taken into account for observations within our solar system (Kaplan, 2005). This changed with the advent of highly precise space geodetic techniques like VLBI and Lunar Laser Ranging (LLR) in the 1960s and 1970s. Mostly based on very accurate timing, the purely Newtonian formulation was not sufficient any more and one began to include so-called post-Newtonian corrections to account for relativity. Although such treatment as second-order corrections to Newtonian formulas fulfills nowadays demands concerning accuracy (Müller *et al.*, 2008), it is not satisfying regarding the theory and the aspired comprehensive approach. Following the GGOS aim for a consistent treatment of the observations of geometry, gravity field and rotation, a complete relativistic treatment is mandatory for measurements of all geodetic techniques (Plag & Pearlman, 2009).

In 2000, the International Astronomical Union (IAU) adopted a rigorous post-Newtonian approach for the definition of a system of space-time coordinates for the solar system and the Earth, within the framework of general relativity (Soffel *et al.*, 2003). The solar system Barycentric Celestial Reference System (BCRS) is appropriate for the solution of the equations of motion of

solar system bodies (e.g. the development of solar system ephemerides) as well as for modeling light propagation from distant celestial objects. More suitable for the description of processes closely around the Earth (e.g. the Earth's rotation, or the motion of Earth satellites) is to define the origin in the center of the Earth rather than in the barycenter, realized with the Geocentric Celestial Coordinate System (GCRS). In modern astronomical and space-geodetic observations the use of several relativistic reference systems is essential. Consequently, also the transformation between them is relevant. While in the IAU 2000 resolutions and the appropriate publication by Soffel *et al.* (2003) the full relativistic framework with its metric tensors is presented, in this thesis the focus is on a consistent application of the formalism with a basic understanding behind. For geodetic processing, the Conventions of the International Earth Rotation and Reference Systems Service (IERS; Petit & Luzum, 2010) provide the appropriate models and tools. They are based on the resolutions of international scientific unions (e.g. IAU) and are the basis for a consistent derivation of the IERS products. Unfortunately, following the goal of easy usage, relativity affairs are often well hidden in complex formulas which sometimes makes it difficult to clearly identify the various effects. When one wants to use the given mathematical framework for slightly different applications, as it is done in this work, a careful treatment concerning the underlying reference systems is essential. Besides the discourse below, the explanation to the IAU resolutions by Kaplan (2005) as well as the work of Klioner (2008) are recommended for a basic understanding of the necessity and its implications of relativity in astronomical processing.

Another aspect of the highly precise measurements and the big distances in space is, that for the first time relativity became actually measurable. In order to describe the accuracy of such measurements, one usually makes use of the parameterized post-Newtonian (PPN) formalism (e.g. Will, 1993). For this, the post-Newtonian approximations, which can be seen as simplified Einstein gravity, were expanded by several PPN-parameters. These parameters, e.g. γ , allow for a violation of Einstein's theory of gravity and also other than Einstein's gravitational theories can be employed. In general relativity $\gamma = 1$. Gravitational light deflection due to massive bodies (e.g. the Sun) has a considerable effect in geodetic VLBI, hence VLBI measurements can be used to determine the space curvature parameter γ (e.g. Fomalont *et al.*, 2010; Heinkelmann & Schuh, 2010). A recent reprocessing of astrometric and geodetic VLBI data since 1979 by Lambert & Poncin-Lafitte (2011) yielded $\gamma = 0.99992 \pm 0.00012$.

2.2 Time Scales

As mentioned in the previous section, time is not absolute but different for observers on various space-time trajectories. In order to measure time, one has to define appropriate time scales. Therefore, a specific phenomenon must be determined which defines a period under certain conditions. Furthermore, one has to agree on the rate of advance, connecting the period with a specific number of time units, as well as an initial epoch corresponding to the time reading at some definite event. A time scale is realized by any kind of clock, which always only provides

an approximation to these idealized specifications.

In geodetic astronomy two different kinds of time scales are in use (Kaplan, 2005). One group is in accordance with the *Système International* (SI; BIPM, 2006), namely based on the SI second (2.2.1), the other group of time scales relies on the variable rotation of the Earth. While with the advent of atomic clocks SI time scales can be realized much more accurate than the ones of the latter kind, the two ways have their justification and the worldwide system of civil time is actually a combination of both of them (see section 2.2.2). Another important aspect of time scales is the question if they are actually measurable or not. One speaks of proper time, when the clock is co-moving with its observer along the same trajectory and in the same gravity field. Proper time is always measurable, but only from the co-moving observer himself. Coordinate time, by contrast, is meant to be some independent argument and is a purely theoretical construct, hence can nowhere be represented by a clock reading.

2.2.1 Time Scales based on the SI-Second

The definition of the SI-second as the unit of time reads (BIPM, 2006):

The second is the duration of 9 192 631 770 periods of the radiation corresponding to the transition between the two hyperfine levels of the ground state of the caesium 133 atom.

In full agreement with general relativity, this definition gives every observer a recipe how the SI-second can be realized in situ. Independent from the location, the gravitational potential, and the state of motion, the SI-second is the same for all observers and represents the unit of proper time (Klioner, 2008). As the proper time of an observer is only defined on his trajectory, in order to compare different proper times of two different observers, one has to introduce so-called coordinate time scales. Coordinate time scales are then defined everywhere in the solar system and can be computed from the reading of a real clock using the theoretical relation following general relativity. Additionally to the trajectory of the observer, that theoretical relation involves the trajectories and mass parameters of the massive bodies of the solar system.

In accordance with the BCRS and GCRS (see section 2.3), certain coordinate time scales are part of the mathematical model of space-time, that is called a reference system (Klioner, 2008). These are the Barycentric Coordinate Time (TCB) and its scaled version, the Barycentric Dynamical Time (TDB), and the Geocentric Coordinate Time (TCG) with its scaled version named Terrestrial Time (TT) respectively. Being defined as coordinate time scales, these four time scales cannot be directly measured, but they can be computed from the readings of some real clock for any space-time event (Klioner, 2008). While TCB and TCG are mainly used as independent time argument for theoretical developments, rather than they appear in practical applications, their scaled counterparts TDB and TT were defined in a way that the difference between proper time of an Earth-bound observer and these two coordinate time scales evaluated along his trajectory is as small as possible and hence are widely used (Klioner, 2008). On the surface of the Earth

TT is defined to run at the same rate as a time scale based on the SI-second, meaning, that the proper time of an observer situated on the rotating geoid is quite close to TT computed along his trajectory. In terms of barycentric time scales, when the transformation between TT and TDB is evaluated at the geocenter, the mean rates of TT and TDB coincide. The difference does not exceed 0.002 seconds and it can be neglected for many applications (Klioner, 2008). The rates of TCG and TCB have been fixed to advance an SI time scale on the surface of the Earth for the defined constants (e.g. Petit & Luzum, 2010, Ch. 1) of L_G and L_B .

$$\frac{dT_T}{dT_{CG}} = 1 - L_G \quad \text{with} \quad L_G = 6.969290134 \cdot 10^{-10} \quad (2.1)$$

$$\frac{dT_{DB}}{dT_{CB}} = 1 - L_B \quad \text{with} \quad L_B = 1.550519768 \cdot 10^{-8} \quad (2.2)$$

In mixed models, where a scaled version of BCRS and a scaled version of GCRS appear, sometimes the constant L_C is used, defined as (Petit & Luzum, 2010, Ch. 1):

$$L_C = 1 - \frac{dT_{CG}}{dT_{CB}} = 1.48082686741 \cdot 10^{-8}. \quad (2.3)$$

The most precise physically realized time scale is the International Atomic Time (TAI). TAI is a coordinate time scale defined in a geocentric reference frame with the SI-second as realized on the rotating geoid as the scale unit (BIPM, 2006, Appendix 2). TT then can be seen as an idealized form of TAI with a constant offset.

$$TT = TAI + 32.184 \text{ sec} \quad (2.4)$$

2.2.2 Coordinated Universal Time UTC

Since most astronomic observations are carried out from the Earth, it is crucial to know at which direction in space the observer's telescope points. Therefore, the independent atomic time scales must be connected with the current Earth Rotation Angle (ERA). ERA is defined as the geocentric angle in the equatorial plane between the Celestial Intermediate Origin (CIO) and the Terrestrial Intermediate Origin (TIO), measuring the rotational motion of the Earth. Universal Time (UT), or rather UT1, is then defined to be linearly proportional to the ERA (Petit & Luzum, 2010, Ch. 5).

$$ERA(T_u) = 2\pi (0.7790572732640 + 1.00273781191135448 \cdot T_u) \quad (2.5)$$

where

$$T_u = \text{Julian UT1 date} - 2451545.0. \quad (2.6)$$

Julian date is a widely used steadily running calendar, whose calculation is easy to implement (e.g. Karttunen *et al.*, 2007) and is available via plenty of Web-services. Since the Earth's rate of rotation is unpredictable and routinely has to be measured e.g. by space-geodetic techniques, the UT1 second is not precisely constant when expressed in a uniform timescale such as TT.

The worldwide system of civil time is based on the Coordinated Universal Time (UTC). The different time zones around the globe follow UTC, differing from it usually by an integral number of hours. UTC is a hybrid time scale, with the SI-second on the geoid as its unit, but kept in accordance with UT1 by introducing so-called leap seconds. Whenever the difference between UTC and UT1 exceeds 0.9 seconds, a leap second can be added to UTC on agreed dates maximal twice a year. This process is coordinated by the IERS and is announced in the Bulletin C¹. The deviation of the actual Earth rotation is quantified with the parameter $dUT1$.

$$dUT1 = UT1 - UTC \quad (2.7)$$

Due to the fact that the Earth's rotation is slowing down due to tidal friction, and that the SI-second was effectively made equivalent to an astronomical second based on a mean solar day of 86400 sec around the year 1820 (Nelson *et al.*, 2001), UT1 is constantly drifting away from TAI. With the last leap second introduced in 2012, since July 1st 2012 the difference amounts to 35 seconds.

$$TAI - UTC = 35 \text{ sec} \quad (2.8)$$

2.3 Conventional Celestial Reference System and Frame

With January 1st 1998, the International Celestial Reference System (ICRS) replaced the FK5 star catalogue as the fundamental celestial reference system for astronomical applications (IAU Resolution B2, 1997). The ICRS is an idealized BCRS, with its axes kinematically non-rotating with respect to distant objects in the universe. These axes are defined through the directions to extragalactic radio sources, respectively quasars (sec. 2.3.2), as determined in the most precise realization of the ICRS, namely the International Celestial Reference Frame (ICRF). It is stipulated that the principal plane of the ICRS is close to the mean equator and that the origin of right ascension is close to the dynamical equinox, both at epoch J2000.0. The second realization of the ICRS at radio wavelengths, ICRF2 (Fey *et al.*, 2009), was constructed in 2009 using nearly 30 years of VLBI observations. It contains the positions of 3414 compact radio sources, including a selected set of 295 defining sources. The axis stability lies at approximately $10 \mu\text{as}$, making ICRF2 nearly twice as stable as its predecessor, ICRF1 (Ma *et al.*, 1998). Further, with a noise level of about $40 \mu\text{as}$ and a more uniform sky distribution, the two largest weaknesses of ICRF1

¹available at: <http://www.iers.org/IERS/EN/Publications/Bulletins/bulletins.html>

could be minimized. The source positions are given in right ascension α and declination δ in a celestial system, which can be easily transformed to a vector \vec{r} , representing the direction on the sky.

$$\vec{r} = \begin{pmatrix} \cos\delta \cos\alpha \\ \cos\delta \sin\alpha \\ \sin\delta \end{pmatrix} \quad (2.9)$$

Coordinates directly obtained from the ICRF are barycentric ones (BCRS), and are independent of the Earth's motion, respectively independent of the equator, equinox, ecliptic, and any epoch. As in VLBI station positions, respectively baselines, are determined in the GCRS, in the following, the transition from the geocentric to the barycentric system is discussed. In a purely Newtonian thinking, the relation between the position $x(t)$ in BCRS and GCRS is trivial:

$$t_{\text{GCRS}} = t_{\text{BCRS}} = t \quad \text{and} \quad x_{\text{GCRS}} = x_{\text{BCRS}} - x_E(t), \quad (2.10)$$

where $x_E(t)$ denotes the barycentric position of the geocenter. In relativity theory, BCRS and GCRS are related by a 4-dimensional space-time transformation, that can be understood as a generalized Lorentz transformation of special relativity. When dealing with directions only (e.g. to the quasars in VLBI), for most applications in geodetic practice it is sufficient to apply simple correction terms for annual aberration and parallax. The former accounts for the relative velocity of the observer to the barycenter, the latter corrects for the position of the Earth on its yearly revolution around the Sun. If station positions are needed in BCRS however, this might not be sufficient any more. As usual in relativity theory, the effort of full theoretical consistency has to be balanced with the needed accuracy. In Chapter 11 of the IERS Conventions, Petit & Luzum (2010) give a simplified version for the transformation of a geocentric position vector \vec{x} to the barycentric one \vec{X} with an uncertainty below 1 mm:

$$\vec{X} = \vec{X}_E + \vec{x} \cdot \left(1 - \frac{W_E}{c^2}\right) - \frac{\vec{V}_E \cdot \vec{x}}{2c^2} \vec{V}_E. \quad (2.11)$$

W_E is the gravitational potential at the geocenter (equation (3.10)) and \vec{V}_E is the barycentric velocity of the Earth. In equation (2.11) approximations of integrals to constants over a certain time period were made and contributions from accelerations due to the Earth's spin and orbital motion were eliminated, as described e.g. in the appendix of Sekido & Fukushima (2006). Additional caution is called for when scaled systems are used, like coordinates in TT or TDB-frames. Besides the time component (as described in section 2.2), also the coordinates must be scaled with the corresponding factor. Hence, e.g.

$$[\vec{X}]_{TCG} = (1 - L_G)^{-1} [\vec{x}]_{TT}. \quad (2.12)$$

Once in the GCRS, the ICRF is tied to the TRS (see 2.4) by the Earth Orientation Parameters (EOP) that are permanently observed by the IERS. This tie is available with daily resolution and an accuracy of ± 0.1 mas (Petit & Luzum, 2010).

While with ICRF the realization at radio wavelengths is certainly the most precise, but only available with VLBI, the optical realizations are sometimes more open to the users. The Hipparcos Catalogue (ESA, 2007) provides ICRS coordinates and velocities of optically bright stars with a median astrometric precision of about 1 mas in position. With the upcoming ESA mission Gaia (Lindegren *et al.*, 2008), to be started in 2013, a new era of optical reference systems will begin. With a target accuracy of some tens of μas for the brightest stars on the sky, once the Gaia catalog is available, the optical and radio celestial reference frame will be of similar accuracies. For establishing an accurate tie between the two frames, sources will have to be identified, that have enough brightness both in radio and optical wavelength to be observed by both techniques (Bourda *et al.*, 2010, 2011).

2.3.1 Ephemerides

An ephemeris (pl. ephemerides) depicts a list of positions of one or more solar system bodies as a function of time. Aligned with the ICRF, ephemerides represent the dynamical realization of that very one. Commonly used, also in the course of this work, is the planetary and lunar ephemeris DE 421 (DE 421; Folkner *et al.*, 2008) from the Jet Propulsion Laboratory (JPL). It includes the positions and velocities of the Sun, the Earth and its Moon, the seven planets and Pluto, with respect to the solar system barycenter. The ephemeris is derived using the Einstein-Infeld-Hoffmann equations of motion of massive bodies, with the dynamical time argument being consistent with TDB. It is distributed by JPL as plain-text (ASCII) files of Chebychev series coefficients and may be downloaded from <ftp://ssd.jpl.nasa.gov/pub/eph/planets/ascii/de421>. It shall be noted here, that DE 421 gives numerical values of TDB-compatible coordinates in SI-units, hence, if TCB-compatible values are desired, they have to be rescaled accordingly. As described in detail in Klioner (2008), this is true for planetary mass parameters μ and positions \vec{x} , whereas the TCB-compatible velocity \vec{v} coincides with the TDB-compatible one.

$$[\vec{x}, \mu]_{TCB} = (1 - L_B)^{-1} [\vec{x}, \mu]_{TDB} \quad (2.13)$$

$$[\vec{v}]_{TDB} = \frac{d\vec{x}_{TDB}}{dt_{TDB}} = \frac{d\vec{x}_{TCB}}{dt_{TCB}} = [\vec{v}]_{TCB} \quad (2.14)$$

Accurate ephemerides need to be updated frequently and steadily improve their accuracy through the use of more observational data and improved dynamical modeling. With the inclusion of additional measurements to recent interplanetary space probes, DE 421 provides the lunar orbit to sub-meter accuracy, the orbits of Venus, Earth, and Mars to sub-kilometer accuracies, and the

orbit of Mercury to several kilometers (Folkner *et al.*, 2008). The orbits of the outer planets and Pluto are not as well determined. The axes of the ephemeris are oriented with respect to the ICRF and VLBI observations of spacecrafts orbiting Venus, Mars, Jupiter, and Saturn serve to tie the ephemeris to the ICRF with an accuracy of 0.25 mas (Petit & Luzum, 2010, chapter 3).

2.3.2 Quasars

Quasi-stellar radio sources, designated as quasars, are among the most luminous sources in the Universe (Schneider, 2010). They belong to the family of active galactic nuclei (AGN), that are supermassive black holes located in foreign galaxies and producing radiation by matter falling towards this black hole. Quasars emit at all wavelengths, from the radio to the X-ray domain, with the quality that this radiation originates from a very small spatial region (Schneider, 2010). For the establishment of a fundamental catalogue of radio sources only the most compact and powerful quasars are chosen, usually having a signal strength of a few tenths of Jansky¹. Relying on objects that are billion of light years away, the ICRF (2.3) is based on the hypothesis that the measured extragalactic radio sources are at rest. However, the ideal definition of a point source with no apparent variation in position cannot be fulfilled in reality. Typically quasars have structure that varies with both time and frequency, an effect that might be necessary to be accounted for in the next generation's geodetic VLBI system (e.g. Petrachenko *et al.*, 2009).

2.4 International Terrestrial Reference System and Frame

For the description of points attached to the surface of the Earth, e.g. the precise positions of geodetic instruments, terrestrial reference systems (TRS) are used. A TRS is co-rotating with the Earth, hence station coordinates undergo only small variations with time rather than the daily revolution. With the International Terrestrial Reference System (ITRS), the IERS provides a geocentric terrestrial reference system that was formally adopted by the International Union of Geodesy and Geophysics (IUGG). The origin is defined as the center of mass for the whole Earth, including oceans and atmosphere, and the unit of length shall be the SI-meter, consistent with TCG. The orientation is equatorial, with the z-axis in the direction of the pole and the x-axis towards the Greenwich meridian. It was adopted from a previous system, with epoch 1984, and maintained ever since by using a no-net-rotation condition. The realizations of ITRS are named International Terrestrial Reference Frames (ITRF), with the latest version ITRF2008 (Altamimi *et al.*, 2011). The provision of ITRF happens via tables of station coordinates, modeled linearly, which means there are coordinates \vec{X}_0 calculated for a certain reference epoch t_0 and the corresponding velocity $\dot{\vec{X}}$ for each station. These coordinates are calculated for regularized positions, in order to remove high frequency variations. The variations $\Delta\vec{X}_i$, predominantly of

¹The frequency-dependent strength of the emitted radio signal received from a source is known as spectral flux density and is measured in watts per square meter per hertz. The unit is the jansky (Jy), with $1 \text{ Jy} = 10^{-26} \text{ W m}^{-2} \text{ Hz}^{-1}$ (Walter & Sovers, 2000).

geophysical origin, are accounted for with conventional models, as described in chapter 7 of the IERS Conventions (Petit & Luzum, 2010). The instantaneous station position \vec{X} at epoch t composes to:

$$\vec{X}(t) = \vec{X}_0 + \dot{\vec{X}} \cdot (t - t_0) + \sum_i \Delta \vec{X}_i. \quad (2.15)$$

ITRF2008 is the result of a combination of single-technique solutions, respectively normal equation matrices, by the four space geodetic techniques, VLBI, Satellite Laser Ranging (SLR), Global Navigation Satellite Systems (GNSS), and Doppler Orbitography and Radiopositioning Integrated by Satellite (DORIS). Besides the gain of redundancy, in the combination the potential of each technique is optimally utilized. Consequently, the ITRF2008 origin solely relies on the SLR time series, its scale is de facto a mean scale of VLBI and SLR, and GNSS with by far the most measurement sites serves for densification and hence strongly controls the orientation, respectively rotation. The accuracy of the ITRF2008 origin is thought to be better than 1 cm and the current scale accuracy is at the level of 1.2 ppb¹, or respectively 8 mm at the equator (Altamimi *et al.*, 2011). Although the contributing single-technique solutions might have a higher internal accuracy, comparing the ITRF2008 coordinates with the technique solutions' time series reveal discrepancies of a few millimeters.

Finally it shall be noted that the actual scale of the ITRF is consistent with TT rather than with TCG, as actually demanded in the definition of the ITRS. This is due to practical reasons, as all contributing analysis centers deliver their solutions compatible with TT and one decided to refrain from a hence inevitable re-scaling to TCG compatible values according to equation (2.12).

2.4.1 Inter-technique ties

Besides the quality of the single-technique solutions, the ITRF2008 depends on local ties at co-location sites, where more than one technique was measuring. The geometrical relationship between antennas of the different techniques are locally measured by classical surveying, delivering the tie between the single-technique frames. According to Ray & Altamimi (2005), such tie vectors measured with accuracies of 1 mm or better at several sites, enable a global alignment of the VLBI and GPS frame to less than 1 mm in each Helmert component. Unfortunately, the already poor number of tie vectors for ITRF2008 do not give this quality and discrepancies between the local ties and the tie vectors determined through space geodesy estimates of several millimeters up to centimeters exist (Seitz *et al.*, 2012). Reasons for this misfit are outdated measurements, problems when measuring the tie vector, e.g. due to the difficult accessibility of the real antenna reference point or an actual movement of that very one (e.g. Sarti *et al.*, 2011), a lack of full variance covariance information of the tie vectors for proper weighting or unidentified systematic inter-technique errors in the ITRF solution. In any case, a good treatment of the

¹1 part per billion means 10⁻⁹; on a global scale with $R = 6371$ km, 1 ppb \approx 6 mm.

available local ties is a major challenge in the derivation of an ITRF realization and according to Altamimi *et al.* (2011), future ITRF improvement resides in improving the consistency between local ties at co-location sites and space geodesy estimates.

The potential of using co-locations of several techniques on satellites for the improvement of inter-technique ties is twofold. On the one hand, multi-technique satellite measurements could be used as an independent validation of a TRF realization (e.g. proposed by Seitz *et al.*, 2012), and on the other hand the inclusion of so-called space ties in the derivation of the TRF might be a promising alternative to the connection with station ties. The latter concept is followed by Thaller *et al.* (2011), who successfully combine GNSS and SLR observations using satellite co-locations. In figure 2.1 the concept of a satellite realizing a space-tie and dedicated to the improvement of TRF frame ties is illustrated. Assuming a precise relative positioning of the different technique-specific sensors on the satellite platform, such configuration combines the frames of the various techniques. This can happen either on the satellite itself, comparing the actual satellite position

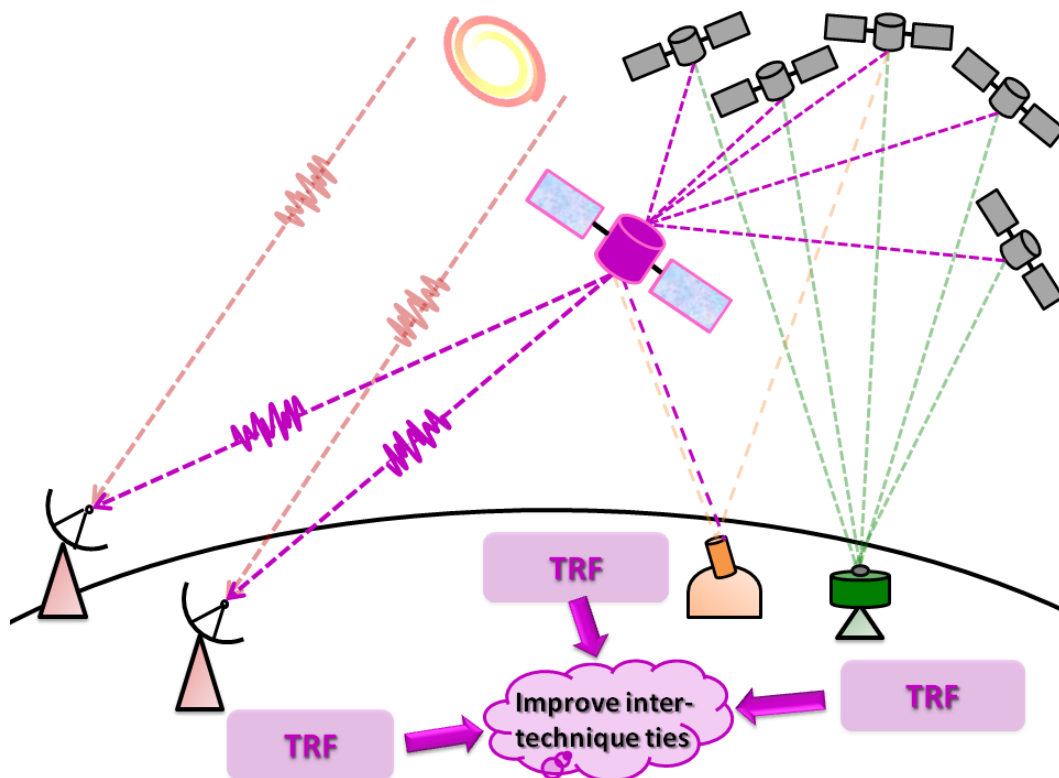


Figure 2.1: The principle of a satellite tracked by different techniques, realizing a so-called space tie.

as determined through the various techniques, or, by the precise determination of the positions of the tracking antennas on Earth in the satellite's system. As an example for the first concept, the proposed GRASP mission is described in chapter 5.2, while the latter concept is the one applied for the simulation studies in chapter 6.

Besides the combination of the various space geodetic techniques via the above mentioned ties in terms of rigorously determined positions of system components on Earth or in space, also

common by-products of the geodetic analysis can be used in this aspect. One example for this are the Earth rotation parameters, that are well determined through several techniques, e.g. VLBI and GPS. Including the polar motion parameters in a combination of the two techniques, through this co-location of the daily pole of rotation the determination of the rotation about the x- and the y-axis, as determined in a subsequent Helmert-transformation between the GPS and the VLBI frame, is considerably stabilized (Ray & Altamimi, 2005). On the other hand, a difference in the determined Earth rotation in two different frames might indicate a relative rotation between the two reference frames. Besides Earth rotation, when using microwave techniques, as e.g. VLBI and GNSS, the troposphere is one of the main error sources and has to be determined during analysis. Additionally, in the estimation process the tropospheric parameters are highly correlated with the station coordinates, especially the stations heights (also see chapter 3.1.3). At co-location sites, assuming an identical troposphere above antennas of both techniques, the determined tropospheric parameters can be used to validate local ties and might even be included in the combination process itself (Krügel *et al.*, 2007).

2.4.2 Transformation between TRS and CRS

Chapter 5 of the IERS Conventions (Petit & Luzum, 2010) gives a detailed recipe how the transformation from the ITRS to the GCRS shall be performed. Having the same origin, namely the geocenter, this transformation is a rotation composed of three rotation matrices arising from polar motion x_p, y_p , the rotation around the Earth Rotation Angle ERA and the motion of the celestial pole in the celestial reference system, described by the coordinates X and Y :

$$\vec{x}_{\text{GCRS}} = Q_{X,Y} \cdot R_{\text{ERA}} \cdot W_{x_p,y_p} \cdot \vec{x}_{\text{ITRS}} = T_2C \cdot \vec{x}_{\text{ITRS}}. \quad (2.16)$$

In the following, this matrix is called the Terrestrial-to-Celestial matrix T_2C , which can be calculated for every time epoch applying the actual EOP. Once in the GCRS, for the following transformation to the BCRS equations (2.10) or (2.11) can be used.

Chapter 3

Very Long Baseline Interferometry

Very long baseline interferometry (VLBI) has its origin in local, two-element interferometry, used by astronomers to study the location and structure of far distant objects in space. The advance of atomic clocks in the 1970s enabled the full separation of two antennas by delivering a stable frequency standard at each station. Now interferometric data is recorded independently at both sites, and, via clock synchronization, can be correlated centrally afterwards. Soon after the first observations in 1967, VLBI attracted the geodesists' interest. The fact, that besides the direction to the radio source, the observation equation also implies the orientation and length of the (global) baseline, opened up new dimensions in terms of precise relative positioning on Earth at that time. With the success of GPS/GNSS a few decades later VLBI shares its pioneering tasks in measuring plate tectonics, but nowadays is still irreplaceable and unique in its ability to measure the Earth's orientation in an inertial frame (Sovers *et al.*, 1998). Today VLBI plays a key role in radio astronomy and geodesy, but has also found its way into space research. In the following, the basic principle of (geodetic) VLBI is illustrated (3.1), after which the theoretical delay modeling is presented in detail (3.1.2). As a basic understanding of the influence of the troposphere on VLBI measurements is important for the upcoming chapters of this work, this is treated in section 3.1.3. Introducing the next generation's VLBI system, in section 3.1.5 some prospects of geodetic VLBI are given. The second part of this chapter is devoted to VLBI measurements to alternative sources than quasars, with an overview of VLBI spacecraft tracking systems (3.2.2) and the necessary formalism to model the measured time delay for moving sources at finite distances (3.2.3). For a profound description of VLBI the reader may be referred to alternative literature, e.g. Sovers *et al.* (1998), Schuh & Böhm (2013), Takahashi *et al.* (2000), or Schuh & Behrend (2012).

3.1 Geodetic VLBI

Geodetic VLBI is coordinated by the International VLBI Service for Geodesy and Astrometry (IVS; Schuh & Behrend, 2012). About 50 antennas, mostly operated by national research organizations, contribute with their facilities to the international IVS observing program. At the moment this covers at least two global 24-hour sessions per week and one so-called intensive-

session of 1 hour duration per day. While the first configuration observes Earth orientation and global station motions, the latter are used to monitor the Earth's spin velocity, respectively dUT1, with daily resolution. Additionally, the IVS schedules dedicated sessions for the determination and maintenance of the ICRF, as well as from time to time special research and development sessions. In the last years, under the header *VLBI2010*, efforts have been made to go towards a full 24/7 coverage, meaning continuous monitoring of Earth orientation parameters with VLBI. Combined with the technological development, VLBI2010 will also entail an increase in precision of VLBI-products (Petrachenko *et al.*, 2009). More information on the IVS activities, as well as all observational data since the year 1979 and derived VLBI products are freely available at <http://ivscc.gsfc.nasa.gov>.

3.1.1 Basics

VLBI observations are performed with a net of at least two radio telescopes receiving signals from numerous extragalactic radio sources distributed across the sky. Each pair of antennas, that observes the same source at the same time, forms a baseline. Radiation from sources beyond our galaxy, such as the commonly observed quasars or galaxies, arrives at the Earth as plane wave fronts, leading to a simple geometric principle that is illustrated in figure 3.1. When the baseline \vec{b} is defined as the vector from station 1 to station 2 and \vec{k}_0 is the direction to the radio source, the distance $c \cdot \tau$ is the projection of the baseline onto the source vector, represented via the scalar product. By dividing with the light velocity c , the basic equation of VLBI reads:

$$\tau = -\frac{\vec{k}_0 \cdot \vec{b}}{c}. \quad (3.1)$$

The observable of a VLBI experiment is the time delay τ , expressing the difference in arrival times of the signal at stations 1 and 2. After signal reception, the observable is time-tagged, amplified, and down-converted, using the time and frequency of a highly stable atomic clock. The signal is split into two frequency bands, usually S-band and X-band for geodetic VLBI, which cover wavelengths at 13 respectively 3.6 cm. Taking the advantage of bandwidth synthesis, six respectively eight channels are recorded for each frequency band, what enables to cover a high bandwidth while keeping the limits of finite recording bandwidths. The actual measurement of

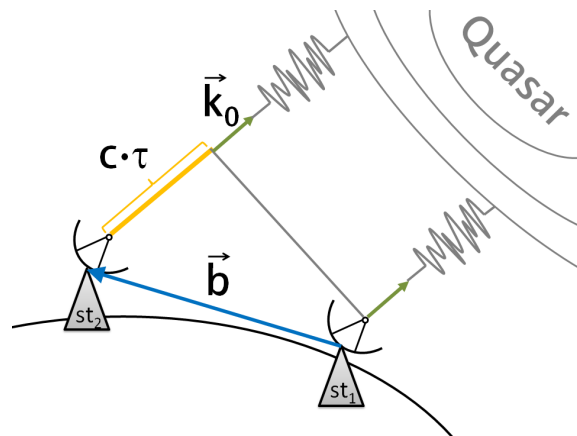


Figure 3.1: Basic geometrical principle of VLBI. The measured time delay τ is modeled as the projection of the baseline \vec{b} onto the direction to the radio source \vec{k}_0 .

the group delay happens in post processing via cross-correlation. Hereby the signals of the participating antennas are compared and shifted in time against each other, until the cross-correlation function reaches its maximum at the time shift τ . The achieved accuracy of the correlation σ_τ is reciprocally proportional to the bandwidth B and the signal-to-noise ratio SNR (eq. 3.2), which in turn depends on the strength of the observed radio source, the size of the antenna, and the duration of the observation, i.e. the scan length.

$$\sigma_\tau = \frac{1}{2\pi} \cdot \frac{1}{SNR \cdot B}. \quad (3.2)$$

Today's systems measure the delay with a precision of 10 – 30 ps (Schuh & Behrend, 2012).

3.1.2 Delay model

The VLBI delay is defined as the difference in arrival time of the measured signal at two separated stations. It is the quantity of interest in a geodetic VLBI experiment and is determined in the correlator for each baseline separately. For Earth-based VLBI observations the delay is at most the light time of one Earth radius, about 20 milliseconds. In order to delimit a searching window for the correlator on the one hand and to deliver most precise a priori values for the analysis on the other, this delay has to be modeled in advance. While the result of the measurement is depicted as observed delay τ_o , the theoretically computed delay is named τ_c in the following. By far the biggest contribution comes from the geometric delay, describing the location and movement of the source and antennas during the measurement. Its calculation is a complex procedure of various coordinate transformations that are necessary to connect the celestial system in which the location of the sources is determined with the terrestrial system of the station positions and of the measurement itself. Chapter 11 of the IERS Conventions (Petit & Luzum, 2010) gives a recipe how to calculate the delay. The model given therein, called the Consensus model, is the result of a dedicated workshop on the relativistic models for use in space geodesy (Eubanks, 1991) where several models available at that time were compared and combined, with the goal to present a model that can be used also by non-specialists in relativity theory. The only imposed restriction was that the new model shall include all relativistic effects necessary to make the actual VLBI results look as simple as possible. In other words, it is desired that the model does not leave or introduce any relativistic changes in estimated parameters larger than the model cutoff. Though easy to implement, drawback of the Consensus model is the fact that all operations are combined in one formula (3.9) which makes it hard for the interested analyst to understand the theory behind. As for this work, especially for chapters 3.2.3 and 5.4.3, understanding the theory is of importance, the model will be inspected more closely in the following.

According to Sovers *et al.* (1998), the construction of the VLBI delay model can be summarized in seven steps (figure 3.2):

1. Determine the location of the two antennas in the Earth-fixed reference frame. Time epoch shall be the time t_1 of reception at antenna 1, measured in the Earth-fixed frame.

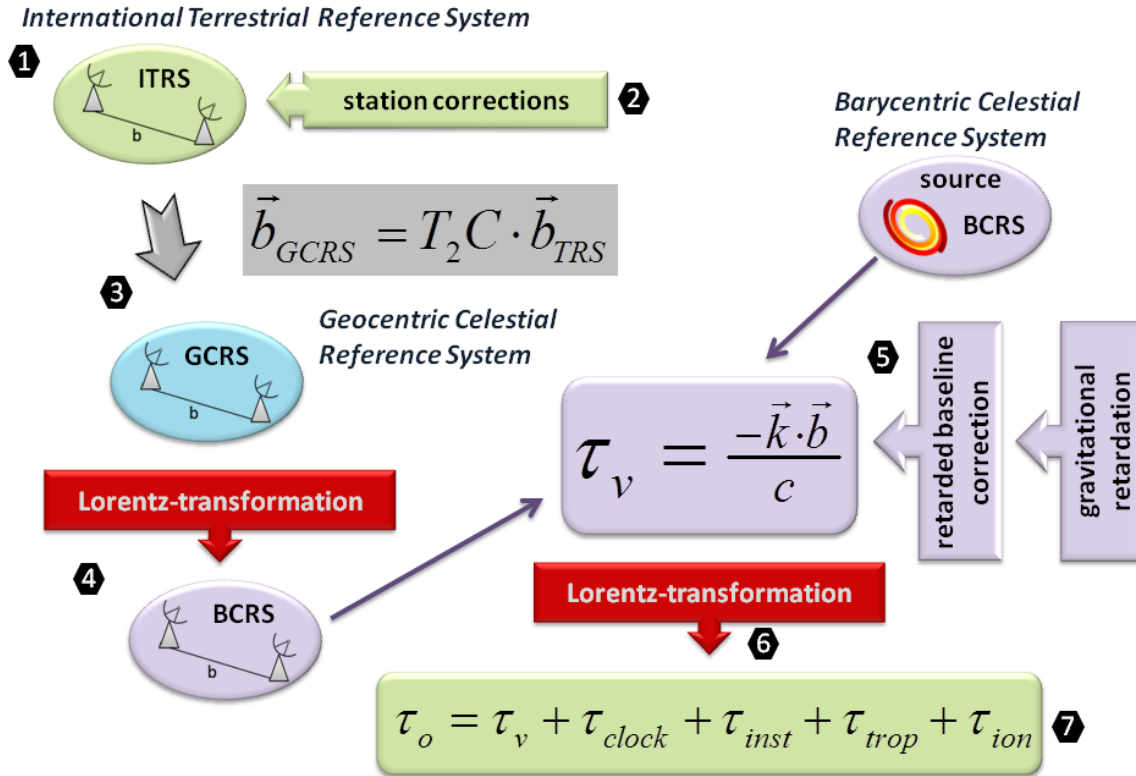


Figure 3.2: The derivation of the VLBI delay model in 7 steps.

2. Correct these station positions for Earth-fixed effects, such as solid Earth tides, plate tectonics, loading effects, and further local station and antenna displacements. Steps 1 and 2 are usually united by applying equation (2.15), delivering the TRF station positions.
3. Transform the ITRF positions into the GCRS-frame, the Earth-fixed, Earth-centered non-rotating celestial frame. This is done by a series of rotations using the Earth Orientation Parameters, as described in equation (2.16). This gives the GCRS positions $x_1(t_1)$ and $x_2(t_1)$ and the baseline

$$\vec{b} = \vec{x}_2(t_1) - \vec{x}_1(t_1). \quad (3.3)$$

4. Perform a Lorentz transformation following equation (2.11), from the moving GCRS (lowercase letters) to the frame at rest relative to the solar system barycenter, the BCRS (uppercase letters).
5. The BCRS is the most suitable system to compute the proper time delay as well as the most important corrections due to gravitative retardation caused by celestial bodies close to the signal path. Here, the basic equation (3.1) is valid, imposing the restriction that the BCRS

baseline \vec{B} is calculated between station 1 at reception time T_1 and station 2 at its reception time T_2 . Following the standard that all quantities are calculated at reception time T_1 , the movement of station 2 during the difference $T_2 - T_1$ has to be respected. This effect is commonly known as retarded baseline correction. Approximating linear station motion, formula (3.1) becomes to:

$$\tau_{BCRS} = T_2 - T_1 = -\frac{\vec{K} \cdot \vec{B}_{T_1}}{c} - \frac{\vec{K} \cdot \vec{V}_2 \cdot (T_2 - T_1)}{c} \quad (3.4)$$

and, after isolating τ on the left side, one gets

$$\tau_{BCRS} = \frac{-\frac{\vec{K} \cdot \vec{B}_{T_1}}{c}}{1 + \frac{\vec{K} \cdot \vec{V}_2}{c}} \quad (3.5)$$

It shall be noted here, that equation (3.5) approximates the arrival of the signal at Earth as plane wavefront. Aiming at the 1 ps accuracy level, the wave-front curvature is diminishing for sources further away than $R = 3 \cdot 10^{14}$ km or approximately 30 light years (Sovers *et al.*, 1998), what holds easily true for the usual quasar targets in VLBI (see chapt. 2.3.2). When observing sources close-by, like spacecrafts or satellites, adaptation of the delay model is required, as described in section 3.2.3. When the signal is traveling trough the space, according to general relativity it is affected by the gravity of massive bodies along its path. This results in a retardation and a bending of the signal. In principle, the ray path follows a so-called null geodesic, where the gravitational influence of the Sun and the planets are modeled carefully. Because VLBI observations are affected differentially, meaning that only the residual effect of two light rays arriving at station 1 and station 2 is measured, the calculation of ΔT_{grav} simplifies tremendously. In the Consensus model it is approximated as a sum over the contributions of the various massive bodies J in the solar system.

$$\Delta T_{grav} = \sum_J \Delta T_{grav,J} \quad (3.6)$$

For the J^{th} body, the general relativistic delay $\Delta T_{grav,J}$ is given by

$$\Delta T_{grav,J} = (1 + \gamma) \frac{GM_J}{c^3} \ln \frac{R_{1,J} + \vec{K} \cdot \vec{R}_{1,J}}{R_{2,J} + \vec{K} \cdot \vec{R}_{2,J}} \quad (3.7)$$

with the space curvature parameter γ , which was already introduced in chapter 2.1.1, the gravitational constant G , the mass of the J^{th} gravitating body M_J , and $\vec{R}_{i,J}$ being the vector from the J^{th} gravitating body to the i^{th} receiver, with length $R_{i,J}$.

$$\vec{R}_{i,J} = \vec{X}_i - \vec{X}_J \quad (3.8)$$

6. Perform a Lorentz transformation back from BCRS to GCRS system and, if necessary, scale the calculated time delay in order to fit the scale of your measurement. In the Consensus model steps 4 to 6 are combined in one equation.

$$\tau_v = \frac{\Delta T_{grav} - \frac{\vec{K} \cdot \vec{b}}{c} \left[1 - \frac{(1+\gamma)W_E}{c^2} - \frac{|\vec{V}_E|^2}{2c^2} - \frac{\vec{V}_E \cdot \vec{v}_2}{c^2} \right] - \frac{\vec{V}_E \cdot \vec{b}}{c^2} (1 + \vec{K} \cdot \vec{V}_E / 2c)}{1 + \frac{\vec{K} \cdot (\vec{V}_E + \vec{v}_2)}{c}} \quad (3.9)$$

It is assumed that the source vector \vec{K} is given in the barycentric system and the baseline \vec{b} in the geocentric one and equation (3.9) is designed in order to spare the users troubles with explicit (relativistic) coordinate transformations. Nevertheless, for skilled users the contributions from the various effects can be clearly identified. Hence, the denominator comes from the retarded baseline described in equations (3.4) and (3.5). Term 2 and 3 in the square brackets connect the geocentric and the barycentric time scales, as shown in equation (2.11). The gravitational potential at the geocenter W_E is calculated neglecting the effects of the Earth's mass.

$$W_E = \sum_{J \neq E} \frac{GM_J}{|\vec{R}_{E,J}|} \quad (3.10)$$

At the picosecond level, only the solar potential needs to be included in W_E (Petit & Luzum, 2010, chapter 11). The terms with the barycentric velocity of the Earth V_E describe effects of the annual aberration and the ones with the geocentric station velocity v_2 account for the Earth's spin or daily aberration. The velocity of station 2 relative to the geocentric origin can be calculated with sufficient accuracy (Sovers *et al.*, 1998) with the mean rotation rate of the Earth $\omega_E = 7.292115 \cdot 10^{-5}$ rad/sec:

$$\vec{v}_{2,TRS} = \vec{\omega} \times \vec{x}_{2,TRS} = \begin{pmatrix} 0 \\ 0 \\ \omega \end{pmatrix} \times \begin{pmatrix} x_2 \\ y_2 \\ z_2 \end{pmatrix} = \begin{pmatrix} -\omega \cdot y_2 \\ \omega \cdot x_2 \\ 0 \end{pmatrix} \quad (3.11)$$

and transferred to GCRS by multiplication with the combined rotation matrix T_2C from equation (2.16)

$$\vec{v}_{2,GCRS} = T_2C \cdot \vec{v}_{2,TRS}. \quad (3.12)$$

The barycentric velocity V_2 follows as

$$\vec{V}_2 = \vec{V}_E + \vec{v}_2. \quad (3.13)$$

For the calculation of ΔT_{grav} following equations (3.6) and (3.7), the Consensus model again chooses a simplified way. At sufficient accuracy, the barycentric coordinates are set

up in the Newtonian way:

$$\vec{X}_i = \vec{X}_E + \vec{x}_i. \quad (3.14)$$

The position of the celestial body is usually taken from one's preferred ephemeris, as described in section 2.3.1. However, due to the motion of the gravitating body, in contrast to the other variables the epoch for this coordinates is not t_1 , but the time of closest approach of the light-ray to the disturbing body t_J . Using the position and velocity of the object at signal reception time, the position of closest approach can be determined iteratively (e.g. Sovers *et al.*, 1998):

$$\vec{X}_{J,n}(t_J) = \vec{X}_J(t_1) - \Delta t \cdot \vec{V}_J(t_1) \quad (3.15)$$

with the time interval determined as the Newtonian light time from the gravitating body to the station

$$\Delta t = t_1 - t_J = t_1 - \frac{|\vec{X}_{J,n-1} - \vec{X}_1|}{c}. \quad (3.16)$$

Alternatively to equation (3.16) the Conventions suggest a formulation where also the geometry between the source and the gravitative body is taken into account.

$$t_J = \min \left[t_1, t_1 - \frac{\vec{K} \cdot (\vec{X}_{J,n-1} - \vec{X}_1)}{c} \right] \quad (3.17)$$

Due to the slow motion of the Sun with respect to the barycenter, this effect is negligible for the Sun, but might get several hundred picoseconds for Jupiter (e.g. Schuh, 1987). With either formulation, equation (3.16) or (3.17), 1-picosecond accuracy can be reached with a single iteration for solar system objects. Finally, for the calculation of $\vec{R}_{2,J}$, the motion during propagation time between station 1 and 2 has to be taken into account.

$$\vec{R}_{2,J} = \vec{X}_2(t_1) - \frac{\vec{V}_E}{c} (\vec{K} \cdot \vec{b}) - \vec{X}_J(t_J) \quad (3.18)$$

The general relativistic effect is strongly dependent on how close the ray passes the gravitating body. Investigating seven years of routine IVS-VLBI experiments, Soja *et al.* (2012) concluded that the effects of the Sun, the Earth, Jupiter, Saturn, the Earth's moon, and Venus reach the level of significance and hence should be included in ΔT_{grav} . For the effect of the Earth, equation (3.7) simplifies to

$$\Delta T_{grav,E} = (1 + \gamma) \frac{GM_E}{c^3} \ln \frac{x_1 + \vec{K} \cdot \vec{x}_1}{x_2 + \vec{K} \cdot \vec{x}_2}. \quad (3.19)$$

The delay as given above was derived for a target accuracy of 1 picosecond. Therefore,

all effects of the order of 0.1 ps are included, while the rest is neglected. The model is simplified as much as possible, meaning that it accepts theoretical errors in terms of theory of relativity wherever the effect is negligible. This is a point of criticism for some specialists (e.g. Kopeikin & Schäfer, 1999), but the very same authors conclude, that despite theoretical deficiencies, the derived delays fulfill the demands on accuracy. Especially in terms of ΔT_{grav} only the most important effect is taken into account. For a clear view on additional effects the reader is referred to the work of Klioner (1991).

7. To this geocentric vacuum delay τ_v several further corrections have to be added in order to get agreement with the measurement τ_o . In Cannon (1999) the following categorization in found:

$$\tau_o = \tau_g + \tau_{clock} + \tau_{inst} + \tau_{trop} + \tau_{ion} + \tau_{rel}. \quad (3.20)$$

Hereby the classical geometric delay (3.4) is depicted τ_g and the relativistic corrections τ_{rel} . In the model derived above, τ_v of (3.9) combines τ_g and τ_{rel} . Media effects, above separated into a part from the troposphere τ_{trop} and from the ionosphere τ_{ion} , and errors due to the station clocks τ_{clock} are described in the following sections (3.1.3 and 3.1.4). τ_{inst} comprises instrumental delays acting differently on each participating telescope. In order to precisely model the way from the arrival of the signal at the main reflector until the moment the time stamp is set, either an independent calibration system is used or the effect can be controlled by adequate models. Representatives for the first type are the phase calibration and the cable calibration systems, where artificial test signals are injected into the front end of the receiver to calibrate the instrumental phase and the variable cable length. The effects of antenna deformations due to temperature (Nothnagel, 2009) or the so-called axis offset (e.g. Sovers *et al.*, 1998), when the pointing axes of the telescope do not intersect, can be largely removed through the corresponding models. All other necessary corrections are not directly related to the topic of this work and the reader is referred to the standard VLBI literature as mentioned in the introduction to this chapter.

3.1.3 Atmospheric delay models

On its journey from the radio source to the Earth-based receivers the radio wave front must pass through intergalactic, interstellar, interplanetary, and terrestrial atmospheric media, producing a delay relative to propagation in vacuum (Sovers *et al.*, 1998). However, only in the immediate vicinity of the Earth the paths of the two signals diverge enough, so that in practice only the effects due the atmosphere need to be taken into account. Following the dominant influences, in the ionosphere charged particles modify the propagation speed and in the troposphere neutral molecules slow down the signal and refractive bending changes the actual ray path.

For microwaves, the ionosphere acts as a dispersive medium, meaning that the propagation delay varies for each individual wavelength. Usual VLBI observations are performed at two

frequency bands, allowing the elimination of the ionospheric delay through linear combination (e.g. Hobiger, 2006) with sufficient accuracy. If a second band is not available, one either has to approximate the ionospheric delay through adequate modeling (e.g. Sovers *et al.*, 1998), or, as done in chapter 4.2.3, use a priori information about the instantaneous ionosphere. Global maps of the total electron content (TEC), as determined by GNSS at the Center for Orbit Determination in Europe (CODE), can be used for this purpose (Tierno Ros *et al.*, 2011). Once determined, τ_{ion} occurs as advance in the phase delay while it delays the group delay measurement with the same magnitude (Sovers *et al.*, 1998).

In contrast to the ionosphere, that is well under control through observations at two frequency bands, the troposphere remains one of the most challenging limitations for all space geodetic techniques (Niell *et al.*, 2006). In the common formalism the tropospheric delay at one station $\Delta L(e)$ at the elevation angle e is separated into a hydrostatic (h) and a wet (w) part, represented as the product of the corresponding zenith delay ΔL^z and the elevation-dependent mapping function $mf(e)$ (Schuh & Böhm, 2013):

$$\Delta L(e) = \Delta L_h(e) + \Delta L_w(e) = \Delta L_h^z \cdot mf_h(e) + \Delta L_w^z \cdot mf_w(e). \quad (3.21)$$

As the delay is proportional to the path length through the atmosphere, the mapping function relates the delay in zenith direction to the slant delay at elevation angle e . In its simplest form, neglecting the Earth's curvature, it can be written as (e.g. Sovers *et al.*, 1998):

$$mf(e) = \frac{1}{\sin(e)}. \quad (3.22)$$

This means, that at 30° elevation the slant delay is twice the size of the zenith delay. Hence, the atmospheric delay rapidly grows with decreasing elevation angle. For highest accuracies nowadays the Vienna Mapping Functions (VMF; Böhm *et al.*, 2006) are recommended by the IERS (Petit & Luzum, 2010), where data of numerical weather models provided by the European Centre for Medium Range Weather Forecasts (ECMWF) are used to approximate reality.

The residual effect of the troposphere on the observation follows by the difference between the two stations:

$$\tau_{trop} = \Delta L_2(e_2) - \Delta L_1(e_1). \quad (3.23)$$

While the hydrostatic part can be modeled a priori very accurately, the wet part of the atmosphere changes rapidly and is usually estimated within data analysis (e.g. Nilsson *et al.*, 2013). Alternatively, for low accuracies or when the zenith wet delays cannot be estimated within the analysis, initial values for ΔL_w^z can also be calculated with appropriate models (Nilsson *et al.*, 2013).

Due to strong correlations, errors in the applied mapping functions or in poor tropospheric delay modeling in general are predominately reflected in estimated station heights (e.g. Böhm,

2004). According to Treuhaft & Lanyi (1987), the estimated zenith delays reflect spatial and temporal averages and the dominant remaining tropospheric errors are due to random fluctuations in the wet troposphere. Following this theory and assuming an adequate model for such tropospheric turbulences, Nilsson *et al.* (2007) developed a method to simulate this effect and use it for investigations on the expected accuracies of future observations. More information on such simulations is given in chapter 5.4.4.

3.1.4 The role of clocks

In VLBI, the basic observable is the time difference of signal reception at two antennas. Because the signals are time tagged with local clock time, differences between the clocks of the separated stations will add directly to the delay measurement (Herring *et al.*, 1990). These clock errors ΔClk_i are usually accounted for in analysis by the estimation of a clock offset and a piecewise parameterized polynomial for each station i . So, the total effect on the delay yields:

$$\tau_{clock} = \Delta Clk_2 - \Delta Clk_1. \quad (3.24)$$

As a quality feature of clocks one can take the frequency stability, which is commonly expressed in terms of the two-sample Allan standard deviation (ASD; e.g. Thompson *et al.*, 1986).

Besides the contributions purely from the clocks, τ_{clock} also absorbs other “clocklike” errors, mainly of instrumental origin.

3.1.5 Prospects

With significant contributions to the ICRF, the EOP series, and the ITRF, the IVS with all its components holds an important position in geodesy. This will not change in near future, as VLBI is unique in its ability to measure precisely the positions of the radio sources realizing the CRF and to monitor precession/nutation and the Earth’s rotation rate (dUT1) over longer time scales. Nevertheless, confronted with aging systems and outdated technology as well as new goals in terms of precision and delivery of the results, the IVS is about to change its observing system completely. The VLBI2010 Global Observing System (VGOS) is the result of the profound VLBI2010 study, defining the design aspects of a next-generation VLBI system. Meeting the goals of GGOS, the key targets of VGOS are (Petrachenko *et al.*, 2009):

- 1-mm position accuracy on global scales,
- continuous measurements for time series of station positions and Earth orientation parameters,
- turnaround time to initial geodetic results of less than 24 hours.

The investigation of a new type of observations within this thesis also requires the discussion of some practical technical issues. Here, several changes coming along with VGOS in the future (as

defined in Schuh & Behrend, 2012) shall be respected. This includes the plan for small and fast antennas, with a proposed dish size of about 12 m and a slew speed of $6 - 12^\circ/\text{s}$, enabling a high number of observations in different directions in a short time interval. The second important change is the covered frequency range. While today's receiving system is optimized (and mostly limited) to observations at 2.2 – 2.4 GHz and 8.2 – 8.95 GHz, VLBI2010 receivers will cover the entire frequency range from 2 – 14 GHz. The precision of the measured delay is expected to be about 4 ps instead of nowadays 10 – 30 ps. With the start of VLBI2010 operations planned for the year 2015, by 2018 approximately 20 new radio telescopes operated by the IVS network institutions will be available, with additional stations possible to join (Hase *et al.*, 2013). This will not only heavily increase the total observing time for geodetic VLBI, but will also significantly improve the global VLBI antenna coverage. Finally, the last point that shall be mentioned in the course of this section is the timeliness of results and data transfer. Taking advantage of the rapid developments in computing and high speed data networks, VGOS clearly strives for electronic data transfer and minimal turnaround times. If successful, this brings VLBI into play for real time applications, like e.g. for navigation purposes.

3.2 VLBI for space applications

While the most popular applications of VLBI are in the field of radio astronomy, where it is mainly used for source imaging and astrometry, and besides the comparatively small area of geodetic VLBI (section 3.1), soon after its invention this technique has been used for locating and navigation of spacecrafts. With its high angular resolution most of the time VLBI is sensitive in the direction perpendicular to the line of sight (LoS), the component common tracking methods sometimes have problems with. Although until today VLBI has never become the mission-critical navigation method, there is another reason why more and more missions implement it as a backup tool on their space probe: with the alternate observations of a well determined quasar given in the ICRS and a spacecraft whose trajectory is usually modeled in some dynamical system, the tie between both systems can be determined directly, meaning the spacecraft can be located in the ICRS. This, on the other hand, improves the achievements of the other Earth-based tracking techniques, as they strongly rely on an accurate position of the tracking station, which is best determined in the ITRS and hence indirectly connected to the ICRS rather than to the dynamic system. Consequently, VLBI is a well proved method to determine frame ties, the reason why it is selected for the solution of the problems treated in the present work. As VLBI for spacecraft tracking is not well known within the geodetic community, this section starts with an overview on the evolution of this application (section 3.2.1). As described there, today's realizations of VLBI tracking systems are strongly mission dependent and differ heavily in terms of signal, observation duration, antenna network and achieved accuracy. An overview of some present systems is given in section 3.2.2. In this thesis the focus is on the adapted delay model for sources other than quasars (section 3.2.3), the advantage of differential VLBI (chapter 4), and future possibilities of

using VLBI for the connection of reference frames (section 3.2.4).

For completeness, this paragraph ends with a few words on space VLBI. Motivated through the straightforward connection of the length of the baseline with angular resolution, the idea of space VLBI is to set up a VLBI telescope in space and perform observations together with Earth-fixed antennas. In 2011 this was realized with the Russian RadioAstron Project¹, where a 10-m space radio telescope orbits around the Earth at distances between 7000 and 350000 km. With the enormous baselines of such space-ground VLBI observations, astrometry can be done with unprecedented precision. From a geodesist's view one has to remark that RadioAstron was designed to carefully observe single sources rather than for fast switching from one source to the next. Hence, its immediate value for geodetic purposes is limited.

3.2.1 Technical evolution

Investigating the history of tracking vehicles in deep space with VLBI (e.g. Border, 2009) certainly the efforts by the NASA Deep Space Network (DSN) can be identified as the pioneering work in that area. From the beginning of the first deep space missions in the 1960s and 1970s, that are space probes at lunar or planetary distances, tracking is accomplished through a variety of radio and optical techniques (Thornton & Border, 2003). Depending on the necessary accuracy and the mission stage, either Earth-based or onboard systems are chosen. That is for example during the approach phase the use of optical systems which provide the relative spacecraft position to the target body by taking images against a known star background, especially when there are large uncertainties in the target-body ephemeris. During a mission's cruise phase on the other hand, radio-tracking systems from Earth have become the standard tool. By measuring the signal travel time (ranging) and the frequency shift (Doppler) the line-of-sight range and range-rate between a tracking station and a spacecraft can be obtained. Performing these measurements over several hours, due to the Earth's rotation imposing a diurnal signature on the measured signal depending on the spacecraft's angular coordinates, finally the trajectory of the spacecraft can be determined. Though undisputed success of the range and Doppler techniques, when accuracy demands increased over time, people were looking for methods augmenting the existing systems and improving the expected accuracy of the derived trajectory. That was the time VLBI found its way into spacecraft tracking. This concept used by astronomers so far helped to solve two pending problems: first, the low sensitivity in declination of Doppler measurements when the spacecraft was near Earth's equatorial plane and second, the errors from insufficient knowledge of dynamic forces mainly due to mismodeled solar pressure accelerations leaking into the direction least well determined by Doppler, declination. Looking at the VLBI technique from the perspective of spacecraft tracking, it is a method of Differential One-way Ranging (DOR, e.g. DSN Telecommunications Link Design Handbook, 2004). This means that by only using a down-link signal a range difference, namely the one between the signal traveling from the transmitter

¹<http://www.asc.rssi.ru/radioastron/>

to antenna 1 and to antenna 2 respectively, is measured. Though, for a significant improvement in orbit determination compared to Doppler and Range, once-differenced VLBI measurements are not accurate enough. A solution is the so-called Differential or Delta VLBI technique (D-VLBI, Δ -VLBI), where a spacecraft is observed alternately to a well-known reference source and the measurements are differenced afterwards. By that, the before delimiting uncertainties in media delays, clock offsets, instrumental delays, and station locations become common-mode errors which are reduced largely through cancellation when differencing the two delay measurements. The method of differential VLBI and its advantages in terms of error cancellation are explained more detailed in chapter 4 of this work.

Developed as a backup system, especially in the beginning VLBI tracking systems were adapted to a mission's own characteristics rather than vice versa. As a result, today several practical tracking systems exist which partly differ fundamentally in their technical realization. Lanyi *et al.* (2007) identified and compared four such techniques, namely Δ DOR as realized by ESA and NASA, the Phase referencing method demonstrated with the Very Long Baseline Array (VLBA), the use of Radio Frequency Synthesis, and Earth Rotation Synthesis. Δ DOR is a well proved operational technique that is described in detail below. The use of Phase referencing for spacecraft tracking was demonstrated at the VLBA (Lanyi *et al.*, 2005) and is also realized in the recently presented VLBI spacecraft tracking technique presented by Duev *et al.* (2012). The other two techniques in Lanyi *et al.* (2007) are only described conceptually. In the Radio-Frequency Synthesis technique the phase ambiguity is solved by forming group delay observables with a sufficiently large bandwidth synthesis, what is more or less comparable with the multi-frequency approach as realized at the SELENE spacecraft described in chapter 4.2. The last proposed method makes use of the varying geometry of baselines induced by Earth rotation. For the so-called Earth Rotation Synthesis, continuous observations over a long time period are needed, which might be a reason why this technique has not been realized so far. The probably most characteristic feature to distinguish various techniques is the number of stations that are involved in the observations. Then, the core question is the chosen method to resolve the phase cycle ambiguities in the measured differential propagation time. This finally determines the covered bandwidth of the measured signal as well as the required observation duration.

Border (2009) distinguishes the narrowband and the wideband technique. This arises from the two successfully performed D-VLBI realizations at the DSN, either measuring phase delay rate over a relatively long time interval of several hours, or observing time delay over a shorter interval. While for the phase delay rate technique a narrowband signal, e.g. the spacecraft carrier, is sufficient, the time delay technique requires a wideband signal enabling a group delay measurement (Border, 2009). The first demonstrations of D-VLBI used only the phase delay rate technique. By analogy with Doppler measurements, the information content arises through Earth rotation, having the same drawback of loss of sensitivity in spacecraft declination for sources near the Earth's equatorial plane. In terms of observation strategy, the crucial thing is to follow the signal phase of each source and especially to connect the integer cycles of phase during the switching gap. In the case of delay measurements, only a few observations of much shorter

duration are sufficient to determine the angle between the baseline vector and the direction to the radio source, or, in case of D-VLBI, the angle between the two sources. Though the advantage of less antenna time needed for navigation, there are more demands on the spacecraft and the recording capabilities of the receiving system. In order to form a group delay, a signal covering a broader bandwidth is needed and recording is usually done on multiple channels, as it is done in geodetic VLBI (chapt. 3.1.1).

But not only recording bandwidth respectively maximum sampling rates are decisive for the success of VLBI spacecraft tracking. In contrast to geodetic VLBI, where people are used to a turnaround time of several days to weeks between the observation and the results of interest, that is impossible for mission-supportive tracking. Hence, in spacecraft VLBI people had to find ways for fast data transfer right from the beginning, creating another restriction on data volume respectively recorded information. On the other hand, in terms of automation, e-transfer and reliability, sometimes VLBI tracking systems are ahead of today's geodetic VLBI observing program.

3.2.2 Overview of VLBI tracking systems

When in the last years space agencies other than NASA began to explore planetary and deep space by launching dedicated missions, sooner or later also VLBI tracking has been incorporated into their tracking systems. Considering different prerequisites, accuracy demands and stages of development, today there are several working VLBI tracking systems that shall be described in the following:

DSN Δ DOR: The NASA DSN began its Δ VLBI tracking with observations to the Voyager spacecrafts in 1979 (Brunn *et al.*, 1978; Christensen *et al.*, 1980). Since then, this technique has evolved significantly, as described in detail by Border (2009), mainly driven by NASA's ambitious planetary exploration program at that time. NASA DSN consists of three observation sites, maintaining antennas at Goldstone (U.S.), Madrid (Spain), and Canberra (Australia). The key enabling technology are group delay measurements of DOR tones with wide spanned bandwidth (Lanyi *et al.*, 2007). In detail, a Δ DOR measurement is generated by comparing, at two ground stations, the phase of two or more tones emitted by a spacecraft, and by measuring the difference in time of arrival, at the same two stations, of a broadband quasar signal (Border & Koukos, 1993). Measurements are usually taken on two baselines of relatively short duration compared to the conventional tracking techniques. Normally a Δ DOR pass consists of three scans (Berry & Border, 2005), each with a duration of a few minutes and containing either the observation sequence spacecraft-quasar-spacecraft or quasar-spacecraft-quasar. Basic requirement for this technique is the availability of DOR tones on the spacecraft, that are generated by modulation of the downlink carrier at S-band, X-band, or Ka-band, hence, telemetry reception is usually interrupted during the measurement. Concerning the accuracy of Δ DOR measurements, one has to distinguish between the precision of the DOR, respectively quasar delay, measurements and

the errors due to the transmission media (mainly the troposphere), baseline errors, and instrumental delays. While most errors scale down with the angular separation between the spacecraft and the quasar, instrumental errors depend more on the characteristics of the radio signals and the spanned bandwidth (Thornton & Border, 2003). The current Δ DOR VLBI tracking systems routinely deliver reliable operation at the 98% goal with accuracies approaching 1 nanoradian (Border, 2009), supporting a multitude of deep space missions and providing valuable information to tie the radio reference frame to the planetary frame (e.g. Folkner *et al.*, 2008).

ESA Δ DOR: While ESA missions have been supported by the NASA DSN with Δ DOR since 1986, with the Cebreros (Spain) DSA-2 antenna coming into operation late 2005, ESA had the potential for making delta-DOR measurements on its own (ESA, 2006). Following a number of technical and organizational upgrades (receiving system, rapid data transfer, correlator, and flight dynamics software), as described by James *et al.* (2009), ESA's Delta-DOR system was validated with observations of the missions Rosetta, Mars Express and Venus Express (VEX). The system was implemented with an accuracy demand of 1 ns uncertainty, corresponding to an angular accuracy of about 25 nrad, with usual separation angles between the target and a reference source of up to 10° (James *et al.*, 2009).

As a delta-DOR measurement is directly related to the geometry of the baseline(s) with relation to the position of the spacecraft, the observing network, including shared visibility from the antennas to the target, is decisive for the angular accuracy between the spacecraft and the reference source. In practice, space agencies help each other with Δ DOR observations in mission-critical manoeuvres and efforts for standardization to ease the collaboration are undertaken, e. g. by the Consultative Committee for Space Data Systems (CCSDS, 2011). Especially the implementation of a third ESA DSA station in Malargüe, Argentina, entering full service in 2013, will intensify such collaborations from both sides, ESA and NASA, as it is the first deep space station in South America.

VLBA Phase referencing: Phase referencing for the precise determination of angles between radio sources is routinely done at the VLBA as part of source imaging (e.g. Lestrade *et al.*, 1990). By using this technique to locate the Mars Exploration Rover B (MER-B) relative to a quasar, Lanyi *et al.* (2005) showed its applicability also for spacecraft tracking. Without the need of a special spacecraft tone, the carrier phase differences were measured on 25 baselines using the 10 VLBA antennas on and around the North-American continent. The various lengths and orientations of the baselines enable the resolution of the carrier phase ambiguities, yielding a potentially higher accuracy than the group delay differences used in the DSN VLBI tracking. A comparison of the results with the DSN tracking revealed a precision advantage of the VLBA phase referencing for X-band measurements at that time, with the restriction that only quasars within 4° of the spacecraft could be used (Lanyi *et al.*, 2005). Nevertheless, despite the advantages of high accuracy, independence of a

dedicated spacecraft tone and not disturbing telemetry operations, the possibility to use weaker, multiple quasar sources, as well as saving antenna time at the DSN, the VLBA is not designed for operational tracking responsibilities mainly due to insufficient timeliness in data transfer and processing. Further, with the future transition from X- to Ka-band, DSN Δ DOR group delay will improve its performance to a similar level as obtained from phase delays. But instead of a replacement of one system through another, Martín-Mur *et al.* (2006) identify the role of the VLBA in spacecraft navigation more in the determination of quasar catalogs, especially at higher frequency bands (e.g. Ka-band) and in periodic measurements of planetary orbiting spacecrafts to improve the planetary ephemerides and the tie to the ICRF. A nice example for the latter is the VLBA imaging between 2006 and 2009 of the Cassini spacecraft orbiting Saturn. Providing positions of Saturn in the ICRF with accuracies of about 0.3 mas (1.5 nrad), these observations, amongst others, were used to constrain a new ephemeris, the DE 422 (Jones *et al.*, 2011).

PRIDE phase referencing: With the Planetary Radio Interferometry and Doppler Experiment (PRIDE) the Joint Institute for VLBI in Europe (JIVE) has started an initiative to support planetary science missions by providing ultra-precise estimates of spacecraft state vectors based on phase-referenced VLBI tracking and radial Doppler measurements (Duev *et al.*, 2012). Similar to the VLBA approach, PRIDE uses the imaging technique with a multi-station network imposing only minimal requirements on the on-board instruments. From the spacecraft signal two observables are derived, a group delay from the wide-band signal and a phase delay from the narrow-band carrier tone. So, with the help of the group delay, the ambiguities for the phases can be resolved for most of the baselines. Test observations to the VEX spacecraft revealed accuracies that are compatible with those of the other systems described in this section, with good expectations for further improvement (Duev *et al.*, 2012). Despite the high flexibility of the PRIDE system – Duev *et al.* (2012) mention the use for near-Earth targets like GNSS satellites – a drawback of this technique might be the need of very close-by ($< 2.5^\circ$ or even same-beam) calibrator sources, what requires a careful quasar-search and observing program in advance.

JAPAN: In Japan, in the beginning of the 21st century, the Japan Aerospace Exploration Agency (JAXA), respectively the Institute of Space and Astronautical Science (ISAS), the National Institute of Information and Communications Technology (NICT), and the National Astronomical Observatory of Japan (NAOJ) have started collaboration to use VLBI for spacecraft navigation (Sekido *et al.*, 2007). Development of software and hardware (e.g. Takeuchi *et al.*, 2006) was followed by a series of test observations to Japanese spacecrafts (e.g. Ichikawa *et al.*, 2004; Kikuchi *et al.*, 2004; Kono *et al.*, 2003; Sekido *et al.*, 2004, 2007). Finally, all efforts led to the well developed differential phase delay tracking applied in the Japanese lunar mission SELENE. This system uses narrow bandwidth signals at multiple frequencies and, in same-beam mode, achieves accuracies of several pico-seconds at S-band phase delays (Hanada *et al.*, 2010). More information on the SELENE tracking

system and appropriate data analysis is given in chapter 4.2 of this thesis.

Chinese CVN: With the construction of the Chinese VLBI Network (CVN) and the establishment of a VLBI data processing center at Shanghai Astronomical Observatory, Chinese Academy of Science, in 2001, China began its VLBI spacecraft tracking. In the first years, hard- and software developments (e.g. Shu *et al.*, 2008) came along with test observations to a series of deep space and near Earth probes (e.g. Huang *et al.*, 2006; Qian & Ping, 2006), with the goal to use advanced technique for tracking in the Chinese lunar exploration program Chang'E (Yan *et al.*, 2010). Emphasis was put on real time VLBI, with the capability of a quick orbit determination for a spacecraft in less than one hour after the observation (Qian & Ping, 2006). Time delay and delay rate observations were performed in a sequence of 20 minutes quasar – 40 minutes Chang'E-1 – 20 minutes quasar, enabling correction of the Chang'E observations for long term systematic effects through the quasar observations (Huang *et al.*, 2011). For Chang'E-2, the system was improved for a digital base-band converter and an improved estimation of the station clocks with GPS (Li *et al.*, 2012). In dependence of the observing mode, ranging from S-band in real time or post-processing, over X-band bandwidth synthesis, to X-band Δ DOR tests, data noise levels from 0.1 to a few nanoseconds can be achieved (Li *et al.*, 2012; Yan *et al.*, 2010).

Besides these mature systems described above, there are some other applications of VLBI successfully supporting space research that are worth to be mentioned here. In 1973/74 radio signals transmitted from five Apollo lunar surface experiments packages (Alsep's) were observed with differential phase VLBI, contributing to studies on Lunar dynamics and Selenodesy (King *et al.*, 1976). In the VEGA project, where differential VLBI measurements to balloons in the Venus atmosphere were performed, in 1985 VLBI entered the field of planetary atmospheric studies (Sagdeyev *et al.*, 1992). Following an assessment study (Pogrebenko *et al.*, 2004) and specific technical preparations at 17 VLBI telescopes, in January 2005 the Huygens probe (e.g. Lebreton *et al.*, 2005) was tracked by differential phase referencing on its descent through the atmosphere landing on Titan, the largest moon of Saturn. Despite the extraordinarily weak signal at 2.04 GHz, that was originally designed for communication with the mother ship Cassini rather than for traveling $1.2 \cdot 10^9$ km to the Earth, the landing trajectory was derived from VLBI observations with sub-mas accuracy, respectively about one kilometer rms (van 't Klooster, 2007). This technique was also used to follow ESA's SMART-1 spacecraft on its final moments and impact on the Moon in 2006 ¹.

3.2.3 Delay model for sources at finite distance

If VLBI targets are within our solar system, the delay model presented in section 3.1.2 is not applicable. Due to the finite distance from the antennas to the sources, the assumption of a plane wavefront has to be replaced by that of a curved one. In addition, finite sources are normally moving with respect to the solar system barycenter, hence the source trajectory has to

¹press release of 15th October 2007: http://www.express-eu.org/SMART1_Imact.html

be included in the processing software. It was already shown in previous sections, that a practical delay model is somehow a compromise solution between a correct (relativistic) formulation and simplifications or cancellations of effects below the level of significance.

As shown in figure 3.3, VLBI observations to sources at finite distance can be seen as the difference between the distances, respectively the light travel times, between the antennas and the source:

$$\tau = R_2(T_2) - R_1(T_1) \quad (3.25)$$

with the antenna reception times T_1 and T_2 and

$$R_i(T_j) = X_{SC}(T_0) - X_i(T_j). \quad (3.26)$$

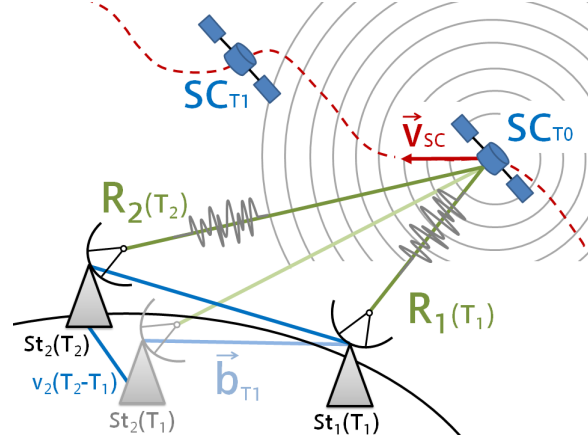


Figure 3.3: VLBI to moving sources at finite distance

Prerequisite for this simple formulation is to know the position of the spacecraft SC at the signal transmission time T_0 . This can be calculated iteratively by solving the light time equation (Moyer, 2003):

$$T_0 = T_1 - \frac{R_{1,SC}}{c} - RLT_{1,SC} \quad (3.27)$$

where $R_{1,SC}$ depicts the geometric straight-line distance between the spacecraft at the time of emission and the antenna at the time of signal reception

$$R_{1,SC} = |\vec{X}_{SC}(T_0) - \vec{X}_1(T_1)| = |\vec{R}_{1,SC}| \quad (3.28)$$

and the relativistic light-time (RLT) delay due to the Sun and other disturbing bodies is calculated as

$$RLT_{1,SC} = \sum_J \frac{(1 + \gamma)GM_J}{c^3} \ln \frac{R_{SC,J} + R_{1,J} + R_{SC1,J}}{R_{SC,J} + R_{1,J} - R_{SC1,J}}. \quad (3.29)$$

In equation (3.29) the vectors from location $i = 1, 2, SC$ to the disturbing body J are defined as

$$\vec{R}_{i,J} = \vec{R}_{i,J}(T_i) = \vec{X}_i(T_i) - \vec{X}_J(T_i) \quad (3.30)$$

where the time epoch T_i is the moment when the signal passes the corresponding point, hence the time of transmission T_0 or reception T_1 and T_2 . Finally,

$$\vec{R}_{SC1,J} = \vec{R}_{1,J}(T_1) - \vec{R}_{SC,J}(T_0). \quad (3.31)$$

The relativistic retardation in (3.29) is calculated for solar system bodies where the signal passes by, for practical standardization one can run it over the solar system planets and the Earth's moon. In the case of the Sun, according to Moyer (2003) an additional bending term shall be included:

$$RLT_{1,SC} = \frac{(1+\gamma)GM_S}{c^3} \ln \frac{R_{SC,S} + R_{1,S} + R_{SC1,S} + \frac{(1+\gamma)GM_S}{c^2}}{R_{SC,S} + R_{1,S} - R_{SC1,S} + \frac{(1+\gamma)GM_S}{c^2}}. \quad (3.32)$$

Complete formulations of a VLBI delay model for sources at finite distances were developed by several authors: Moyer (2003) provides a model applicable for spacecraft observations. In principle it is described by the formulation given above, based on a precise solution of the light-time equations from the source to the two antennas. In Sovers *et al.* (1998), besides the quasar solution described in 3.1.2, a corresponding formalism for a curved wave front is presented, applicable at the 1 ps accuracy level for source distances between $2 \cdot 10^5$ and $3 \cdot 10^{14}$ km. A lunar VLBI observation model for Earth-based observations of emitters as close as the Earth's moon was developed by Fukushima (1994), relying on an iterative vector formalism expressed in the same way as for quasi infinite sources. The model also includes a good description on partial derivatives of the delay with respect to station and source positions. The most substantial work in the area of VLBI delay models is by Klioner (1991). With an emphasis on gravitational effects due to general relativity, Klioner (1991) provides three delay models: one for VLBI observations to remote sources like quasars and pulsars, a second one for interplanetary spacecraft and one for VLBI observations to Earth satellites and near-Earth spacecrafts. The second and third model are used within this thesis in chapters 4 and 5. For all other formalisms, the reader is referred to the corresponding publication.

A small drawback of the models presented above might be the fact that they are given in some independent, non-rotating reference system, mostly BCRS or a scaled version of it (see chapter 2 for more information). This requires care and knowledge about time and coordinate transformations for a potential user when implementing a finite-distance model into existent VLBI software. Exactly this problem was faced by Sekido & Fukushima (2006) by the development of an analytical representation of a VLBI delay expressed in TT-scale for ground-based VLBI observations of radio sources at finite distance. The authors describe it as an expansion of the Consensus model (see 3.1.2) with the same target accuracy of 1 ps. Hereby, the direction to the source is replaced with the pseudo source vector \vec{K}_p composed of the directions $\vec{R}_i(T_j)$ from the antenna to the source according to (3.26).

$$\vec{K}_p = \frac{\vec{R}_1(T_1) + \vec{R}_2(T_1)}{R_1(T_1) + R_2(T_1)} \quad (3.33)$$

\vec{K}_p can be obtained after solving the light-time equation following (3.27). In contrast to the Newtonian calculation of (3.14), now the barycentric station coordinates in TDB-frame are calculated

combining equations (2.11) and (2.3) to

$$\vec{X}_{i,TDB}(T_1) = \vec{X}_{E,TDB}(T_1) + \left(1 - \frac{W_E}{c^2} - L_C\right) \cdot \vec{x}_{i,TT}(t_1) - \frac{\vec{V}_E \cdot \vec{x}_{i,TT}(t_1)}{2c^2} \vec{V}_E. \quad (3.34)$$

Similar to (3.9), with the baseline vector \vec{b} defined in TT-frame, the delay τ_f , also in TT, is then computed as

$$\tau_f = \frac{\Delta RLT - \frac{\vec{K}_p \cdot \vec{b}}{c} \left[1 - \frac{(1+\gamma)W_E}{c^2} - \frac{|\vec{V}_E|^2}{2c^2} - \frac{\vec{V}_E \cdot \vec{v}_2}{c^2} \right] - \frac{\vec{V}_E \cdot \vec{b}}{c^2} \left[1 + \frac{\hat{R}_2 \cdot \vec{V}_2}{c} - \frac{(\vec{V}_E + 2\vec{v}_2) \cdot \vec{K}_p}{2c} \right]}{\left[1 + \frac{\hat{R}_2 \cdot \vec{V}_2}{c} \right] (1 + H)}. \quad (3.35)$$

\hat{R}_2 is the TDB direction vector of station 2

$$\hat{R}_2 = \frac{\vec{R}_2}{R_2}. \quad (3.36)$$

Due to the fact that \vec{b} is defined following equation (3.3), with antenna positions at station 1 receiving epoch t_1 , again the movement of station 2 between t_1 and t_2 must be taken into account. Assuming linear station motion as in (3.4), Sekido & Fukushima (2006) include a second order correction term H for the retarded baseline, which is defined as

$$H = \left| \frac{\vec{V}_2}{c} \times \hat{R}_2 \right|^2 \frac{\vec{K}_p \cdot \vec{b}}{2R_2}. \quad (3.37)$$

Finally, the differential gravitative delay is obtained by subtracting the effects of the two ray paths following equation (3.29)

$$\Delta RLT = RLT_{2,SC} - RLT_{1,SC}. \quad (3.38)$$

Converting the subtraction of two logarithms into the invers product of its argument then gives

$$\Delta RLT = \sum_J \frac{(1+\gamma)GM_J}{c^3} \ln \left[\frac{R_{2,J} + R_{0,J} + R_{20,J}}{R_{2,J} + R_{0,J} - R_{20,J}} \cdot \frac{R_{1,J} + R_{1,J} - R_{10,J}}{R_{1,J} + R_{0,J} + R_{10,J}} \right]. \quad (3.39)$$

The correction term given above accounts only for the most significant Post-Newtonian effect. Further effects, which might get important under certain circumstances, are not discussed here and the reader is referred to e.g. Klioner (1991) for more information.

3.2.4 Future potential

Analyzing the numerous efforts in VLBI spacecraft tracking, the trend clearly goes into more mission-critical inclusion of this alternative tracking technique, expecting a number of success-

ful applications in space navigation, planetary science and the calculation of ephemerides in the future. Several developments supporting this perspective are on their way at the moment: already mentioned several times in this work is the upcoming transition from X-band to Ka-band (32 GHz). The move to higher frequencies used in spacecraft tracking is driven by better communication performance, but also increases the accuracy of radiometric tracking techniques by the use of shorter wavelengths and its reduced sensibility to charged particles in the ionosphere and the solar plasma (Thornton & Border, 2003). Work on a CRF realization at X/Ka-band has already been started accordingly (Jacobs *et al.*, 2012). If the VLBI tracking is included in a mission's scenario right from the beginning, its performance can also be improved. This includes a mutual coordination of the used signals, a careful planning of critical manoeuvres in terms of good visibility from a predefined antenna network on Earth and sufficient time for substantial preparation in advance, like a thorough quasar search in the area of interest. Rapid advances in electronics and telecommunication contribute with wider recorded bandwidth and faster data transfer. Very positive is also the ongoing establishment of new antennas around the globe; in this aspect van 't Klooster (2007) and Pogrebenko *et al.* (2004) mention the upcoming Square Kilometer Array, that could be used for VLBI tracking achieving a much better SNR of weak signals from a spacecraft than today's systems and allowing even small probes to transmit telemetry information directly to the Earth. Finally, also new types of observations are possible, as e.g. the tracking of a planetary lander and an appropriate rover in same-beam interferometry, which reduces the errors that are dependent of the separation-angle to a minimum (see also chapter 4.1.4).

In the end of this chapter one can conclude that besides the (in geodesy) well known geodetic VLBI, there is a considerably large area of VLBI space applications. While the former relies on the voluntary global cooperation mostly of national research facilities under the auspices of the IVS, the latter predominantly is controlled by the big space agencies. Aiming at possible synergies between these two groups, from 2009 to 2013 the IVS maintained the IVS Working Group 5 (WG5) on Space Science Applications (Nothnagel *et al.*, 2013). This can be the first step for a mutual transfer of knowledge, where, on the one hand the geodetic community might profit from the experience gained in spacecraft tracking when observing satellites in the future (see chapter 5), and, on the other hand, the IVS can support future space missions through the expertise of its members or by providing appropriate infrastructure in terms of hardware and software.

Chapter 4

Differential VLBI

As pointed out in chapter 3.2, differential VLBI (D-VLBI) is commonly used in VLBI spacecraft tracking in order to reach sufficient accuracy. Despite the simple concept of measuring a spacecraft's angular distance to a well known quasar, this method also holds some characteristics that are worth closer inspection. In the first section of this chapter (4.1) the measurement principle is demonstrated and some basic thoughts on the observation sequence and the resultant scan gaps (4.1.1) as well as on the separation angle between the reference source and the spacecraft (4.1.2) are presented. This is followed by some geometrical reflections on the similarity of the transmission media (4.1.3) and the introduction of the special case of same beam VLBI (4.1.4). The second part (4.2) describes the processing with the Vienna VLBI software (VieVS) of same-beam differential VLBI tracking data of the lunar mission SELENE, including an empirical determination of the level of cancellation of uncalibrated errors.

4.1 Measurement principle

The classical principle of D-VLBI is illustrated in figure 4.1. A spacecraft is observed alternately to a quasar, with the goal to minimize uncontrollable error sources and to angularly locate the spacecraft relative to the quasar with highest precision. These error sources include for example station clock offsets and instrumental delays, baseline errors due to inaccurate station coordinates or unmodeled station variations, and uncalibrated media effects. The extent, to which the error sources are eliminated in the observed differential delay, depends on the resemblance of the signal path, the temporal separation of the observations, and the degree to which the spectral characteristics of the signals match each other (Thornton & Border, 2003). The last point is of importance in the classical quasar - spacecraft method, as a natural quasar source typically emits a broadband signal with a flat spectrum over many gigahertz, while the spacecraft signal is band-limited, usually containing several narrow tones that can be used for VLBI.

D-VLBI experiments are usually run in a way that observations to one source are flanked by that to the other source. This can be either done in the sequence quasar-spacecraft-quasar, or spacecraft-quasar-spacecraft. In principle one can say that the shorter the switching intervals

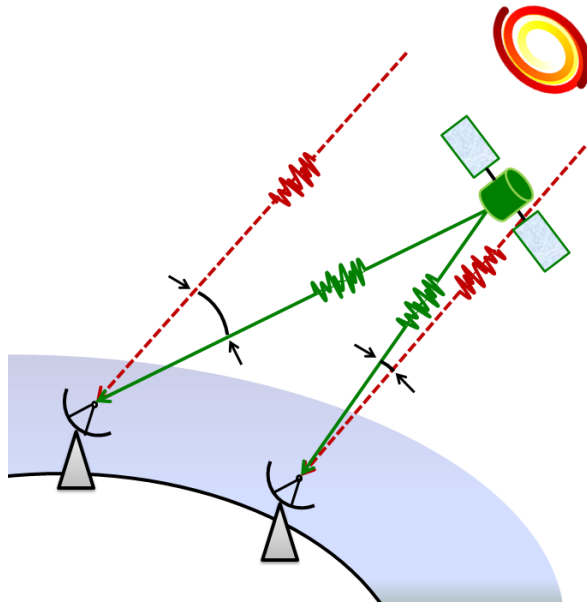


Figure 4.1: Classical D-VLBI principle. The direction to a space probe is determined relative to that of a reference source.

and the closer the sources, a higher resemblance between the ray paths can be assumed and the better the result will be. Depending on the realization, switching sequences of several minutes and separation angles of a few degrees (with extremes up to 25°) are common.

4.1.1 Scan gaps

In D-VLBI, the observation of one source automatically means a scan gap for the other source. In the case of group delay observations, integration times of several minutes are common, in order to get sufficiently high SNR for accurate measurements. As one usually has to deal with weaker radio sources, bigger antennas with e.g. 34 m in the case of the DSN network are used for these measurements. Changes on the signal path within this gap of several minutes, e.g. due to short-term media fluctuations, are therefore not canceled when subtracting the delays and affect the final accuracy of the measurement.

More critical is the scan gap length for phase observations, as it more or less decides on success or failure of the measurement itself in this case. For the astrometric phase-referencing method (e.g. Shapiro *et al.*, 1979) and also for narrow-band Δ VLBI phase observations (e.g. Wu, 1979), computer-aided schemes have been developed to connect fringe phases among consecutive scans assuming linear or polynomial phase variation during the gap. For the task of ambiguity solution, also the measured fringe rates might be used (Shapiro *et al.*, 1979). Wrobel *et al.* (2000) identify the dynamic atmosphere as the dominating constraint on the determination of a possible switching time and propose a value of 300 sec for the switching time¹ in

¹The switching time involves a target observation of 180 sec, bracketed by calibrator observations each lasting

phase-referencing at 8.4 GHz under typical atmosphere conditions. A more advanced method is introduced by Kondo *et al.* (2009), who propose to control the scan-gap time dynamically according to the actual weather conditions. In the next section (4.2) the VLBI observations of the SELENE mission are described, where the integration time was set to 50 sec. Including a slewing time of 10 sec, this results in a switching time of 60 sec (Kikuchi *et al.*, 2008).

4.1.2 Separation angles

Most errors in D-VLBI scale down with the angular separation between the spacecraft and the reference source (Thornton & Border, 2003). Ideally, one would like to find strong (1-Jy) sources within a few degrees of the spacecraft, but this situation is more the exception than the rule (Thornton & Border, 2003). In the case of X-band, according to Lanyi *et al.* (2007), there are enough sources with sufficient flux and adequate distribution to allow selection of reference sources with a mean angular separation of 6° from the spacecraft at most points along the ecliptic, where the majority of deep space missions are located. In practice however, for today's missions often a thorough quasar search in the corresponding area of the sky precedes the actual mission, especially when the observing technique is restricted to very close-by sources (see 3.2.2). With the gradual change of tracking frequency from S/X-band to shorter wavelengths, there is also the need of a corresponding radio source catalog satisfying the demands on availability and accuracy of reference sources.

For deep space missions, the length of the baseline between the observing antennas is small compared to the distance of the spacecraft to the antennas, and the directions in space are approximately identical. Consequently, when at one station a reference source is close to the target source, yielding a small separation angle, this is also true for the other station. If the distance to the space probe decreases, this situation changes and the LoS from the antennas to the probe become more and more different. In figure 4.3 the relation of height of the space probe h , baseline length b , elevation angle ϵ and elevation difference $\Delta\epsilon$ is shown. According to the simplified two-dimensional geometry of figure 4.2, for this investigation the elevation angle ϵ is defined as the angle between the baseline and the direction to the target. For satellites at heights h of 10000, 20000, 30000, 50000, 100000, and 400000 km measured from the direct line b between two antennas, the difference in elevation $\Delta\epsilon = \epsilon_2 - \epsilon_1$ at the two stations in dependence of the elevation at station 1 ϵ_1 , varying from 1° to 90° is illustrated. This is calculated for baseline lengths from 100 km to twice the Earth's radius, what is indicated with the varying colors.

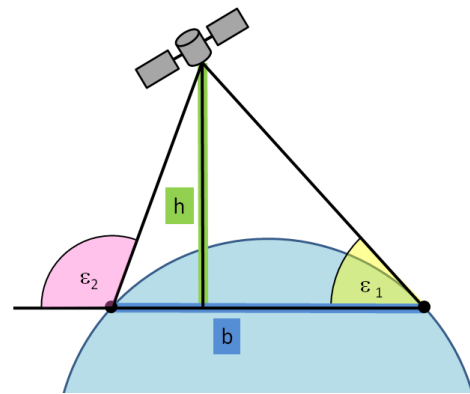


Figure 4.2: Geometrical relation used to calculate the difference in elevation angles ϵ_1 and ϵ_2 in dependence of the baseline length b and the satellite height h .

While for sources at a distance of 400000 km, about the distance from the Earth to the Moon, the elevation-dependent effect of the baseline length with maximal 2° is rather negligible, this geometric contribution to the separation angle roughly lies in the range of $5 - 10^\circ$ for a target height of 50000 km. For the conventional GNSS-satellite height of about 20000 km and below, the difference in the elevation angle is mainly above 10° , leading to the conclusion that the conventional D-VLBI technique as used in spacecraft tracking might not be applicable in the same way for VLBI satellite tracking. Further, one is urged to carefully distinguish between the separation angle as seen in an (absolute) barycentric reference system and the topocentric separation angle seen from a single station. The importance of the latter can be seen when investigating the

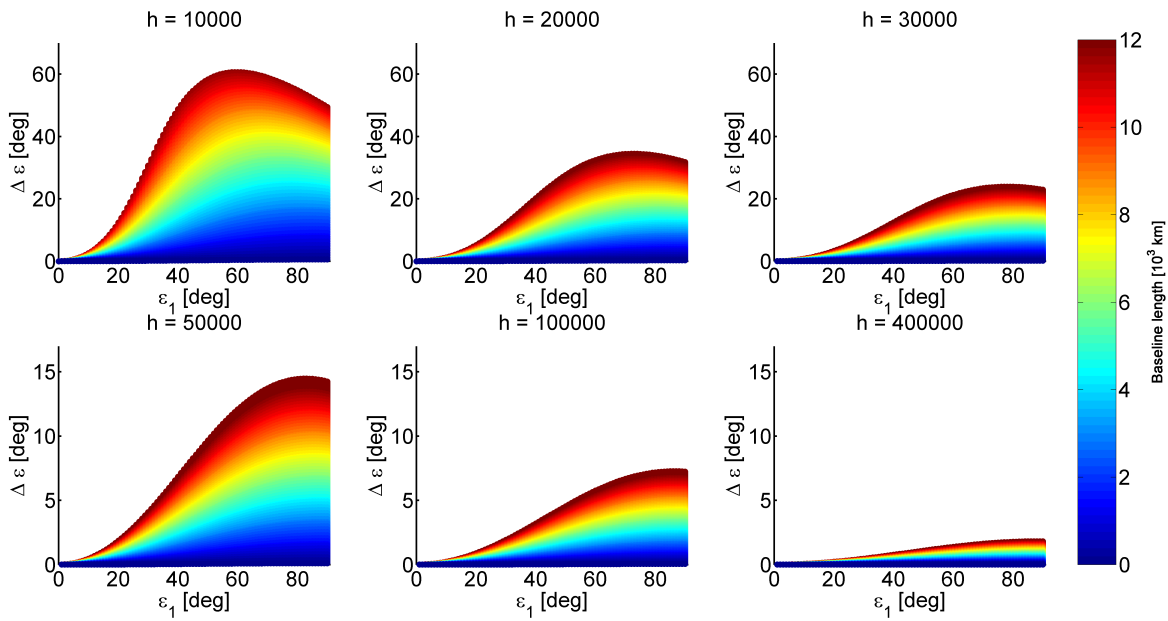


Figure 4.3: Separation angle $\Delta \epsilon$ versus elevation ϵ_1 for various baseline lengths (indicated by different colors) and target heights of 10000, 20000, 30000, 50000, 100000, and 400000 km.

cancellation of the atmospheric delay, which is strongly elevation-dependent.

4.1.3 Common media

Making use of cancellation of media effects requires strong resemblance between the actual media the two signals pass through. Kikuchi *et al.* (2008) present such investigations for separation angles in elevation of up to 1° , here some assessments are made for larger angular separation.

When separation angles are small, as e.g. in the SELENE D-VLBI observations described in section 4.2, during analysis it can be sufficient to model the hydrostatic troposphere delay and omit the estimation of the wet contribution (see section 3.1.3). As shown in figure 4.4, this is not true for larger separation in elevation. With the simplest mapping function of (3.22) and assuming a zenith wet delay of 150 mm, the residual effect on the slant wet delay of two ray

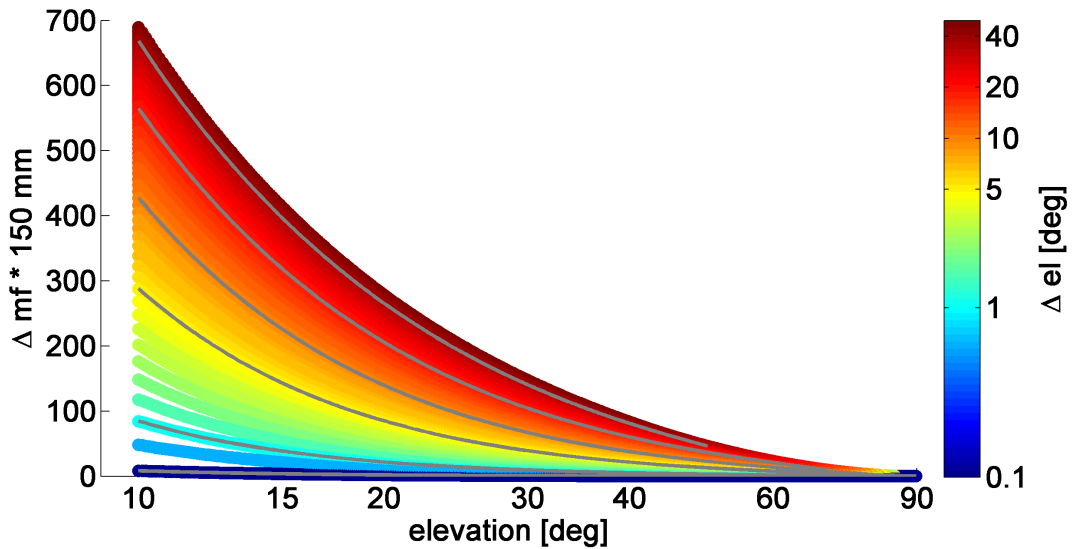


Figure 4.4: Residual effect on the slant wet delay of two ray paths, separated by $\Delta el = el_2 - el_1$, in dependence of the elevation angle el_1 . A zenith wet delay of 150 mm is assumed.

paths, separated by $\Delta el = el_2 - el_1$, in dependence of the elevation angle el_1 is shown. For better readability, the gray lines indicate the curves for a Δel of 0.1, 1, 5, 10, 20, and 40 degrees. For an angular separation of 5° in elevation (yellow area), at an elevation of 30° , the passed media is different for half of an assumed wet delay in zenith direction, in this case about 75 mm. Clearly evident is the strong increase of the effect at low elevations. Overall it can be noted, that at Δel greater than 1° , wet troposphere is not canceled to a good extent any more.

Next, the influence of rapid changes in the wet troposphere over time and azimuthal separation is investigated. For the derivation of figure 4.5, slant wet delays are simulated following the procedure described in chapter 5.4.4 and using the parameters given in table 5.1. Shown are the differences in the delay of two consecutive ray paths, that are separated by time and by azimuth direction. Therefore, calculations were done 50 times and the determined rms indicates the expected error. At an elevation angle of 30° (green line), the residual delay induced by tropospheric turbulence between an initial observation and a second observation, (a) 30 seconds later and at an azimuth 20° away from the initial azimuth, is expected to be about 5 mm. With increasing switching interval, e.g. 5 minutes (b), even for the same azimuth, differences of several millimeters can be caused by tropospheric turbulence.

Concerning the ionosphere, respectively the influence of charged particles on the ray path, it is assumed that additional delays can be controlled either by the use of two or more frequencies or by applying an alternative way of correction (see section 3.1.3). However, when in D-VLBI cancellation through common media is chosen to control this effect, care must be taken for sources at different distances, e.g., when observations to a near Earth satellite shall be corrected through observations to an extragalactic reference radio source. While the signal from the satellite is disturbed by the Earth's ionosphere, the signal from the quasar is additionally influenced by in-

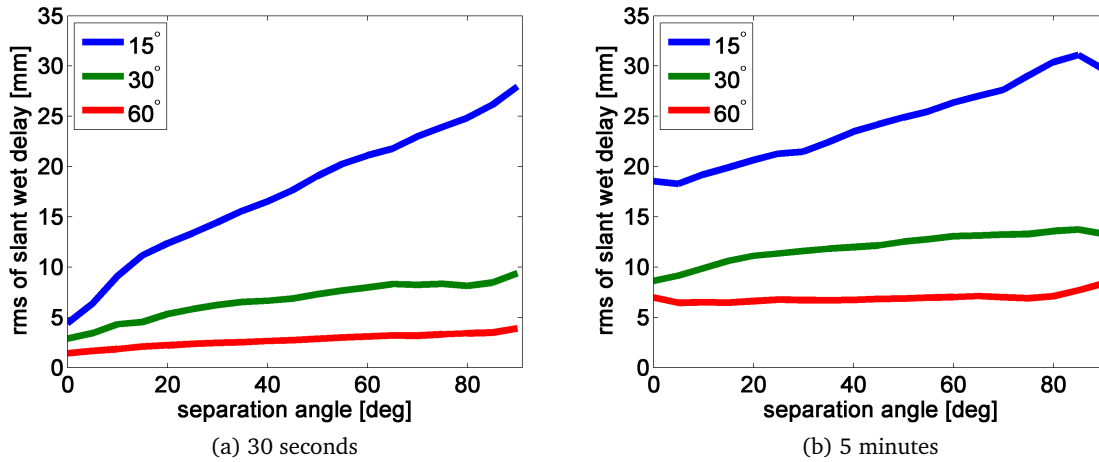


Figure 4.5: Simulated rms of the slant wet delay in dependence of the azimuthal separation angle for a switching interval of (a) 30 seconds and (b) 5 minutes. The effect is calculated for observations at an elevation angle of 15° (blue line), 30° (green), and 60° (red).

terplanetary and interstellar plasma, which can cause delays of considerable size (e.g. Sovers *et al.*, 1998).

4.1.4 Same beam interferometry

A special case of D-VLBI is the same beam interferometry. Here, two target sources are so close together, that they can be observed simultaneously within the same antenna beam. This technique is applicable mostly in deep space and planetary science, when e.g. several space probes orbit a planet or if a mission consists of a lander and its rover. In same beam interferometry, extremely accurate relative positions can be provided, as there are no errors due to the inevitable scan gaps in classical D-VLBI and as a result of the minimum separation between the targets. Thornton & Border (2003) calculated the error budget for same beam observations to space probes on and around Mars, where all targets would be visible within the 1-mrad beamwidth of a 34-m antenna at X-band.

Whether two sources can be observed by one antenna simultaneously is mainly dependent on the size of the antenna (diameter D) and the wavelength of the observed signal λ . Commonly used in this aspect is the half-power beam width $HPBW$, that is the angular distance where the antenna gain drops to half of the maximum value. Though several antenna parameters are needed to calculate the actual $HPBW$, it can be approximated as:

$$HPBW = \frac{\lambda}{D}. \quad (4.1)$$

The VLBI observations to the SELENE spacecrafts, that are treated in the following section, were made in same beam mode.

4.2 D-VLBI by the example of SELENE

The Japanese lunar mission SELENE (SELenological and ENgineering Explorer), orbiting the Moon in the years 2007-2009, was developed to remote-sense the lunar surface globally (Kato *et al.*, 2008). It carried instruments for the study of various topics of lunar science, as e.g. described in Kato *et al.* (2010). The mission consisted of three spacecrafts, the three-axis stabilized main satellite Kaguya and two small spin-stabilized sub-satellites, called Okina (or Rstar) and Ouna (or Vstar). With this special constellation shown in figure 4.6, apart from standard two-way range and Doppler tracking to each separate satellite, the so-called four-way Doppler tracking technique was employed: whenever the main satellite was over the far side of the Moon, the Doppler signal from an earthbound antenna was relayed via the relay satellite Rstar. Additionally, highly precise differential VLBI measurements were performed to Rstar and the VLBI satellite Vstar, involving an improvement of the final orbit consistency from several hundreds to several tens of meters (Goossens *et al.*, 2011a).

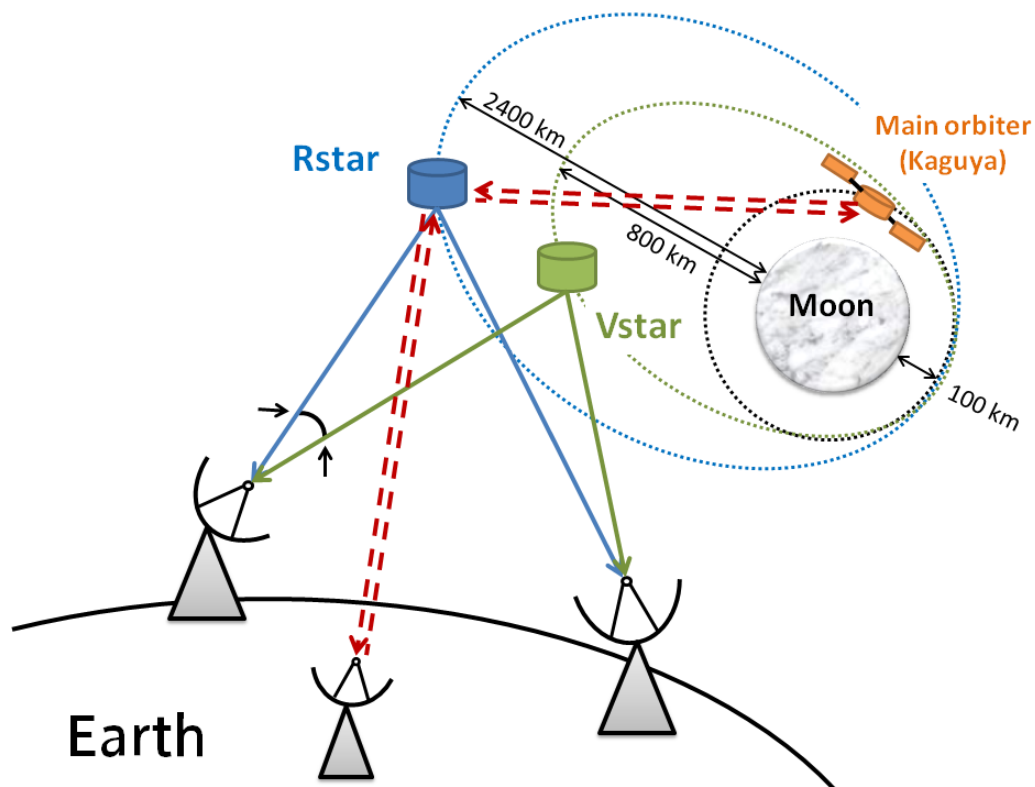


Figure 4.6: SELENE mission overview with D-VLBI measurements between Rstar and Vstar and 4-way-Doppler tracking of Kaguya via the relay satellite.

4.2.1 SELENE differential VLBI tracking

As pointed out in chapter 3.2, the common Δ DOR spacecraft tracking is based on group delay observation and its resolution is inversely proportional to both the signal to noise ratio

(SNR) and the signal bandwidth of the measurement signal (see eq. 3.2; Sekido *et al.*, 2007). Facing the conditions of limited signal bandwidth of the previously designed spacecraft and a main domestic VLBI network with only short baselines, the VLBI phase delay technique was adopted for the purposes of SELENE. In the phase technique, the profit of higher delay resolution and hardly any requirements on signal bandwidth comes along with the $2\pi N$ ambiguity problem. Here, the multi-frequency VLBI (MFV) method serves as an alternative to the imaging with the VLBA described in 3.2.2. Finally, as in switching differential VLBI mode the aimed accuracies still could not be reached, observations were performed in same-beam mode, where signals from the two satellites are received within one antenna beam when pointing towards the midpoint of the sources.

In SELENE, Rstar and Vstar transmit 4 narrowband carrier signals, three in S-band and one in X-band, with center frequencies given in table 4.1.

Table 4.1: Frequencies of VLBI signals in SELENE (e.g. Hanada *et al.*, 2008)

$S_1 = 2212$ MHz,	$S_2 = 2218$ MHz,	$S_3 = 2287$ MHz,	$X_1 = 8456$ MHz
-------------------	-------------------	-------------------	------------------

After reception, these signals are processed with a specifically developed narrow bandwidth sampling and recording system, stored on hard disk and correlated on a software correlator (Kikuchi *et al.*, 2004). For details on the transmitted signal structure, bandwidth and strength, as well as on technical specifications of the instruments on-board and at the ground stations the reader is referred to Hanada *et al.* (2010). With Φ indicating the phase difference of the signals registered at antenna 1 and antenna 2, by again differencing between the two sources $sc1$ and $sc2$, one gets four doubly differenced fringe phases $\Delta\Phi$, one for each frequency.

$$\Delta\Phi = \Phi_{sc1} - \Phi_{sc2} \quad (4.2)$$

In order to determine the final differential phase delay unambiguously, it either must be smaller than one cycle of the applied frequency or the $2\pi N$ ambiguity can be solved anyhow else. The trick in MFV is to use the three signals in S-band and combinations of them in a multi-step procedure to derive the X-band differential phase delay in the end. As described in detail by Kono *et al.* (2003) or Kikuchi *et al.* (2008), first the cycle ambiguity resolution of the wide lane $S_2 - S_1$ is solved, followed by the one of $S_3 - S_1$, which then enables to resolve the S_1 and eventually the X_1 carrier ambiguity. However, for a successful MFV application several conditions need to be fulfilled during the observation process, which were worked out in detail by Kono *et al.* (2003) and Kikuchi (2006). To sum them up, in the SELENE MFV the demands on the initial geometric delay are fulfilled via sufficient a priori orbit accuracy through alternative tracking data and most error sources are canceled thanks to the differential approach. Unfortunately, tropospheric fluctuations with periods shorter than the switching interval and traveling ionospheric disturbances may still corrupt the measurements (Kikuchi, 2006). As a consequence, in SELENE VLBI observations the cycle ambiguity can be resolved using same-beam mode while they cannot usually be resolved

for switched VLBI when the conditions are bad (Liu *et al.*, 2010).

For the same beam case, the requirement for a maximum separation angle between Rstar and Vstar of 0.56° was adopted, after consideration of not only the phase characteristics and power characteristics of the telescopes, but also correlation results from previous observations (Liu *et al.*, 2010). In practice, the midpoint of the two sources was tracked enabling X-band same beam observations for separation angles of less than 0.1° and S-band same beam observations when the angular separation was less than 0.56° . The fixed limits basically correspond to twice the half-power beam width *HPBW* of an antenna with 20 m diameter (Hanada *et al.*, 2010), that can be approximated by the relation of the observed wavelength λ and the diameter of the antenna D as given in equation 4.1.

SELENE VLBI tracking was performed between November 2007 and June 2009 with the Japanese VERA (VLBI Exploration of Radio Astrometry; Kobayashi *et al.*, 2003) stations in Mizusawa, Iriki, Ishigaki, and Ogasawara regularly about 100 hours per month. Additionally, two international campaigns with participating stations in Shanghai, Urumqi (both in China), Hobart (Australia), and Wettzell (Germany) were organized (Hanada *et al.*, 2010). As shown by Kikuchi (2006), the accuracy of the determined differential phase delay depends on the mean elevation angle and the elongation between the two sources. In the analysis of SELENE same beam differential VLBI data Liu *et al.* (2010) achieved a measurement error of less than 1 mm rms for small separation angles and about 2.5 mm for separation angles up to 0.56° . Goossens *et al.* (2011a) and Goossens *et al.* (2011b) applied the VLBI tracking data in orbit determination of the SELENE satellites and the derivation of a lunar gravity field with data weights of 1 cm for the same beam data. Their findings identified the VLBI data to improve the positions of the sub-satellites, mainly in terms of orbit consistency. Consequently, it increases the accuracy of the 4-way Doppler tracking and indirectly supports the derivation of the gravity field.

4.2.2 Processing SELENE D-VLBI data in VieVS

The SELENE VLBI data that is used within this work was provided by the National Astronomical Observatory of Japan (NAOJ) in Mizusawa. The input data are the differential phase delays $\Delta\tau$, as well as the "final" orbits of Rstar and Vstar, as determined with all available measurements (Range, Doppler, and VLBI) after the end of the mission. Consequently, the critical tasks of correlation and ambiguity solution are not part of the presented work. For the processing, the Vienna VLBI Software (VieVS, Böhm *et al.*, 2012, see chapter 5.4.1) is used after several adaptations for the delay model, the possibility of processing differential VLBI data, and the treatment of moving sources given in a lunar reference system. The differential phase delays $\Delta\tau$ are calculated by differencing the "single" delays of Rstar and Vstar:

$$\Delta\tau = \tau_{Vstar} - \tau_{Rstar}. \quad (4.3)$$

Concerning the delay modeling, there is neither a difference between S-band and X-band observations nor one between same beam and switching data, as the observations are referred to a common epoch during the process of correlation. For the calculation of the single delays, the standard finite distance model was implemented in VieVS following Sekido & Fukushima (2006), as described in chapter 3.2.3. Alternatively, and primarily for control reasons, also the formalisms by Fukushima (1994) and by Klioner (1991) were fully implemented and can be selected by the user. The data used for the subsequent investigations descend from two observing periods, one with only domestic Japanese stations and the other with also intercontinental baselines (figure 4.7):

- October 2008, 17th – 22nd: Japanese VERA stations Iriki (IRI), Ishigaki (ISI), Mizusawa (MZW), and Ogasawara (OGW); 3197 observations, 2% in switching mode.
- January 2008, 12th – 16th: IRI, ISI, MZW, OGW, Hobart (HOB, Australia), Urumqi (URQ, China), Shanghai (SHA, China), and Wettzell (WTZ, Germany); 2766 observations, 45% in switching mode.

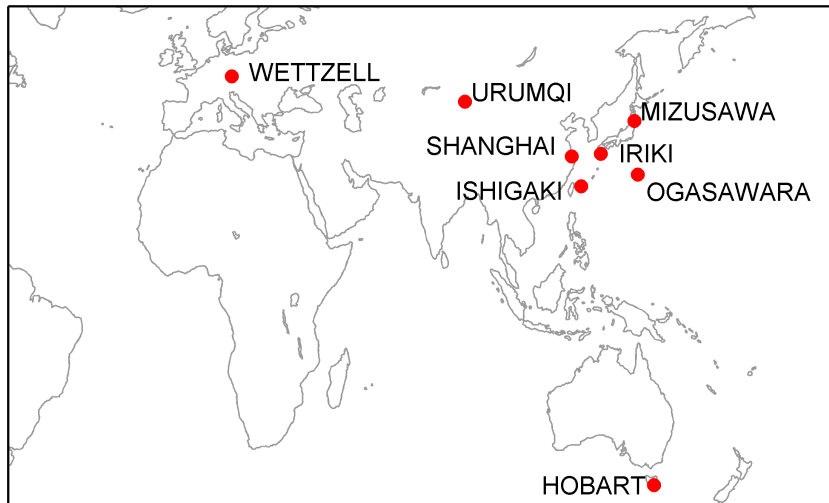


Figure 4.7: Antenna network for the SELENE observations.

In figure 4.8 the temporal distribution of the used data is shown for the two periods, given in number of observations per hour. Observations with contributions of the international stations are printed in pink.

The orbital periods of Rstar and Vstar were about 4 and 2.5 hours respectively (Goossens *et al.*, 2011a). VLBI observations were performed on arcs of 20 to 60 minutes, with an interval of 1 minute for the same beam data and 2 minutes for the switching data. The result of the processing is inspected in terms of residuals, meaning the difference between the observed and

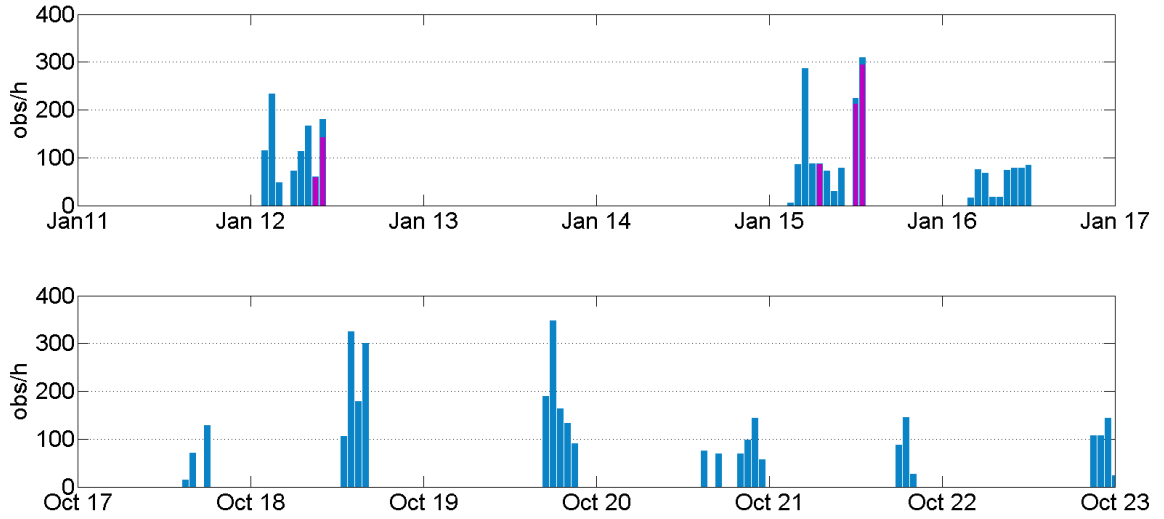


Figure 4.8: Temporal distribution of the SELENE D-VLBI data, given in number of observations per hour in January and October 2008. The international campaigns are printed in pink.

the computed values for the differential delay $\Delta\tau$.

$$\text{residuals} \equiv \Delta\tau_{\text{observed}} - \Delta\tau_{\text{computed}} \quad (4.4)$$

When the VLBI data is included in SELENE orbit determination, biases per pass per baseline are estimated, in order to absorb a) remaining cycle ambiguities that slipped through the correlation and b), to a smaller extent, residual media effects (Goossens *et al.*, 2011a). In VieVS, only ambiguity cycle slips of the S-band carrier ($\lambda_{S_1} = c/2212 \text{ MHz} = 0.135 \text{ m}$) and the group delay ($\lambda_g = c/75 \text{ MHz} = 3.997 \text{ m}$)¹, as determined during the processing, are applied. Possible sources of the remaining signal due to residual media effects are studied in section 4.2.3. In figures 4.9 and 4.10 the obtained residuals after ambiguity solution for the January and October data are shown per baseline, with the separation angle between Rstar and Vstar plotted in the back. For better visibility, and because the absolute time is not important for the following investigations, the black vertical lines indicate bigger time gaps that were cut out. One can see immediately, that the October residuals are slightly better than the January residuals, what is due to the longer international baselines and resultant lower elevation angles on the one hand, and because of the much bigger part of switching data on the other hand. Nevertheless, most of the residuals of both investigated data series are smaller than $\pm 50 \text{ ps}$, respectively $\pm 15 \text{ mm}$. Figure 4.11 shows the distribution of the residuals, divided into classes of 20 ps. On closer inspection, one can clearly identify a systematic signal in the residuals of some passes. That signal was also identified by the

¹The bandwidth of the group delay corresponds to the spanned bandwidth of the S-band carriers, thus $S_3 - S_1 = 75 \text{ MHz}$.

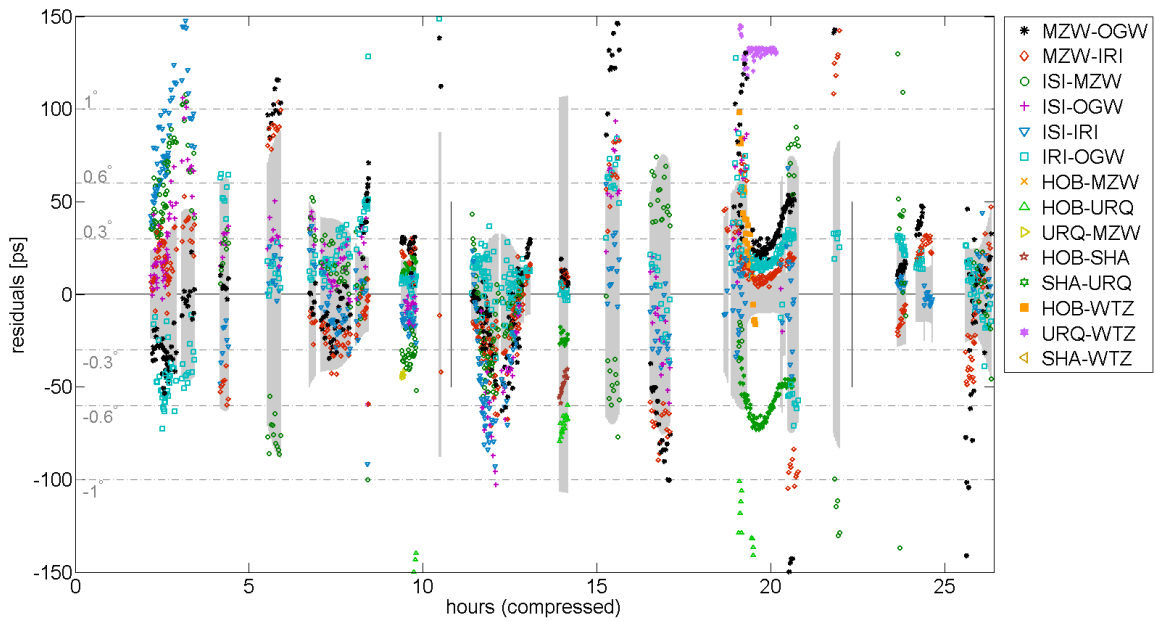


Figure 4.9: January residuals after ambiguity solution. The results are plotted in different colors for each baseline with the time axis interrupted and compressed at the vertical lines. In the back, the magnitude of the separation angle is plotted positive and negative in gray.

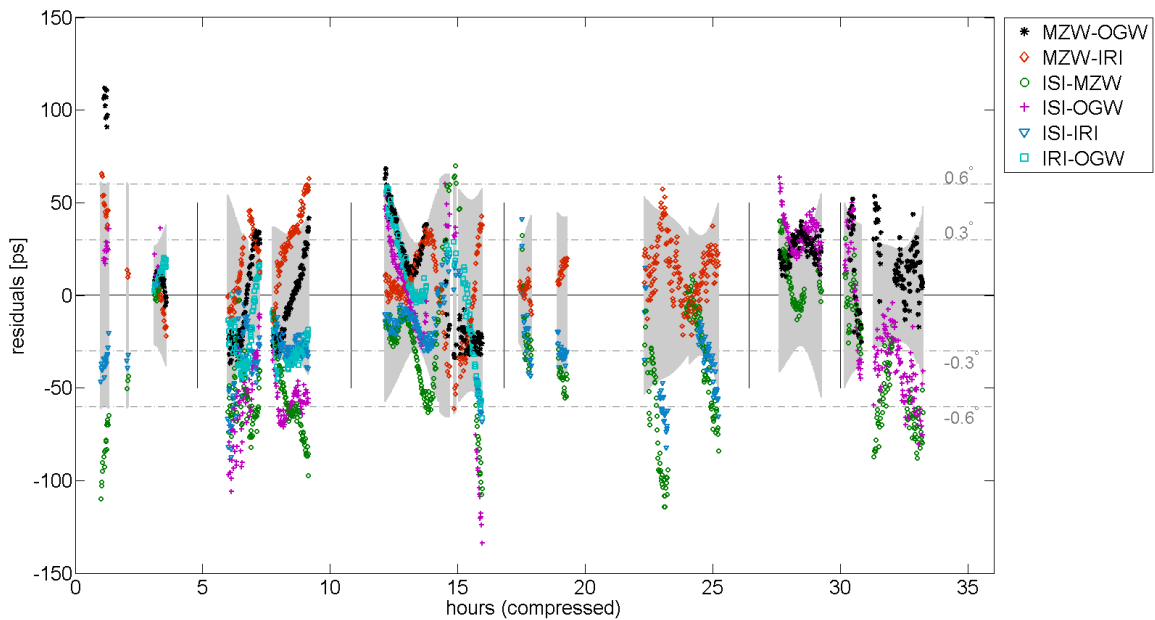


Figure 4.10: October residuals after ambiguity solution. The results are plotted in different colors for each baseline with the time axis interrupted and compressed at the vertical lines. In the back, the magnitude of the separation angle is plotted positive and negative in gray.

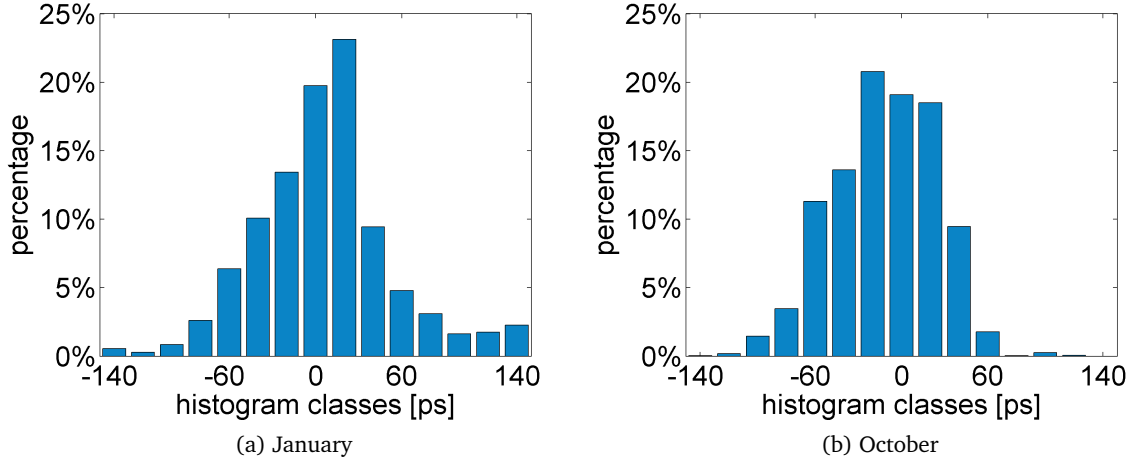


Figure 4.11: Distribution of the residuals, divided into classes of 20 ps.

analysts of the NAOJ (e.g. Goossens *et al.*, 2011a), who finally state that its origin is not directly related to a gravity feature but might rather be some residual orbital signal with the synodic period of the two sub-satellites¹ (Hanada *et al.*, 2010).

SELENE D-VLBI observations were used to support the orbit determination of the SELENE satellites (e.g. Goossens *et al.*, 2011b). In VieVS, the estimation of the relative position of Vstar to Rstar is realized with the partial derivative of the differential delay $\Delta\tau$ with respect to the position of Vstar \vec{X}_V yielding:

$$\frac{\partial \Delta\tau}{\partial \vec{X}_V} = -\frac{\vec{X}_V - \vec{X}_1}{R_{1,V}} + \frac{\vec{X}_V - \vec{X}_2}{R_{2,V}}, \quad (4.5)$$

where $R_{i,V}$ denotes the distance from Vstar to station i . In the case of VLBI-only orbit estimation, one has to respect the sensitivity of the system being restricted to the differential angle between the baseline and the observed sources. Without any constraints, the residuals shown in figures 4.9 and 4.10 result in orbit corrections for Vstar up to the kilometer-level. However, when the distance to the satellite is constrained and only movement perpendicular to the LoS is allowed, results on the order of some meters are achieved (see Plank *et al.*, 2013). This is a reasonable result, as Goossens *et al.* (2011b) determined the orbit errors of Rstar and Vstar to be smaller than 30 m. Nevertheless, these constrained orbit corrections can not explain the present residuals and further D-VLBI-only orbit estimation did not reveal new insights.

¹Using $P_{Rstar} = 4$ h and $P_{Vstar} = 2.5$ h, one gets $1/P_{syn} = 1/P_{Rstar} + 1/P_{Vstar}$ and a synodic period of $P_{syn} = 1.53$ h (Goossens *et al.*, 2011a).

4.2.3 Investigation of residual effects & level of cancellation

This section aims for two goals: for first, the degree of cancellation of errors in certain a priori parameters through the D-VLBI approach instead of standard single-target VLBI is estimated, and secondly it is investigated whether some of the residual effects might be the cause of the remaining signal determined in the section above. Parts of this study are also presented in Plank *et al.* (2013). Concerning the presented investigations to the atmospheric and ionospheric delays, the interested reader is also referred to the work by Liu *et al.* (2009).

The findings are summarized in table 4.2, presenting the empirically determined magnitude of remaining errors in the single delay to one source τ , and in the differential delay $\Delta\tau$. The given values represent the maxima of the majority of the observables, certain extreme values, originating from extremely low elevation or geometrically bad conditions, are given in brackets. The values are mostly given in time delay, the corresponding distance is obtained by multiplication with the velocity of light c . To remember, 10 ps correspond to about 3 mm.

Antenna: Errors in the antenna position can arise from badly determined station coordinates, which might be the case when antennas are used that are more utilized for astronomy than for geodetic observations and consequently did not participate in many experiments that can be used for a precise coordinate determination. But also effects of the antenna itself or other station dependent errors fall into this category. An error of $\pm 0 - 5$ cm in xyz -directions is added randomly at each station for every observation, what results in an error of up to 300 ps in τ for the given observations. After differencing between the two sources, this station-induced error reduces to 1 – 2 ps at most. Considering the correlations with other parameters of the observation, it can be said that the error slightly reduces with increasing baseline length but is fairly independent from the separation angle between the two targets.

Orbit: In order to investigate the effect of errors in the a priori orbit, the position of one satellite is changed for $\pm 0 - 20$ m in xyz -directions. While this results in errors of 300 ps with extremes up to 3 ns in τ , the effect in $\Delta\tau$ is only 1 – 10 (25) ps. The size of the error is direct proportional to the length of the baseline and, in case of $\Delta\tau$, the error also linearly increases with the separation angle.

EOP: In conventional tracking, badly determined Earth Orientation Parameters are directly translated into spacecraft angular position errors. In D-VLBI, the demands are a little bit lower. For the SELENE data set, the EOP were changed randomly for every observing epoch up to $\pm 5 \mu\text{s}$ in $dUT1$, $\pm 200 \mu\text{as}$ in polar motion x_p and y_p , and $\pm 300 \mu\text{as}$ in the celestial pole offsets dX and dY . This results in errors of 2 ps with extremes up to 30 ps in τ . The effect for the differential observable $\Delta\tau$ is linearly proportional to the separation angle, but stays below 0.2 ps for all investigated observations.

Relativity: The term relativity here stands for the entire theoretical delay modeling, including the necessary transformations between the various time and space reference sys-

tems. In order to get some redundancy, the modeling was implemented following three different recipes for VLBI observations to sources at finite (lunar) distance, namely Sekido & Fukushima (2006), which is described in section 3.2.3, Fukushima (1994), and Klioner (1991). The results in τ between the formalisms by Sekido & Fukushima (2006) and Fukushima (1994) are equivalent at the order of $(V_E/c)^2$, about 100 ps at maximum. The deviation to the implementation following Klioner (1991) is a bit bigger and amounts up to 400 ps. In $\Delta\tau$, these errors are reduced to 1 – 4 ps and, as shown in figure 4.12, are

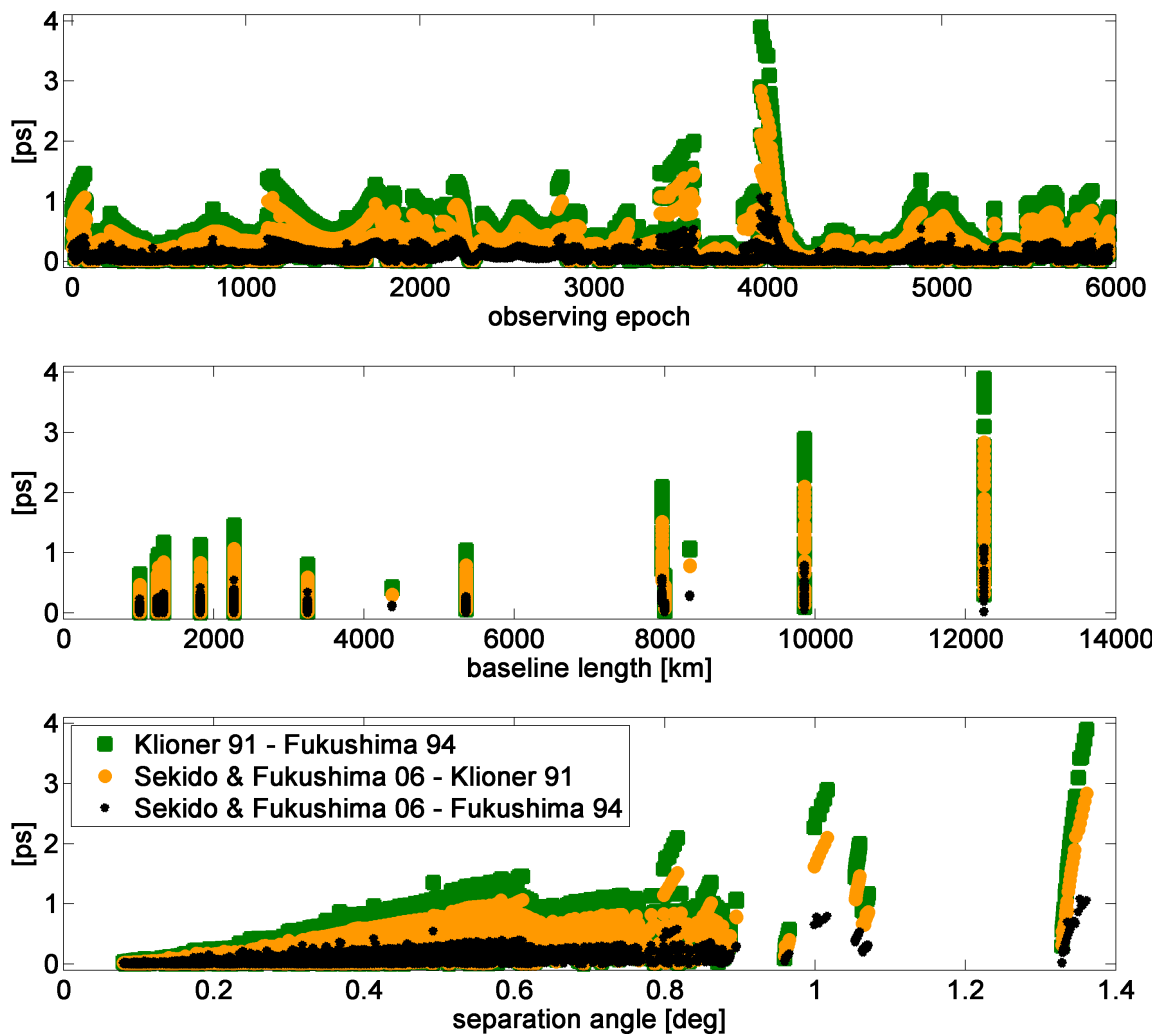


Figure 4.12: Divergence in $\Delta\tau$ of three implemented delay models for each observation (top) and versus baseline lengths (middle) respectively the separation angle (bottom).

directly proportional to the baseline lengths and separation angles. It is important to state that only a part of the differences between the models comes from the theory itself, the other part emerges from operations that are not treated in the respective literature¹ and

¹E. g. the model of Fukushima (1994) is given in TCB time scale and the corresponding transformations to TT

might reflect errors induced by imperfect implementation.

To sum up the geometrical error sources of the antenna, the orbit of the sources, and the EOP as well as errors in the relativistic delay modeling, a factor of cancellation of about 100 is found. With remaining signals < 10 ps (≈ 3 mm), these geometric effects are almost totally canceled and can be neglected in the following search for alternative contributors to the residuals.

This is not true for errors introduced by the atmosphere. In case of atmospheric delay a new parameter becomes increasingly important, namely the elevation angle of the observation. About 90% of the observations were taken at elevations above 20° , only for a few observations, especially those with the intercontinental baselines, the elevation angles decrease to 10° or even 5° . Of course, the strong correlation with the separation angle remains valid.

Hydrostatic troposphere, a priori: The total hydrostatic tropospheric delay that is modeled a priori following standard VLBI analysis (see chapter 3.1.3) amounts up to 10 ns, respectively 60 ns for very low elevations. Generally, the above determined factor of cancellation of 100 also applies here, though certain maxima in $\Delta\tau$ are found around 1 ns. Hydrostatic atmospheric delays, neglecting turbulent effects, are assumed to be modeled a priori very accurately. As possible errors are even scaled down by a factor of 100, this source can be deleted from the list of causes for the remaining residuals.

Wet troposphere: The influence of the wet part of the troposphere usually has to be estimated in VLBI analysis. As here only the o-c values are investigated, this is not done in the present SELENE D-VLBI processing with VieVS. In order to estimate its scale, the effect in τ and $\Delta\tau$ is calculated using a priori estimates for the zenith wet delays and the wet mapping functions as available with the Vienna Mapping Functions (Böhm *et al.*, 2006). Absolutely, the wet troposphere delays the signal for about 1 ns, at very low elevations for up to 4 ns. Due to the narrow separation angle this effect widely reduces to < 2 ps and can be neglected. Only at the very low elevation angles on the intercontinental baselines the wet troposphere can influence the measurements critically, and in these cases it might explain some of the residuals of figures 4.9 and 4.10.

Tropospheric turbulence: As already pointed out earlier in this work, tropospheric turbulence causes short-term fluctuations in time and spatial domain. Following the approach already used in section 4.1.3, the effect of the residual slant wet delay versus azimuthal separation is shown for three elevations in figure 4.13. In the left figure (a) simulations are done for same beam observations (sb), i.e. there is no time component, and the effects are relatively small (a few picoseconds). On the right (b), the switching interval of the switching (sw) data (60 seconds) is included, resulting in a considerably bigger effect of 10 – 20 ps. In combination with separation in elevation, residual errors due to the wet troposphere might explain some of the residuals of the processing; especially at low elevations. Under cer-

scale are not treated explicitly.

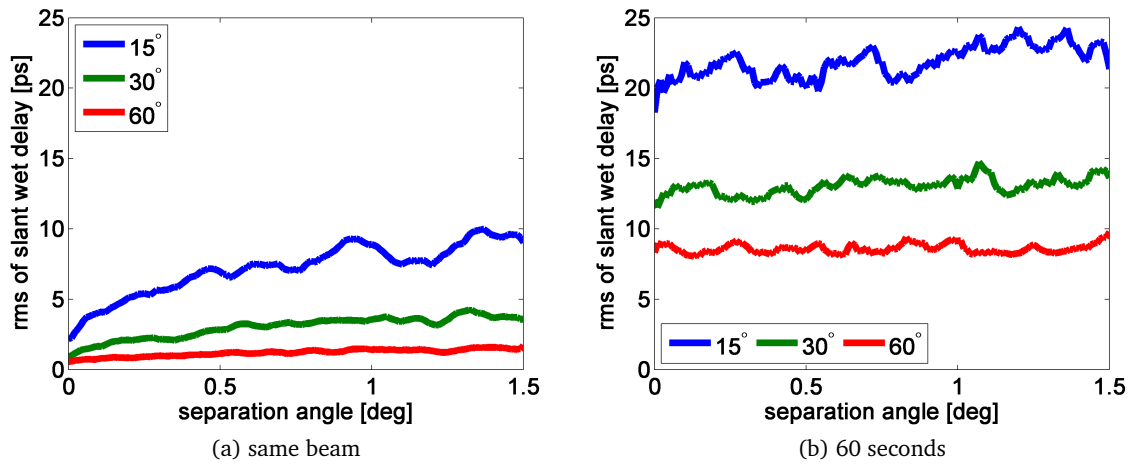


Figure 4.13: Simulated rms of the slant wet delay in dependence of the azimuthal separation angle for (a) same beam observations and (b) a switching interval of 60 seconds. The effect is calculated for observations at an elevation angle of 15° (blue line), 30° (green), and 60° (red).

tain circumstances, tropospheric turbulence can also corrupt the successful measurement itself. Therefore, Kikuchi *et al.* (2008) defined minimum elevation angles for the SELENE observations to avoid a possible failure.

Ionosphere: Moderate ionospheric fluctuation is a stringent requirement for the successful derivation of the differential phase delay observable. Long-term variations can be eliminated when observations in S-band and X-band are available. However, when only S-band same beam observations are made, the ionosphere is not treated separately and might not get fully canceled through differencing between Rstar and Vstar. Following Tierno Ros *et al.* (2011), this residual effect is determined by using GNSS-derived maps of the total electron content (TEC). For the SELENE observations, absolute errors of 500 ps are found, which scale down to 5 ps in the residual delay. For a few observations extremes reach 5 ns in τ and respectively 20 ps in $\Delta\tau$. When comparing these residual errors with the observations, one has to remember that for phase observations the signal is accelerated rather than delayed.

To sum up the residual differences in the atmospheric delays, it can be stated that errors in particular due to the ionosphere and the wet troposphere can be of significance in the processing. However, attempts in applying adequate corrections for these effects were not too promising. While the calculated corrections decrease some of the large residuals to a minimum, some other observations get enlarged. Reason for this could be that the errors of different origin nearly cancel in the original processing and when applying an actual correction, the cancellation vanishes and the other errors remain. Further, tropospheric turbulence could not be corrected, as the investigations above rely on simulations only.

In the end of this chapter, some final conclusions of the performed SELENE D-VLBI processing

Table 4.2: Effect in the calculated τ and $\Delta\tau$ due to varying a priori parameters. The values represent the maxima of the observables' majority, particularly extreme values are given in brackets. When distinguished, *sb* stands for the same beam data and *sw* for the switching data.

	τ	$\Delta\tau$
GEOMETRY		
Antenna ± 5 cm	300 ps	1 – 2 ps
Orbit ± 20 m	300 ps (3 ns)	1 – 10 (25) ps
EOP	2 (30) ps	< 0.2 ps
<i>dUT1: 5 μs/x_p, y_p: 200 μas/dX, dY: 300 μas</i>		
RELATIVITY		
Divergence of implemented delay models	100 – 400 ps	1 – 4 ps
ATMOSPHERE		
Hydrostatic troposphere, a priori	< 10 (60) ns	< 100 ps (1 ns)
Wet troposphere, ECMWF	< 1 (4) ns	< 2 (40) ps
Troposphere turbulence	-	< 10 (sb) 25 (sw) ps
Ionosphere, TEC-maps	500 ps (5) ns	5 (20) ps

shall be drawn: the SELENE data could be used to successfully verify the option of processing D-VLBI data in VieVS. With the high precision of the measurements, errors causing residuals larger than a few picoseconds could be identified and removed. Then, using the observation setup of the SELENE data, the effect of possible poor modeling on the residuals and the level of cancellation when using differential rather than conventional, single target, VLBI was investigated. Geometrical modeling is traditionally done very carefully in geodetic VLBI, but due to the high level of cancellation, it can be said that it is of minor importance in D-VLBI and no room for improvement could be identified in that area. This is different for the omnipresent media delays, which cause errors right at and slightly above the level of accuracy of the measurements. To account for this, it can be a good idea to install additional methods to scan the troposphere and to precisely determine the ionospheric disturbances parallel to possible future D-VLBI observations. In the case of SELENE, however, the most prominent residuals can not be related with a cause investigated within this work, strengthening the thesis of an unmodeled orbital signal, e.g. due to solar radiation pressure (Goossens *et al.*, 2011a).

Chapter 5

VLBI satellite tracking

VLBI satellite tracking is the simultaneous observation of a signal emitted on board of a satellite with at least two antennas on Earth (fig. 5.1). The reasons to apply this technique are manifold (sec. 5.1): starting with the purposes of orbit determination, navigation and Earth surveying in the past, VLBI observations to satellites have served to prove the concept applied in various (deep) space missions or they were proposed to support the GPS system in the critical task of phase center determination. Today this technique is more and more mentioned in the context of reference frames, either for establishing a direct link between terrestrial systems, realized e.g. by the GNSS-satellite orbits, with the quasi-inertial ICRF, or for improving the consistency of the ITRF through a thorough connection of the various space geodetic techniques, e.g. in terms of space ties. Despite a multitude of applications, VLBI satellite tracking has not been performed on a routine basis yet. There are still a number of open questions, with some of them being treated here.

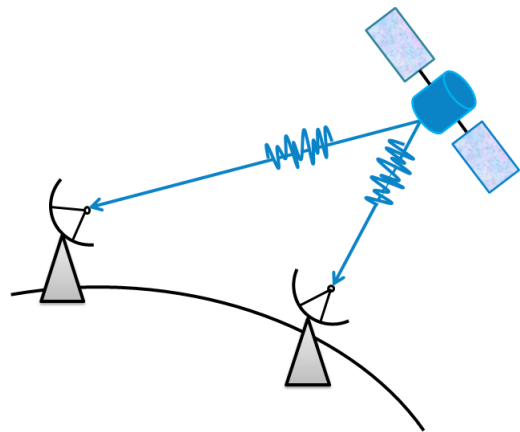


Figure 5.1: VLBI satellite tracking.

In the beginning of this chapter (sec. 5.1) an overview of the various (future) applications of VLBI satellite tracking is given, actually representing additional justification for this work. In section 5.2 the GRASP concept is introduced, the probably most complete study for the realization of VLBI satellite tracking at the moment. The most important issues in terms of the technical realization of such observations are treated in section 5.3, with explicit studies on shared visibility (5.3.1) and antenna slewing (5.3.2). In section 5.4 the *VieVS₂tie* software is introduced, a VLBI analysis software capable to simulate and process VLBI observations to satellites. The expositions there include the formalism for the satellite delay model (5.4.3) as well as a description of the *VieVS* simulator that is used to derive the results of chapter 6.

5.1 Motivation and previous work

The idea of observing artificial Earth satellites with interferometric methods is not a completely new one. Soon after the development of VLBI, a series of applications to satellites were presented and implemented. This includes the tracking and orbit determination of synchronous satellites (e.g. Preston *et al.*, 1972; Rosenbaum, 1972), or the use of interferometer terminals for Earth surveying (Counselman & Gourevitch, 1981). The advance of GNSS and improvements of alternative tracking methods pushed this concept into oblivion, before it was rediscovered in the recent years. In preparation for the VLBI tracking to their lunar probes SELENE and Chang'E, Japanese and Chinese tracking teams tested the mostly newly developed hardware and software also with observations to near Earth orbiters and satellites (e.g. Hanada *et al.*, 2008; Huang *et al.*, 2006). Following the successful application in the space missions (see chapters 3.2 and 4.2), now the VLBI-tracking shall be used for precise orbit determination of geostationary satellites, e.g. of China's COMPASS/BeiDou satellite navigation system (Huang *et al.*, 2011).

In geodesy, and disregarding the immediate goal of improved orbit determination, the driving force behind is the improvement of reference frames. In particular, the tie between the quasi-inertial CRF and some TRF, as e.g. determined by space geodetic techniques, is of interest. This interaction is the topic of the IAG Sub-Commission 1.4¹, with, amongst others, the objectives to *analyze VLBI observations to GNSS satellites* and to *simulate future micro satellite missions like GRASP in VLBI analysis software packages*. In principle, one can distinguish between two possible scenarios for VLBI satellite observations:

- Use available infrastructure, e.g. satellites of the GNSS. Most space geodetic techniques use microwave signals either for communication or for the measurement itself. If one can observe such signals with VLBI, this would enable a rigorous connection of e.g. GNSS with VLBI on the one hand, and, on the other, would do without new hardware in space and hence would be rather cost-saving.
- The other option is the launch of a new satellite, carrying a VLBI transmitter in addition to sensors of the other space geodetic techniques, like GNSS, SLR, and DORIS. In this case one has the advantage to choose the best signal in advance and to precisely locate the antennas of each technique aboard the satellite relative to each other.

Hase (1999) proposed the observation of GPS satellites with VLBI, with the goal to tie the satellite transmitters of the GPS system directly to the ICRF. This approach would also enable direct access to the Earth's center of mass determined in the ICRF, which is not possible with classical VLBI (Dickey, 2010). With VLBI tracking of GLONASS satellites at L-band, Tornatore *et al.* (2011a,b) successfully demonstrated the technical realization of such observations, with further developments in that area to be expected.

¹<http://iag.geo.tuwien.ac.at>

The second idea is followed in the mission concept GRASP (Bar-Sever *et al.*, 2009, see section 5.2), where a VLBI transmitter is mounted on a satellite platform together with components of other space geodetic techniques, acting as a highly precise space tie. A mission idea that is followed by several groups at the moment and which might be realized in one way or another in medium-term.

Building on a different way of operation but worth mentioning in this context is the GPS-VLBI Hybrid system (Kwak *et al.*, 2010). Here, GPS signals received by standard GPS antennas, are recorded and correlated in general VLBI way, enabling the combination of GPS and simultaneously recorded VLBI data at observation level.

5.2 GRASP

The Geodetic Reference Antenna in Space (GRASP) is a micro satellite mission concept dedicated to the enhancement of all the space geodetic techniques, and promising revolutionary improvements to the definition of the Terrestrial Reference Frame (TRF), its densification, and accessibility (Bar-Sever et al., 2009).

GRASP was proposed to NASA in 2011 and, though not granted yet, the mission concept was found to be good and might be realized in the future with slight modifications and international partnerships (Bar-Sever, personal communication 2012). In this work GRASP serves as a probable application of satellite VLBI, representative for other similar mission concepts under development, e.g. MicroGEM at the GeoForschungsZentrum Potsdam¹ (Brieß *et al.*, 2009). The key-technique of GRASP is the co-location of sensors for all the space geodetic techniques contributing to the TRF, namely GNSS, SLR, VLBI, and DORIS. A careful a priori calibration of the sensors and the entire satellite platform, the simplicity of the spacecraft itself without any moving parts, and the orbit configuration shall enable a spacecraft orbit determination with 1 mm absolute accuracy and 0.1 mm/year stability for the mean radial component (Nerem & Draper, 2011). GRASP will serve as a geodetic fundamental station in space with inter-technique ties exceeding those of existent co-location sites and enable the derivation and dissemination of a new TRF meeting the demands of GGOS. In principle, all sensors and measurement concepts are well tested through the employment on other satellites, except the VLBI instrument. For this, technology from the past GRAIL² mission shall be inherited for GRASP, transmitting signals in S-band and X-band that can be tracked by all geodetic VLBI sites (Nerem & Draper, 2011). This yields basically two observing modes: for first, real VLBI observations with multiple ground antennas, on the condition of common visibility, and for second, the observation of GRASP with a single VLBI telescope, what would correspond to a one-way integrated Doppler measurement.

¹MicroGEM is a feasibility study for future GNSS-remote sensing satellites of the GeoForschungsZentrum (GFZ) Potsdam. The concept, that in the meanwhile has been prolonged under the names "NanoGEM" and "NanoX", also includes a VLBI transmitter aboard the satellite.

²Gravity Recovery and Interior Laboratory; e.g. www.nasa.gov/grail/

Within this study, only the first option is treated. Once realized, GRASP shall produce weekly TRF realizations, consistently combining data from all involved techniques. Applying the second way of observation, simulations of VLBI point-positioning revealed station positions determined better than 1 cm using seven days of GRASP tracking (Nerem & Draper, 2011). Corresponding simulations for the VLBI mode were not done so far.

5.3 Technical aspects

The focus of the present work is on the geometrical point of view, as well as on the investigation of expected accuracies, under consideration of the most important stochastic error sources of geodetic VLBI today. Certainly, VLBI observations to satellites involve a number of further obstacles, mainly of technical origin. Some of them are briefly discussed here.

Let's start with the signal. In contrast to the broadband, noise-like signal emitted by natural radio sources, artificial sources on satellites by definition are limited in bandwidth. If one can design a dedicated signal on a satellite, different concepts need to be considered, as the broad range of realizations of VLBI spacecraft tracking (chapt. 3.2.2) shows. Whatever concept is chosen, attention should be paid on good compatibility with the common geodetic VLBI sites and also the future VGOS system. When a signal is utilized for VLBI that was originally designed for a different purpose, e.g. for communication or ranging, the technical realization might become even more complicated. In the case of GNSS for example, the transmitted signals are in L-band and hence below the usual S-band frequencies of the IVS receivers. Consequently, one has to find antennas with L-band receivers, as was done in the experiment by Tornatore *et al.* (2011b), with the precaution of signal attenuation. This is necessary because the GNSS signals are much stronger than the usually observed radio sources and the sensitive hardware would be endangered getting destroyed (Tornatore & Haas, 2009). The other possibility is to use the common receiving systems that are optimized for S-band and X-band observations and test if some of the strong L-band signal can slip through. In this case, the sensitivity in L-band is extremely low, and some changes, as e.g. additional amplifiers, are required in the signal chain¹. Investigations on the observability of GNSS signals were done e.g. by Tornatore & Haas (2009) and Hase (1999), with the latter one explicitly mentioning the issue of phase center determination. In the case of GPS, the center of phase, where the received signal is emitted, and the center of mass of the satellite, to which the orbit determination is referred to, are offset by more than one meter. Additionally, the orientation of this eccentricity vector varies with time. Studying the possibility of mapping these phase centers of the GPS satellites with VLBI was the purpose for installing the IVS Working Group 1 (WG1) on GPS Phase Center Mapping. Following the discussions within WG1², one learns of an additional obstacle for observing the GPS signal with VLBI. This is the

¹U. Schreiber and J. Kodet from Wettzell Observatory and Technical University Munich are working on a hardware realization of L-band observations (personal communication).

²available at <http://ivscc.gsfc.nasa.gov/about/wg/wg1>

fact that the GPS signal, enabling a beam coverage of the whole globe, is generated in a phased antenna array rather than ideally transmitted from a compact antenna. As a consequence, the signals received at different VLBI antennas might not be leaving the transmitter aboard the GPS satellite with identical phase from one center.

Besides frequency and signal power, the actual tracking of the satellites is a point to examine carefully. Shared visibility, a prerequisite for VLBI observations, and antenna slewing are described in more detail in the sections below (5.3.1 and 5.3.2).

Concerning the method of D-VLBI applied for satellite-tracking, some thoughts were already mentioned in the previous chapter (4.1.3). Despite the advantage of cancellation of errors, the parallax on the satellite between the two ends of the baseline is rather big. This means that if a reference source is in line with the satellite for one station, it is several degrees away from the satellite for the other station. In the case of GPS, for a baseline of 6000 km with one station observing the satellite in zenith direction, according to figure 4.3, the parallax will be about 15° for the other station. Additionally, when the reference source, i.e. the weak quasar, is observed close to a GPS-satellite, it might happen that the strong GPS signal leaks into the weak quasar signal, corrupting the measurement. Consequently, the D-VLBI technique in VLBI satellite tracking is not part of the present thesis. In the course of this work, all investigations to VLBI satellite tracking are done for "single-target" mode VLBI, meaning that there is only one target observed by a station at one time epoch.

A last point, what one should keep in mind, is the availability of the antennas. Geodetic VLBI works on the basis of collaboration between countries and research facilities all over the world, coordinated by the IVS. Whenever VLBI observations are performed, one needs at least two antennas (preferably at different sites), meaning at least one partner antenna. Hence, also for test observations a careful planning and a certain lead time is required.

5.3.1 Shared visibility

Satellite VLBI only works on the condition that the target satellite is in shared visibility from the observing stations. In particular the height of the satellite, together with its orbit characteristics, decide about the possibility of VLBI observations. The second restriction is given by the available network of VLBI antennas that are capable to observe the satellite. In the following, the common visibility for two stations with various baseline lengths in dependence on the satellite height is calculated, with the underlying two-dimensional geometrical concept shown in figure 5.2: the maximal separation of two stations (baseline length b), where a satellite at height h can still be observed is achieved when the satellite is above the midpoint of the baseline. Following the fig-

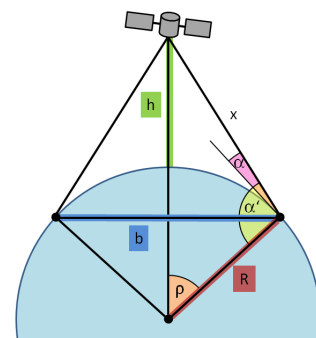


Figure 5.2: Geometrical relation between the maximum baseline length b and the satellite height h .

ure, the sine of ρ equals the ratio of half of the baseline b to the mean Earth radius $R = 6371$ km. The law of cosines relates the auxiliary variable x to the known parameters and applying the rule of sines then gives the angle α' . The maximal elevation angle α , under which the satellite can be seen from both stations is finally generated by subtracting $\pi/2$ from α' . Figure 5.3 illustrates the result for baseline lengths from 100 km to the Earth's diameter and satellite heights from 500 to 20000 km. For a better understanding, the relation for the 7 selected satellite heights written next to the colorbar is shown with gray lines. Hence, a satellite at 2000 km can be observed from two stations with a maximal separation of 8000 km, though under very low elevation of a few degrees only. For a cut-off elevation of 15° , a maximum baseline length of 6000 km is possible.

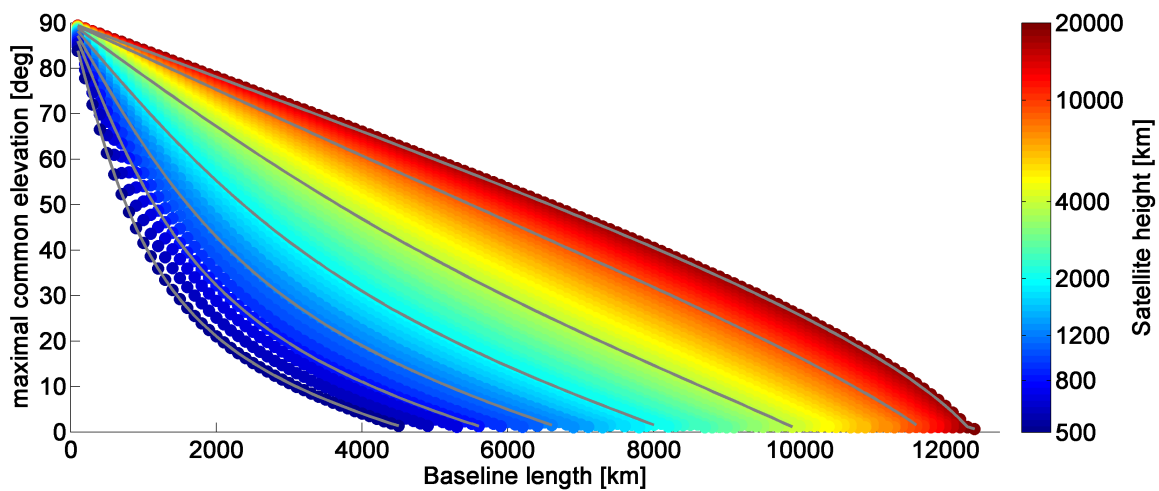


Figure 5.3: Common visibility for various baseline lengths in dependence of the satellite heights. The gray lines indicate the relation for the satellite heights written next to the colorbar.

5.3.2 Antenna slew speed

In geodetic VLBI, the pointing direction of an antenna needs to be corrected for Earth's rotation constantly during an observation. At a maximum, this correction amounts to 0.25° per minute. More important than the tracking is a fast switching between sources in different directions, which is the reason that pure geodetic VLBI antennas are usually faster than antennas designed for astronomical purposes. The currently used IVS VLBI system includes antennas with slew speeds of about $0.4 - 3^\circ$ per second and the target for the upcoming VLBI2010 antennas lies at $6 - 12^\circ$ per second (Schuh & Behrend, 2012).

When observing satellites, the antennas must be capable to follow the satellite on its way through the sky. Hereby, predominantly the height of the satellite is decisive for its speed, meaning that low satellites cross the sky faster than high satellites. Ignoring the ellipticity of the orbit and assuming constant velocity, at lower elevations a lower tracking speed is needed than at higher elevations. With the target getting close to zenith direction, the demands, especially for slew rates in azimuth, increase rapidly. While the tracking normally should not be a problem for

the quite slow satellites of the GNSS (Tornatore & Haas, 2009), in the case of lower satellites, fast antennas are required. In figure 5.4, the necessary slew rates are shown for the four satellites that are used in chapter 6 of this work, with the working names *GPS*, *LAGEOS*, *GRASP2000* and *GRASPELL*. The corresponding orbital parameters can be found in table 6.1. What is shown in

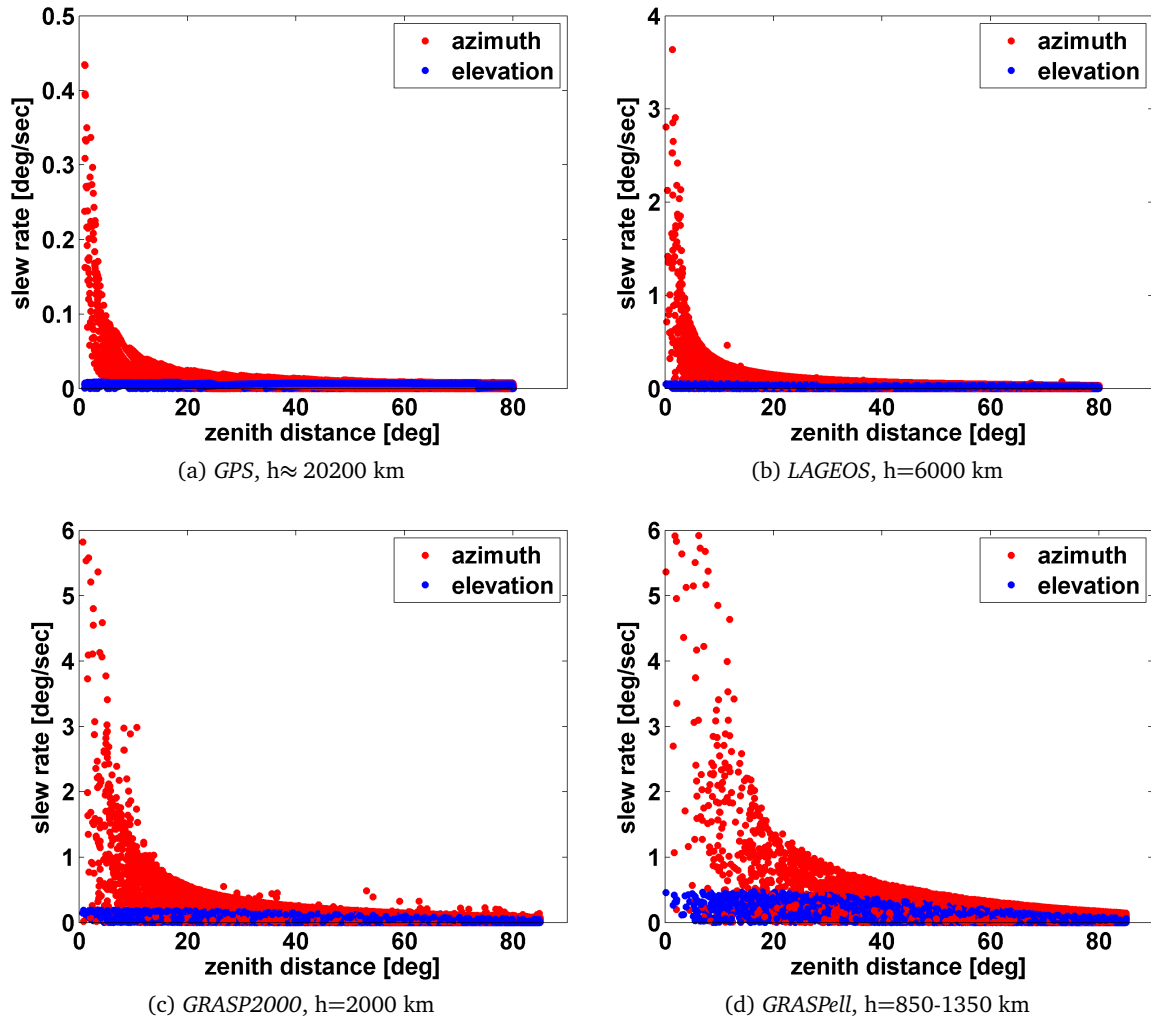


Figure 5.4: Antenna slew rates in azimuth (red) and elevation (blue) that are needed for the observations presented in chapter 6.

figure 5.4 are the slew rates calculated for almost all investigated schedules of chapter 6, plotted versus the corresponding zenith distance of the observation. Hereby, the elevation range goes from $0 - 90^\circ$, while the azimuthal turn is unlimited. It has to be noted, that the slew speed is calculated on the basis of the distinct observation epochs, without taking care of the antenna movement during the observation. Rather uncritical is the needed slew speed in elevation, revealing maximum values of $0.01^\circ/\text{s}$ for *GPS*, $0.05^\circ/\text{s}$ for *LAGEOS*, $0.2^\circ/\text{s}$ for *GRASP2000* and $0.5^\circ/\text{s}$ for the *GRASPELL* satellite. Different is the situation for the azimuthal slew rates. While it is no problem to observe *GPS*, *LAGEOS* or *GRASP2000* at low elevations, with decreasing zenith

distance the maximum needed slew rate increases rapidly. For *GPS* this increase starts at a zenith distance of about 5° , with a maximum slew rate of $< 0.5^\circ/s$ for observations up to an elevation of 89° . Slew speeds of $0.5^\circ/s$ might be needed for observing *LAGEOS* at 6000 km above ground already at 80° elevation. When observations are done even closer to the zenith, antennas with azimuthal slew speeds of up to $4^\circ/s$ are needed. For the lower *GRASP2000* satellite at 2000 km and the elliptical orbit of *GRASPELL* with heights between 850 and 1350 km, maximum slew rates of $6^\circ/s$ will be needed. For these satellites high slew speeds are also necessary for tracking at lower elevations, i.e. *GRASP2000* crosses the $1^\circ/s$ -border at a zenith distance of 20° , *GRASPELL* at 30° .

In conclusion, figure 5.4 shows that the maximum needed slew speeds for observing the investigated schedules in some cases lie above the capabilities of nowadays standardly used antennas. But even for the future VGOS antennas, the feasibility of such scheduled VLBI observations needs to be examined thoroughly for each antenna prior the actual observation. The considerations above only give the angular change between two consecutive observations in azimuth and elevation. This is adequate for antennas with their two axes mounted in azimuth and elevation directions, but does not give information for the tracking with antennas of a different design, e.g. with hour angle-declination mount. Further, as e.g. pointed out by Sun (2013), for a precise calculation of antenna slewing times, in addition to the axes' velocities also their abilities in acceleration has to be considered.

Besides the assessments based on artificial schedules above, there are additional matters for the practical realization of VLBI satellite tracking. In a mature scheduling tool, possible complications due to cable wrap have to be considered. In practice, antennas cannot move unlimited in one direction, but they are restricted to cable lengths (azimuth) or mechanical reasons (elevation). This means, that when a satellite is tracked at high elevation close to zenith, at some point the antenna might not be able to go further overhead and needs to turn for 180° in azimuth and continue within its feasible elevation window. It is also possible that certain antennas are not capable to observe directly into zenith direction or within an area close to it.

All these practical issues are not included in the scheduling within this thesis and are subject of a corresponding extension of the scheduling tool. As complications mostly appear for observations close to zenith, it might also be useful to exclude observations in a certain area around the zenith direction of each antenna.

As a last point concerning the tracking, the actual realization in the antenna's operation system shall be mentioned. VLBI antennas are able to correct for Earth rotation automatically, but they are usually not capable of following satellites. Hence, Tornatore *et al.* (2010) recommend the installation of a satellite tracking module in the VLBI field system as e.g. realized by Moya Espinosa & Haas (2007).

5.4 VieVS₂tie

The necessary software used for the studies described in this work is mainly newly created, and primarily consists of adapted parts of the Vienna VLBI software VieVS. They are united in the general heading *VieVS₂tie*.

5.4.1 Vienna VLBI software VieVS

The Vienna VLBI software VieVS (Böhm *et al.*, 2012) has been developed at the Vienna University of Technology since 2009. It is written in the commercial programming language MATLAB, whose huge number of in-built functions for mathematical operations eases the understanding and modification of the code tremendously. VieVS represents a complete state of the art geodetic VLBI software suitable for the routine matters of scheduling, geodetic processing or the derivation of geodetic parameters, exactly the same as for research tasks like the generation and testing of new models and analysis strategies. VieVS is operated through a graphical user interface, where all parts of the software are integrated. This includes the scheduling of observations (*Vie_{sched}*– Sun, 2013), the data read in, the calculation of the theoretical delay (see chapter 3.1), the parameter estimation (*Vie_{ism}*– Teke, 2011), the determination of global parameters, a TRF or a CRF within a global solution (*Vie_{glob}*– Krásná *et al.*, 2013), as well as a plotting tool for an ad hoc interpretation of the results. For more information about VieVS the reader is referred to <http://views.geo.tuwien.ac.at> and the documentation there.



Figure 5.5: Vienna VLBI software.

5.4.2 Satellite tracking in VieVS

Starting from VieVS Version 2.0, adaptations are done in order to schedule, simulate and process VLBI satellite observations in *VieVS₂tie*. It is not intended to give the full source code here, but the main changes and strategies for their implementation shall be described in this section briefly. Comprising the most important steps of the delay calculation, a flowchart of the developed program is shown in figure 5.6.

As no real observations are used within this work, in the beginning one needs to create an observation file. Therefore, an independent routine was created that enables the scheduling of VLBI satellite observations. Starting from an antenna network and a satellite orbit, the scheduling is based on shared visibility only, neglecting any constraints due to signal strength, antenna characteristics or slewing times. Hereby, the stations are chosen from standard TRF catalogs and the orbit data is available via standard sp3 files in the case of GNSS¹ or ASCII-lists of satellite

¹Orbit data for the GNSS satellites can be downloaded from the IGS (Dow *et al.*, 2009) in the standard sp3 format (e.g. <http://igsb.jpl.nasa.gov/igsb/data/format/sp3c.txt>)

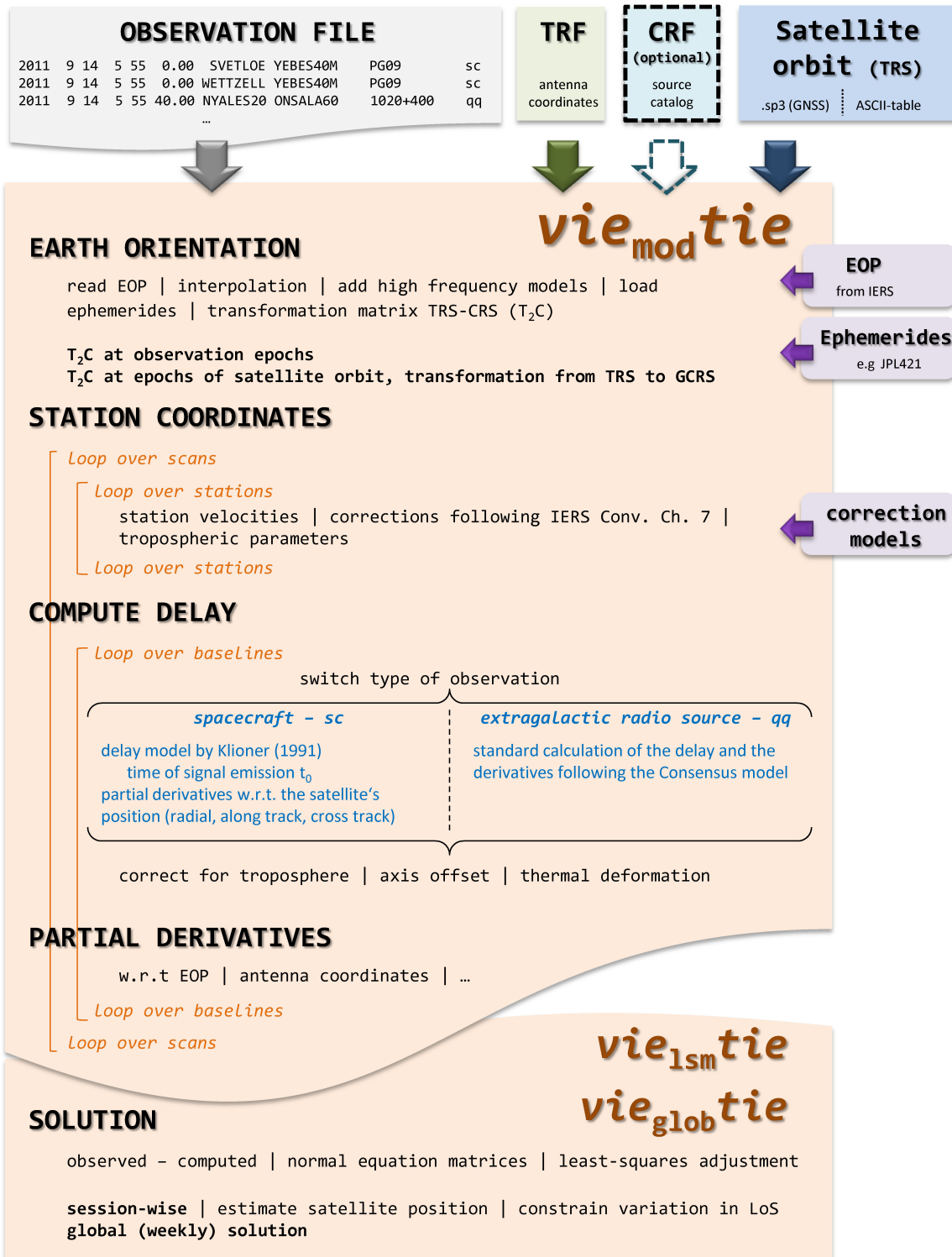


Figure 5.6: Flowchart of the developed program VieVS₂tie.

positions. Result from the scheduling is an observation file containing for each observation the observation time, the observing stations, the source name and the source type. In the case of combining VLBI satellite observations with classical VLBI (as is done in chapter 6.4.1), the standard Vie_{sched} can produce the same format, with the observation type qu for the classical quasar observations while observations to spacecrafts or satellites are of type sc . The format of the observation file can be seen in the upper left of figure 5.6. This file is then read by the VieVS software, replacing the otherwise used ngs-card files. The actual calculation of the delay happens in the program $Vie_{\text{mod}}tie$, following the flowchart given in figure 5.6. In a first step, the Earth orientation is computed using the corresponding tables provided by the IERS and applying standard high frequency models. This is done for all observing epochs, respectively scans, as well as for the epochs at which the satellite orbit is given. Once the T_2C matrices are built, according to equation (2.16), the orbit data that is initially given in some TRS can be transformed to the GCRS. In this step, also the positions of the Earth and the other solar system bodies, as provided by the ephemerides, are loaded for each observing epoch. At this point, a loop over all scans, respectively observing epochs, is started. Following equation (2.15), the actual antenna positions are calculated applying plate tectonics and a number of geophysical models as listed in the IERS Conventions (Petit & Luzum, 2010, ch. 7). The calculation of the theoretical delay is done in a loop over all baselines, respectively observations, per scan. For each observation it is distinguished between the two types, applying standard VieVS analysis for qu -observations and running the newly implemented satellite-delay model for sc -observations. In the latter case, the model by Klioner (1991), as described in the next section (5.4.3), is used. Main new features compared to the standard Consensus model (sec. 3.1.2) are the calculation of the time of signal emission at the satellite t_0 and the calculation of the partial derivatives of the delay with respect to (w.r.t) the satellite's position in radial, along track, and cross track components. This is done following equation 4.5, or, for higher accuracies is obtained by the derivative of the delay model, described in the next section, with respect to the source position. Identical for both types of observations is the delay due to the troposphere, the antenna axis offsets and due to thermal deformation. In a last step, all further partial derivatives, e.g. w.r.t. antenna coordinates and EOP are calculated.

Using real observations or following a simulation procedure as described in section 5.4.4, parameters can be estimated either for each session or within a global solution. Both parts of VieVS, Vie_{lsm} and Vie_{glob} were modified accordingly. So, in $Vie_{\text{lsm}}tie$ the normal equation system is set up allowing a single-session analysis, while $Vie_{\text{glob}}tie$ combines the normal equation matrices of several sessions allowing for a global solution. For estimating station positions there is the option to use all observations, or, in case of combined observations (sc & qu) only use the observations of one type. Also implemented but not treated within this work is the option of estimating the satellite's position. This can either be done for each observing epoch or is modeled as piecewise linear offsets with variable intervals. With the usually poor sensitivity in the radial component, there is also the option to constrain the variation in radial direction, along the line of sight (LoS).

VieVS₂tie, as described above, is capable to process VLBI satellite observations and derive common target parameters as e.g. antenna positions or satellite coordinates. However, for the lack of actual VLBI satellite observations, the approval of the software with real data is pending. Concerning the developed scheduling tool, it is to say that at the moment this tool is only suitable for scheduling artificial observations, e.g. for the purpose of simulations. For real observations, this tool has to be refined, including various restrictions as e.g. pointed out in section 5.3.2.

5.4.3 Satellite delay modeling

The theoretical delay for VLBI observations to satellites can be modeled following the formalism of chapter 3.2.3. However, as both the source and the observing stations are located in the neighborhood of the Earth, in *VieVS₂tie* the approach suggested by Klioner (1991) is implemented, where all coordinates are defined in GCRS rather than in the BCRS. The coordinate time delay Δt is defined as the difference of reception times t_2 and t_1 .

$$\Delta t = t_2 - t_1 = \Delta t_0 \left[1 - \frac{\vec{n}_2 \cdot \vec{v}_2(t_1)}{c} \right] + \Delta t_{gr,E} \quad (5.1)$$

Δt_0 is the time calculated from the difference of the distances l_2 and l_1 , determined at reception time t_1 . The time of the signal emission at the satellite t_0 has to be calculated iteratively solving the light time equation, e.g. given in eq. (3.27).

$$\Delta t_0 = 1/c(l_2 - l_1) \quad \text{with} \quad \vec{l}_i = \vec{x}_0(t_0) - \vec{x}_i(t_1) \quad \text{and} \quad l_i = |\vec{l}_i| \quad (5.2)$$

\vec{n}_2 represents the direction to the source from station 2

$$\vec{n}_2 = \frac{\vec{l}_2}{l_2} \quad (5.3)$$

and $\Delta t_{gr,E}$ is the relativistic light-time delay due to the Earth.

$$\Delta t_{gr,E} = \frac{(1 + \gamma)GM_E}{c^3} \ln \frac{(r_2 + r_s + r_{2s})(r_1 + r_s - r_{1s})}{(r_2 + r_s - r_{2s})(r_1 + r_s + r_{1s})} \quad (5.4)$$

The arguments r_i of equation 5.4 are calculated as:

$$r_{1,2,s} = |\vec{r}_{1,2,s}(t_{1,2,0})| \quad \text{and} \quad r_{is} = |\vec{r}_i - \vec{r}_s|. \quad (5.5)$$

With all quantities above scaled to GCRS, for comparison with the observed delay τ , Δt finally has to be rescaled according to equation 2.1.

$$\tau = \Delta t(1 - L_G) \quad (5.6)$$

5.4.4 Simulations

Simulations are performed in order to approximate real data, allowing to draw conclusions that are transferable to reality. Therefore, first the behavior of real observations has to be abstracted through a realistic model and second, a suitable simulation method must be chosen. The VieVS simulator (Vie_{sim} – Pany *et al.*, 2010) realizes the simulation method used for design decisions of the VLBI2010 system (Petrachenko *et al.*, 2009), comprising the three most important stochastic error sources in VLBI, namely wet troposphere delay, station clock, and measurement errors. Pany *et al.* (2010) give a detailed description on these simulations and justify its applicability through comparisons with real observations. In this work the description is restricted to the basic models and its use when deriving the results of chapter 6.

Vie_{sim} uses Monte Carlo simulations, which simulate above mentioned errors on the basis of random numbers and allow a subsequent statistical interpretation of the derived results, e.g. in terms of mean values or variance. The simulations are set up as follows (fig. 5.7): on the basis

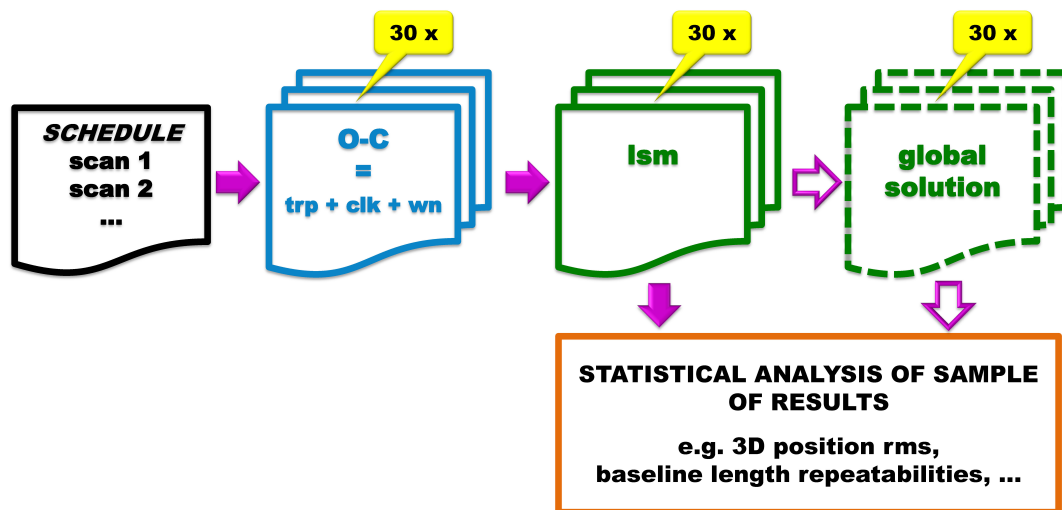


Figure 5.7: Simulation setup in VieVS. For a predefined schedule, the observed minus computed (o-c) values are set up as the sum of effects due to the wet troposphere, clocks and measurement errors. The simulated o-c values are then analyzed like normal observations, delivering estimates either for single session solutions or within a global solution combining several schedules. The sample of 30 repetitions allows a statistical analysis e.g. in terms of 3D position rms.

of a designated observation schedule, following adequate models the effects of the wet troposphere ($\tau_{trp,1,2}^s$) and the station clocks ($\tau_{clk,1,2}^s$) are simulated for each station and observation and a measurement noise ($\tau_{wn,bl}^s$) is calculated per baseline and observation. For a convincing sample, this is done 30 times using new random numbers each run. Assuming that there are no further errors sources, the sum of the simulated effects form the observed-minus-computed

values $\tau_o - \tau_c$, which are then used in the estimation process.

$$\tau_o - \tau_c = \tau_{trp,1,2}^s + \tau_{clk,1,2}^s + \tau_{wn,bl}^s \quad (5.7)$$

This means, that the simulated observations do not depend on a dedicated delay model according to section 5.4.3. The decisive values are the time of the observation as well as the spatial direction to the source in terms of the elevation angle and azimuth. The simulated observations (or rather o-c values) are then analyzed like normal data, first session-wise and optionally also within a global solution. Finally, the sample of 30 results allows a statistical interpretation, usually in the form of 3D position rms or baseline length repeatabilities. The basic models of the three error sources are:

Wet troposphere delay: In Vie_{sim} , the formalism by Böhm *et al.* (2007) is implemented. Following the strategy proposed by Nilsson *et al.* (2007), it applies turbulence theory (Treuhaft & Lanyi, 1987) to account for correlations between the observations in dependence on elevation, azimuth and time epoch when calculating the zenith wet delays (zwd). Following (3.21), the simulated wet delay for station i at elevation e is obtained by

$$\Delta L_{w,i}(e_i) = zwd_i \cdot mf_{w,i}(e_i). \quad (5.8)$$

For the simulation of the zwd , the characteristic of the wet troposphere is described by several parameters, as listed in table 5.1. If not explicitly stated otherwise, the given numbers are the ones used in the simulations throughout this work. For detailed information on their definition the reader is referred to Nilsson *et al.* (2007), Nilsson & Haas (2010), or Pany *et al.* (2010).

Table 5.1: Parameters for the simulation of the wet troposphere.

parameter	value	description
zwd_0	150 mm	initial zenith wet delay at the beginning of the time series
C_n	$2.5 \cdot 10^{-7} \text{m}^{-1/3}$	structure constant of a turbulent troposphere
H	2 km	effective height of the troposphere
v_e	8 m/s	wind speed in east direction
v_n	0 m/s	wind speed in north direction
dh	200 m	height increment for numerical integration
dh_{seg}	8 h	correlation interval

Clock: The influence of the station clocks is simulated as the sum of a random walk and an integrated random walk process. This follows the idea of Herring *et al.* (1990), the according source code can be found in Böhm *et al.* (2007). The input number represents the Allan standard deviation (ASD) of the station clocks. Throughout this work, the value of $1 \cdot 10^{-14}$ at 50 minutes is used.

Measurement noise: The measurement noise shall reflect the precision of the measured delay. It is simulated as white noise and one random value is added per baseline, respectively per observation. The standard value used is 30 ps, what is typical for today's VLBI systems.

Applying all three stochastic errors and following equation (5.7), the simulated residuals can be put together to

$$\tau_o - \tau_c = (zwd_2 \cdot mf_{w,2}(e_2) + clk_2) - (zwd_1 \cdot mf_{w,1}(e_1) + clk_1) + wn_{bl}. \quad (5.9)$$

The simulations used in this work were also utilized when designing the next generation VLBI system, VLBI2010 (Petrachenko *et al.*, 2009). Concerning the different impact of the single error sources, Pany *et al.* (2010) concluded that the wet troposphere is the most important of these three parameters. Relatively small was the impact of the measurement error and there was no positive impact found if clocks better than $1 \cdot 10^{-14}$ at 50 min were used. These statements coincide with the findings of chapter 6.2.4, where the effect of the simulation parameters on the results of this thesis is investigated.

Concerning the effect of the tropospheric errors on derived station positions, one has to understand the model behind more closely. On the one hand, the simulator is based on temporal and spatial correlations, meaning that observations in similar directions and separated only by a short time will have similar tropospheric delays. As a consequence, such observations do not help to reduce tropospheric errors as they would do in a model purely based on random numbers. On the other hand, the estimation of troposphere parameters is highly correlated with the station heights. For a good separation, observations at low elevations have to be included in the schedule. In standard VLBI scheduling, a common way to achieve good results is to strive for a good sky coverage over each station, i. e. one wants to do observations in different directions and at different elevation angles to be able to resolve the troposphere.

Chapter 6

Simulation studies and results

With the following simulations it is investigated whether VLBI observations to satellites allow a precise derivation of antenna coordinates in the satellite frame. Revealing proper results, the VLBI satellite technique can be pursued as a true alternative for a direct connection of the VLBI and the satellite frame. The chapter starts with some background on the study (6.1), before presenting results achieved with observations in small regional antenna networks (6.2). Here, the characteristics of the simulation study are examined in detail. In section 6.3 results for global networks are presented, before observations to GNSS-satellites are treated separately in section 6.4. Finally, the most important results are summarized in section 6.5.

6.1 Composition of the study

For the upcoming investigations, the *VieVS₂tie* software, as described in chapter 5.4, is used. The presented results are obtained within weekly solutions, meaning that the satellite is observed during 7 days. As shown in figure 6.1, this is achieved by scheduling 7 consecutive days and a combination of the daily sessions within a global solution. The sample of 30 repetitions for the simulations allows a statistical analysis of the results, e.g. in terms of 3D position rms. In the following sections, the decisive individual steps and input options for this study are discussed. This covers information about the observed satellites (6.1.1) and the observing networks (6.1.2), the scheduling procedure (6.1.3), an overview on the used processing options (6.1.4) and the mathematical definition of station position repeatability (6.1.5).

6.1.1 Satellite orbits

Satellites used in geodesy are mostly in orbits with small eccentricities, thus nearly circular orbits with high inclination for a uniform global coverage. The observational targets of this study are satellites at three different height classes, with orbits based on real missions or mission proposals. The satellites with their orbital parameters are given in table 6.1. Representative for a low Earth orbiting satellite (LEO) is the proposed GRASP satellite (chapt. 5.2). The orbital

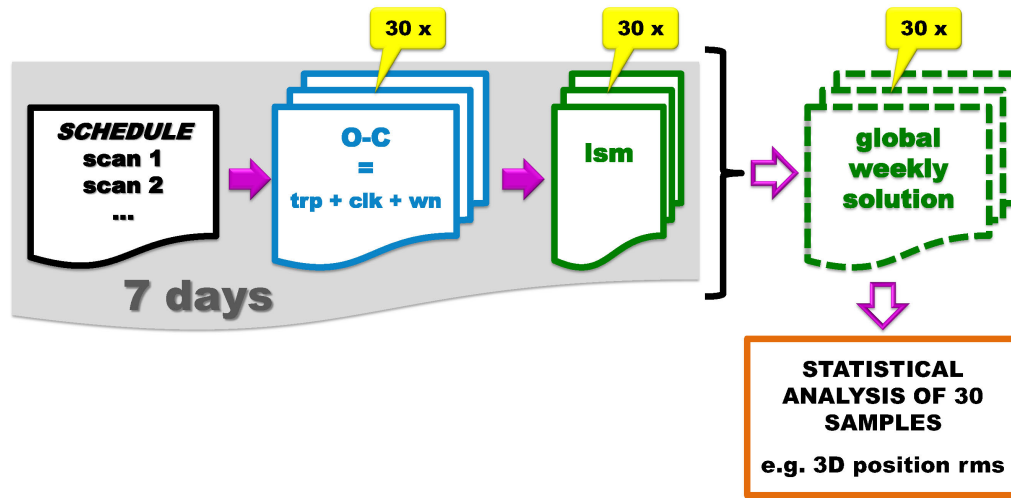


Figure 6.1: Set-up of the weekly solutions. Following 7 consecutive schedules of 24 hours each, the observations are simulated 30 times and processed session-wise first. Weekly coordinates are estimated within a global solution, with the sample of 30 repetitions allowing statistical analysis in terms of 3D position rms.

elements for the *GRASP2000* satellite at 2000 km height go back to an earlier stage of this mission’s planning stage¹, while the lower, elliptical orbit of *GRASPELL* is given in the mission proposal (Nerem & Draper, 2011). For *GRASPELL*, the satellite height varies between 850 and 1350 km. Much higher, at heights of about 6000 km fly the laser ranging satellites *LAGEOS*, that give the orbit elements for the second satellite type. Third, observations to satellites of the GPS system are examined, having a mean altitude of about 20200 km above ground.

Table 6.1: Orbital parameters of the target satellites.

	height h	inclination i	eccentricity e
<i>GRASP2000</i>	2000 km	104.89°	0.0001
<i>GRASPELL</i>	850 – 1350 km	99.92°	0.0334
<i>LAGEOS</i>	6000 km	109.84°	0.0045
<i>GPS</i>	20200 km	55°	nearly circular

For the simulations, the orbits of *GRASP* and *LAGEOS* are integrated over seven days, under consideration of the Earth’s oblateness. In this context, the approach of weekly solutions gives some independence from the arbitrarily chosen remaining orbital elements, which are the right ascension of the ascending node, the argument of the perigee and the mean anomaly. The input to the software happens via a table of xyz -coordinates with 1 min intervals. In the case of *GPS*, orbit files in sp3-format, as provided by the International GNSS Service (IGS; Dow *et al.*, 2009), are used. In order to get an impression of the Earth’s coverage, in figure 6.2 the ground

¹Y. Bar-Sever, personal communication

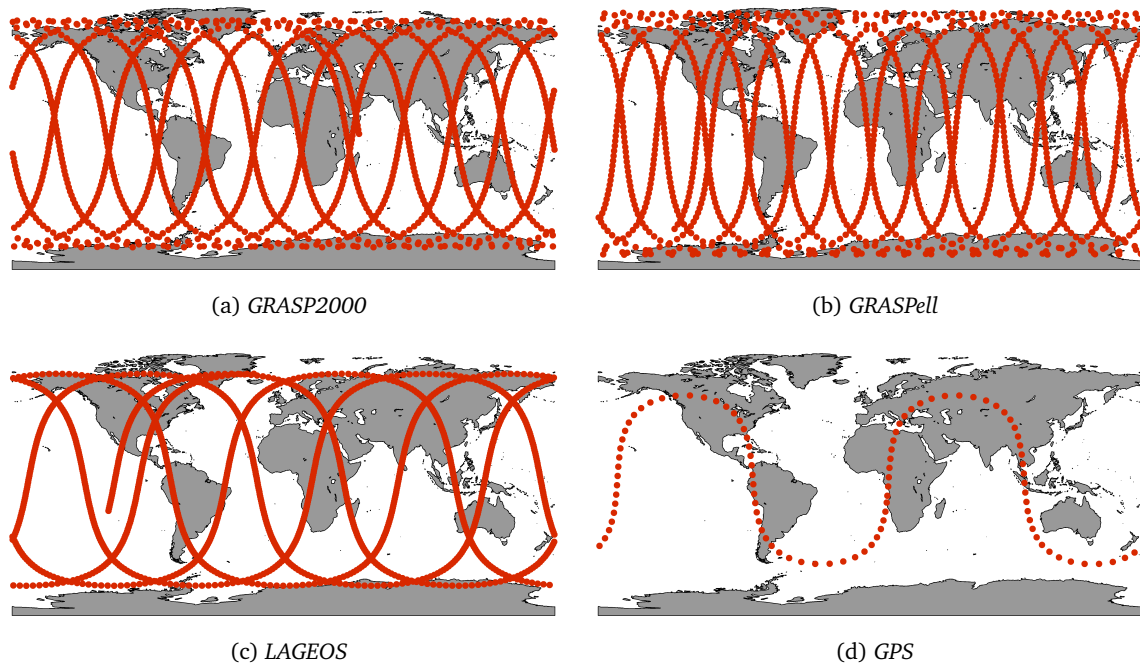


Figure 6.2: Ground tracks of 1 day for (a) *GRASP2000*, (b) *GRASPELL*, (c) *LAGEOS* and (d) one satellite of the *GPS*. Each dot represents the nadir of the satellite's position on the Earth's surface, calculated with 1 minute intervals for (a)-(c) and with 15 minutes intervals for (d).

tracks of the four used satellites are shown for one day. Both *GRASP* satellites and the *LAGEOS* satellite orbit the Earth several times per day and hence cover new areas each revolution. The *GPS* satellite, by contrast, keeps the virtually identical ground track each day, as a result of its orbital period of 12 sidereal hours.

6.1.2 Station networks

In this study, different station networks are used. As shown in chapter 5.3.1, prerequisite for VLBI observations to satellites at low altitudes are sufficiently short baselines in the network. Therefore, besides the usual global networks, also regional constellations are investigated.

Regional networks: Inspired by the (more or less) actual active antenna network, regional networks are selected in three regions, in Europe (EUR, blue), Asia (ASIA, green), and Australia/Oceania (AUS, red). They include 7, in the case of AUS 6 stations and their spatial distribution is shown in figure 6.3. The participating stations are:

EUR: Ny Ålesund, Metsähovi, Onsala, Svetloe, Wettzell, Yebes, Zelenchukskaya

ASIA: Aira, Badary, Kashima, Kunming, Mizusawa, Shanghai, Urumqi

AUS: DSS45, Hobart, Katherine, Parkes, Warkworth, Yarragadee

In the regional networks, the majority of the formed baselines have a length between 2000 and 3000 km. According to figure 5.3.1, this should enable common visibilities also for the

6.1 Composition of the study

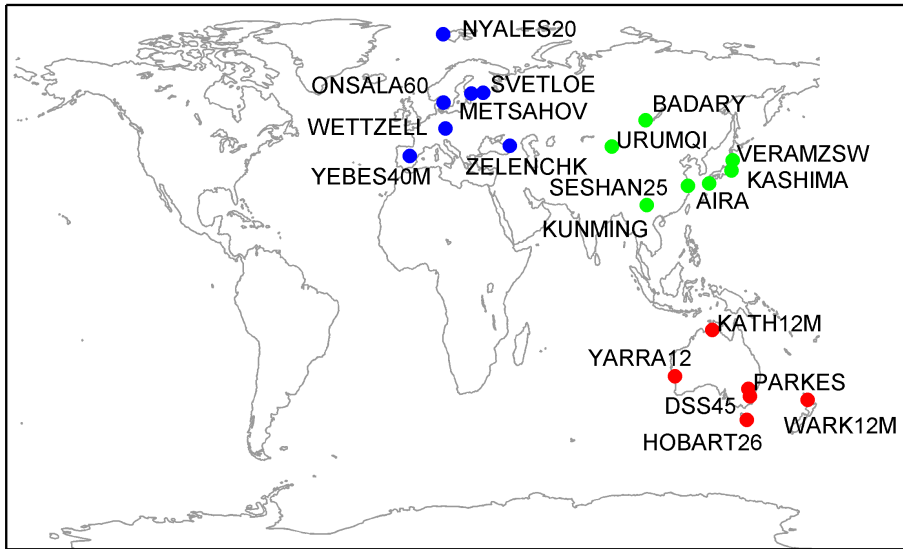
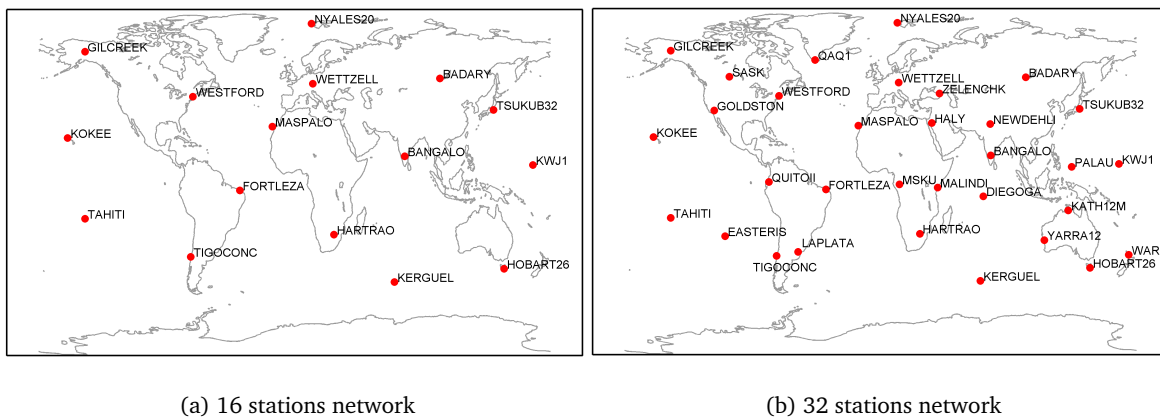


Figure 6.3: Map of the regional antenna networks with 7 stations in Europe (blue) and Asia (green), and 6 stations in the Australia/Oceania region (red).

GRASP2000 and *GRASPELL* satellites.

Global networks: For the global networks, the simulation networks of the VLBI2010 simulations, as proposed by Niell (2007), are used. Advantage of these networks is an intended homogeneous global distribution of the antennas, under the conditions of land coverage, existing stations and possible upcoming stations. Observations are scheduled for the two global networks shown in figure 6.4, one with 16 stations (a) and one consisting of 32 stations (b). The coordinates of the used antennas are given in appendix A.



(a) 16 stations network

(b) 32 stations network

Figure 6.4: Maps of used global antenna networks including (a) 16 stations and (b) 32 stations.

6.1.3 Scheduling

The scheduling of the observations is done purely geometrical, using the corresponding routine within *VieVS₂tie* (see chapt. 5.4). Following input parameters like date, antenna network, target satellite, and scan duration, whenever common visibility for two stations is given, the observation is scheduled. Restrictions due to maximum antenna slew rates are not considered. As will be shown later in this work (sec. 6.2.2 and 6.2.3), in particular the choice of the cut-off elevation angle and of the observation interval during scheduling is decisive.

6.1.4 Processing options

The processing options concern the settings in the least squares adjustment. Hereby, standard VLBI processing options are applied, with some exceptions and specifications as given in table 6.2:

Table 6.2: Processing options within the simulation study.

Earth orientation	fixed
Troposphere zwd	30 min pwl offsets 1 cm relative constraints
gradients	none
Clock	60 min pwl offsets + rate + quadratic term 1.3 cm relative constraints
Station coordinates	NNT, NNR applied

Earth Orientation Parameters (EOP) are not estimated during the analysis. Despite the fact, that they are sensitive to possible rotational distortions between the VLBI and the satellite frame, what can be important for real observations, such effects are not simulated and investigations in this direction are left for further studies. Zenith wet delays (zwd) are estimated as piecewise linear (pwl) offsets every 30 minutes for each station. During estimation and especially important at periods without any observations, loose constraints of 1 cm after 30 minutes are applied. Troposphere gradients to address azimuthal asymmetry are not estimated. The clocks are set up as 60 minutes pwl offsets, plus a rate and a quadratic term, with 1.3 cm constraints after 60 minutes. Station coordinate estimation is done once per session, applying a no-net-rotation (NNR) and no-net-translation (NNT) condition. In the subsequent global solution, parameters for clocks and zenith wet delays are reduced while the normal equation matrices for the antenna coordinates are stacked and solved together within the weekly solution. For detailed information on the procedure of the global solution the reader is referred to Krásná *et al.* (2013).

The influence on the results when these processing options are changed is investigated in section 6.2.5.

6.1.5 Station position repeatability

The parameter that is used to assess the simulation results is the repeatability of antenna coordinates, named station position repeatability or 3D position rms in the following. Starting from seven daily sessions, each simulated 30 times, one has 210 processed sessions for each schedule. In the global solution, seven consecutive days are combined and one set of antenna coordinates (dx, dy, dz) is estimated for each station, repeated 30 times. For a better geometrical interpretation, dx , dy and dz are converted to local up- (dr), east- (de) and north- (dn) components. The standard deviation σ of these estimates gives a measure of the expected accuracy of derived antenna coordinates. Exemplarily, the standard deviation σ_{dr} for $n = 30$ samples with the mean value dr_m is calculated:

$$\sigma_{dr} = \sqrt{\frac{1}{n-1} \sum_{i=1}^n (dr_i - dr_m)^2}. \quad (6.1)$$

The 3D position rms is then defined as:

$$3D \text{ rms} = \sqrt{\sigma_{dx}^2 + \sigma_{dy}^2 + \sigma_{dz}^2} = \sqrt{\sigma_{dr}^2 + \sigma_{de}^2 + \sigma_{dn}^2}. \quad (6.2)$$

As will be shown in the results below, the number of observations is often highly correlated with the achieved accuracy. In the following figures the number of observations per day is defined as the mean value per station:

$$n_{obs} = \text{mean}(n_{obs}^{\text{day1}} \dots n_{obs}^{\text{day7}}). \quad (6.3)$$

For a better visibility in the plots, n_{obs} is mostly given in units of 1000.

6.2 Regional networks

First, observations are analyzed for the dense European network. The results shown in figure 6.5 (a)-(d) are given in weekly 3D position rms (orange), as well as in repeatability of the height (blue), east (green) and north (brown) component. The observation settings are those of table 6.3, which are found to reveal the best solutions.

Table 6.3: Observation settings for the regional networks.

	interval	cutoff angle
<i>GRASP2000</i>	1 min	10°
<i>GRASPELL</i>	30 sec	5°
<i>LAGEOS</i>	1 min	10°
<i>GPS</i>	5 min	10°

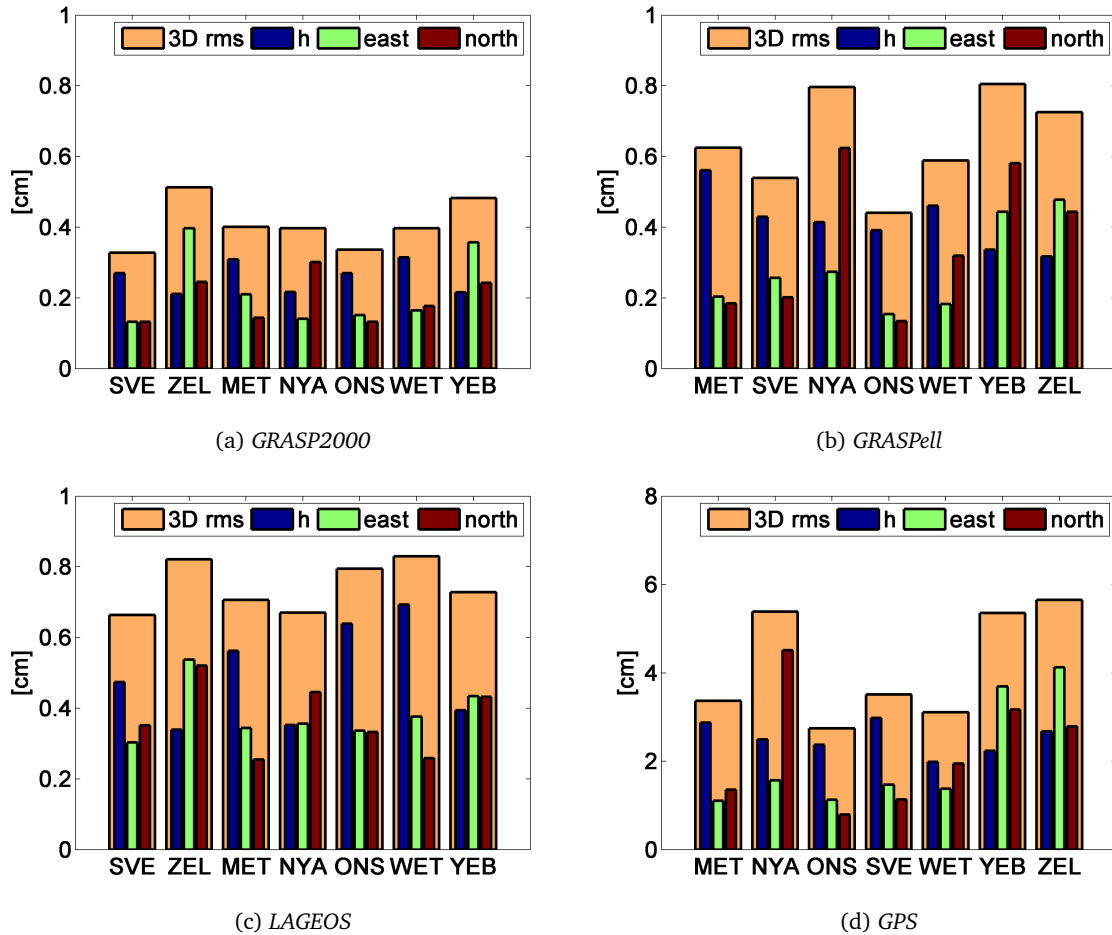
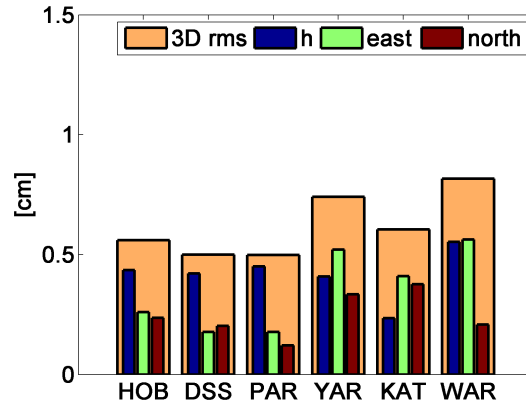


Figure 6.5: Station position errors in terms of weekly 3D position rms (orange), as well as repeatability of the height (blue), east (green) and north (brown) component if a satellite (a)-(d) was observed with the regional European network.

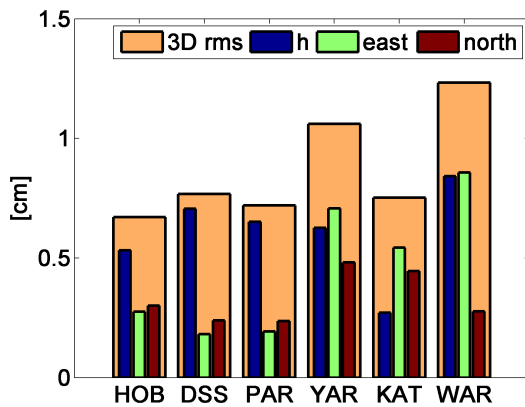
The best results are achieved with the *GRASP2000* satellite, with a mean weekly 3D position rms of 4 mm. For *GRASPell* and *LAGEOS* the geometry is not so good, revealing results slightly below the 1 cm level, with mean 3D position rms of 6 mm and 7 mm respectively. Really bad accuracies, at the 5 cm level, are found for the *GPS* satellite. For the time being, observations to *GPS*-satellites are not used in further investigations. They are treated separately in section 6.4. Studying figures 6.5 (a)-(c) it is evident, that the height component shown in blue is significantly worse than the horizontal position error. This is due to the strong correlation of estimated height and troposphere, which is the main contributor to the simulated observation error. Exceptions are found for the stations Ny Ålesund (NYA), Zelenchukskaya (ZEL) and Yebes (YEB). The reason for this is their location in the network. VLBI is only sensitive to variations within the plane of the triangle station 1 - source - station 2. As the above mentioned stations are situated at the edges of the network and only form baselines with other stations in one direction, their horizontal components are not as well determined as at the stations in the center of the antenna network (see fig. 6.8). This behavior is observed in all investigated regional networks and is named the

"network effect" in the following.

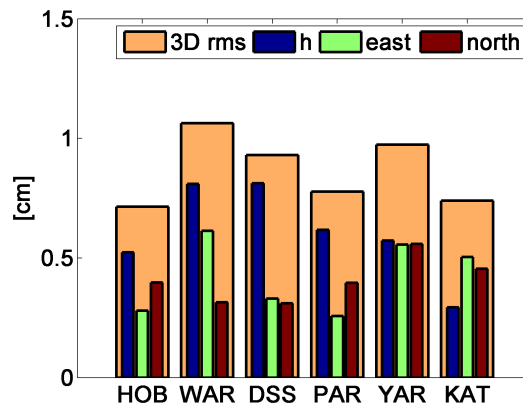
Besides the European network, observations to *GRASP2000*, *GRASPELL* and *LAGEOS* from other regional networks are investigated. Results achieved with the Australian AUS network are presented in figure 6.6. The determined mean weekly 3D position rms is 6 mm for *GRASP2000*



(a) *GRASP2000*



(b) *GRASPELL*



(c) *LAGEOS*

Figure 6.6: Station position errors in terms of weekly 3D position rms (orange), as well as repeatability of the height (blue), east (green) and north (brown) component if a satellite (a)-(c) was observed with the regional Australian network.

and 8 mm for both, *GRASPELL* and *LAGEOS*. Equivalent to the EUR network, the stations at the edges, namely Yarragadee (YAR), Katherine (KAT) and Warkworth (WAR), are slightly worse. This is also connected with the significantly fewer observations of those three stations compared to the other antennas. Table 6.4 shows the mean number of observations for each station. When observing one of the *GRASP* satellites, YAR, KAT and WAR have about 40 % less observations than the other stations HOB, DSS and PAR and about 30 % less when observing *LAGEOS*.

Finally, results are presented for the Asian network in figure 6.7. With a mean weekly 3D position rms of 6 mm, 1 cm and 8 mm for *GRASP2000*, *GRASPELL* and *LAGEOS*, they are comparable to the station position repeatabilities achieved with the EUR and AUS network.

Table 6.4: Mean number of observations per station in the AUS network.

	HOB	DSS	PAR	YAR	KAT	WAR
<i>GRASP2000</i>	295	310	301	175	176	199
<i>GRASPELL</i>	457	477	461	251	237	292
<i>LAGEOS</i>	1007	1021	1013	807	703	829

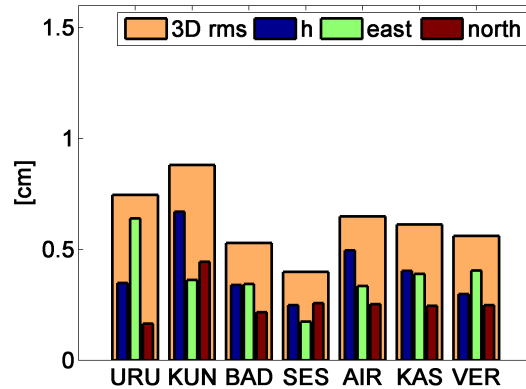
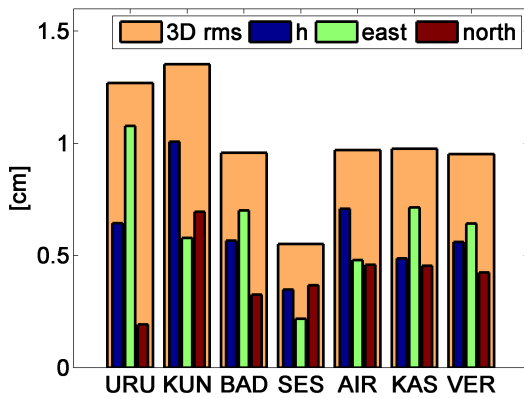
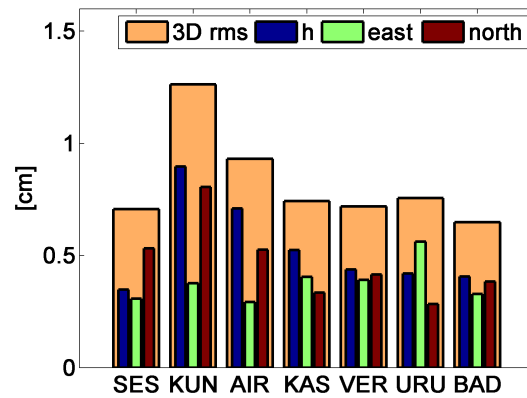
(a) *GRASP2000*(b) *GRASPELL*(c) *LAGEOS*

Figure 6.7: Station position errors in terms of weekly 3D position rms (orange), as well as repeatability of the height (blue), east (green) and north (brown) component if a satellite (a)-(c) was observed with the regional Asian network.

Summing up the investigations above shows, that with observations of regional networks to satellites at heights between ~ 1000 and 6000 km, station position repeatabilities of a few millimeters up to about 1.4 cm are achieved. Testing the three networks EUR, AUS and ASIA described in 6.1.2, similar results are found, allowing the conclusion that the findings are valid for all further networks with comparable characteristics. In figure 6.8 an overview of the observing baselines for the three networks is given. As can be seen in plot 6.8 (a)-(c), all possible baselines,

6.2 Regional networks

meaning a combination of two stations, are actually observed. This is true also for the quite low *GRASPELL* satellite. Concerning the lengths of the baselines, 6.8 (d)-(f) give the distribution of the baseline lengths for EUR, AUS and ASIA. It can be stated, that networks with the majority of their baselines having lengths between 2000 and 3000 km are appropriate for such observations.

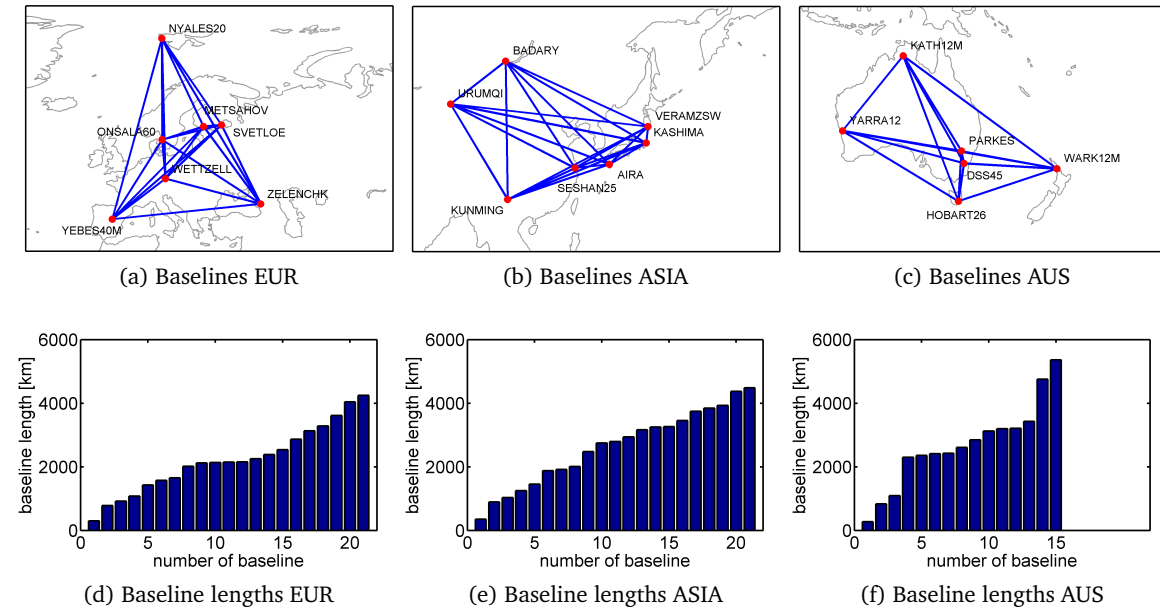


Figure 6.8: Networks with baselines of the regional European (EUR), Asian (ASIA), Australian (AUS) networks (a-c) and the lengths of the observed baselines (d-f).

In the end of this section the importance of the total number of observations is emphasized. In figure 6.9 the weekly 3D position rms of figures 6.5, 6.6 and 6.7 is printed versus the mean number of observations per station per day. Especially for the extremely low satellites *GRASP2000* and *GRASPELL* a clear correlation between a higher number of observations and an increase in precision is evident. For *LAGEOS* this connection is not that strong, but therefore the total number of observations per station is between 700 and 1500, what is twice as many as for the other two satellites.

In the upcoming sections, the results are examined more closely with regard to the settings of the presented study. This covers the concept of weekly solutions (6.2.1), the influence of the cutoff elevation angle (6.2.2), the observation interval (6.2.3) and the effect on the results when changing the simulation parameters (6.2.4) or the processing options (6.2.5). Further, the importance of a certain number of satellite passes over a station per day for the results is shown (6.2.6). A quick estimation of the influence of orbit errors on the results (6.2.7) and the assessment of the representativeness of the investigated time span (6.2.8) end this section.

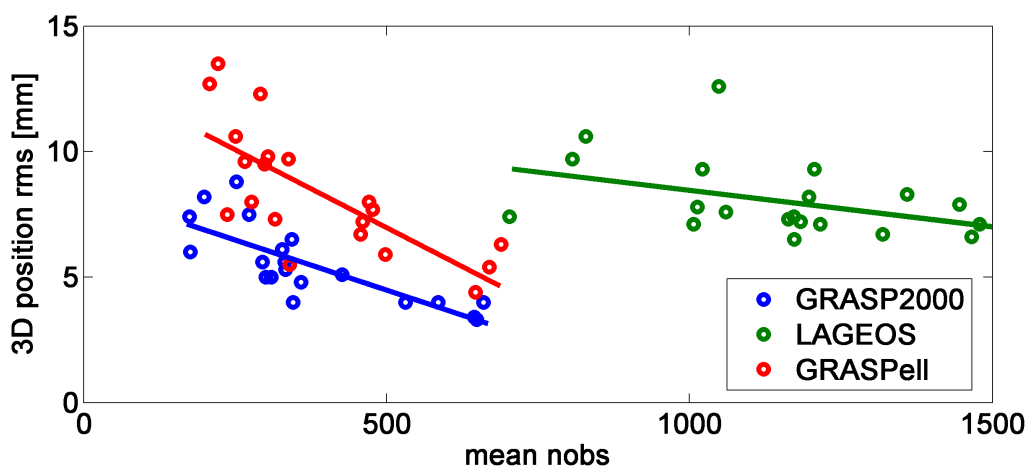


Figure 6.9: Weekly 3D position rms versus the mean number of observations per day for *GRASP2000* (blue), *LAGEOS* (green) and *GRASPELL* (red) with fitted linear trends. The data is derived from all three regional networks, with one point representing the weekly 3D position rms for one station.

6.2.1 Weekly solution

In this work, the approach of weekly solutions is chosen. This is common in TRF calculation, as e.g. the services for SLR (ILRS; Pearlman *et al.*, 2002) and GNSS (IGS; Dow *et al.*, 2009) at the moment deliver weekly solutions of station coordinates. Also the GRASP proposal (Nerem & Draper, 2011) follows this concept. For the investigated VLBI satellite observations, predominantly due to the limited number of observations, solutions for antenna coordinates over seven days are much more stable than derived coordinates after 1 or 2 days. Shown in figure 6.10 is the improvement of the derived mean 3D position rms when solving the global solution for 1 to 7 days. For the three investigated satellites, the improvement of the weekly solution compared to a one-day solution is approximately a factor of 2.

6.2.2 Cutoff elevation angle

The optimum cutoff elevation angle manages the right mixture between observations at low, but not too low elevations, enabling the separation of the station heights and the tropospheric and clock parameters during estimation. While for low elevation angles the influence of the troposphere increases strongly, the total number of observations decreases if the cutoff angle is set too high. MacMillan & Ma (1994) found the optimum elevation cutoff for VLBI at $7 - 8^\circ$, where the correlations between station height error and zenith delays are sufficiently reduced and the errors of the mapping functions are still tolerable. For the VLBI satellite observations, cutoff elevation angles of 5° , 7° , 10° , and 15° are tested. In figure 6.11 the results are shown for observations to the *GRASP2000* satellite from the European network. It is evident, that an elevation cutoff of 5° (blue) and 15° (brown) mostly give worse results than the other two options. Considering also investigations with observations to *LAGEOS* and *GPS* satellites, the standard cutoff angle is set with 10° . Worth to notice is the reduction of the total number of

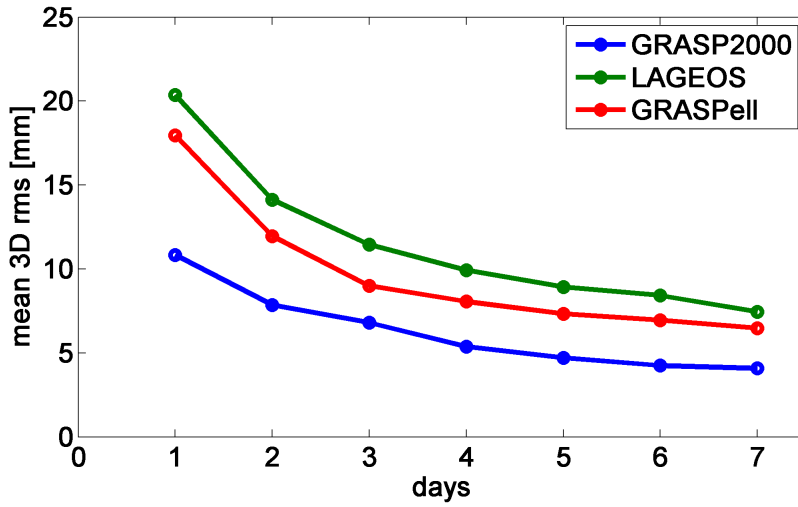


Figure 6.10: Results for processing n days up to a weekly solution (n=7). The results are calculated for the three satellites observed by the EUR network.

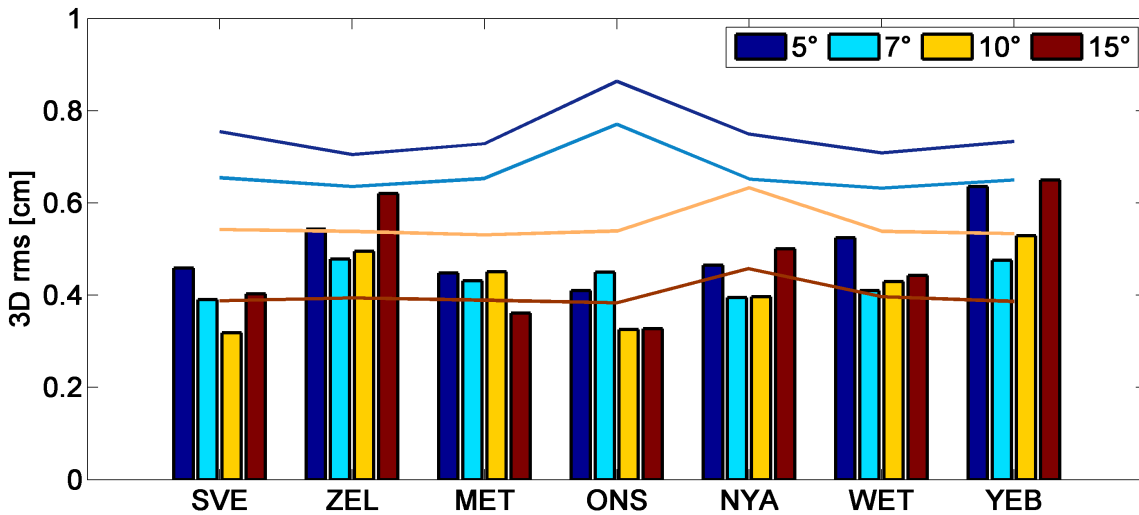


Figure 6.11: Weekly 3D position rms for cutoff elevation angles of 5° (blue), 7° (light blue), 10° (orange), and 15° (brown). The colored lines indicate the corresponding number of observations per day, divided by 1000. The results are based on simulated observations to the GRASP2000 satellite with 1 minute intervals.

observations with increasing cutoff angle, as indicated in units of 1000 observations per day with the four colored lines. Hence, for a cutoff angle of 15° there are approximately half of the observations in the solution than at a cutoff angle of 5°. This fact becomes principal for observations to the extremely low GRASPELL satellite, where, despite an observation interval of 30 seconds, the number of observations is that low, that there is no improvement with a higher cutoff angle. Consequently, for GRASPELL the cutoff angle is set at 5°. The standardly used cutoff angles for each satellite are summarized in table 6.3.

6.2.3 Observation interval

A VLBI-observation is not performed at a single epoch, but is integrated over a certain time. However, after correlation, the determined time delay is referred to a certain time epoch with the interval between two consecutive observations called the observation interval. While in geodetic scheduling this interval depends on antenna specifications like the dish size, the antenna SNR, the signal strength of the observed source, as well as on the time that needs to be reserved for the slewing from one source to the next, these aspects are not considered in the investigations presented here. The point of interest in this section is to find the appropriate interval for each investigated satellite, which basically determines the total number of observations.

For the simulation, in principle one could schedule observations with any interval. In practice, as mentioned above, one needs to respect the duration of the observation, the antenna slewing and the fact that generating a high number of observations also means a high amount of data that has to be recorded, transferred, correlated and processed. Further, the simple increase of the observation interval does not always mean a gain in information and might be useless in terms of better accuracies.

If one assumes the observations uncorrelated and flawed with random Gaussian noise, when increasing the number of observations n one would expect an improvement of the derived standard deviation σ , compared to the accuracy of a single observation σ_i , by the square root of n :

$$\sigma = \frac{\sigma_i}{\sqrt{n}}. \quad (6.4)$$

For the observations investigated here, however, this is not completely true. Consecutive observations that are close in time and space are affected by a similar troposphere. Hence, such observations do not give new information and do not help to derive more accurate results. This is evident when studying table 6.5 and figure 6.12.

For table 6.5 the weekly 3D position rms in the EUR network is calculated for observations to the four satellites using different observation intervals. The numbers after the verticals give the corresponding number of observations per day for each station. Hereby one has to consider, that when testing the different schedules each time a new simulation is run using new random numbers. Therefore, when comparing different solutions, this can only be done up to the level of repeatability of the solution, shown in figure 6.13 (d). Studying the results, the optimal observation interval for each satellite was determined and is highlighted in the table. It becomes evident, that at a certain interval there is no further improvement for another shortening of the interval. This is also visualized in figure 6.12, where the improvement in 3D position rms is plotted versus the number of observations for each station. For comparison, the gray shaded line shows the improvement following the law of equation 6.4. There is strong improvement for *GRASP2000* when the interval is decreased from 5 minutes to 1 minute and hardly any further improvement when an interval of 30 seconds is used. For *LAGEOS* four different intervals are

6.2 Regional networks

Table 6.5: Station position repeatability and number of observations for the four satellites observed by the EUR network testing different observation intervals. The values are given in terms of weekly 3D position rms in cm, the numbers behind the verticals are the numbers of observations per day. The highlighted rows indicate the determined best observation interval for the corresponding satellite. Besides the observation interval, additional variation in the results is induced by the simulation of the observations.

	SVE	ZEL	MET	ONS	NYA	WET	YEB
<i>GRASP2000</i>							
30 sec	0.33 1295	0.47 857	0.34 1320	0.33 1288	0.38 1058	0.35 1172	0.50 715
1 min	0.33 649	0.51 427	0.40 660	0.34 645	0.40 531	0.40 585	0.48 359
5 min	0.72 132	0.92 88	1.02 134	0.57 129	0.75 106	0.62 120	0.84 74
<i>GRASPELL</i>							
15 sec	0.52 1378	0.58 1342	0.75 941	0.58 1294	0.52 997	0.79 558	0.93 633
30 sec	0.63 689	0.54 670	0.80 471	0.44 647	0.59 498	0.80 277	0.73 316
1 min	0.78 345	0.60 336	0.88 236	0.46 324	0.62 248	0.91 138	0.93 157
<i>LAGEOS</i>							
30 sec	0.87 2935	0.79 2395	0.82 2961	0.62 2890	0.69 2640	0.71 2718	0.82 2327
1 min	0.66 1466	0.82 1197	0.71 1479	0.79 1446	0.67 1319	0.83 1359	0.73 1163
5 min	0.85 292	0.86 240	0.84 294	0.90 288	0.77 264	0.80 271	0.73 231
10 min	0.94 145	1.11 119	1.04 148	0.90 144	0.94 131	1.17 135	0.97 116
<i>GPS</i>							
1 min	3.83 2144	8.45 1863	3.38 2149	2.65 2045	9.43 1951	3.76 1876	9.28 1878
5 min	3.42 428	5.87 373	3.50 430	3.00 408	6.41 390	3.35 374	6.60 375
10 min	4.15 214	8.49 187	3.52 215	3.65 204	7.44 195	4.17 187	8.26 188
15 min	4.51 143	7.28 125	3.91 143	4.89 136	6.41 130	4.36 124	7.37 125

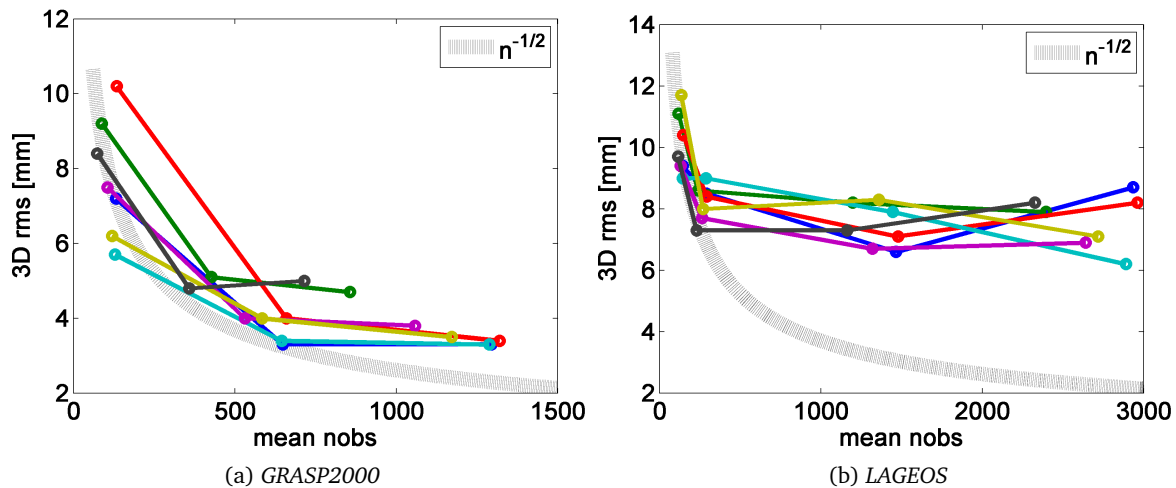


Figure 6.12: Weekly 3D position rms versus the number of observations for (a) *GRASP2000* and (b) *LAGEOS*. The colored lines represent one station each, for which the results are marked for different observing intervals according to table 6.5. The gray shaded line shows the expected improvement following equation 6.4.

tested, with a clear blip after the second marker, representing 5 minutes intervals. With these investigations, together with some desire for uniformity, the optimal observing interval is found to be 1 minute for *GRASP2000* and *LAGEOS*. For *GRASPeII*, due to its low altitude and the according severe restrictions on common visibility, the interval is set to 30 seconds, while for the slow *GPS* satellites an interval of 5 minutes is sufficient. These values, that are summarized in table 6.3, are standardly used for the investigations within this work.

6.2.4 Influence of simulation parameters

As already pointed out in chapter 5.4.4, experiences with the VieVS simulator showed that the influence of the wet troposphere dominates the derived results. In this section this is confirmed for the presented results within this thesis. In figure 6.13 (a)-(c) the influence of varying input values for models of the wet troposphere, the clock error and the measurement noise on the mean weekly 3D position rms is shown. The curves are calculated for the three test satellites, *GRASP2000*, *GRASPeII* and *LAGEOS* and show good agreement in their behavior. The mean weekly 3D position rms is the mean value over the 7 stations of the EUR network. For the clock (b), it is evident that there is no further improvement of the results when better clocks than those with an ASD of $1 \cdot 10^{-14}$ at 50 minutes are used. As common clocks are already better than that, there is no danger to get bad results because of poor clock performance. A similar behavior is found for the impact of the measurement error (c). The results seem to be resistant to white noise up to 100 ps, while the influence rapidly grows for noise bigger than that. Hence, in the case of the presented weekly solutions, the precision of the measured delay shall be at least 0.1 ns or about 3 cm.

Things are more complicated when defining the structure constant Cn for the simulation of the wet troposphere (a). In real, these values are strongly connected with the other deterministic parameters of the troposphere (see table 5.1) and significantly vary from station to station and in time. Here, the rather conservative value of $Cn = 2.5 \cdot 10^{-7} \text{m}^{-1/3}$ is chosen for all stations. In dependence of the real situation, according to figure 6.13 (a), the presented results might get better for up to a factor of 2 for very dry conditions (e.g. $Cn = 1.0$), but they can also be a little worse for extremely wet and turbulent conditions (e.g. $Cn = 3.5$).

The last parameter that is investigated is the number of simulation runs and the ensuing validity of the shown results. As described in chapter 5.4.4, the presented results are based on the statistical interpretation of a sample of 30 simulation runs. In order to find out if the derived solutions are representative, the *GRASP2000* result was calculated for five independent simulation runs and compared in figure 6.13 (d). As can be seen, the solutions for the weekly 3D position rms vary at a level below 1 mm, with one exception of 1.5 mm for Yebes. The corresponding mean 3D position rms of all stations varies between 4.1 mm and 4.8 mm. It is therefore concluded that, at the millimeter-level, the sample of 30 runs gives representative results.

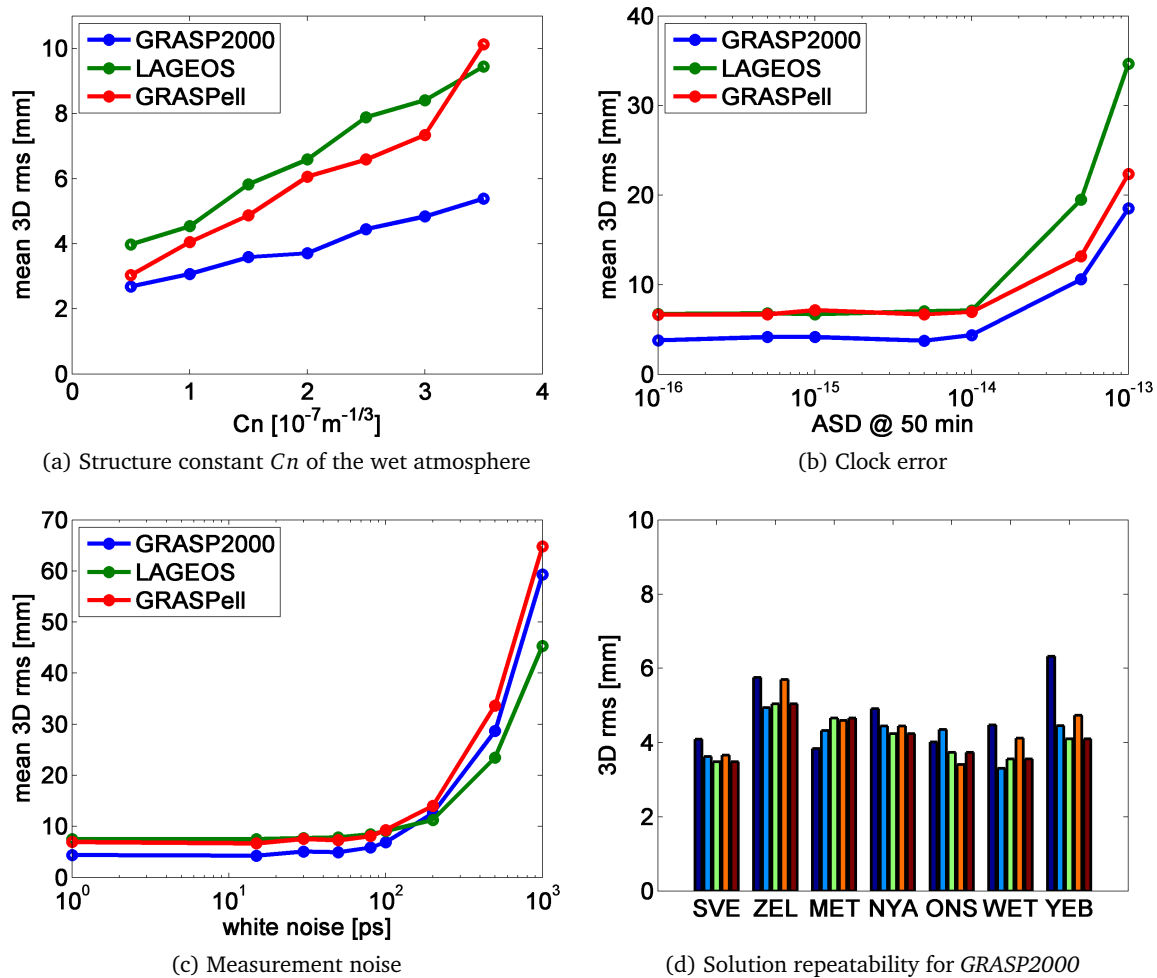


Figure 6.13: Influence of the simulation parameters for modeling the tropospheric turbulence (a), the clock error (b) and the measurement noise (c) on the results. In (d) the solution repeatability if GRASP2000 was observed with the EUR network is shown for 5 runs.

6.2.5 Influence of processing options

The processing options are given in section 6.1.4. Here it is investigated whether any changes there might change the results and if so how big these changes are.

Unlike in usual VLBI analysis, EOP are not estimated in the simulation. However, tests show that if EOP are determined once per day during the processing, the derived results for station repeatabilities do not change significantly, i. e. the numbers differ in the sub-millimeter level only. Similar behavior is found for tropospheric gradients. Not included by default, with a maximum change of 1 mm in weekly 3D position rms for isolated stations they hardly effect the derived results when estimated. Clock parameters are estimated once per hour. Changes of this interval (30 min, 2 h, 3 h) are reflected in the results at the sub-millimeter level.

More decisive is the estimation interval of the troposphere. By default, the zenith wet delay is estimated for each station every 30 minutes, with 1 cm relative constraints. In order to test the

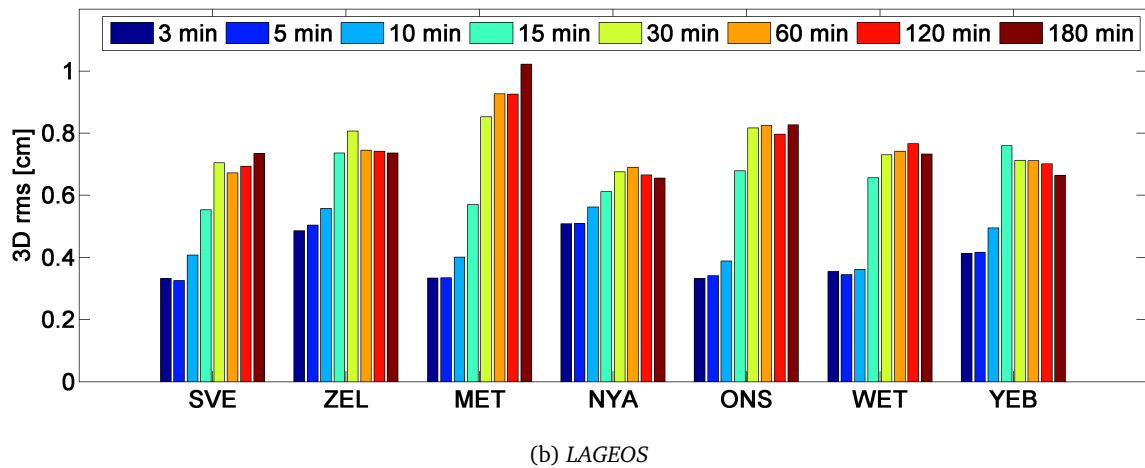
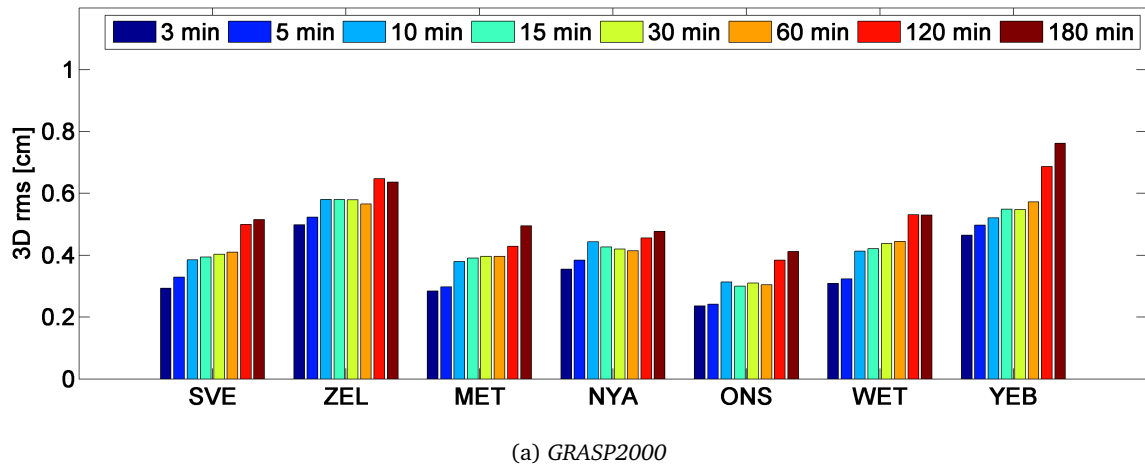


Figure 6.14: Effect on weekly 3D position rms of different intervals for the estimation of the troposphere zenith wet delay, for (a) *GRASP2000* and (b) *LAGEOS*. The observation interval is 1 minute in both cases.

influence of this estimation interval on the results, the solution is repeated for the same simulated data with an estimation interval of 3 min, 5 min, 10 min, 60 min, 120 min, and 180 min. In figure 6.14 the variation of the weekly 3D position rms is shown for the European network observing (a) *GRASP2000* and (b) *LAGEOS*. For *GRASP2000* the results are a little bit better for the short intervals of 3 and 5 minutes, about the same for an interval between 10 and 60 minutes and a little bit worse for the longer intervals. With a maximal variation of 2 to 4 mm, the variation is rather small and the default interval of 30 minutes is found to be okay. This is not the case for *LAGEOS* observations. Here, the variation range is bigger, about 5 mm, with a clear improvement for the shorter intervals of 3, 5, and 10 minutes. The reason for this is not fully understood yet. Following the idea that in the case of *GRASP2000* a further improvement for shorter estimation intervals might be restricted through the influence of other error sources, the investigations were repeated with strongly reduced errors due to the clock and the measurement noise. Therefore, a clock error of $1 \cdot 10^{-16}$ at 50 minutes and a measurement noise of 1 ps were used. But, the

resultant weekly 3D position rms for *GRASP2000* does not get better than the apparent 2 – 3 mm border and the derived figures are almost identical with the ones of figure 6.14, with only a small improvement for *GRASP2000* and a big one for *LAGEOS* when using shorter estimation intervals.

In order to investigate the different behavior in this matter of *GRASP2000* and *LAGEOS* more deeply, in the following the estimated zenith wet delays, as determined during the analysis using different estimation intervals, are compared to the initially simulated zwd. In figure 6.15, the simulated zwd for each observation are shown with blue circles for one day at station Wettzell, while the estimated ones are represented by a green line when an estimation interval of 3 minutes is used, a red line for an interval of 10 minutes and a black line in the case of 30 minutes. One

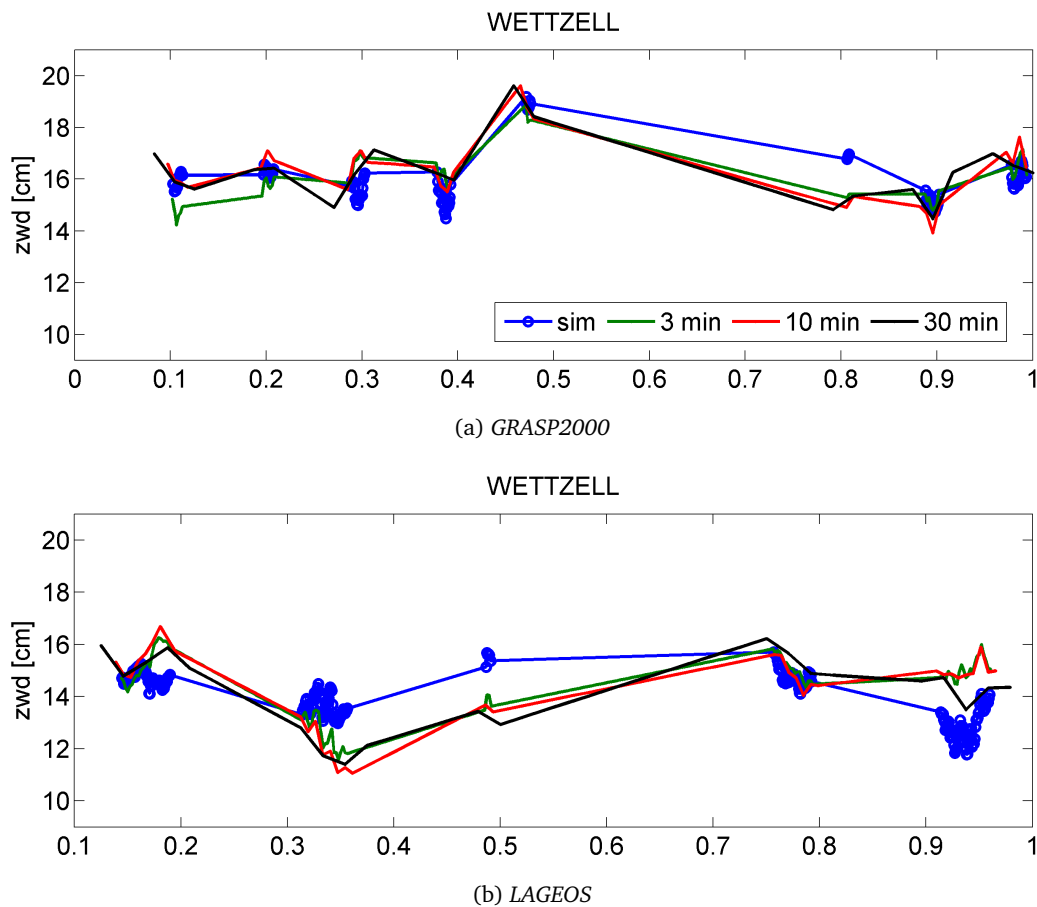


Figure 6.15: Comparison between the simulated zwd (blue) and the estimated ones at station Wettzell observing (a) *GRASP2000* and (b) *LAGEOS* for one day. The observation interval is 1 minute in both cases and the estimation interval for the zwd is 3 minutes (green), 10 minutes (red) and 30 minutes (black). The time axis is given in units of days, starting at midnight of the observed day.

clearly sees, that for both satellites and for all three estimation intervals, the estimates do not fit the simulated zwd very well. This becomes even more clear, when the estimates are interpolated to the observation epochs and compared with the simulated zwd for each observation, as done in figure 6.16. While the big markers represent the zenith wet delays, the small dots in the bottom of the figure show the (absolute) differences between the simulated and the estimated values

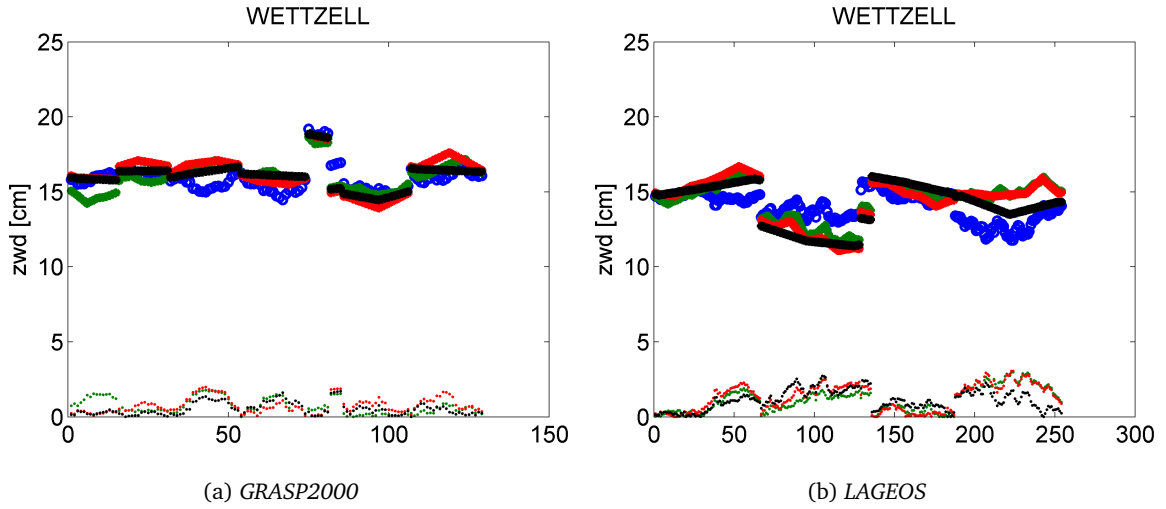


Figure 6.16: Comparison between the simulated zwd (blue) and the estimated ones at station Wetzell observing (a) *GRASP2000* and (b) *LAGEOS* for one day. The observation interval is 1 minute in both cases and the estimation interval for the zwd is 3 minutes (green), 10 minutes (red) and 30 minutes (black), with the estimated values interpolated to the observation epochs. Besides the total values printed with the bigger markers, the small dots represent the absolute deviation from the simulated value. The numbers on the x-axis indicate the number of observation.

in their corresponding color. One can learn, that the estimated zwd deviate from the initially simulated ones for up to some centimeters. Comparing the different estimation intervals, it can also be seen that neither interval reveals considerably better or worse agreement than the others. This comparison, as shown for station Wetzell in figure 6.16, is done for all stations within the EUR network, with the corresponding figures given in appendix B. In table 6.6, the mean deviations during one day are given for each station.

Table 6.6: Deviation of the estimated zwd from the simulated ones in cm, as calculated as the mean value for each station during one day from the results shown in figures 6.16, B.1 and B.2. Values are given for the EUR network observing *GRASP2000* and *LAGEOS* during one day with 1 min intervals, using different estimation intervals of 3 min, 10 min and 30 min. The last column gives the mean values over the 7 stations.

	SVE	ZEL	MET	NYA	ONS	WET	YEB	\emptyset
<i>GRASP2000</i>								
3 min	0.63	0.80	0.53	0.74	0.67	0.71	0.50	0.65 cm
10 min	0.43	0.79	0.62	0.73	0.45	0.76	0.60	0.62 cm
30 min	0.45	0.78	0.54	0.49	0.52	0.53	0.45	0.54 cm
<i>LAGEOS</i>								
3 min	0.78	1.03	0.98	1.03	0.68	1.15	1.55	1.03 cm
10 min	0.76	1.33	0.93	0.78	0.88	1.31	1.93	1.13 cm
30 min	1.11	0.52	1.34	0.91	0.81	1.12	2.77	1.23 cm

On average, the deviation is about 6 mm in the case of *GRASP2000* and about twice the size,

namely 1.1 cm, for *LAGEOS*. Keeping in mind that for a good determination of the zwd one needs observations in different directions and elevations, the better result for the lower *GRASP2000* satellite is reasonable, as it moves much faster across the sky than the higher *LAGEOS* satellite. Considering these relatively big disagreement, the variation in the daily means for the individual stations due to different estimation intervals of 2 – 3 mm is small. Also the variation of the mean values over all stations (last column) is small, with almost no effect visible for *GRASP2000* and a slight improvement of 2 mm in the agreement of simulated and estimated zwd when the estimation interval is decreased from 30 min to 3 min in the case of *LAGEOS*. Unfortunately, repeated evaluation like the one above for several days, attempting to explain good results in 3D position rms by better agreement between simulated and estimated zwd did not reveal a clear relation. Obviously, the complete procedure of estimating station coordinates in a regional VLBI network, together with the other necessary parameters is more complicated and such a connection is not as straightforward as one might wish. Possibly, also the fact that a regional network is investigated and that the NNT and NNR conditions are applied is of importance in this aspect.

Considering the quite large disagreement of a few centimeters between the simulated and the estimated zwd, the applied relative constraints of 1 cm after 30 min are not that loose any more. As a consequence, different constraints are tested. For the derivation of figure 6.17, the European experiments are simulated once and analyzed using constraints of 10 cm, 1 cm and 3 mm after 30 min, always applying three different estimation intervals of 5 min, 10 min and 30 min. Once again, the effects on the determined weekly 3D position rms of applying different constraints during the estimation of the zwd are bigger for *LAGEOS* than for *GRASP2000*. Generally, figure 6.17 shows that constraints of 10 cm after 30 min are too loose and give worse results. When applying very tight constraints, namely 3 mm after 30 min, for both satellites the results are rather unaffected by different estimation intervals and also in the case of *LAGEOS* the mysterious jumps in the results when going from a 30 min interval to a 10 min interval vanish. Concluding, one can say that the choice of the applied constraints and the estimation interval of the zwd shall be taken carefully as it can influence the results noticeably. For the results within this thesis, the standard values of 1 cm constraints after 30 min and the estimation interval of 30 min are used.

As a last point investigating the peculiar behavior of *GRASP2000* and *LAGEOS*, and presenting an idea for future studies, a probable relation with the different pass lengths of the satellites being visible for the regional network is mentioned. Shown in figure 6.18 is the duration of each satellite pass, i. e. the time between the first and the last observation of a pass, when (a) *GRASP2000* and (b) *LAGEOS* were observed with the regional EUR network for seven days. As can be seen, the maximum pass length, i.e. the duration while the satellite can be observed from at least two station of the network, for *GRASP200* is about 20 – 27 min, while *LAGEOS* can be observed up to 75 min without interruption. In the case of *GRASP2000* this means, that when an estimation interval of 30 min is used there is only one zenith wet delay estimated for one pass. Following this idea, one could adapt the software accordingly, enabling to determine the estimation interval not on fixed time intervals but in dependence of the particular pass length,

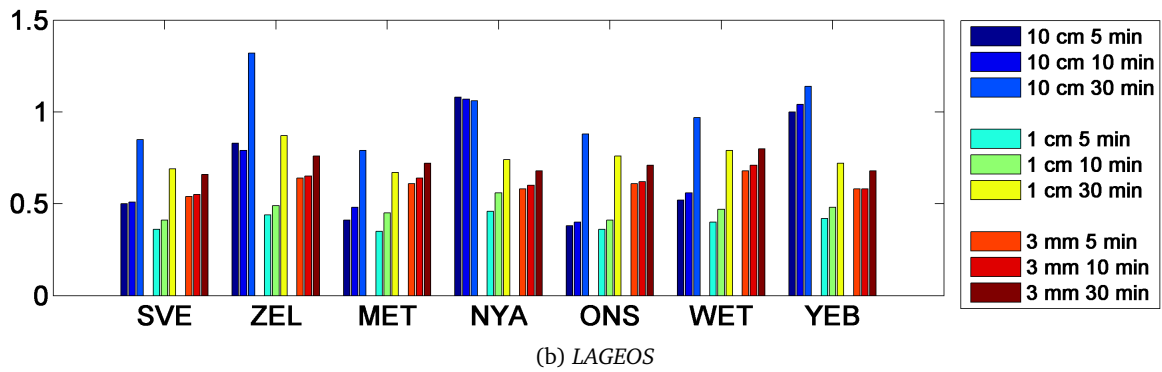
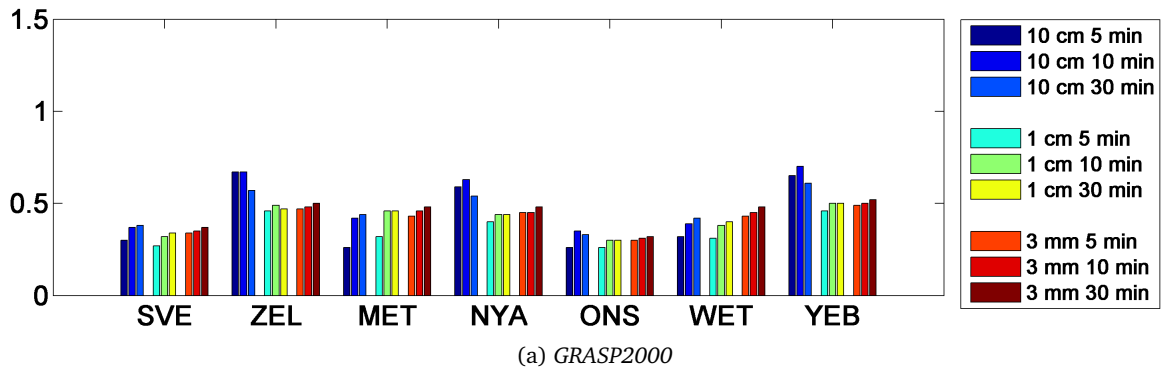


Figure 6.17: Effect on the weekly 3D position rms when different constraints and estimation intervals for the zwd are used for (a) GRASP2000 and (b) LAGEOS. Both satellites are observed with the EUR network with 1 minute intervals for 7 days. The results are shown for each station, arranged in blocks of using the same constraints for different estimation intervals of 5 min, 10 min and 30 min. The applied constraints are 10 cm (blue bars), 1 cm (green) and 3 mm (red), always after 30 min.

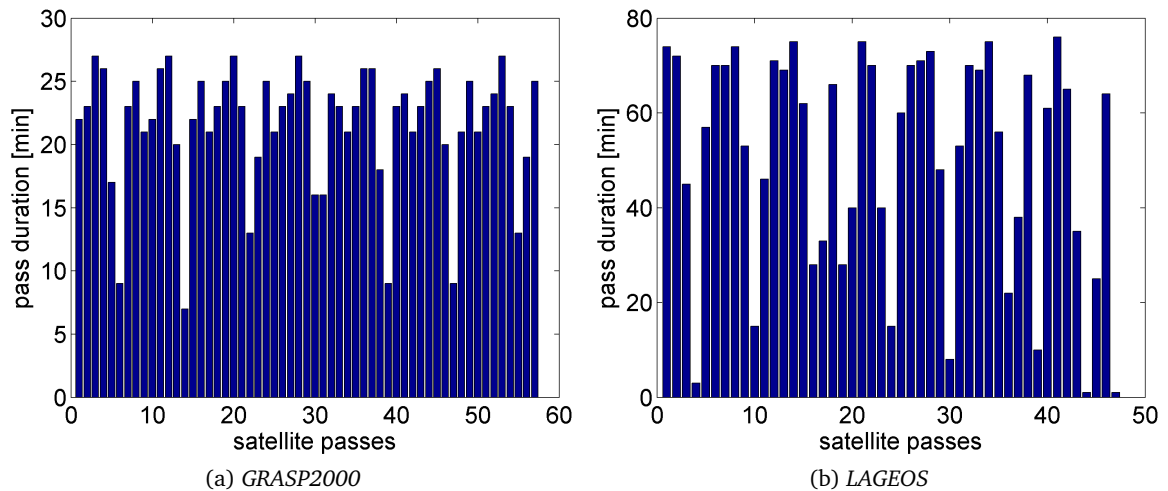


Figure 6.18: Duration of the satellite passes, i.e. the time between the first and the last observation of a pass, for (a) GRASP2000 and (b) LAGEOS, observed with the regional EUR network for seven days.

e.g. estimating 1, 2 or n zwd for one pass.

In the end of this section, the question may arise why station position repeatabilities of a few millimeters can be achieved with the troposphere determined that bad. The solution here are the multiple satellite passes which seem to stabilize the solution for antenna positions. This is investigated more closely in the following section.

6.2.6 Satellite passes

The observational concept of VLBI satellite tracking proposed in this thesis strongly relies

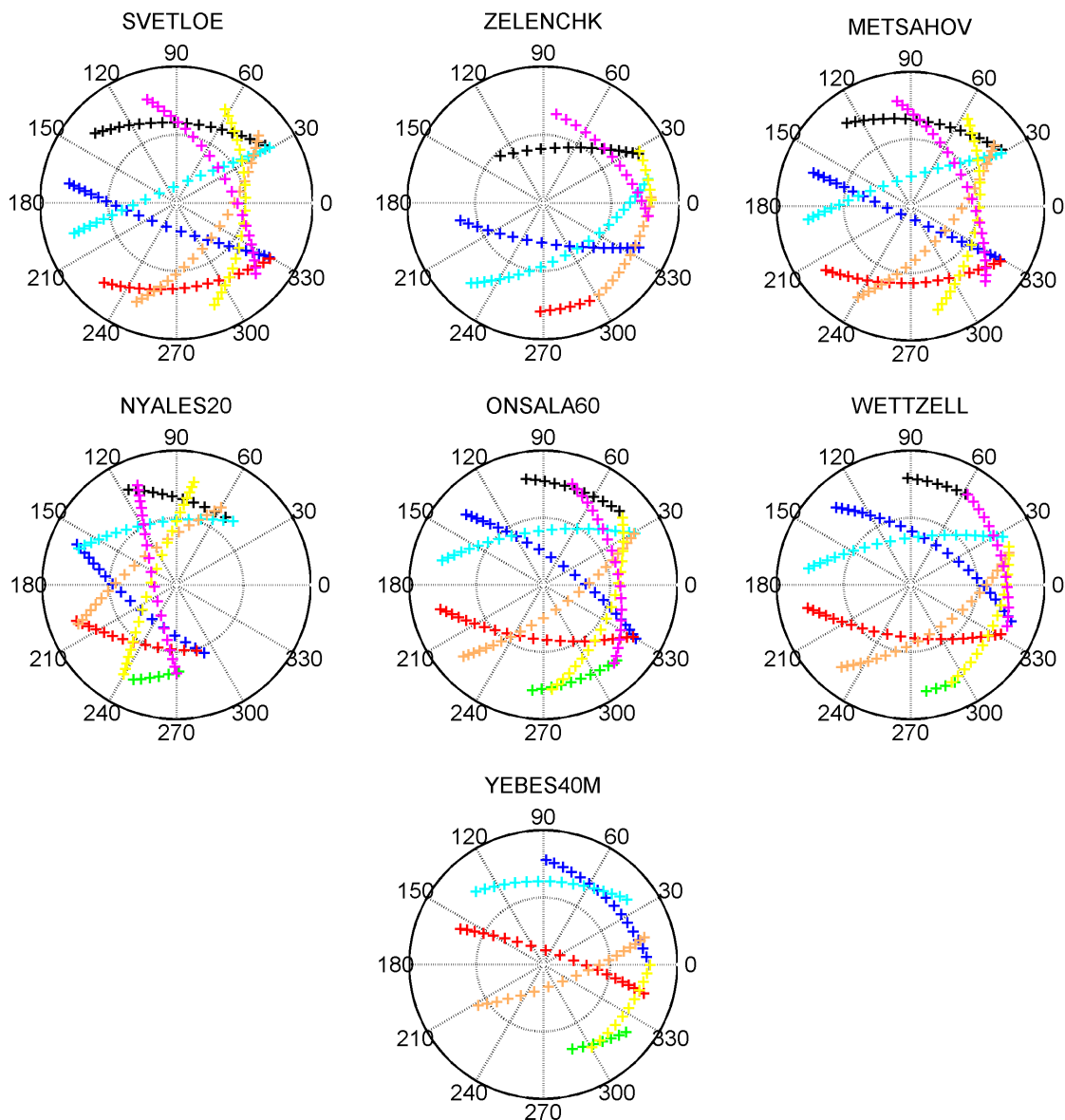


Figure 6.19: 1-day satellite passes of *GRASP2000* observed with the 7 stations of the EUR network. Each new pass is colored differently.

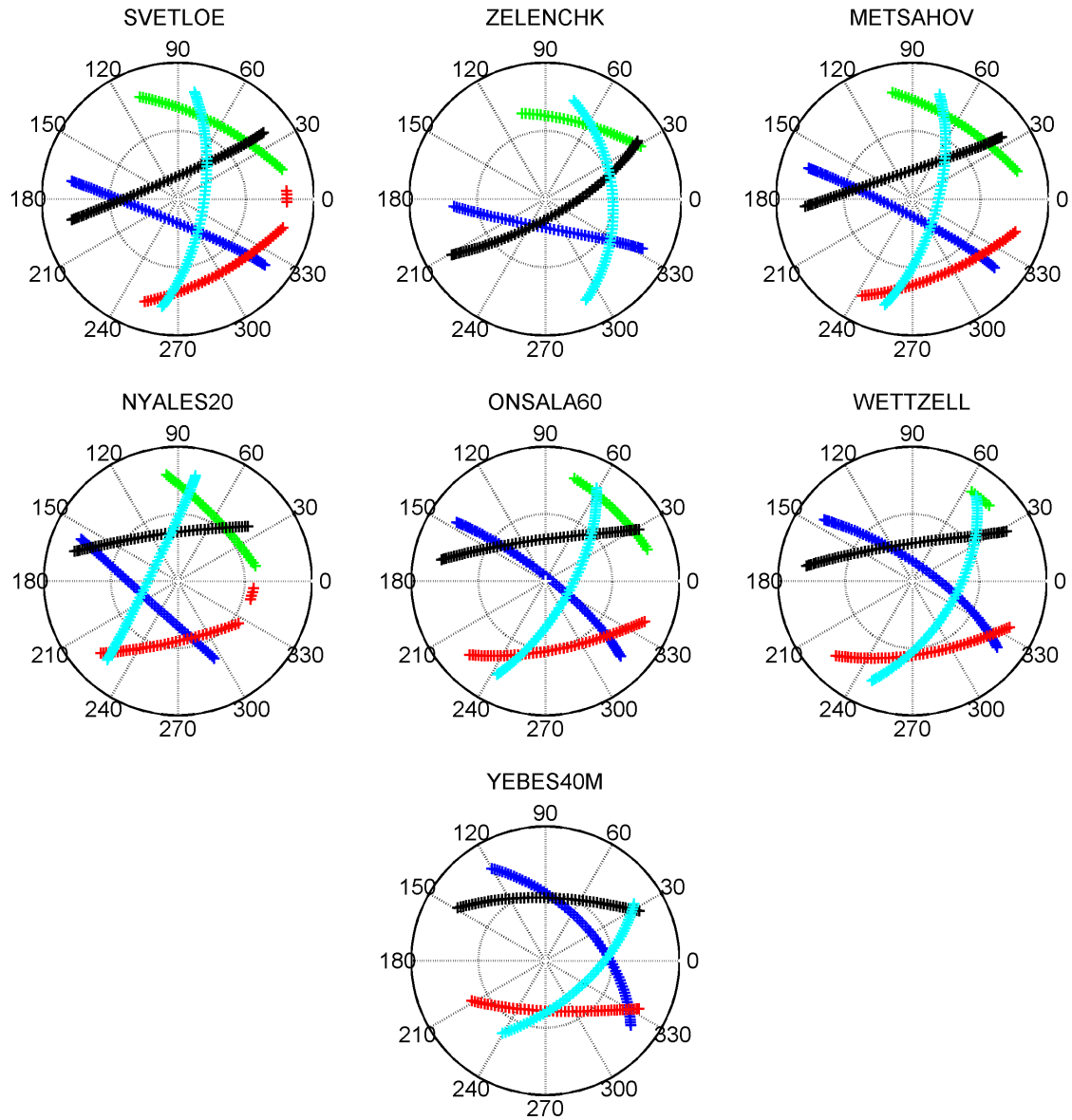


Figure 6.20: 1-day satellite passes of *LAGEOS* observed with the 7 stations of the EUR network. Each new pass is colored differently.

on several satellite passes over a station, creating new geometry each pass. This influence of the number of passes on the results is investigated in this section. Therefore, the schedule for one day observing *GRASP2000* and *LAGEOS* with the EUR network is split into separate schedules, each including one pass more than the previous schedule. In figures 6.19 and 6.20 these schedules are illustrated by showing the skyplots for each station, with each new pass printed in a new color. In the case of *GRASP2000* the satellite passes Europe 8 times during the day, for *LAGEOS* 5 passes are counted.

For the 1-day schedules, including 1 to 8 passes, respectively 1 to 5 in the case of *LAGEOS*, mean station position repeatabilities are calculated. The results, plotted against the number of

satellite passes, are shown in figure 6.21. It can be concluded that, in order to get good results,

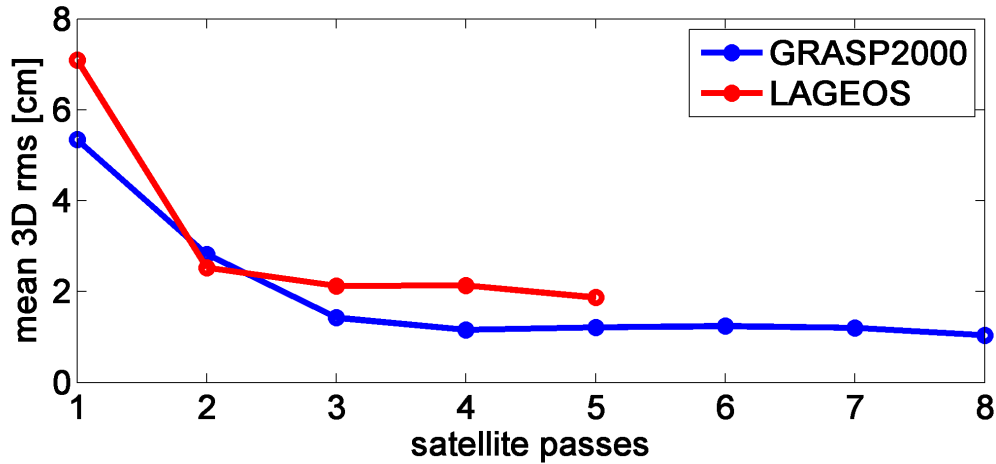


Figure 6.21: 1-day mean 3D position rms versus satellite passes for *GRASP2000* (blue) and *LAGEOS* (red). The mean values are calculated from the results of the 7 stations within the EUR network.

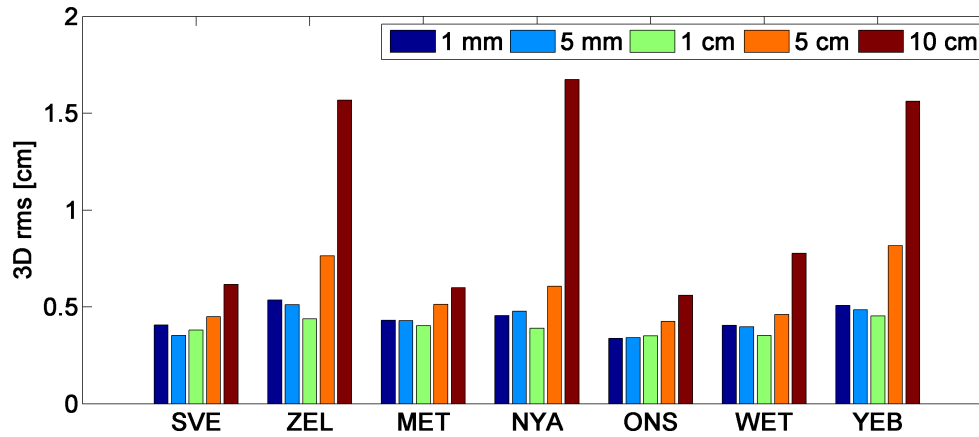
at least three satellite passes are required. One further sees that for both satellites from three passes on the results are good and stay constant for more passes. Hereby one has to respect that the results are not comparable to those of the weekly solutions shown in the other sections of this thesis (also see sec. 6.2.1) and that small variation is due to the fact that for each schedule new simulations are done (see also figure 6.13-d).

6.2.7 Orbit error

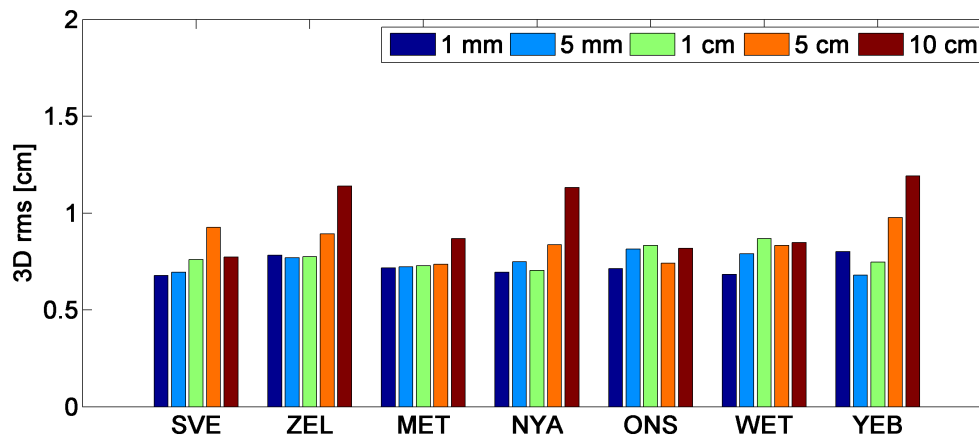
The simulation studies presented in this work concentrate on the derivation of antenna positions on Earth in the system of the observed satellite. It is assumed that the satellite's position is well known and orbit determination is not a primary goal. However, in order to be able to quantify the effect of possible orbit errors on the results, a simple investigation is performed in this context. Orbit errors are implemented in the simulation study as follows: first, the simulated observations using the default simulation parameters are created using the standard - *correct* - orbit. In the processing, every 15 minutes the satellite position (xyz) is moved by a new set of translation (Δxyz), that is determined by a random number between ± 1 times the maximal orbit error σ_o .

$$xyz_{\text{TRS}} = xyz_{\text{TRS}} + \Delta xyz = \begin{pmatrix} x \\ y \\ z \end{pmatrix}_{\text{TRS}} + \begin{pmatrix} \text{rand} \cdot \sigma_o \\ \text{rand} \cdot \sigma_o \\ \text{rand} \cdot \sigma_o \end{pmatrix} \quad (6.5)$$

In fig. 6.22 the weekly 3D position rms are shown for the EUR network, when the orbits of (a) *GRASP2000* and (b) *LAGEOS* are affected by errors σ_o of 1 mm, 5 mm, 1 cm, 5 cm, and 10 cm.



(a) GRASP2000



(b) LAGEOS

Figure 6.22: Effect of orbit errors at the level of 1 mm, 5 mm, 1 cm, 5 cm and 10 cm on the weekly 3D position rms for (a) *GRASP2000* and (b) *LAGEOS*. The observations are scheduled for the EUR network at intervals of 1 minute.

For the investigated schedules, VLBI observations to *GRASP2000* can compensate such systematic errors during a 15 min interval up to a size of 1 cm, before the orbit errors can significantly affect the derived antenna positions on Earth. For the *LAGEOS* satellite the effect of the orbit error is weaker. When σ_o is between 1 mm and 1 cm the derived results reside on the same level, while a worsening can be seen for the higher σ_o of 5 and 10 cm. Despite the very simple procedure to assess the effect of orbit errors on the derived results, one can conclude that, for the investigated schedules, the determination of station positions in the satellite system is resistant to a maximal orbit error of 1 cm.

The investigation of orbit errors on the derived station coordinates is an interesting topic. As already mentioned in chapter 2.4.1, possible distortions of the satellite frame, realized by the satellite orbit(s), with respect to the ITRF or the VLBI frame, can e.g. be reflected in the Earth

rotation parameters. Additionally, systematic errors can affect the determined station positions. In order to investigate this, such effects first need to be simulated during the orbit integration creating an erroneous orbit, that later on is used in the analysis of the simulated schedules. As the simple example above shows, the preparations in the software for testing such effects are done, opening the field for future research in that area.

6.2.8 Investigated time span

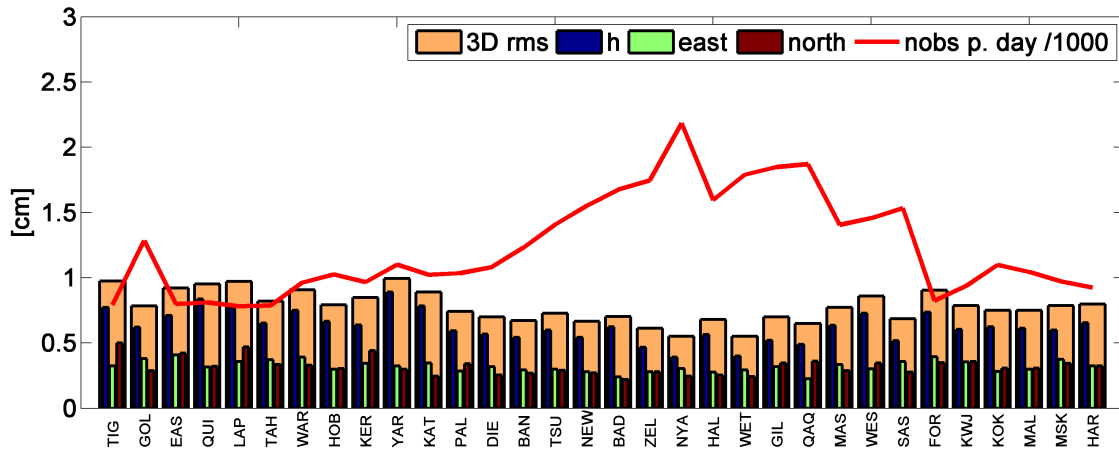
With all the investigations presented within this thesis relying on the identical week of simulated orbits, the question arises whether the results are also valid for other time spans. Decisive for the study is mainly the common visibility for the observing antennas, what is determined through the satellite orbits. Studying the integrated orbits, it is concluded that the presented results are rather independent of the chosen epoch. As shown in figure 6.2, the ground tracks of *GRASP2000*, *GRASPELL* and *LAGEOS* cover the whole globe during one day and repeat further on. Hence, if schedules of at least one day duration are used, the actual date is not of importance. Similar behavior is found for satellites of the *GPS*. With the orbital period of 12 sidereal hours, the ground track repeats twice a day with a short time shift each pass. Consequently, in the case of *GPS* the choice of the satellite is decisive for the visibility conditions while the epoch, as long as the schedule lasts at least 12 hours, is negligible.

6.3 Global networks

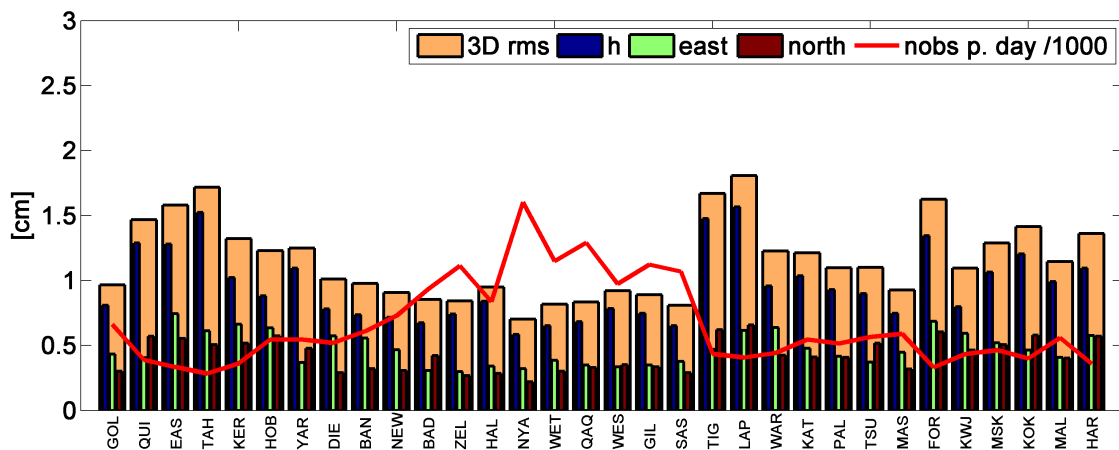
Following the promising results of VLBI satellite observations with regional networks, simulations for global networks are done next. Therefore, the artificial VLBI networks with 32 respectively 16 stations, as introduced in section 6.1.2, are used. The observed satellites are *GRASP2000* and *LAGEOS*.

6.3.1 32 stations

The results for the 32-stations network observing (a) *LAGEOS* and (b) *GRASP2000* are shown in figure 6.23. The standard observation parameters of 1 minute intervals and 10° cutoff angle are used for *LAGEOS*. Due to strong limitations in common visibility and otherwise bad results, for *GRASP2000* the observing interval is decreased to 30 seconds and the cutoff angle is reduced to 5° . For *LAGEOS*, the achieved accuracies with a mean weekly 3D position rms of 8 mm are comparable to that of the regional networks. Stations with more observations are slightly better than stations with less, as indicated by the red line. For *GRASP2000*, the results are about a factor two worse than for the regional networks, with the dependence on the number of observations even more evident. Weekly 3D position rms between 9 and 19 mm are found. The explanation for the difference in the results between the high and the low satellite is found when studying the lengths of the observed baselines. Comparing the baseline geometry shown in figure 6.24 (a) and (b), one sees that no observations over the Pacific e.g. with antennas in Hawaii and Japan



(a) LAGEOS

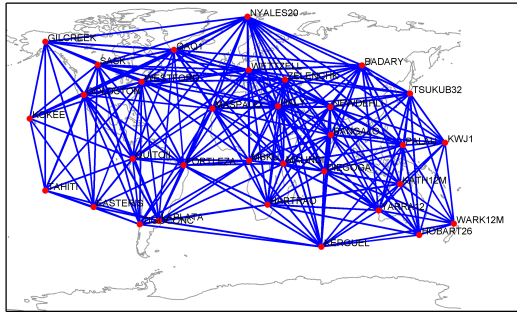


(b) GRASP2000

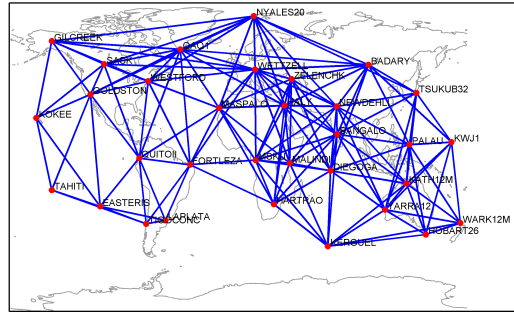
Figure 6.23: Weekly 3D position rms of a global 32-stations network observing (a) *LAGEOS* and (b) *GRASP2000*. The used observation parameters are an interval of 1 minute with 10° cutoff for *LAGEOS* and 30 seconds with 5° cutoff for *GRASP2000*.

or Tahiti and New Zealand are found for both satellites. But it is also clear that the baseline plot for *LAGEOS* is much denser than that for *GRASP2000*. While with *LAGEOS* observations are done on 282 baselines (c), for *GRASP2000* common visibility is found for only 159 baselines (d). In the previous section good results for *GRASP2000* were found for baselines between 2000 and 3000 km, in the global 32-stations network the majority of baselines is much longer. According to figure 5.3, the maximal common elevation angles for a satellite at 2000 km height on baselines between 4000 and 7000 km is quite low, namely below 30° . For the higher *LAGEOS* satellite at 6000 km (yellow area), baseline lengths up to 8000 or 9000 km are not a problem.

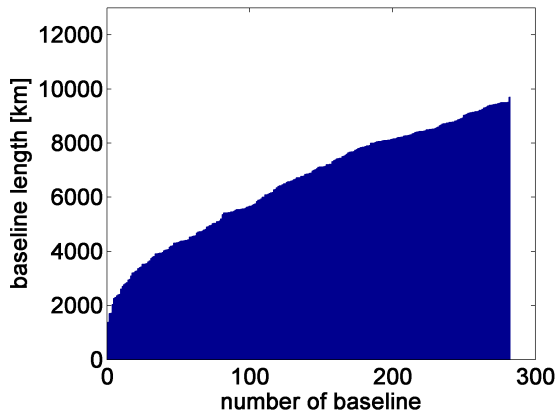
With the simulations for the 32-stations network it can be concluded that (a) *LAGEOS* can be observed revealing same accuracies as in dense regional networks and that (b) for *GRASP2000* the baselines are slightly too long and the results are about a factor of two worse.



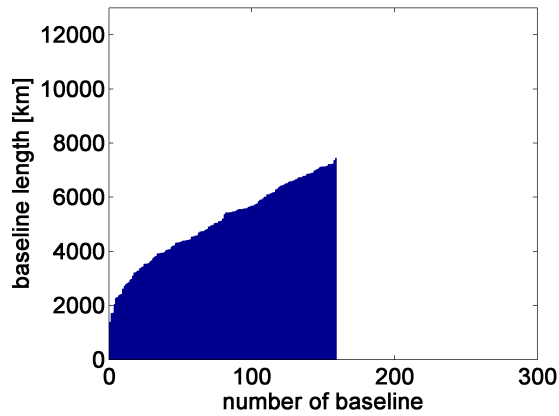
(a) LAGEOS baselines



(b) GRASP2000 baselines



(c) LAGEOS baseline lengths

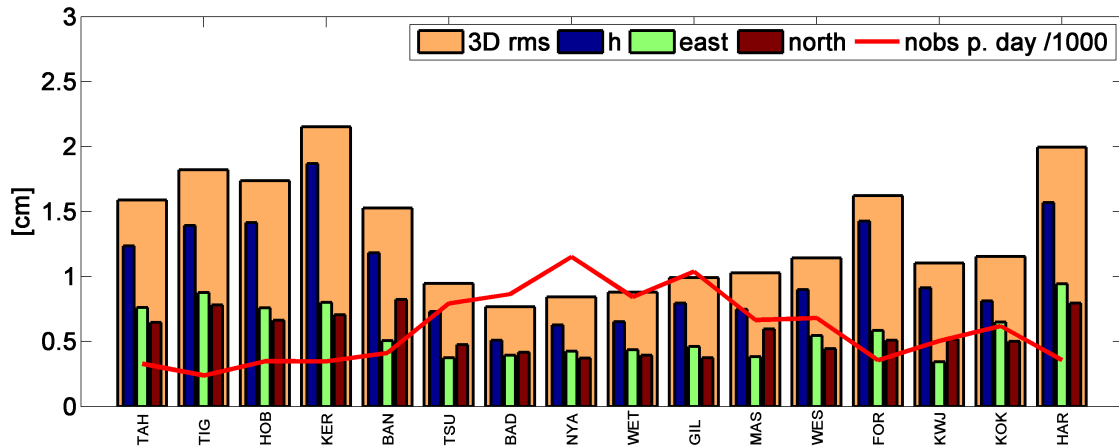


(d) GRASP2000 baseline lengths

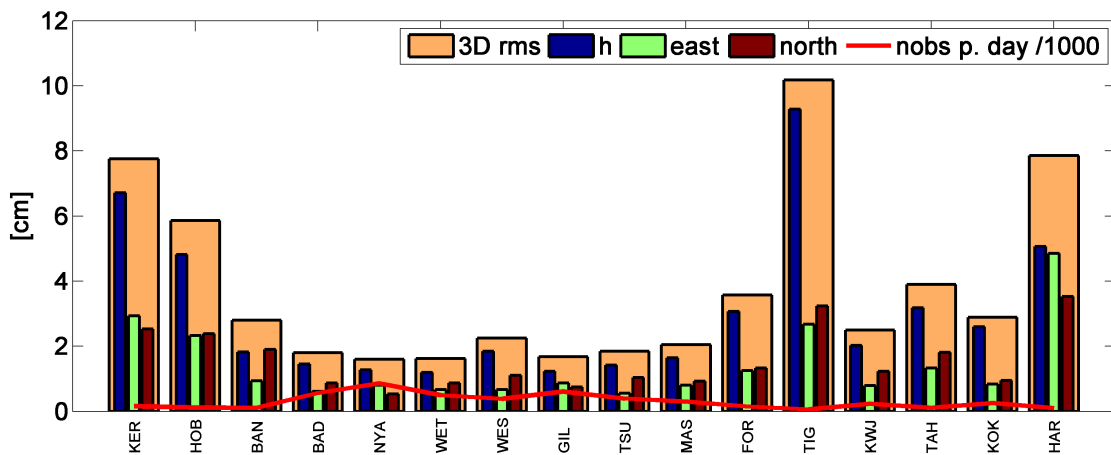
Figure 6.24: Illustration of the observed baselines in the 32-stations network for (a) LAGEOS and (b) GRASP2000 and the corresponding lengths of these baselines for (c) LAGEOS and (d) GRASP2000.

6.3.2 16 stations

With a network comprising 32 antennas being rather big compared to nowadays usual networks, investigations are done for a 16-stations network next. Despite the fact that, for better homogeneity, there are still some antennas included that do not exist (yet), simply the reduced number from 32 to 16 stations is more realistic and meets today's available antenna infrastructure. In figure 6.25 the results for (a) LAGEOS and (b) GRASP2000 are shown. A mean station position repeatability of 1.3 cm is found for observations to the LAGEOS satellite, with strong dependence on the varying number of observations per station. As shown in figures 6.26 (a) and (c), the total number of baselines reduces to 67, with only loose links to the stations on the edges of the network. Consequently, the network effect that was already observed in the regional networks is also evident in the 16-stations network. While the observations between Tsukuba and Gilcreek close the network in the north, revealing good results for these two stations, no observations are found across the Pacific in the south causing poor results for the stations there. Already causing problems for LAGEOS, for GRASP2000 the observed baseline network (figure 6.26-b) is



(a) LAGEOS



(b) GRASP2000

Figure 6.25: Weekly 3D position rms of a global 16-stations network observing (a) *LAGEOS* and (b) *GRASP2000*. The used observation parameters are an interval of 1 minute with 10° cut off for *LAGEOS* and 30 seconds with 5° cut off for *GRASP2000*.

too sparse, resulting in station position repeatabilities of several centimeters. With only three baselines of a total of 39 lying close to the above identified optimal length range below 3000 km (6.26-d), this network is found to be not suitable for observing a low satellite at 2000 km height.

6.3.3 Cluster network

Facing the situation of having optimum baseline lengths but a strong network effect in the regional networks and slightly too long distances between the antennas in the global networks, here the option of cluster networks is tested. This means, that the three regional networks of section 6.2 with short baselines are combined to one cluster network. This ensures dense regional resolution on the one hand and shall lessen the network effect through the global connection on

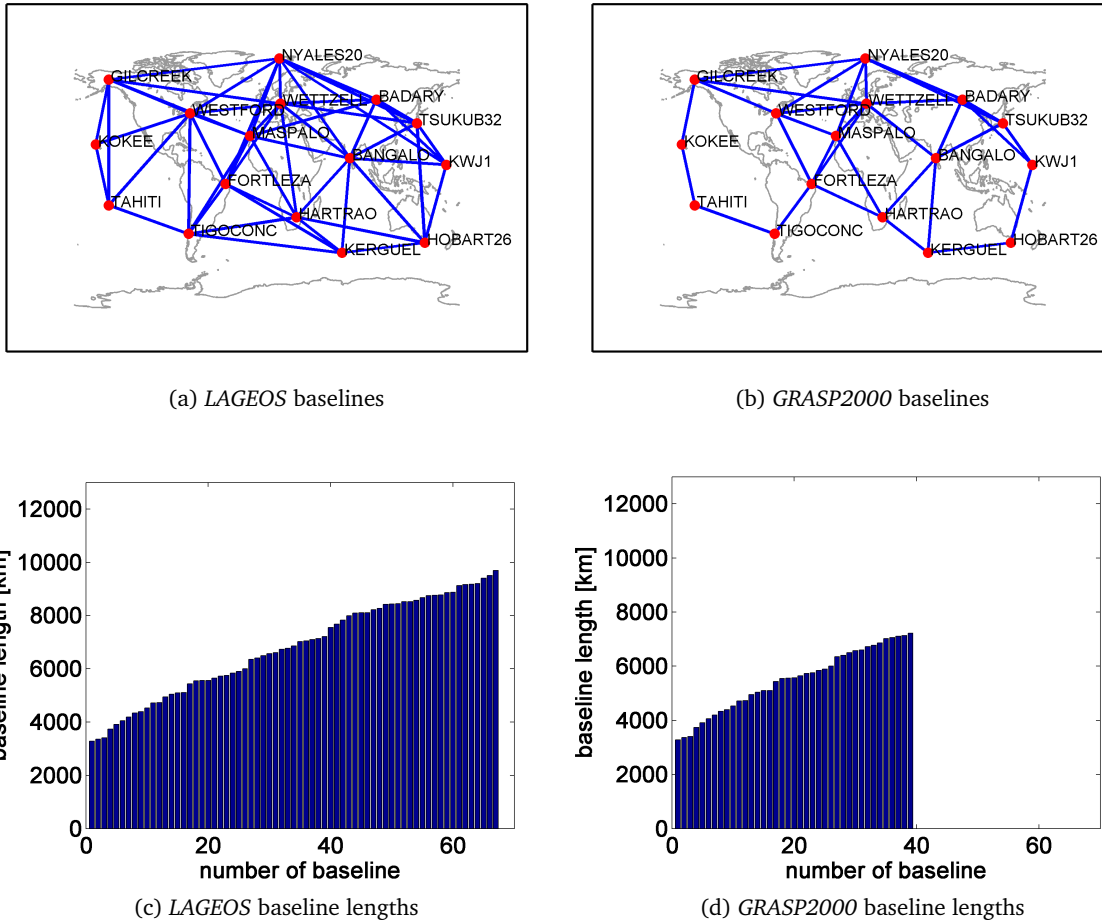


Figure 6.26: Illustration of the observed baselines in the 16-stations network for (a) *LAGEOS* and (b) *GRASP2000* and the corresponding lengths of these baselines for (c) *LAGEOS* and (d) *GRASP2000*.

the other. The results for *LAGEOS* and *GRASP2000* are shown in figure 6.27 with the corresponding observed baselines illustrated in figure 6.28. This time, the standard scheduling parameters of 1 minute intervals and 10° cutoff angle are also used for *GRASP2000*. Through the global connection, the number of observed baselines in the cluster network increases from 57¹ to 144 for *LAGEOS* and respectively 82 for *GRASP2000*. For *LAGEOS*, a mean 3D position rms of 9 mm is found. There are two classes of stations, with HOB, WAR, DSS, PAR, YAR, KAT and YEB having only about half of the observations compared to the rest of the stations and showing worse results. The height component clearly dominates the position errors, indicating that the network effect vanishes through the cluster approach. Compared to the separate regional networks solutions of section 6.2, for *LAGEOS* the results with the cluster approach are at the same level. In the case of *GRASP2000*, a worsening of the results to a mean weekly 3D position rms of 1.2 cm is found. As can be seen in figure 6.28 (d), the additional baselines connecting the sub-networks are predominantly outside the optimum lengths between 2000 and 3000 km. Consequently, the

¹= sum of the baselines in the three regional networks as given in figure 6.8: 21 + 21 + 15 = 57.

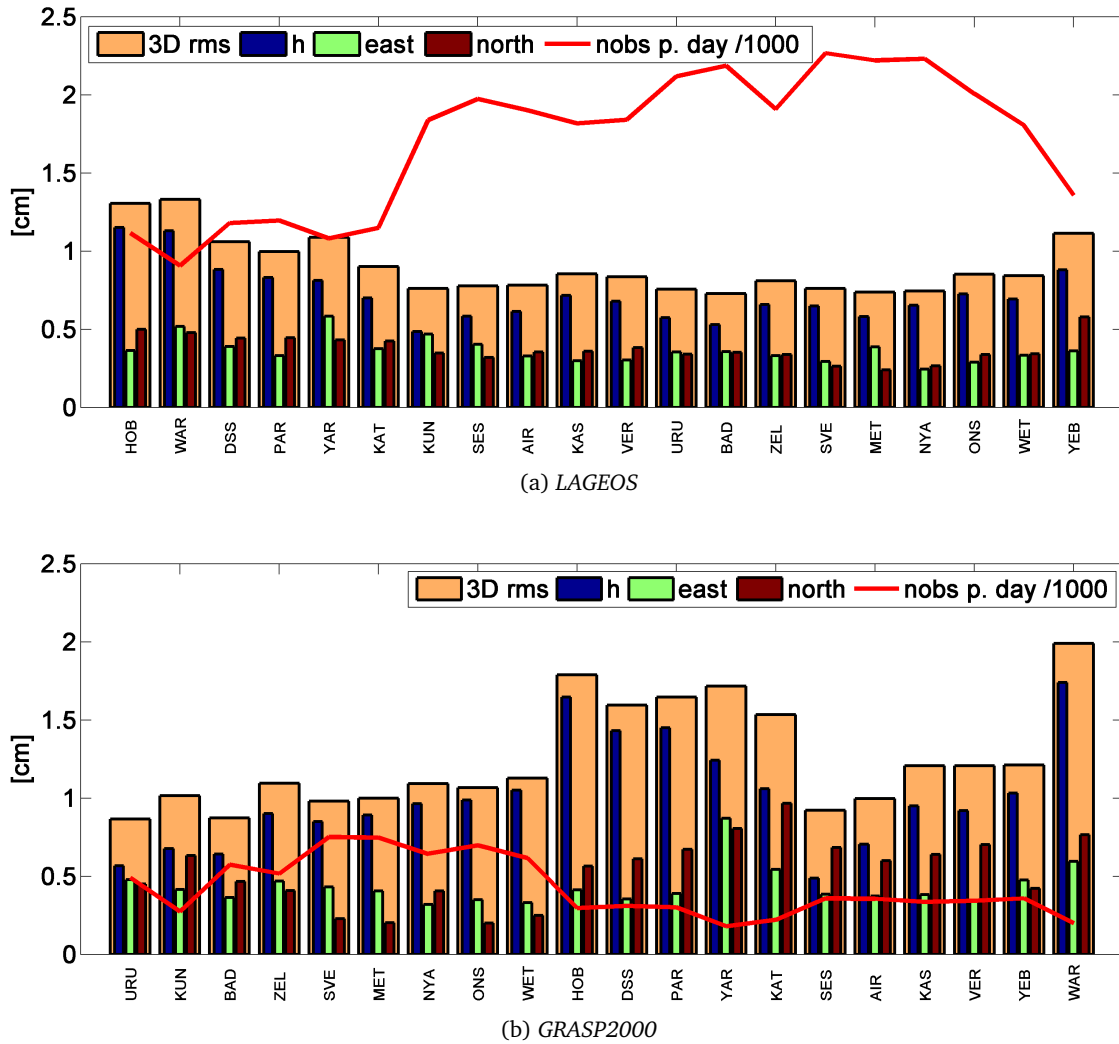


Figure 6.27: Expected station position repeatabilities for a global cluster network observing (a) *LAGEOS* and (b) *GRASP2000*. Observations are scheduled for one week with 1-min intervals and a cutoff elevation angle of 10° .

interconnecting observations have to be performed at low elevations, what might be an explanation for the generally big errors in the height components. The theory of too long baselines for *GRASP2000* is strengthened through the fact that changing the scheduling options to 30 seconds intervals and 5° cutoff angle does not improve the results. Another point is the fact, that in the single regional networks errors are possibly compensated through distribution within the network, what might not be the case to the same extent in the global cluster networks.

Summarizing the investigations on global networks one can conclude that for *LAGEOS* adequate networks can be found, though the number of participating antennas has to be quite high. Despite the intended homogeneously distributed networks, the results differ from station to station. On the one hand this is due to the different number of observations for each station, as controlled by the satellite orbit, on the other hand it is related to the geometry determined by

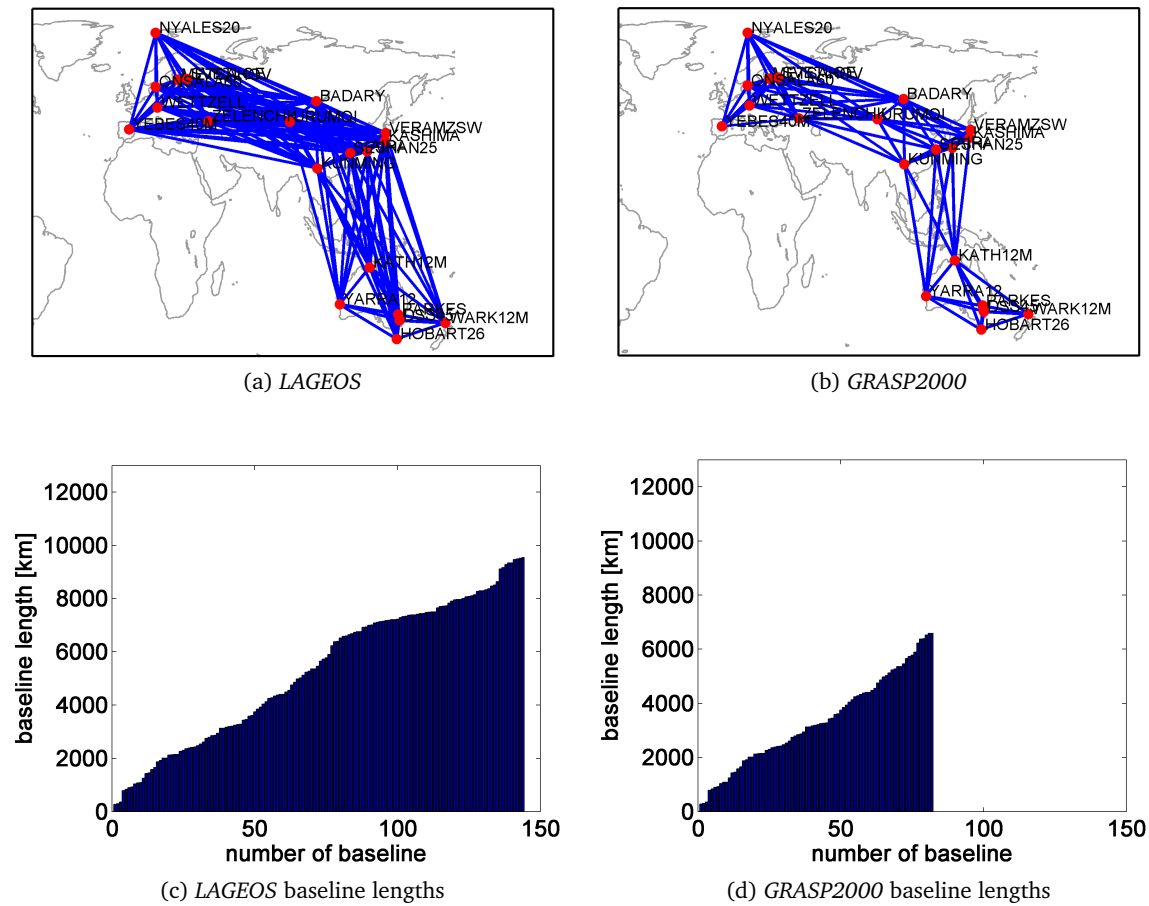


Figure 6.28: Illustration of the observed baselines in the cluster network for (a) *LAGEOS* and (b) *GRASP2000* and the corresponding lengths of these baselines for (c) *LAGEOS* and (d) *GRASP2000*.

the location of the antenna in the antenna network. In the case of *GRASP2000* the global baselines are rather challenging. The best option here probably is to use cluster networks instead of networks striving for a homogeneous global coverage. In general, for all investigated networks the errors in the height component are found to be about a factor of two worse compared to the horizontal components. This is another indication that the troposphere is not determined very well and alternative methods like e.g. additional observations to radio sources to resolve the troposphere might be beneficial.

6.4 Observations to GNSS-satellites

Satellites of the GNSS are situated at heights of about 20000 km above ground and orbit the Earth approximately twice per day. Although this height enables good common visibilities also for large antenna networks, the approach for VLBI satellite observations applied in the previous sections does not deliver good results for satellites of the GNSS. As apparent in figure 6.5 (d), in a regional network weekly 3D position rms of several centimeters are expected. Also evident is

the fact, that the errors do not only effect the height component, what would indicate problems with the troposphere, but also the horizontal positions are badly determined. Reason for this is the poor geometry of the network observing a single GPS-satellite. This can be seen in the station's skyplots of figure 6.29. Here, for station Wetzell the distribution of the observations in the sky during one day is shown, for observing (a) a single GPS-satellite, (b) *GRASP2000* and (c) *LAGEOS*. While *GRASP2000* and *LAGEOS* orbit the Earth several times per day providing good distribution in the sky, the GPS-satellite moves very slowly over the sky and only passes each station twice per day, on the same satellite track. This is neither sufficient for resolving the troposphere nor for a good geometry to accurately determine antenna positions. Also observations

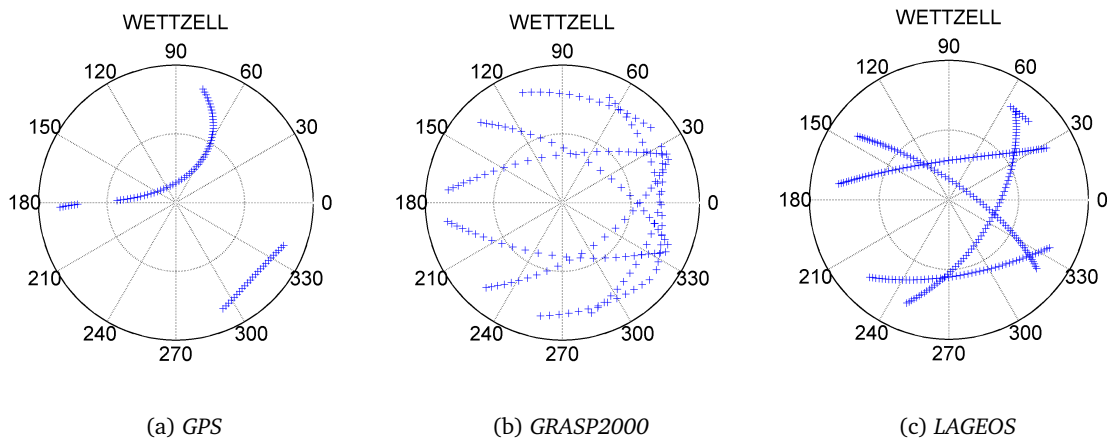


Figure 6.29: 1-day skyplots for station Wetzell observing (a) a GPS-satellite with 5-min intervals and (b) *GRASP2000* and (c) *LAGEOS* with 1-min intervals each.

with the global antenna networks are not very promising. In figure 6.30, the results are shown when one GPS-satellite was observed with the 32-stations network at 5 minutes intervals. Al-

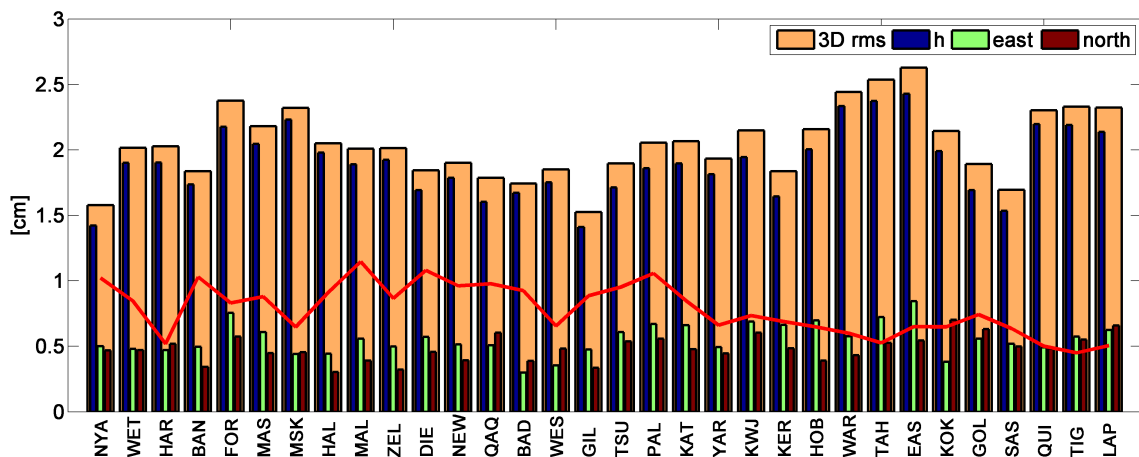


Figure 6.30: Weekly 3D position rms when one GPS-satellite was observed with the 32-stations network with 5-min intervals.

though observations are found for 361 baselines with lengths up to the Earth's diameter, a mean station position repeatability of 2 cm is found. Clearly evident is the difference between the horizontal position errors and the error in the height component. The former can be determined very precisely, at the level of a few millimeters only, what is presumably a result of the high number of baselines connecting the stations to each other tightly. Unfortunately, the height component is only poorly determined, revealing repeatabilities of about 2 cm.

Consequently, if satellites of the GNSS shall be observed with VLBI, alternative methods than the ones applied in sections 6.2 and 6.3 have to be found. In this section, two alternative strategies of observing GNSS-satellites with VLBI are introduced: for first, the idea of including satellite observations into a standard geodetic VLBI session to radio sources is followed (sec. 6.4.1); in the second approach observations are scheduled to a satellite constellation, i. e. several GPS satellites instead of a single satellite are observed (sec. 6.4.2). For the following investigations only satellites of the GPS are used. However, due to the similar system and orbit characteristics of the other GNSS systems, it is assumed that the findings are transferable when satellites of the GLONASS system or of the upcoming Galileo or BeiDou systems were observed.

6.4.1 Combined observations of a satellite and radio sources

In the combined approach the idea is to combine the satellite observations with a normal geodetic VLBI session as illustrated in figure 6.31. The geodetic VLBI sessions are scheduled with

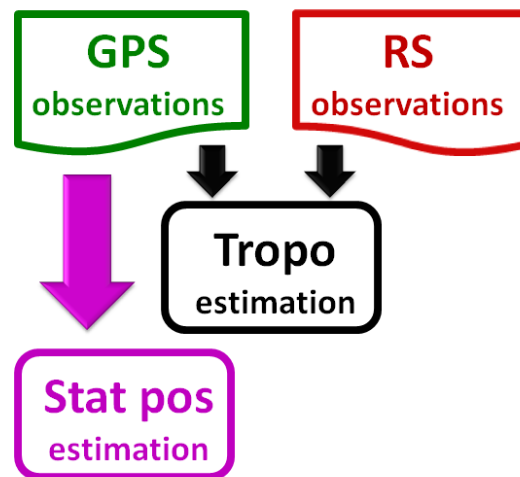


Figure 6.31: Concept of the combined approach. The satellite observations are embedded in a standard VLBI session. In a first step the troposphere parameters are determined using all observations and in a second step station positions are derived using observations to the GPS satellite only.

the scheduling part of the Vienna VLBI Software $Vi_{e_{\text{sched}}}$. As described in detail by Sun (2013), $Vi_{e_{\text{sched}}}$ schedules observations following several commandments. One of them is the aim for good sky coverage for each station, what normally stands for a good resolution of the troposphere enabling precise determination of the target parameters, as e.g. antenna positions. The

geodetic schedule is then merged with the satellite schedule, for the time being without taking care of necessary antenna slewing times or observation durations. For the combined schedule the observations are simulated, meaning that the same troposphere and clocks are assumed for both types of observations. In the processing, while all observations are used for the estimation of zenith wet delays and clocks, for determining the stations' positions only observations to the satellites are utilized. This enables a good resolution of the troposphere on the one hand, but, on the other hand, also delivers the antenna positions in the satellite system. These positions could then be compared to those determined with the radio source positions, delivering a direct frame tie on Earth between the satellite system and the VLBI frame. This approach is applied for the European network observing one GPS satellite with 5-minutes intervals. As shown in figure 6.32 (a), the additional observations to radio sources strongly improve the sky coverage compared to the satellite-only observations shown in figure 6.29 (a). As a result, shown in figure 6.32 (b), a

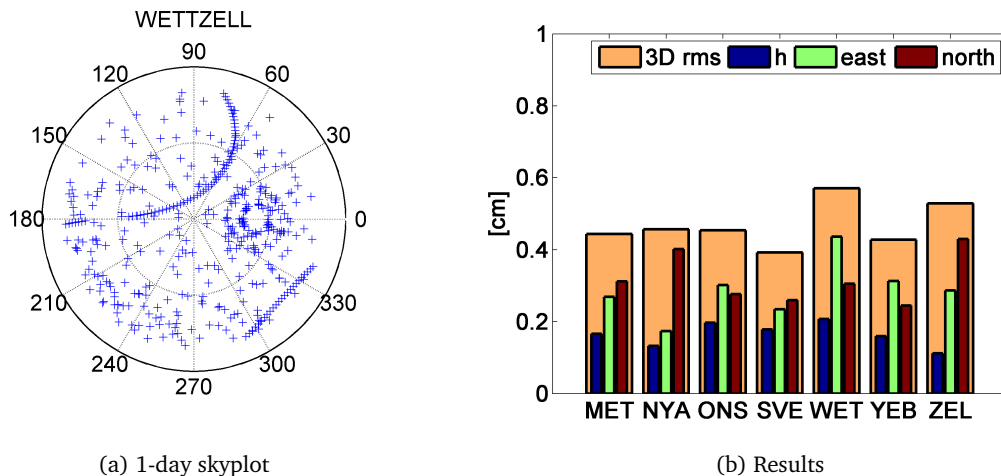


Figure 6.32: 1-day skyplot of station Wetzell for the combined observations (a) and the results in terms of 3D position repeatabilities for the EUR network (b). The results are obtained within a weekly solution with a combined schedule of standard VLBI observations to radio sources and observations to one GPS satellite with 5-min intervals.

mean weekly 3D position rms of 5 mm is found. Compared to the satellite-only solution shown in figure 6.5 (d), this is an improvement of almost a factor of ten for the combined approach. Interesting is the fact that now the height errors are entirely smaller than the horizontal components. On the one hand, this can be explained with the use of a regional network and the already previously observed network effect. On the other hand, as for the estimation for the antenna coordinates only the satellite observations are used, the satellite orbit is also important in this aspect. Differently to the previously investigated *GRASP* and *LAGEOS* satellites, whose track over the station changes each pass (see sec. 6.2.6), in the case of the GPS satellite the geometry used for antenna positioning stays the same for each pass. Consequently, it can happen that one horizontal component is not as well determined as the other.

Overall, the combined approach delivers good results and might also be an option for ob-

servations to the other satellites, as *GRASP2000*, *GRASPELL*, and *LAGEOS*. Apart from precise antenna coordinates and good determination of the troposphere, by a separate processing of the radio source observations also all other commonly determined parameters like highly precise EOP, clock parameters or other antenna specific delays can be determined for the time of the satellite observations. By only giving a short introduction to this method here, there is lots of space for future research in this direction, e.g. in terms of the necessary number of additional observations to radio sources. Nevertheless, in order to realize this combined approach there is an important prerequisite, namely, that observations to satellites and radio sources can be performed with the same receiving system nearly at the same time. When thinking of observing GPS satellites in L-band, there might be some obstacles to overcome, as either the quasar has to be observed in L-band too or the receiver is capable to quickly switch between L-band and the usual S- and X-bands. In this aspect, the use of twin-telescopes could be beneficial. Recently installed or planned at a few sites are so-called twin telescopes, where two telescopes are built at one observatory. By using twins at least at two sites, one telescope at each site, equipped with an adequate receiving unit, could be used for the observation of the satellite while the other telescopes could be operated in standard mode observing radio sources. As a last point, a problem concerning the different signal strength shall be mentioned. As test observations showed¹, when observing a natural radio source close to a GNSS satellite, it might happen that the strong signal of the satellite leaks into the antenna beam, causing problems to identify the weak signal from the quasar.

6.4.2 Observing a satellite constellation

An alternative way to increase the sky coverage is to observe more than one satellite. This does not only help to resolve the troposphere (what is also achieved by the inclusion of observations to radio sources in the schedule), but also considerably improves the geometry of the observations, what is important for the positioning of the receiving antennas.

With the existent and upcoming GNSS systems, in the next years the number of available satellites will increase from today about 50-60 to 100-120 active GNSS satellites in orbit. Provided that all satellites are suitable for VLBI tracking, it is only a natural outcome to observe more than one satellite in a session. This will require careful studies concerning scheduling strategies in the future. For the investigations presented here, a very simple scheduling is used, with the prime aim to show that with VLBI observations to several GNSS satellites, station coordinates of high accuracy can be determined in the satellites' system. Again, only satellites of the GPS are used, representative for the other systems.

Before choosing satellites arbitrarily, it is worth to recall the constellation of the GPS. The nominal constellation of 24 satellites is distributed into six evenly spaced orbital planes (e.g. Hofmann-Wellenhof *et al.*, 2001). In reality, there are up to 32 GPS satellites in orbit, that gives a

¹V. Tornatore, personal communication.

maximum of six satellites for each orbital plane. The importance of a careful choice for the results is illustrated with observations in the European regional network. In figure 6.33 the results for two different schedules are presented. In the first case (a), it was intended to select six satellites

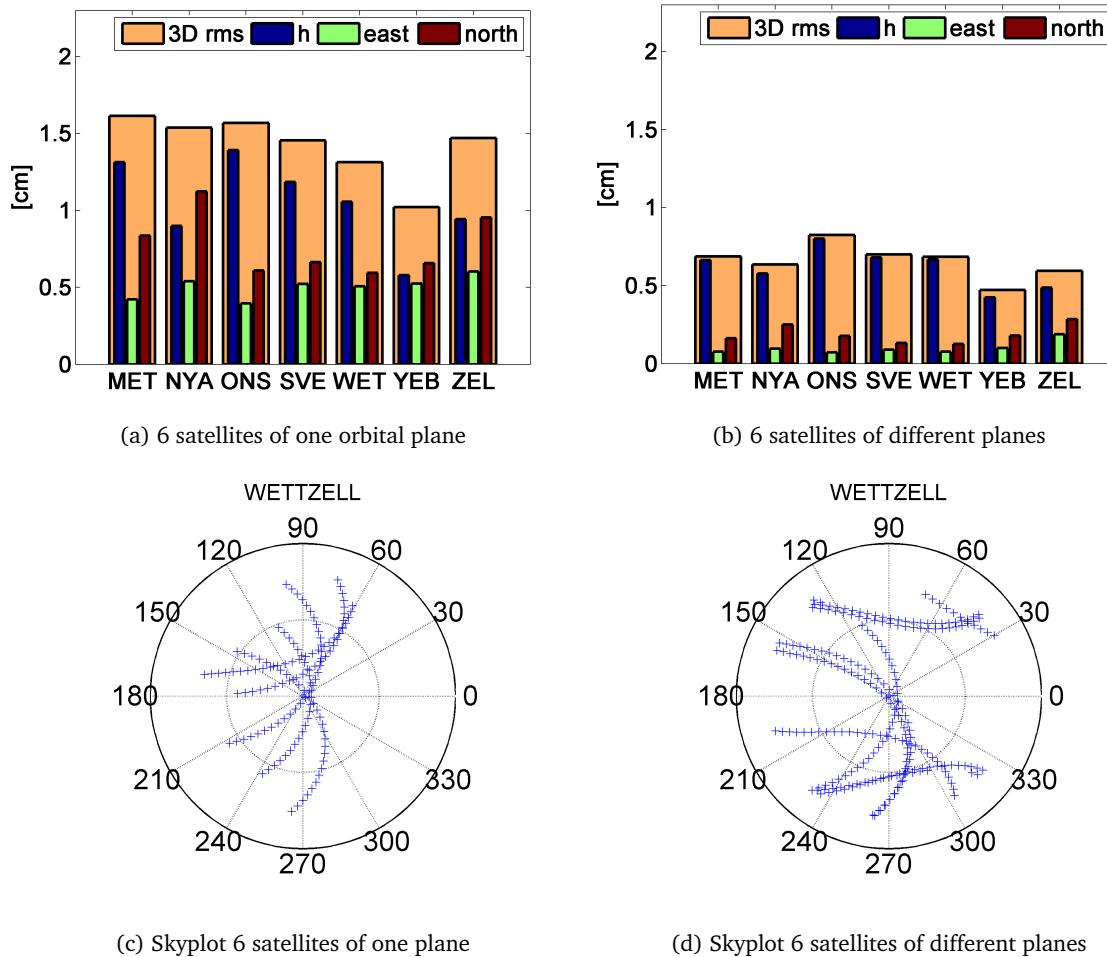


Figure 6.33: Results if stations of the EUR network observe (a) 6 GPS satellites of the same orbital plane and (b) 6 satellites of different orbital planes for one week. The corresponding skyplot for the station Wetzell is given below, in (c) and (d) respectively.

of the same orbital plane, appearing over Europe one after each other (c). The satellite with the highest mean elevation angle for all stations is tracked in 5-min intervals, until the next satellite appears high in the sky. With this schedule, a mean weekly 3D position rms of 1.4 cm is achieved (a). Although using six satellites instead of only one significantly improves the results (see fig. 6.5-d), compared to the combined approach of the previous section this schedule is not better. In addition, similar to the one-satellite solution, a strong network effect for the antennas located at the edges of the network is observed. For the second schedule, with the results shown in figure 6.33 (b), two major things are changed in the scheduling strategy: first, the selection of the satellites is done more carefully, intending to choose satellites of different orbital planes. Second,

the tracking is not done by following one satellite as long as it is visible and then picking the next satellite, but instead, whenever more than one satellite is visible, all possible observations are scheduled with a fast switching between different targets. More specifically, one satellite is only observed once every 10 minutes. In between, in steps of 1 minute, observations for the other satellites are scheduled. This gives consecutive observations into different directions in the sky, similar to the classical geodetic VLBI sessions. Applying this smart scheduling, a mean weekly 3D position rms of 6 mm is achieved. Hereby, the horizontal positions are determined at the level of 1-3 mm only, whereas errors of 5 mm or more are found in the height component. With this observing strategy found to give the best results so far, it is applied in a global network next. The results shown in figure 6.34 are achieved when the same 6 GPS satellites as before, not all of them located in the same orbital plane, were observed with the global 16-stations network. Again, a fast switching between different satellites is scheduled. The results, with a

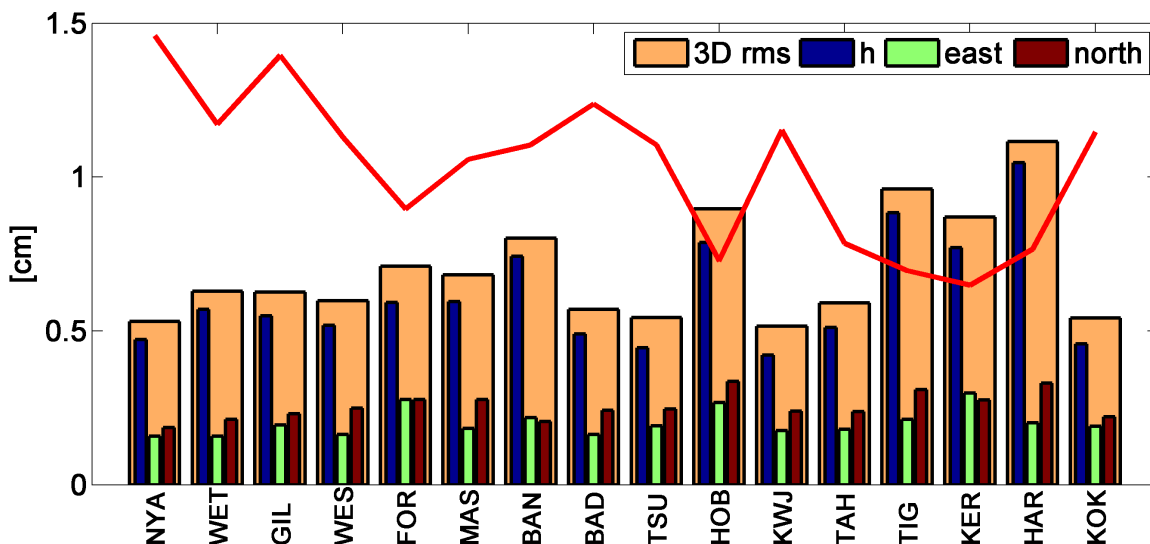


Figure 6.34: Weekly antenna position repeatabilities when 6 GPS satellites of various orbital planes were observed in a 16-stations network. The red line indicates the mean number of observations per day for each station, in units of 1000.

mean weekly 3D position rms of 7 mm, are comparable to those of the regional network. Once more the horizontal positioning accuracies are better than those of the height components. For the worst determined stations, namely HOB, TIG, KER and HAR, an exceptional low number of observations is found.

This scheduling approach shows, that with observations to several GPS satellites the antenna positions can be determined in the satellites' system with high accuracies. With this being the prime intention of the investigations within this thesis, any further studies in this respect are left to future research. For the scheduling procedure, however, a decision has to be made which satellite shall be observed. This task is somehow comparable with the scheduling of classical VLBI observations to radio sources, hence similar scheduling strategies could be used. As additional condition it is proposed to use satellites of different orbital planes, what automatically improves

the variability of the geometrical situation between the target and the observing antennas.

6.5 Summary of the results

Applying the same procedure that was used to support designing the next generation VLBI system, VGOS, VLBI observations to satellites were simulated in order to estimate expected accuracies of determined antenna positions. It is found that if a satellite at a height between 1000 and 6000 km was observed with regional antenna networks, station position repeatabilities of a few millimeters are found for weekly solutions. When global networks shall be used, there is a need for a generally high number of participating stations, i. e. preferably about 30. Hereby, the global networks are challenging for the very low satellites, requiring a careful selection of tracking antennas, e.g. arranged in clusters. Investigations concerning several influences on the results show the importance of a changing geometry of the satellite orbit with respect to the tracking stations. With several satellite passes over a station provided a day, despite a generally poor determination of the tropospheric delays, high accuracies for the determination of antenna positions are enabled. To reach this, the use of optimum observation parameters and schedules is assumed. The lack of a changing geometry is the major reason for a preliminary disqualification of VLBI observations to GNSS-satellites. However, by observing several satellites of the available GNSS-satellite constellation, highest accuracies can also be expected in that area. As a third strategy for VLBI satellite observations, the inclusion into a standard geodetic VLBI session was suggested and studied on the example of a GPS-satellite. This seems to be a good way to go, although there are more capabilities of the observing antennas required. With regard to future scheduling of such observations, some differences to traditional (quasar-) scheduling could be identified. When observing one satellite with VLBI, the task of scheduling is reversed. With the target's position fixed, it is not about the choice of the right source but the choice of a good antenna network to enable good results. Hereby, one has to care about a sufficient number of observations for each station, which strongly influences the expected accuracy of the derived antenna coordinates.

Concluding this chapter one can say, that for the investigated satellites adequate (simple) observing strategies are found, enabling the determination of antenna positions on Earth in the satellites' system with accuracies of a few millimeters.

Chapter 7

Conclusions and Outlook

VLBI satellite tracking is a new technique involving the potential to support a consistent derivation of precise reference frames. Appointing adequate observing strategies, that enable the precise determination of station coordinates in the satellite system, is an important step towards this final goal. As illustrated in figure 7.1, such antenna positions in the satellite system can further on be directly compared to that in the VLBI system, determined through classical observations to radio sources. Possible deviations of the two sets of coordinates would then represent the frame tie between the frame of the satellite and the VLBI frame. Determined at

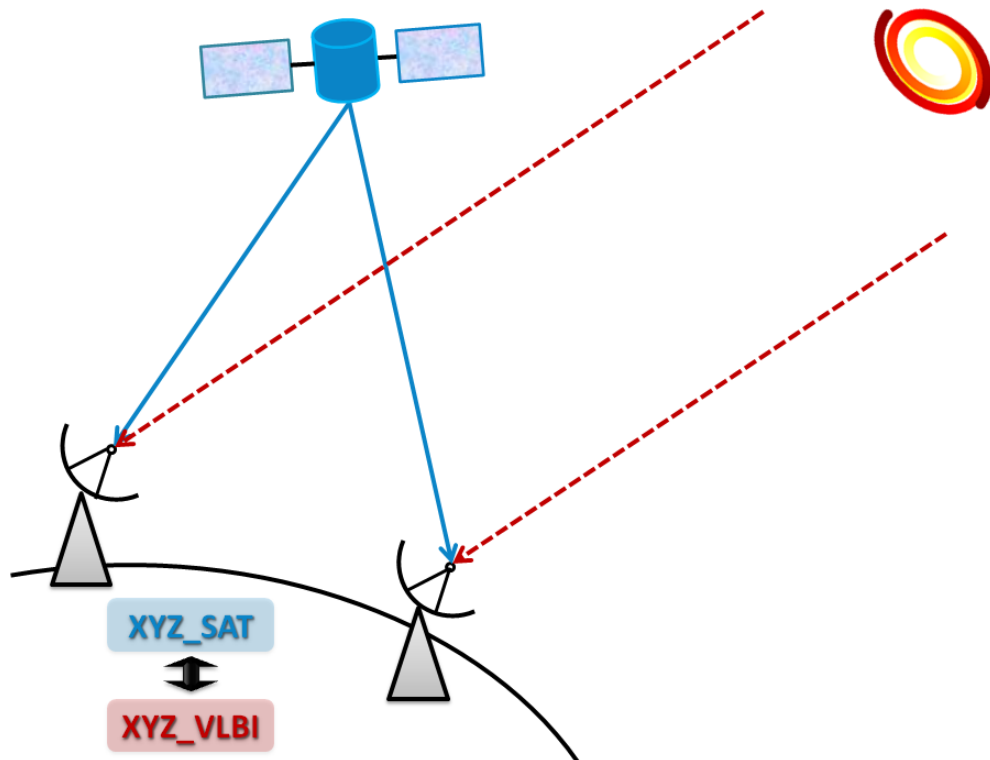


Figure 7.1: Inter-technique ties through the comparison of VLBI antenna coordinates determined in two reference frames.

the level of a few millimeters, these inter-technique ties have the potential to reveal systematic errors between the two frames. Precise coordinates of a VLBI telescope, e.g. determined in the GPS-system, allow the derivation of the vector between the VLBI telescope and a close by GPS antenna in the GPS frame through subtraction of the corresponding coordinates. This would offer the unique chance to compare the locally measured tie vector between the telescope and the GPS receiver with the vector derived from the determined coordinates, independent of the VLBI frame. Globally, a potential distortion of one system relative to the other, scale differences, or translations can be identified using identical stations. In short: immediate applications are manifold.

However, before above mentioned comparisons can be done, the border between simulations and real observations must be crossed. The considerable number of promising research happening in that area at the moment, together with the broad range of well-established realizations in VLBI spacecraft tracking are good indicators for a breakthrough of VLBI satellite tracking soon. Besides the well-known geodetic VLBI technique, starting with the exploration of the deep space, VLBI was also applied to targets within our solar system. Following the pioneering work by NASA, in the recent years also ESA, JAXA or the Chinese space agency developed their own VLBI tracking systems. Spectacular mission support with VLBI tracking, or the employment of the innovative, highly precise multi-frequency same-beam VLBI technique within the lunar SELENE mission are worth to be examined closely for potential technology transfer for geodetic purposes. Though changes in the mathematical model will be required, the corresponding formalisms are available and can be implemented in suitable software with due consideration of a careful (relativistic) treatment of the underlying time and coordinate systems. The observation of satellites with VLBI itself, in terms of common visibility for certain baseline lengths and of tracking the target with the VLBI telescopes, is found to be feasible for satellites at minimum heights of about 1000 kilometers. Solely the realization of D-VLBI for earthbound satellites can be problematic. Due to the parallax between the two stations of a baseline, though a reference radio source might be close to the observed satellite for one station, it is several degrees apart for the other station. The lower the satellite's height, this additional separation angle increases, reducing the level of cancellation e.g. of common tropospheric disturbances.

How can this thesis support progress in the area of VLBI satellite tracking? Detailed simulations like the examples presented have not been available so far. In combination with the expected accuracies, they can support applications for future research, test observations, or new satellite missions. With the choice of the quite simple observing strategies, the demands on eligible VLBI telescopes and receivers could be reduced. It is shown that, for low satellites, good results can also be achieved without additional observations to radio sources. Consequently, receiving antennas that are optimized for the signal emitted by the satellite can be used. For the time being, one can do without applying the D-VLBI technique, that is generally used in VLBI spacecraft tracking; good results can also be achieved with "single-target mode" observations.

The critical question of determining the characteristics for a signal that can be tracked in VLBI mode is not treated in the presented study. An interesting finding though is, that the results of the

weekly solutions are resistant up to a simulated measurement error of 0.1 ns. But, concerning the optimal signal in combination with adequate receiving units, there is definitely more research necessary. When judging the results of chapter 6, one has to keep in mind that all findings are based on simulations only. As shown, the simulations predominantly rely on assumptions about the tropospheric conditions at the observing sites. For sure VLBI observations to satellites will be affected also by other error sources that are not included in the presented simulations so far. The influence of the ionosphere for example, is completely ignored. This is reasonable for classical geodetic VLBI, as the use of two frequency bands allows a sufficient correction of this effect. In the case of satellite observations, however, one can not automatically assume that there will also be a signal available on at least two frequency bands. Further, errors originating in the signal chain between the main reflector to the recording unit, induced by different frequencies or signal strengths are not investigated. Here, the use of the standard S- and X-bands is advisable, but also applying the proposed "single-target mode" instead of the D-VLBI approach or the subsequent combination with radio source observations is probably less critical in this aspect. Other issues that are not treated are those concerning the practical realization of such observations. This includes the complete communication flow between a new scheduling tool, the read-in to the field system of the antenna, a successful correlation and the subsequent analysis of collected data. The existence of new parameters, e. g. the orbit of the moving target, will require changes in the commonly applied data formats. Another point is the availability of suitable VLBI telescopes. The presented results are all derived within weekly solutions of observations, partially done with exceptionally big antenna networks. This might be possible in the upcoming VGOS system, but it will still take some time until this will be fully installed.

In the course of the work, the processing of VLBI observations to satellites was incorporated into the geodetic VLBI analysis software VieVS. As soon as successful measurements will be available in terms of measured time delays, the proposed analysis including the estimation of station parameters can be performed. The extension of the VieVS-simulator for the possibility to process VLBI satellite observations can be used to assess the expected accuracies for future schedules. As chapter 6.4.2 clearly shows, when several satellites of the GNSS constellation are observed, finding best possible schedules is not trivial. Additional to the requirement of a good sky coverage to resolve the troposphere, what is known from geodetic scheduling, in the case of satellite observations, the satellite's trace in the sky is decisive. By comparing various scheduling runs, the simulation tool can be of use for this important task.

Compared to the investigated lower satellites at heights of 2000 and 6000 kilometers, for observing satellites of the GNSS system alternative strategies shall be applied. Promising options are the integration into a standard geodetic VLBI session or the observation of a satellite constellation instead of a single satellite. Only presenting the general ideas for these methods, research needs to be continued in that area. As a result of the multitude of satellites available, it shall be investigated whether good results are also possible with concepts using smaller networks than the investigated ones. Additionally, the observation duration, namely the concept of weekly solutions can be reassessed.

So far, the focus is set on improving the TRF. Considering the complete product of TRF, EOP and CRE, this scope shall be expanded. If telescopes are capable to observe both, a satellite's signal and radiation emitted by the sources of the ICRF, a direct determination of the satellite's position with respect to the ICRF would be a great opportunity. For this, the investigations have to be steered towards the orbit determination of the target rather than to the estimation of antenna coordinates on Earth. Concerning the measurement of the Earth orientation, the necessary combination of several techniques could be brought to the next level with VLBI observations to satellites. By locating the satellites directly in the ICRF, the strong correlations with the determined orbits might become controllable, enabling a more consistent and stable EOP series.

Future progress provided, one can look forward to the next realizations of VLBI satellite tracking. Following the prospects, they might push geodesy one step closer towards the ambitious goals of GGOS, meeting the requirements of our society living on the planet Earth.

Appendix A

List of stations

Table A.1: List of VLBI stations. The coordinates are referred to epoch 1.1.2000.

Antenna code	Abbr.	x [m]	y [m]	z [m]	v_x [m/y]	v_y [m/y]	v_z [m/y]
AIRA	AIR	-3530219.395	4118797.538	3344015.813	0.0	0.0	0.0
BADARY	BAD	-838200.712	3865751.585	4987670.933	-0.0272	-0.0020	-0.0019
BANGALO	BAN	1337936.478	6070317.106	1427876.797	0.0	0.0	0.0
DIEGOGA	DIE	1916269.427	6029977.453	-801719.909	0.0	0.0	0.0
DSS45	DSS	-4460935.506	2682765.701	-3674381.052	-0.0357	0.0010	0.0457
EASTERIS	EAS	-1884993.218	-5357605.161	-2892858.701	0.0	0.0	0.0
FORTLEZA	FOR	4985370.037	-3955020.342	-428472.243	-0.0022	-0.0036	0.0124
GILCREEK	GIL	-2281547.371	-1453645.136	5756993.073	-0.0293	-0.0097	0.0015
GOLDSTON	GOL	-2356171.121	-4646755.845	3668470.596	0.0	0.0	0.0
HARTRAO	HAR	5085442.776	2668263.538	-2768696.960	-0.0007	0.0198	0.0164
HALY	HAL	4509692.341	3283704.168	3081653.132	0.0	0.0	0.0
HOBART26	HOB	-3950236.855	2522347.575	-4311562.414	-0.0387	0.0091	0.0412
KASHIMA	KAS	-3997892.278	3276581.298	3724118.220	-0.0013	0.0058	-0.0076
KATH12M	KAT	-4147354.588	4581542.408	-1573303.300	0.0	0.0	0.0
KERGUEL	KER	1406337.289	3918161.093	-4816167.357	0.0	0.0	0.0
KOKEE	KOK	-5543837.654	-2054567.672	2387852.040	-0.0091	0.0633	0.0322
KUNMING	KUN	-1281152.396	5640863.519	2682653.086	0.0	0.0	0.0
KWJ1	KWJ	-6160874.094	1339908.993	960563.555	0.0	0.0	0.0
LAPLATA	LAP	2780102.995	-4437418.918	-3629404.505	0.0	0.0	0.0
MALINDI	MAL	4865366.343	4110737.607	-331121.571	0.0	0.0	0.0
MASPALO	MAS	5439192.215	-1522055.484	2953454.847	0.0	0.0	0.0
METSAHOV	MET	2892585.070	1311715.422	5512640.062	-0.0165	0.0126	0.0079
MSKU	MSK	6204510.619	1470114.795	-152578.031	0.0	0.0	0.0
NEWDEHLI	NEW	1241601.071	5464927.525	3035051.746	0.0	0.0	0.0
NYALES20	NYA	1202462.712	252734.419	6237766.077	-0.0142	0.0074	0.0104
ONSALA60	ONS	3370605.983	711917.529	5349830.772	-0.0139	0.0144	0.0106
PALAU	PAL	-4434004.683	4512075.946	810538.049	0.0	0.0	0.0
PARKES	PAR	-4554232.051	2816758.909	-3454035.670	-0.0306	-0.0041	0.0536
QAQ1	QAQ	2190822.783	-2271041.880	5524275.233	0.0	0.0	0.0
QUITOII	QUI	1272867.321	-6252772.124	-23801.765	0.0	0.0	0.0
SASK	SAS	-1097511.768	-3767840.011	5011012.391	0.0	0.0	0.0
SESHAN25	SES	-2831687.002	4675733.633	3275327.658	-0.0298	-0.0110	-0.0114
SVETLOE	SVE	2730173.912	1562442.627	5529969.045	-0.0185	0.0121	0.0078
TAHITI	TAH	-5117648.700	-3260301.800	-1958394.300	0.0	0.0	0.0
TIGOCONC	TIG	1492052.727	-4887961.102	-3803541.831	-0.1351	-0.0385	0.0081
TSUKUB32	TSU	-3957408.786	3310229.408	3737494.803	-0.0029	0.0050	-0.0051
URUMQI	URU	228310.629	4631922.781	4367063.996	-0.0319	-0.0021	0.0063
VERAMZSW	VER	-3857241.880	3108784.843	4003900.664	0.0031	0.0040	-0.0124
WARK12M	WAR	-5115324.399	477843.305	-3767192.886	0.0	0.0	0.0
WESTFORD	WES	1492206.541	-4458130.514	4296015.549	-0.0154	-0.0013	0.0036
WETTZELL	WET	4075539.835	931735.313	4801629.402	-0.0157	0.0169	0.0101
YARRA12	YAR	-2388896.057	5043349.968	-3078590.918	0.0	0.0	0.0
YEBES40M	YEB	4848761.717	-261484.229	4123084.913	0.0082	-0.0005	0.0059
ZELENCHK	ZEL	3451207.821	3060375.230	4391914.932	-0.0216	0.0142	0.0097

Appendix B

Figures

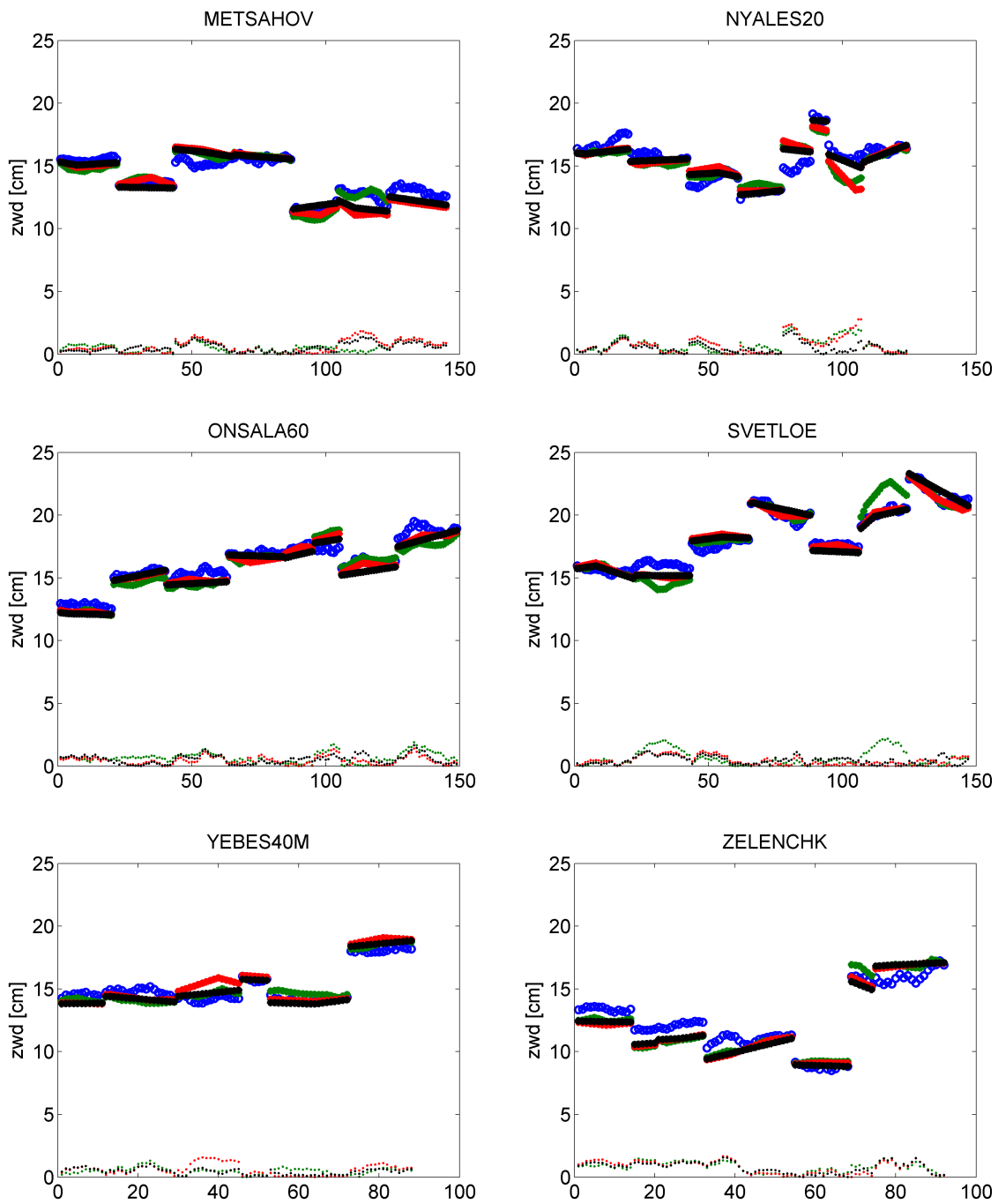


Figure B.1: Comparison between the simulated zwd (blue) and the estimated ones observing *GRASP2000* for one day. The observation interval is 1 minute and the estimation interval for the zwd is 3 minutes (green), 10 minutes (red) and 30 minutes (black), with the estimated values interpolated to the observation epochs. Besides the total values printed with the bigger markers, the small dots represent the absolute deviation from the simulated value.

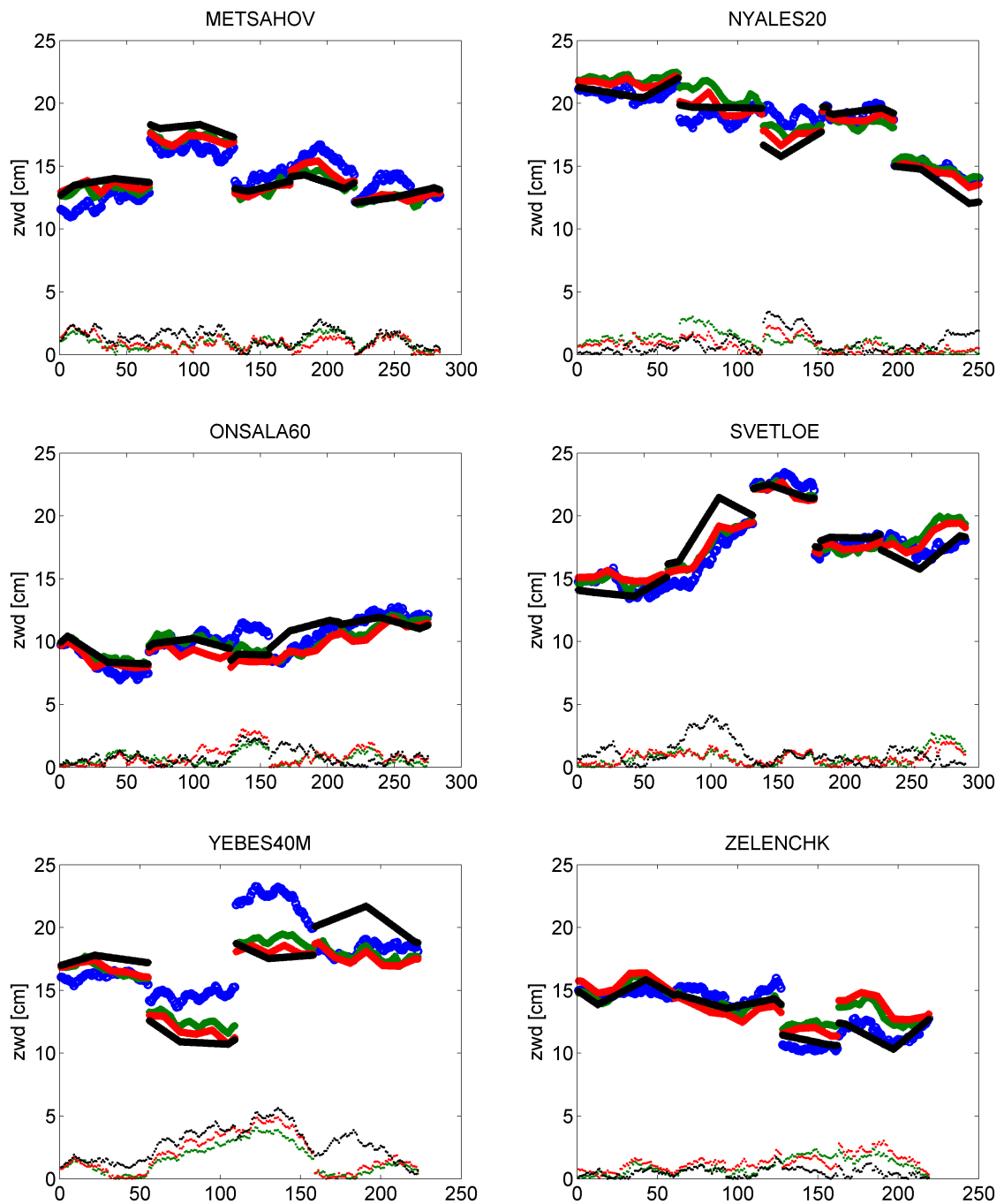


Figure B.2: Comparison between the simulated zwd (blue) and the estimated ones observing *LAGEOS* for one day. The observation interval is 1 minute and the estimation interval for the zwd is 3 minutes (green), 10 minutes (red) and 30 minutes (black), with the estimated values interpolated to the observation epochs. Besides the total values printed with the bigger markers, the small dots represent the absolute deviation from the simulated value.

Abbreviations

Δ-VLBI	Delta VLBI
AGN	Active Galactic Nucleus
ASCII	American Standard Code for Information Interchange
ASD	Allan standard deviation
BCRS	Barycentric Celestial Reference System
CCSDS	The Consultative Committee for Space Data Systems
CIO	Celestial Intermediate Origin
CODE	Center for Orbit Determination in Europe
CVN	Chinese VLBI Network
D-VLBI	Differential VLBI
DORIS	Doppler Orbitography and Radiopositioning Integrated by Satellite
DOR	Differential One-way Ranging
DSA	Deep Space Antenna
DSN	Deep Space Network
ECMWF	European Centre for Medium-Range Weather Forecast
EOP	Earth Orientation Parameters
ERA	Earth Rotation Angle
ESA	European Space Agency
GCRS	Geocentric Celestial Coordinate System
GGOS	Global Geodetic Observing System
GLONASS	Globalnaja Nawigazionnaja Sputnikowaja Sistema
GNSS	Global Navigation Satellite Systems
GPS	Global Positioning System
GRAIL	Gravity Recovery and Interior Laboratory
GRASP	Geodetic Reference Antenna in Space
HOB	Hobart VLBI antenna
IAG	International Association of Geodesy
IAU	International Astronomical Union
ICRF	International Celestial Reference Frame
ICRS	International Celestial Reference System
IERS	International Earth Rotation and Reference Systems Service

IGS	International GNSS Service
IRI	Iriki VLBI antenna
ISAS	ISAS
ISI	Ishigaki VLBI antenna
ITRF	International Terrestrial Reference Frame
ITRS	International Terrestrial Reference System
IUGG	International Union of Geodesy and Geophysics
IVS	International VLBI Service for Geodesy and Astrometry
JAXA	Japan Aerospace Exploration Agency
JIVE	Joint Institute for VLBI in Europe
JPL	Jet Propulsion Laboratory
LEO	Low Earth Orbit
LLR	Lunar Laser Ranging
LoS	Line of Sight
MER-B	Mars Exploration Rover B
MFV	Multi Frequency VLBI
MZW	Mizusawa VLBI antenna
NAOJ	National Astronomical Observatory of Japan
NASA	National Aeronautics and Space Administration
NICT	National Institute of Information and Communications Technology
OGW	Ogasawara VLBI antenna
PPN	Parameterized post-Newtonian
PRIDE	Planetary Radio Interferometry and Doppler Experiment
RLT	Relativistic light-time
SELENE	Selenological and engineering explorer
SHA	Shanghai VLBI antenna
SI	Système International
SLR	Satellite Laser Ranging
SNR	Signal to noise ratio
TAI	International Atomic Time
TCB	Barycentric Coordinate Time
TCG	Geocentric Coordinate Time
TDB	Barycentric Dynamical Time
TEC	Total electron content
TIO	Terrestrial Intermediate Origin
TRF	Terrestrial Reference Frame
TRS	Terrestrial Reference System
TT	Terrestrial Time
URQ	Urumqi VLBI antenna
UTC	Coordinated Universal Time

UT	Universal Time
VERA	VLBI Exploration of Radio Astrometry
VEX	Venus Express
VGOS	VLBI2010 Global Observing System
VieVS	Vienna VLBI Software
VLBA	Very Long Baseline Array
VLBI	Very Long Baseline Interferometry
VMF	Vienna Mapping Functions
WTZ	Wettzell VLBI antenna

List of Figures

2.1	The principle of space-ties	15
3.1	Basic geometrical principle of VLBI.	18
3.2	VLBI delay model in seven steps	20
3.3	VLBI to moving sources at finite distance	34
4.1	Classical D-VLBI principle.	40
4.2	Geometrical relation ϵ_1 , ϵ_2 , b , and h	41
4.3	Separation angle versus elevation for various baseline lengths and target heights	42
4.4	Residual effect in slant wet delay induced by the mapping function	43
4.5	Slant wet delay versus azimuthal separation angle	44
4.6	SELENE mission overview	45
4.7	Antenna network for the SELENE observations	48
4.8	Temporal distribution of SELENE data	49
4.9	January residuals after ambiguity solution	50
4.10	October residuals after ambiguity solution	50
4.11	Distribution of the SELENE residuals	51
4.12	Divergence in $\Delta\tau$ induced by the use of different delay models	53
4.13	Slant wet delay versus azimuthal separation angle for SELENE	55
5.1	VLBI satellite tracking.	57
5.2	Geometrical relation between b and h	61
5.3	Common visibility for various baseline lengths in dependence of h	62
5.4	Antenna slew speeds	63
5.5	Vienna VLBI software.	65
5.6	Flowchart <i>VieVS₂tie</i>	66
5.7	Simulation setup in VieVS	69
6.1	Study set-up for weekly solutions.	74
6.2	1-day satellite ground tracks	75
6.3	Map of the regional antenna networks.	76
6.4	Maps of global antenna networks	76

6.5	Results regional network EUR	79
6.6	Results regional network AUS	80
6.7	Results regional network ASIA	81
6.8	Baselines of regional networks EUR, ASIA, AUS	82
6.9	Weekly 3D position rms versus the number of observations.	83
6.10	Processing of n days versus weekly solution.	84
6.11	Weekly 3D position rms with different cutoff elevation angles.	84
6.12	Weekly 3D position rms versus the number of observations	86
6.13	Influence of simulation parameters	88
6.14	Influence of the estimation interval of the zwd.	89
6.15	Estimated versus simulated zwd.	90
6.16	Estimated versus simulated zwd at observing epochs.	91
6.17	Testing different constraints and estimation intervals for the zwd.	93
6.18	Duration of satellite passes.	93
6.19	1-day satellite passes <i>GRASP2000</i>	94
6.20	1-day satellite passes <i>LAGEOS</i>	95
6.21	1-day mean 3D position rms versus satellite passes.	96
6.22	Effect of orbit errors on the 3D position rms.	97
6.23	Weekly 3D position rms of a global 32-stations network	99
6.24	Observed baselines in the 32-stations network	100
6.25	Weekly 3D position rms of a global 16-stations network	101
6.26	Observed baselines in the 16-stations network	102
6.27	Weekly 3D position rms of a global cluster network	103
6.28	Observed baselines in the global cluster network	104
6.29	Skyplots Wettzell	105
6.30	Results of a global 32-stations network observing 1 GPS-satellite	105
6.31	Concept of the combined approach	106
6.32	Results for GPS combined approach	107
6.33	Skyplots Wettzell	109
6.34	6 GPS satellites observed in a 16-stations network.	110
7.1	VLBI antenna coordinates in two reference frames.	113
B.1	Estimated versus simulated zwd <i>GRASP2000</i> , all stations.	120
B.2	Estimated versus simulated zwd <i>LAGEOS</i> , all stations.	121

List of Tables

4.1	Frequencies of VLBI signals in SELENE (e.g. Hanada <i>et al.</i> , 2008)	46
4.2	Effect in the calculated τ and $\Delta\tau$ due to varying a priori parameters. The values represent the maxima of the observables' majority, particularly extreme values are given in brackets. When distinguished, <i>sb</i> stands for the same beam data and <i>sw</i> for the switching data.	56
5.1	Parameters for the simulation of the wet troposphere.	70
6.1	Orbital parameters of the target satellites.	74
6.2	Processing options within the simulation study.	77
6.3	Observation settings for the regional networks.	78
6.4	Mean number of observations per station in the AUS network.	81
6.5	Station position repeatability and number of observations for the four satellites observed by the EUR network testing different observation intervals. The values are given in terms of weekly 3D position rms in cm, the numbers behind the verticals are the numbers of observations per day. The highlighted rows indicate the determined best observation interval for the corresponding satellite. Besides the observation interval, additional variation in the results is induced by the simulation of the observations.	86
6.6	Deviation of the estimated zwd from the simulated ones in cm, as calculated as the mean value for each station during one day from the results shown in figures 6.16, B.1 and B.2. Values are given for the EUR network observing <i>GRASP2000</i> and <i>LAGEOS</i> during one day with 1 min intervals, using different estimation intervals of 3 min, 10 min and 30 min. The last column gives the mean values over the 7 stations.	91
A.1	List of VLBI stations. The coordinates are referred to epoch 1.1.2000.	118

Bibliography

- ALTAMIMI, Z., COLLILIEUX, X. AND MÉTIVIER, L. (2011). ITRF2008: an improved solution of the international terrestrial reference frame. *J. Geod.*, 85:8, 457–473.
- BAR-SEVER, Y., HAINES, B., BERTIGER, W., DESAI, S. AND WU, S. (2009). Geodetic Reference Antenna in Space (GRASP) - A Mission to Enhance Space-Based Geodesy. In *COSPAR Colloquium: Scientific and Fundamental Aspects of the Galileo Program*, Padua, Italy, 2009.
- BERRY, D.S. AND BORDER, J.S. (2005). Delta-DOR. *CCSDS Concept Paper*, <http://hdl.handle.net/2014/37674>, CCSDS Fall Meetings 2005, Atlanta, GA, September 12-16, 2005.
- BIPM (2006). The International System of Units (SI). *Bureau International des Poids et Mesures*, 8th edition.
- BÖHM, J. (2004). Troposphärische Laufzeitverzögerungen in der VLBI. *Geowissenschaftliche Mitteilungen*, 68, Schriftenreihe der Studienrichtung Vermessung und Geoinformation, Technische Universität Wien, ISSN 1811-8380 (in German).
- BÖHM, J., WERL, B. AND SCHUH, H. (2006). Troposphere mapping functions for GPS and very long baseline interferometry from European Centre for Medium-Range Weather Forecasts operational analysis data. *J. Geophys. Res.*, 111, doi:10.1029/2005JB003629.
- BÖHM, J., WRESNIK, J. AND PANY, A. (2007). Simulation of wet zenith delays and clocks. *IVS Memorandum 2006-013v03*, <ftp://ivscc.gsfc.nasa.gov/pub/memos/ivs-2006-013v03.pdf>, 4 September 2007.
- BÖHM, J., BÖHM, S., NILSSON, T., PANY, A., PLANK, L., SPICAKOVA, H., TEKE, K. AND SCHUH, H. (2012). The new Vienna VLBI Software VieVS. In *Proceedings of the 2009 IAG Symposium, Buenos Aires, Argentina*, Vol. 136, International Association of Geodesy Symposia, 31 August - 4 September 2009.
- BORDER, J.S. (2009). Innovations in Delta Differential One-Way Range: From Viking to Mars Science Laboratory. In *Proc. 21st Int. Sym. Space Flight Dynamics, Toulouse, France, 28 Sep-02 Oct 2009*, <http://www.mediatec-dif.com/issfd/OrbitdI/Border.pdf>.

- BORDER, J.S. AND KOUKOS, J.A. (1993). Technical Characteristics and Accuracy Capabilities of Delta Differential one-Way Ranging Δ DOR as a Spacecraft Navigation Tool. Presented at CCDS meeting of RF & Modulation Standards Working Group, Munich, Germany, 09/20/1993, <http://hdl.handle.net/2014/35696>.
- BOURDA, G., CHARLOT, P., PORCAS, R.W. AND GARRINGTON, S.T. (2010). VLBI observations of optically-bright extragalactic radio sources for the alignment of the radio frame with the future Gaia frame - I. Source detection. *Astr. & Astroph.*, 520, doi:10.1051/0004-6361:201014248, A113.
- BOURDA, G., COLLILOUD, A., CHARLOT, P., PORCAS, R. AND GARRINGTON, S. (2011). VLBI observations of optically-bright extragalactic radio sources for the alignment of the radio frame with the future Gaia frame - II. Imaging candidate sources. *Astr. & Astroph.*, 526, doi:10.1051/0004-6361:201014249, A102.
- BRIESS, K., KONEMANN, G. AND WICKERT, J. (2009). MicroGEM – Microsatellites for GNSS Earth Monitoring, Abschlussbericht Phase 0/A. 15. September 2009, Helmholtz-Zentrum Potsdam Deutsches GeoForschungsZentrum GFZ and Technische Universität Berlin.
- BRUNN, D.L., PRESTON, R.A., WU, S.C., SIEGEL, H.L., BROWN, D.S., CHRISTENSEN, C.S. AND HILT, D.E. (1978). Δ VLBI Spacecraft Tracking System Demonstration: Part I. Design and Planning. *DSN Progress Report*, 42-45, 111–132, Jet Propulsion Laboratory, Pasadena, California.
- CANNON, W. (1999). Overview of VLBI . In N. Vandenberg and K. Baver, eds., *International VLBI Service for Geodesy and Astrometry 1999 Annual Report*, 13–17, NASA/TP-1999-209243.
- CCSDS (2011). Delta-Differential one way ranging (Delta-DOR) operations. Recommendation for Space Data System Practices, Magenta Book, CCSDS 506.0-M-1, <http://public.ccsds.org/publications/archive/506x0m1.pdf>.
- CHRISTENSEN, C.S., MOULTRIE, B., CALLAHAN, P.S., DONIVAN, F.F. AND WU, S.C. (1980). Δ VLBI Spacecraft Tracking System Demonstration: Part II. Data Acquisition and Processing. *TDA Progress Report*, 42-60, 42–67, Jet Propulsion Laboratory, Pasadena, California.
- COUNSELMAN, C. AND GOUREVITCH, S.A. (1981). Miniature Interferometer Terminals for Earth Surveying: Ambiguity and Multipath with Global Positioning System. *IEEE Transactions on Geoscience and Remote Sensing*, GE-19, 244–252, No. 4.
- DICKEY, J.M. (2010). How and Why do VLBI on GPS. In D. Behrend and K. Baver, eds., *International VLBI Service for Geodesy and Astrometry 2010 General Meeting Proceedings*, 65–69, NASA/CP 2010-215864.
- DOW, J.M., NEILAN, R.E. AND RIZOS, C. (2009). The International GNSS Service in a changing landscape of Global Navigation Satellite Systems. *J. Geod.*, 83, 191–198, doi: 10.1007/s00190-008-0300-3.

- DSN TELECOMMUNICATIONS LINK DESIGN HANDBOOK (2004). Delta-differential one-way ranging. *Jet Propulsion Laboratory, Pasadena, California*, (810-005) Module 210.
- DUEV, D.A., MOLERA CALVÉS, G., POGREBENKO, S.V., GURVITS, L.I., CIMÓ, G. AND BOCANEGRA BAHAMON, T. (2012). Spacecraft VLBI and Doppler tracking: algorithms and implementation. *Astr. & Astroph.*, 541, A43, doi:10.1051/0004-6361/201218885.
- ESA (2006). Delta-DOR A New Technique for ESA's Deep Space Navigation. In A. Wilson and C. Walker, eds., *ESA-Bulletin*, Vol. 128, Nov. 2006.
- ESA (2007). The Hipparcos and Tycho catalogues. *ESA Publications Division, c/o ESTEC, Noordwijk, The Netherlands*, 17 volumes.
- EUBANKS, T.M., ed. (1991). Proceedings of the U.S. Naval Observatory Workshop on Relativistic Models for Use in Space Geodesy. U.S. Naval Observatory Washington D.C. 20392-5100, U.S.A.
- FEY, A., GORDON, D. AND JACOBS, C.S., eds. (2009). The second realization of the international celestial reference frame by very long baseline interferometry. Frankfurt am Main: Verlag des Bundesamts für Kartographie und Geodäsie, Presented on behalf of the IERS / IVS Working Group, IERS Technical Note 35.
- FOLKNER, W.M., WILLIAMS, J.G. AND BOGGS, D.H. (2008). The Planetary and Lunar Ephemeris DE 421. *IPN Progress Report 42-178 August 15, 2009*, 31, http://ipnpr.jpl.nasa.gov/progress_report/42-178/178C.pdf.
- FOMALONT, E., KOPEIKIN, S., JONES, D., HONMA, M. AND TITOV, O. (2010). Recent VLBA/VERA/IVS tests of general relativity. In S.A. Klioner, P.K. Seidelmann and M.H. Soffel, eds., *Relativity in Fundamental Astronomy. Proceedings IAU Symposium*, Vol. 261, 291–295.
- FUKUSHIMA, T. (1994). Lunar VLBI observation model. *Astr. & Astroph.*, 291, 320–323.
- GOOSSENS, S., MATSUMOTO, K., LIU, Q., KIKUCHI, F., SATO, K., HANADA, H., ISHIHARA, Y., NODA, H., KAWANO, N., NAMIKI, N., IWATA, T., LEMOINE, F.G., ROWLANDS, D.D., HARADA, Y. AND CHEN, M. (2011a). Lunar gravity field determination using SELENE same-beam differential VLBI tracking data. *J. Geod.*, 85, 205–228.
- GOOSSENS, S., MATSUMOTO, K., ROWLANDS, D.D., LEMOINE, F.G., NODA, H. AND ARAKI, H. (2011b). Orbit determination of the SELENE satellites using multi-satellite data types and evaluation of SELENE gravity field models. *J. Geod.*, 85, 487–504.
- HANADA, H., IWATA, T., NAMIKI, N., KAWANO, N., ASARI, K., ISHIKAWA, T., KIKUCHI, F., LIU, Q., MATSUMOTO, K., NODA, H., TSURUTA, S., GOOSSENS, S., IWADATE, K., KAMEYA, O., TAMURA, Y., HONG, X., PING, J., AILI, Y., ELLINGSEN, S. AND SCHLÜTER, W. (2008). VLBI for better gravimetry in SELENE. *Adv. Space Res.*, 42, 341–346.

- HANADA, H., IWATA, T., LIU, Q., KIKUCHI, E., MATSUMOTO, K., GOOSSENS, S., HARADA, Y., ASARI, K., ISHIKAWA, T., ISHIHARA, Y., NODA, H., TSURUTA, S., PETROVA, N., KAWANO, N., SASAKI, S., SATO, K., NAMIKI, N., KONO, Y., IWADATE, K., KAMEYA, O., SHIBATA, K.M., TAMURA, Y., KAMATA, S., YAHAGI, Y., MASUI, W., TANAKA, Y., MAEJIMA, H., HONG, X., PING, J., SHI, X., HUANG, Q., AILI, Y., ELLINGSEN, S. AND SCHLÜTER, W. (2010). Overview of Differential VLBI Observations of Lunar Orbiters in SELENE (Kaguya) for Precise Orbit Determination and Lunar Gravity Field Study. *Space Sci. Rev.*, 154, 123–144.
- HASE, H. (1999). Phase Centre Determinations at GPS-Satellites with VLBI. In W. Schlüter and H. Hase, eds., *Proceedings of the 13th Working Meeting of the European VLBI for Geodesy and Astrometry*, 273–277, Bundesamt für Kartographie und Geodäsie, Wettzell, 1999, held at Viechtach, February 12-13, 1999.
- HASE, H., BEHREND, D., MA, C., PETRACHENKO, B., SCHUH, H. AND WHITNEY, A. (2013). The Emerging VGOS Network of the IVS. In D. Behrend and K. Baver, eds., *International VLBI Service for Geodesy and Astrometry 2012 General Meeting Proceedings*, 8–12, NASA/CP-2012-217504.
- HEINKELMANN, R. AND SCHUH, H. (2010). Very long baseline interferometry: accuracy limits and relativistic tests. In S.A. Klioner, P.K. Seidelmann and M.H. Soffel, eds., *Relativity in Fundamental Astronomy. Proceedings IAU Symposium*, Vol. 261, 286–290.
- HERRING, T.A., DAVIS, J.L. AND SHAPIRO, I.I. (1990). Geodesy by radio interferometry: The application of kalman filtering to the analysis of very long baseline interferometry data. *J. Geophys. Res.*, 95 B8, 12561–12581.
- HOBIGER, T. (2006). VLBI as a tool to probe the ionosphere. *Geowissenschaftliche Mitteilungen*, 75, Schriftenreihe der Studienrichtung Vermessung und Geoinformation, Technische Universität Wien, ISSN 1811-8380.
- HOBSON, M.P., EFSTATHIOU, G. AND LASENBY, A.N. (2006). *General Relativity - An Introduction for Physicists*. Cambridge University Press, ISBN-13 978-0-521-82951-9.
- HOFMANN-WELLENHOF, B., LICHTENEGGER, H. AND COLLINS, J. (2001). *GPS - Theory and Practice*. Springer Wien New York, Fifth, revised edition, ISBN: 3-211-83534-2.
- HUANG, Y., HU, X., HUANG, C., JIANG, D., ZHENG, W. AND ZHANG, X. (2006). Orbit Determination of Satellite "Tance 1" with VLBI Data. *Chin. Astr. & Astroph.*, 30, 318–329.
- HUANG, Y., HU, X., ZHANG, X., JIANG, D., GUO, R., WANG, H. AND SHI, S. (2011). Improvement of orbit determination for geostationary satellites with VLBI tracking. *Chinese Sci Bull*, 56, 2765–2772.
- IAU RESOLUTION B2 (1997). On the international celestial reference system (ICRS). *XXIIIrd IAU GA, Kyoto*, http://www.iau.org/static/resolutions/IAU1997_French.pdf.

- ICHIKAWA, R., SEKIDO, M., OHSAKI, H., KOYAMA, Y., KONDO, T., YOSHIKAWA, M., OHNISHI, T., YOSHIKAWA, M., CANNON, W., NOVIKOV, A., BÉRUBÉ, M. AND NOZOMI DVLBI GROUP (2004). An Evaluation of VLBI Observations for Deep Space Tracking of the Interplanetary Spacecrafts. In N.R. Vandenberg and K.D. Baver, eds., *International VLBI Service for Geodesy and Astrometry 2004 General Meeting Proceedings*, 253–257, NASA/CP-2004-212255.
- JACOBS, C.S., CLARK, J.E., GARCÍA MIRÓ, C., HORIUCHI, S., ROMERO-WOLFF, A., SNEDEKER, L. AND SOTUELA, I. (2012). A Celestial Reference Frame at X/Ka-Band (8.4/32 GHz) for Deep Space Navigation. *23rd Symposium on Space Flight Dynamics*.
- JAMES, N., ABELLO, R., LANUCARA, M., MERCOLINO, M. AND MADDÈ, R. (2009). Implementation of an ESA delta-DOR capability. *Acta Astronautica*, 64, 1041–1049.
- JONES, D.L., FOMALONT, E., DHAWAN, V., ROMNEY, J., FOLKNER, W.M., LANYI, G., BORDER, J. AND JACOBSON, R.A. (2011). Very Long Baseline Array Astrometric Observations of the Cassini Spacecraft at Saturn. *The Astronomical Journal*, 141:29, doi: 10.1088/0004-6256/141/2/29.
- KAPLAN, G.H. (2005). *The IAU Resolutions on Astronomical Reference Systems, Time Scales, and Earth Rotation Models - Explanation and Implementation*. U.S. Naval Observatory, Washington, D.C. 20392, USNO Circular; 179.
- KARTTUNEN, H., KRÖGER, P., OJA, H., POUTANEN, M. AND DONNER, K.J. (2007). *Fundamental Astronomy*. Springer-Verlag Berlin Heidelberg, 5th Edition.
- KATO, M., SASAKI, S., TANAKA, K., IJIMA, Y. AND TAKIZAWA, Y. (2008). The Japanese lunar mission SELENE: Science goals and present status. *Adv. Space Res.*, 42, 294–300.
- KATO, M., SASAKI, S., TAKIZAWA, Y. AND THE KAGUYA PROJECT TEAM (2010). The Kaguya Mission Overview. *Space Sci. Rev.*, 154, 3–19.
- KIKUCHI, F. (2006). Differential Phase Delay Estimation by Same Beam Method. *Ph.D. Thesis*, the Graduate University for Advanced Studies.
- KIKUCHI, F., KONO, Y., YOSHIKAWA, M., SEKIDO, M., OHNISHI, M., MURATA, Y., PING, J., LIU, Q., MATSUMOTO, K., ASARI, K., TSURUTA, S., HANADA, H. AND KAWANO, N. (2004). VLBI observation of narrow bandwidth signals from the spacecraft. *Earth Planets Space*, 56, 1041–1047.
- KIKUCHI, F., LIU, Q., MATSUMOTO, K., HANADA, H. AND KAWANO, N. (2008). Simulation analysis of differential phase delay estimation by same beam VLBI method. *Earth Planets Space*, 60, 391–406.
- KING, R.W., COUNSELMAN, C.C. AND SHAPIRO, I.I. (1976). Lunar Dynamics and Selenodesy: Results From Analysis of VLBI and Laser Data. *J. Geoph. Res.*, 84:35, 6251–6256.

- KLIONER, S.A. (1991). General Relativistic Model of VLBI Observables. In *Proceedings of the AGU Chapman Conference on Geodetic VLBI: Monitoring Global Change*, 188–202, NOAA Technical Report NOS 137 NGS 49.
- KLIONER, S.A. (2008). Relativistic scaling of astronomical quantities and the system of astronomical units. *Astr. & Astrophys.*, 478, 951–958.
- KOBAYASHI, H., SASAO, T., KAWAGUCHI, N., MANABE, S., OMODAKA, T., KAMEYA, O., SHIBATA, K.M., MIYAJI, T., HONMA, M., TAMURA, Y., HIROTA, S.T., KUJI, S., HORIAI, K., SAKAI, S., SATO, K., IWADATE, K., KANYA, Y., UJIHARA, H., JIKE, T., FUJII, T., OYAMA, T., KURAYAMA, H., SUDA, H., SAKAKIBARA, S., KAMOHARA, R. AND KASUGA, T. (2003). VERA project. In *New Technologies in VLBI*, Vol. 306, Astronomical Society of the Pacific Conference Series.
- KONDO, T., HOBIGER, T., SEKIDO, M., ICHIKAWA, R., KOYAMA, Y. AND TAKABA, H. (2009). Estimation of scan-gap limits on phase delay connections in Delta VLBI observations based on the phase structure function at a short time period. *Earth Planets Space*, 61, 357–371.
- KONO, Y., HANADA, H., PING, J., KOYAMA, Y., FUKUZAKI, Y. AND KAWANO, N. (2003). Precise positioning of spacecrafts by multi-frequency VLBI. *Earth Planets Space*, 55, 581–589.
- KOPEIKIN, S.M. AND SCHÄFER, G. (1999). Lorentz covariant theory of light propagation in gravitational fields of arbitrary-moving bodies. *Physical Review D*, 60, 124002(44).
- KRÁSNÁ, H., BÖHM, J., PLANK, L., NILSSON, T. AND SCHUH, H. (2013). Atmospheric Effects on VLBI-derived Terrestrial and Celestial Reference Frames. In C. Rizos and P Willis, eds., *IAG Symp. 139. Earth in the Edge: Science for a Sustainable Planet*, ISBN 978-3-642-37221-6, in press.
- KRÜGEL, M., THALLER, D., TESMER, V., ROTHACHER, M., ANGERMANN, D. AND SCHMID, R. (2007). Tropospheric parameters: combination studies based on homogeneous VLBI and GPS data. *J. Geod.*, 81, 515–527.
- KWAK, Y., GOTOH, T., AMAGAI, J., TAKIGUCHI, H., SEKIDO, M., ICHIKAWA, R., SASAO, T., CHO, J. AND KIM, T. (2010). The First Experiment with VLBI-GPS Hybrid System. In D. Behrend and K. Baver, eds., *International VLBI Service for Geodesy and Astrometry 2010 General Meeting Proceedings*, 330–334, NASA/CP 2010-215864.
- LAMBERT, S.B. AND PONCIN-LAFITTE, C.L. (2011). Improved determination of γ by VLBI (Research Note). *Astr. & Astrophys.*, 529, A70.
- LANYI, G., BORDER, J., BENSON, J., DHAWAN, V., FOMALONT, E., MARTIN-MUR, T., MCEL RATH, T., ROMNEY, J. AND WALKER, C. (2005). Determination of angular separation between spacecraft and quasars with the very long baseline array. *IPN Progress Report*, 42–162, August 15.
- LANYI, G., BAGRI, D.S. AND BORDER, J.S. (2007). Angular position determination of spacecraft by radio interferometry. In *Proceedings of the IEEE*, Vol. 95:11, November 2007.

- LEBRETON, J.P., WITASSE, O., SOLLAZZO, C., BLANCQUAERT, T., COUZIN, P., SCHIPPER, A.M., JONES, J.B., MATSON, D.L., GURVITS, L.I., ATKINSON, D.H., KAZEMINEJAD, B. AND PÉREZ-AYÚCAR, M. (2005). An overview of the descent and landing of the Huygens probe on Titan. *Nature*, 438/8, 758–764, doi:10.1038/nature04347.
- LESTRADE, J.F., ROGERS, A.E.E., WHITNEY, A.R., NIELL, A.E., PHILLIPS, R.B. AND PRESTON, R.A. (1990). Phase-referenced VLBI observations of weak radio source. Milliarcsecond position of Algol. *Astronomical Journal*, 99(5), 1663–1673.
- LI, P., HU, X., HUANG, Y., WANG, G., JIANG, D., ZHANG, X., CAO, J. AND XIN, N. (2012). Orbit determination for Chang'E-2 lunar probe and evaluation of lunar gravity models. *Sci China - Phys Mech Astron*, 55, 514–222.
- LINDEGREN, L., BABUSIAUX, C., BAILER-JONES, C., BASTIAN, U., BROWN, A.G.A., CROPPER, M., HØG, E., JORDI, C., KATZ, D., VAN LEEUWEN, F., LURI, X., MIGNARD, F., DE BRUIJNE, J.H.J. AND PRUSTI, T. (2008). The Gaia mission: science, organization and present status. In W.J. Jin, I. Platais and M.A.C. Perryman, eds., *Proceedings IAU Symposium, A Giant Step: from Milli- to Micro-arcsecond Astrometry*, Vol. 248, 217–223.
- LIU, Q., KIKUCHI, F., GOOSSENS, S., MATSUMOTO, K., HANADA, H., PING, J., SHI, X., TAMURA, Y., HARADA, Y., ASARI, K., TSURUTA, Y., ISHIKAWA, T., KAWANO, N., ISHIHARA, Y., NODA, H., SASAKI, S., IWATA, T. AND NAMIKI, N. (2009). S-band Same-Beam VLBI Observations in SELENE (Kaguya) and Correction of Atmospheric and Ionospheric Delay. *J. of the Geodetic Society of Japan*, 55, 243–254, no. 2.
- LIU, Q., KIKUCHI, F., MATSUMOTO, K., GOOSSENS, S., HANADA, H., HARADA, Y., SHI, X., HUANG, Q., ISHIKAWA, T., TSURUTA, S., ASARI, K., KAWANO, N., KAMATA, S., IWATA, T., NODA, H., NAMIKI, N., SASAKI, S., ELLINGSEN, S., SATO, K., SHIBATA, K., TAMURA, Y., JIKE, T., IWADATE, K., PING, J., XIA, B., AN, T., FAN, Q., HONG, X., YANG, W., ZHANG, H., AILI, Y., REID, B., HANKEY, W., MCCALLUM, J., KRNOCHNABL, G. AND SCHLÜTER, W. (2010). Same-beam VLBI observations of SELENE for improving lunar gravity field model. *Radio Sci.*, 45, RS2004.
- MA, C., ARIAS, E.F., EUBANKS, T.M., FEY, A.L., GONTIER, A.M., JACOBS, C.S., SOVERS, O.J., ARCHINAL, B.A. AND CHARLOT, P. (1998). The international celestial reference frame as realized by very long baseline interferometry. *The Astronomical Journal*, 116:1, 516–546.
- MACMILLAN, D.S. AND MA, C. (1994). Evaluation of very long baseline interferometry atmospheric modeling improvements. *J. Geophys. Res.*, 99 B1, 637–651.
- MARTÍN-MUR, T., ANTREASIAN, P., BORDER, J., BENSON, J., DHAWAN, V., FOMALONT, E., GRAAT, E., JACOBSON, R., LANYI, G., MCEL RATH, T., ROMNEY, J. AND WALKER, C. (2006). Use of very long baseline array interferometric data for spacecraft navigation. *19th International Symposium on Space Flight Dynamics, Kanazawa, Japan, June 4-11, 2006*, <http://hdl.handle.net/2014/39896>.

- MOYA ESPINOSA, M. AND HAAS, R. (2007). SATTRACK A Satellite Tracking Module for the VLBI Field System. In J. Böhm, A. Pany and H. Schuh, eds., *Proceedings of the 18th European VLBI for Geodesy and Astrometry Working Meeting, 12-13 April 2007, Vienna*, Vol. 79, 53–58, Schriftenreihe der Studienrichtung Vermessung und Geoinformation, Technische Universität Wien, ISSN 1811-8380.
- MOYER, T.D. (2003). Formulation for observed and computed values of deep space network data types for navigation. In J.H. Yuen, ed., *JPL Deep Space Communications and Navigation Series*, John Wiley & Sons Inc., ISBN: 0-471-44535-5.
- MÜLLER, J., SOFFEL, M. AND KLIONER, S.A. (2008). Geodesy and relativity. *J. Geod.*, 82, 133–145.
- NELSON, R.A., MCCARTHY, D.D., MALYS, S., LEVINE, J., GUINOT, B., FLIEGEL, H.F., BEARD, R.L. AND BARTHOLOMEW, T.R. (2001). The leap second: its history and possible future. *Metrologia*, 38, 509–529.
- NEREM, R.S. AND DRAPER, R.W. (2011). Geodetic Reference Antenna in SPace. *GRASP proposal submitted in response to NNH11ZDA0120*, prepared for National Aeronautics and Space Administration Science Mission Directorate September 29, 2011.
- NIELL, A.E. (2007). Simulation Networks - 1. *IVS Memorandum 2007-001v01*, <ftp://ivscc.gsfc.nasa.gov/pub/memos/ivs-2007-001v01.pdf>.
- NIELL, A.E., WHITNEY, A., PETRACHENKO, B., SCHLÜTER, VANDENBERG, N., HASE, H., KOYAMA, Y., MA, C., SCHUH, H. AND TUCCARI, G. (2006). VLBI2010: Current and Future Requirements for Geodetic VLBI Systems. *IVS Memorandum 2006-008v01*, <ftp://ivscc.gsfc.nasa.gov/pub/memos/ivs-2006-008v01.pdf>.
- NILSSON, T. AND HAAS, R. (2010). Impact of atmospheric turbulence on geodetic very long baseline interferometry. *J. Geoph. Res.*, 115, B03407, doi:10.1029/2009JB006579.
- NILSSON, T., HAAS, R. AND ELGERED, G. (2007). Simulations of atmospheric path delays using turbulence models. In J. Böhm, A. Pany and H. Schuh, eds., *Proceedings of the 18th European VLBI for Geodesy and Astrometry Working Meeting, 12-13 April 2007, Vienna*, Vol. 79, 175–180, Schriftenreihe der Studienrichtung Vermessung und Geoinformation, Technische Universität Wien, ISSN 1811-8380.
- NILSSON, T., BÖHM, D., J. WIJAYA, TRESCH, A., NAFISI, V. AND SCHUH, H. (2013). Path delays in the Neutral Atmosphere. In *Atmospheric Effects in Space Geodesy*, 73–136, Springer Verlag, ISBN: 978-3-642-36931-5.
- NOTHNAGEL, A. (2009). Conventions on thermal expansion modelling of radio telescopes for geodetic and astrometric VLBI. *J. Geod.*, 83:8, 787–792.

- NOTHNAGEL, A., CHARLOT, P., DEHANT, V., FIENGA, A., HASE, H., PLANK, L. AND SCHUH, H. (2013). Short Report of the IVS Working Group 5 (WG5) on Space Science Applications - An IVS Perspective. Available at: <http://ivscc.gsfc.nasa.gov/about/wg/wg5/>.
- PANY, A., BÖHM, J., MACMILLAN, D.S., SCHUH, H., NILSSON, T. AND WRESNIK, J. (2010). Monte Carlo simulations of the impact of troposphere, clock and measurement errors on the repeatability of VLBI positions. *J. Geod.*, 85:1, 39–50.
- PEARLMAN, M.R., DEGNAN, J.J. AND BOSWORTH, J.M. (2002). The International Laser Ranging Service. *Adv. Space Res.*, 30:2, 135–143.
- PETIT, G. AND LUZUM, B., eds. (2010). IERS Conventions 2010. Frankfurt am Main: Verlag des Bundesamtes für Kartographie und Geodäsie, IERS Technical Note No. 36.
- PETRACHENKO, B., NIELL, A., BEHREND, D., COREY, B., BÖHM, J., CHARLOT, P., COLLIOD, A., GIPSON, J., HAAS, R., HOBIGER, T., KOYAMA, Y., MACMILLAN, D., MALKIN, Z., NILSSON, T., PANY, A., TUCCARI, G., WHITNEY, A. AND WRESNIK, J. (2009). Progress Report of the IVS VLBI2010 Committee: Design Aspects of the VLBI2010 System. *NASA/TM-2009-214180*, <ftp://ivscc.gsfc.nasa.gov/pub/misc/V2C/TM-2009-214180.pdf>.
- PLAG, H.P. AND PEARLMAN, M., eds. (2009). Global geodetic observing system: Meeting the requirements of a global society on a changing planet in 2020. Springer-Verlag Berlin Heidelberg.
- PLANK, L., BÖHM, J., MADZAK, M., TIERNO ROS, C. AND SCHUH, H. (2013). Processing SELENE Differential VLBI Data. In D. Behrend and K. Baver, eds., *International VLBI Service for Geodesy and Astrometry 2012 General Meeting Proceedings*, 291–295, *NASA/CP-2012-217504*.
- POGREBENKO, S.V., GURVITS, L.I., M., C.R., AVRUCH, I.M., LEBRETON, J.P. AND VAN'T KLOOSTER, C.G.M. (2004). VLBI tracking of the Huygens probe in the atmosphere of Titan. In A. Wilson, ed., *Proceedings of the International Workshop Planetary Probe Atmospheric Entry and Descent Trajectory Analysis and Science, 6-9 October 2003, Lisbon, Portugal*, 197–204, ESA SP-544, Noordwijk, Netherlands: ESA Publications Division, ISBN 92-9092-855-7.
- PRESTON, R.A., ERGAS, R., HINTEREGGER, H.F., KNIGHT, C.A., ROBERTSON, D.S., SHAPIRO, I.I., WHITNEY, A.R., ROGERS, A.E.E. AND CLARK, T.A. (1972). Interferometric Observations of an Artificial Satellite. *Science*, 178-4059, 407–409.
- QIAN, Z. AND PING, J. (2006). The Orbit Determination of the CHANG'E-1 Lunar Orbiter by VLBI. In *SICE-ICASE International Joint Conference 2006*, Oct. 18-21, 2006 in Bexco, Busan, Korea.
- RAY, J. AND ALTAMIMI, Z. (2005). Evaluation of co-location ties relating the VLBI and GPS reference frames. *J. Geod.*, 79, 189–195.
- ROSENBAUM, B. (1972). The VLBI Time Delay Function for Synchronous Orbits. *NASA/TM-X-66122*, GSFC.

- SAGDEYEV, R.Z., KERZHANOVITCH, V.V., KOGAN, L.R., KOSTENKO, VI., LINKIN, V.M., MATVEYENKO, L.I., NAZIROV, R.R., POGREBENKO, S.V., STRUCKOV, I.A., PRESTON, R.A., PURCEL, J., HILDEBRAND, C.E., GRISHMANOVSKIY, V.A., KOZLOV, A.N., MOLOTOV, E.P., BLAMONT, J.E., BOLOH, L., LAURANS, G., KAUFMANN, P., GALT, J., BIRAUD, F., BOISCHOT, A., ORTEGA-MOLINA, A., ROSOLEN, C., PETIT, G., MEZGER, P.G., SCHWARTZ, R., RÖNNÄNG, B.O., SPENCER, R.E., NICOLSON, G., ROGER, A.E.E., COHEN, M.H., MARTIROSYAN, R.M., MOISEYEV, I.G. AND JATSKIV, J.S. (1992). Differential VLBI measurements of the Venus atmosphere dynamics by balloons: VEGA project. *Astron. & Astrophys.*, 254, 387–392.
- SARTI, P, ABBONDANZA, C., PETROV, L. AND NEGUSINI, M. (2011). Height bias and scale effect induced by antenna gravitational deformations in geodetic VLBI data analysis. *J. Geod.*, 85:1-8, doi:10.1007/s00190-010-0410-6.
- SCHNEIDER, P. (2010). *Extragalactic Astronomy and Cosmology - An Introduction*. Springer-Verlag Berlin Heidelberg, ISBN 978-3-642-06971-0.
- SCHUH, H. (1987). Die Radiointerferometrie auf langen Basen zur Bestimmung von Punktverschiebungen und Erdrotationsparametern. *DGK Reihe C, Dissertationen*, Heft Nr. 328, (in German).
- SCHUH, H. AND BEHREND, D. (2012). VLBI: A fascinating technique for geodesy and astrometry. *J. of Geodynamics*, 61, 68–80.
- SCHUH, H. AND BÖHM, J. (2013). Very long baseline interferometry for geodesy and astrometry. In G. Xu, ed., *Sciences of Geodesy - II*, doi:10.1007/978-3-642-28000-9-7, Springer-Verlag Berlin Heidelberg.
- SEITZ, M., ANGERMANN, D., BLOSSFELD, M., DREWES, H. AND GERSTL, M. (2012). The 2008 DGFI realization of the ITRS: DTRF2008. *J. Geod.*, 86:12, 1097–1123.
- SEKIDO, M. AND FUKUSHIMA, T. (2006). A VLBI delay model for radio sources at a finite distance. *J. Geod.*, 80, 137–149.
- SEKIDO, M., ICHIKAWA, R., OSAKI, H., KONDO, T., KOYAMA, Y., YOSHIKAWA, M., OHNISHI, T., CANNON, W., NOVIKOV, A., BÉRUBÉ, M. AND NOZOMI VLBI GROUP (2004). VLBI Observation for Spacecraft Navigation (NOZOMI) - Data Processing and Analysis Status Report. In N.R. Vandenberg and K.D. Baver, eds., *International VLBI Service for Geodesy and Astrometry 2004 General Meeting Proceedings*, 258–262, NASA/CP-2004-212255.
- SEKIDO, M., RYUICHI, I., YOSHIKAWA, M., TAKEUCHI, H., KATO, T., MOCHIZUKI, N., MURATA, Y. AND ICHIKAWA, T. (2007). Evaluation of Differential VLBI Phase Delay Observable for Spacecraft Navigation - Δ VLBI observation of Hayabusa to ITOKAWA -. *SICE Annual Conference*, 3029–3036, Kagawa University, Japan.

- SHAPIRO, I.I., WITTELS, J.J., COUNSELMAN, C.C., ROBERTSON, D.S., WHITNEY, A.R., HINTEREGGER, H.F., KNIGHT, C.A., ROGERS, A.E.E., CLARK, T.A., HUTTON, L.K. AND NIELL, A.E. (1979). Submilliarcsecond Astrometry via VLBI. I. Relative position of the radio sources 3C 345 and NRAO 512. *The Astronomical Journal*, 84/10.
- SHU, F., ZHANG, X. AND KONDO, T. (2008). Development of correlator model for differential VLBI observations of satellites. In *ICMMT 2008 Proceedings*, 443–446, doi: 10.1109/ICMMT.2008.4540413.
- SOFFEL, M., KLIONER, S., PETIT, G., WOLF, P., KOPEIKIN, S., BRETAGNON, P., BRUMBERG, V., CAPITAINE, N., DAMOUR, T., FUKUSHIMA, T., GUINOT, B., HUANG, T., LINDEGREN, L., MA, C., NORDTVEDT, K., RIES, J., SEIDELMANN, P., VOKROUHLICKY, D., WILL, C. AND XU, C. (2003). The IAU 2000 resolutions for astrometry, celestial mechanics and metrology in the relativistic framework: explanatory supplement. *Astron. J.*, 126, 2687.
- SOJA, B., PLANK, L. AND SCHUH, H. (2012). General relativistic delays in current and future VLBI. In H. Schuh, S. Böhm, T. Nilsson and N. Capitaine, eds., *Earth rotation, reference systems, and celestial mechanics: Synergies of geodesy and astronomy. Journées 2011, Vienna, 19-21 September*, 41–44, Department of Geodesy and Geoinformation Vienna University of Technology and Observatoire de Paris, ISBN:978-2-901057-67-3.
- SOVERS, O.J., FANSELOW, J.L. AND JACOBS, C.S. (1998). Astrometry and geodesy with radio interferometry: experiments, models, results. *Reviews of Modern Physics*, 70:4, 1393–1454.
- SUN, J. (2013). VLBI scheduling strategies with respect to VLBI2010. *Geowissenschaftliche Mitteilungen*, 92, Schriftenreihe der Studienrichtung Vermessung und Geoinformation, Technische Universität Wien, ISSN 1811-8380.
- TAKAHASHI, F., KONDO, T., TAKAHASHI, Y. AND KOYAMA, Y. (2000). *Wave Summit Course: Very Long Baseline Interferometer*. IOS Press, ISBN: 1-58603-076-0.
- TAKEUCHI, H., KIMURA, M., NAKAJIMA, J., ICHIKAWA, R., SEKIDO, M., KONDO, T. AND KOYAMA, Y. (2006). A VSI-compliant 2-Gbps DAS for Spacecraft Differential VLBI. In D. Behrend and K. Baver, eds., *International VLBI Service for Geodesy and Astrometry 2006 General Meeting Proceedings*, 221–225, NASA/CP-2006-214140.
- TEKE, K. (2011). Sub-daily Parameter Estimation in VLBI Data Analysis. *Geowissenschaftliche Mitteilungen*, 87, Schriftenreihe der Studienrichtung Vermessung und Geoinformation, Technische Universität Wien, ISSN 1811-8380.
- THALLER, D., DACH, R., SEITZ, M., BEUTLER, G., MAREYEN, M. AND RICHTER, B. (2011). Combination of GNSS and SLR observations using satellite co-locations. *J. Geod.*, 85, 257–272.
- THOMPSON, A.R., MORAN, J.M. AND SWENSON, G.W.J. (1986). *Interferometry and Synthesis in Radio Astronomy*. Wiley, New York.

- THORNTON, C.L. AND BORDER, J.S. (2003). Radiometric Tracking Techniques for Deep Space Navigation. In Joseph H. Yuen, ed., *JPL Deep Space Communications and Navigation Series*, John Wiley & Sons Inc., ISBN: 0-471-44534-7.
- TIERNO ROS, C., BÖHM, J. AND SCHUH, H. (2011). Use of GNSS-derived TEC maps for VLBI observations. In W. Alef, S. Bernhart and A. Nothnagel, eds., *Proceedings of the 20th Meeting of the European VLBI Group for Geodesy and Astrometry*, Vol. 22, 114–117, Institut für Geodäsie und Geoinformation der Universität Bonn.
- TORNATORE, V. AND HAAS, R. (2009). Considerations on the observation of GNSS-signals with the VLBI2010 system. In G. Bourda, P. Charlot and A. Collioud, eds., *Proceedings of the 19th European VLBI for Geodesy and Astrometry Working Meeting*, 151–155, Université Bordeaux 1 - CNRS Observatoire Aquitain des Sciences de l'Univers Laboratoire d'Astrophysique de Bordeaux, 24-25 March 2009, Bordeaux.
- TORNATORE, V., HAAS, R., MACCAFERRI, G., CASEY, S., POGREBENKO, S.V., MOLERA, G. AND DUEV, D. (2010). Tracking of GLONASS satellites by VLBI radio telescopes. In ESA, ed., *5th ESA International Workshop on Tracking, Telemetry and Command Systems for Space Applications (TTC 2010) Proceedings*, ESA-ESTEC, Noordwijk, The Netherlands, 21-23 September 2010, Special publication ESA WPP-318.
- TORNATORE, V., HAAS, R., DUEV, D., POGREBENKO, S., CASEY, S. AND MOLERA CALVÉS, G. (2011a). Determination of GLONASS satellite coordinates with respect to natural radio sources using the VLBI technique: preliminary results. In Association Astronautique et Aéronautique de France e SEE (Société de l'Electricité, de l'Electronique et des Technologies de l'Information et de la Communication), ed., *ETTC2011, European Test and Telemetry conference, 14-16 Giugno 2011, Toulouse France*, electronic publication, http://publications.lib.chalmers.se/records/fulltext/local_150623.pdf.
- TORNATORE, V., HAAS, R., DUEV, D., POGREBENKO, S., CASEY, S., MOLERA CALVÉS, G. AND KEIMPEMA, A. (2011b). Single baseline GLONASS observations with VLBI: data processing and first results. In W. Alef, S. Bernhart and A. Nothnagel, eds., *Proceedings of the 20th Meeting of the European VLBI Group for Geodesy and Astrometry*, Vol. 22, 162–165, Institut für Geodäsie und Geoinformation der Universität Bonn.
- TREUHAFT, R.N. AND LANYI, G.E. (1987). The effect of the dynamic wet troposphere on radio interferometric measurements. *Radio Science*, 22:2, 251–265.
- VAN 'T KLOOSTER, K. (2007). VLBI-Observation of 'Huygens' Probe. In *Proceedings of International Conference on Antenna Theory and Techniques*, 57–58, 17-21 September, 2007, Sevastopol, Ukraine.

- WALTER, H.G. AND SOVERS, O.J. (2000). *Astrometry of Fundamental Catalogs - The Evolution from Optical to Radio Reference Frames*. Astronomy and Astrophysics Library, Springer-Verlag Berlin Heidelberg.
- WILL, C. (1993). *Theory and Experiment in Gravitational Physics*. Cambridge University Press, Cambridge.
- WROBEL, J.M., WALKER, R.C., BENSON, J.M. AND BEASLEY, A.J. (2000). Strategies for Phase Referencing with the VLBA. *VLBA Scientific Memorandum 24*, <http://www.vlba.nrao.edu/memos/sci/sci24memo.ps>.
- WU, S.C. (1979). Connection and Validation of Narrow-Band Δ VLBI Phase Observations. *DSN Progress Report*, 42-52, Jet Propulsion Laboratory, Pasadena, California.
- YAN, J., PING, J., LI, F., CAO, J., HUANG, Q. AND FUNG, L. (2010). Chang'E-1 precision orbit determination and lunar gravity field solution. *Adv Space Res*, 46, 50–57.

CURRICULUM VITAE

Lucia Plank
Project Assistant, Dipl.-Ing.
Vienna University of Technology
Department of Geodesy and Geoinformation
Research Group Advanced Geodesy, E120-4
Gußhausstraße 27-29
1040 Vienna, AUSTRIA
Phone: +43-1-58801-12867
lucia.plank@tuwien.ac.at
www.hg.tuwien.ac.at

Personal

Dipl.-Ing. Lucia Maria Plank

Born on June 3rd, 1984 in Wels, Austria

Nationality: Austria

Parents: Dipl.-Ing. Maria and Johann Plank

Employment Record

2012-now

Project assistant, Department of Geodesy and Geoinformation, Vienna University of Technology (30 hours)

Project: *Ties between kinematic and dynamic reference frames (D-VLBI)*; within the Research Unit *Space-Time Reference Systems for Monitoring Global Change and for Precise Navigation in Space*, funded by the German Research Foundation (DFG)
Project leaders: Harald Schuh and Johannes Böhm

2008-2012

University assistant, Institute of Geodesy and Geophysics, Vienna University of Technology (25 hours, four-year fixed contract)

Head of the Institute: Harald Schuh

University and Education

2009-2013

Doctoral programme (Dr. techn.) at Vienna University of Technology

2012

2-weeks research stay at Jet Propulsion Laboratory (JPL) Pasadena, USA

August 2012, invited by Christopher Jacobs

2010

2-weeks research stay at the National Astronomical Observatory of Japan (NAOJ) in Mizusawa (Japan)

2008

**Dipl.-Ing. degree (equiv. MSc.) in “Geodesy and Geophysics“,
Vienna University of Technology**

Thesis: “*Calculation of the Earth Rotation Vector with VLBI and Ringlaser measurements.*” Supervisors: Harald Schuh and Rüdiger Haas

2007

**ERASMUS student exchange programme at Chalmers University
of Technology in Gothenburg and Onsala Space Observatory
(Sweden)**

Sept. 2007-March 2008

2002-2008

**Master programme of the Vienna University of Technology
Geodesy and Geophysics**

2002

**Matura (school leaving examination), Bundesgymnasium
Brucknerstraße Wels (High School)**

Awards

**Best Presentation Award, Geodetic Week 2009, Karlsruhe
(Germany)**

Memberships and committees

2011-now

**Member of IAG SC 1.4 WG2: Co-location on Earth and in Space
for the Determination of the Celestial Reference Frame**

2011-now

Member of IVS Working Group 6 on Education and Training

2010-now

**Faculty representative in the “Arbeitskreis für
Gleichbehandlungsfragen (AKG)” (committee for non-
discrimination) at the Vienna University of Technology**

2010-2013

**Member of the study commission “Vermessung und
Geoinformation” at the Vienna University of Technology**

2009-now

**Associate member of the International VLBI Service for Geodesy
and Astrometry (IVS)**